Functions of CFTR and anoctamins in kidney and other epithelial organs

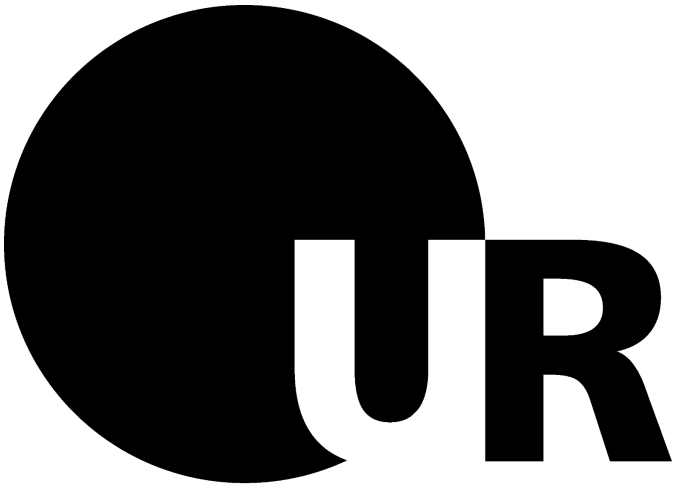

DISSERTATION ZUR ERLANGUNG DES DOKTORGRADES
DER NATURWISSENSCHAFTEN (DR.RER.NAT.)
DER FAKULTÄT FÜR BIOLOGIE UND VORKLINISCHE MEDIZIN
DER UNIVERSITÄT REGENSBURG

vorgelegt von
Inês Maria Santos Cabrita Bustorff Silva
aus
Amadora, Portugal

im Juni
2020

DAS PROMOTIONSGESUCH WURDE EINGEREICHT AM:
12.06.2020

DIE ARBEIT WURDE ANGELEITET VON:
PROF. DR. KARL KUNZELMANN

UNTERSCHRIFT:

_____

DIE ARBEIT WURDE ANGELEITET VON: PROF. DR. KARL KUNZELMANN

PRÜFUNGSAUSSCHUSS:

VORSITZENDER: PROF. DR. MED. ARMIN KURTZ

1.GUTACHTER: PROF. DR. MED. KARL KUNZELMANN

2.GUTACHTER: PROF. DR. RER. NAT. CHRISTIAN WETZEL

3. PRÜFER: PROF. DR.MED. FRANK SCHWEDA

ERSATZPERSON: PROF. DR. RER. NAT. JENS SCHLOSSMANN

SUMMARY

Autosomal dominant polycystic kidney disease (ADPKD) is characterized by the development of bilateral renal cysts that continuously expand, leading to impaired renal function. ADPKD is originates when mutations occur in the *PKD1* or *PKD2* genes, whose protein products are collectively called polycystins. Polycystin-1 (encoded by *PKD1*) is a membrane protein with large extracellular domains, probably working as a receptor for an unidentified ligand. Polycystin-2 (encoded by *PKD2*) is also a membrane-associated protein that works as a non-selective ion channel with high permeability for calcium ions (Ca^{2+}). Together, these proteins are thought to form a functional complex, which can regulate intracellular Ca^{2+} signaling. One of the hallmarks of ADPKD is the transepithelial Cl^- secretion towards the cyst lumen. This secretion is thought to occur mainly through the cAMP-activated Cl^- channel Cystic Fibrosis Transmembrane Conductance Regulator (CFTR). CFTR is expressed in the apical membrane of epithelial cells of several organs, such as airways and kidney. Its function is proposed to be upregulated in cystic epithelial cells. However, heterogeneity in CFTR expression suggests that this channel may not be the only Cl^- channel responsible for transepithelial chloride (Cl^-) secretion in ADPKD. In fact, Ca^{2+}-activated Cl^- channels (CaCCs) activated through purinergic receptors seem to play a fundamental role in this process. TMEM16A, TMEM16F and TMEM16K represent members of a family of CaCCs and phospholipid scramblases, which are also expressed in airways and renal epithelial cells. Together with CFTR, they could participate in Cl^- secretion and may therefore contribute to cyst development. Also, aberrant Ca^{2+} signaling in ADPKD may further enhance Ca^{2+}-activated Cl^- secretion and cell proliferation.

In the present thesis I demonstrate that TMEM16 paralogs facilitate compartmentalized Ca^{2+} signaling in various tissues. TMEM16A and TMEM16K are shown to enhance Ca^{2+}-dependent intestinal ion secretion. Apart from supporting ion secretion, basic cellular functions such as volume regulation and apoptosis are supported by TMEM16K. Mutations in TMEM16K cause cellular defects and genetic disorders through dysfunctional local Ca^{2+} signaling. It is concluded that intracellular Ca^{2+} signals augmented by TMEM16A and TMEM16F support ATP-dependent constitutive mucus secretion in airways and intestine. By knockdown of *PKD1* or *PKD2* in the mouse collecting duct cell line M1, a cystic phenotype could be induced in an organoid model *in vitro*. Kidneys of mice with a renal tubular knockdown of *Pkd1* or *Pkd2* developed a cystic phenotype similar to ADPKD. Cells lacking expression of PKD1 or PKD2 present increased constitutive and ATP-stimulated Cl^- secretion, mainly through upregulation of TMEM16A. These cells also show an increase in proliferative activity. It is shown that the increase in TMEM16A-activity enhances endoplasmic reticulum Ca^{2+} store content and intracellular Ca^{2+} signaling.

In additional studies it is demonstrated that inhibition of TMEM16A by the FDA-approved drugs niclosamide or benzbromarone, reduces airway inflammation, attenuates mucus secretion, and promotes bronchorelaxation. The same inhibitors are shown to potently suppress cyst formation in a mouse model for ADPKD, essentially by inhibiting increased intracellular Ca^{2+} signals, Cl^- secretion and cell proliferation. Thus, therapeutic inhibition of TMEM16 paralogs lays the groundwork for a novel treatment of both inflammatory airway disease and polycystic kidney disease. The results presented here may also establish a novel therapeutic concept for several additional diseases in which TMEM16A and other TMEM16 paralogs play a central role.

ZUSAMMENFASSUNG

Die autosomal dominante polyzystische Nierenerkrankung (ADPKD) ist durch die Entwicklung bilateraler Nierenzysten gekennzeichnet, die sich kontinuierlich ausdehnen und zu einer Beeinträchtigung der Nierenfunktion führen. ADPKD entsteht durch Mutationen in den Genen *PKD1* oder *PKD2*, deren Proteine kollektiv als Polyzystine bezeichnet werden. Polyzystin-1 (kodiert durch *PKD1*) ist ein Membranprotein mit großer extrazellulärer Domäne, das vermutlich als Rezeptor für einen bislang nicht identifizierten Liganden dient. Polycystin-2 (kodiert durch *PKD2*) ist ebenfalls ein membranassoziiertes Protein, das als nicht-selektiver Ionenkanal mit hoher Permeabilität für Kalzium- (Ca^{2+}) Ionen operiert. Man nimmt an, dass beide Proteine zusammen einen funktionellen Komplex bilden, der intrazelluläre Ca^{2+} -Signale reguliert. Eines der Kennzeichen der ADPKD ist die transepitheliale Chloridionensekretion in Richtung des Zystenlumens. Bisherige Untersuchungen ließen vermuten, dass die Sekretion hauptsächlich durch den cAMP-aktivierten Cl^--Ionenkanal CFTR (Cystic Fibrosis Transmembrane Conductance Regulator) erfolgt. CFTR ist in der apikalen Membran von Epithelzellen verschiedener Organe wie z.B. solchen in Luftwegen und der Niere exprimiert. Die Funktion von CFTR scheint in Epithelzellen, die das Zystenlumen auskleiden, hochreguliert zu sein. Heterogenitäten der CFTR-Expression legen jedoch nahe, dass dieser Kanal möglicherweise nicht alleinig für die transepitheliale Chloridsekretion bei ADPKD verantwortlich ist. Tatsächlich dient eine weitere Klasse von Chloridionenkanälen der Chloridsekretion, die sog. Ca^{2+} aktivierten Cl^- Kanäle (CaCCs). Diese werden beispielsweise über purinerge Rezeptoren aktiviert. TMEM16A, TMEM16F und TMEM16K gehören zu einer Familie von Proteinen, die CaCCs und Phospholipid-Scramblasen bilden. Diese sind ebenfalls in Epithelzellen der Luftwege und in Nierentubuli exprimiert. Wahrscheinlich nehmen diese TMEM16-Paraloge zusammen mit CFTR an der Cl^- Sekretion teil und tragen so zur Zystenentwicklung bei. Die aberranten Ca^{2+}-Signale bei ADPKD könnten die Ca^{2+}-aktivierte Cl- Sekretion sowie die Zellproliferation weiter verstärken.

In der vorliegenden Arbeit zeige ich, dass TMEM16-Paraloge intrazelluläre submembranär lokalisierte Ca^{2+} -Signale in verschiedenen Geweben verstärken. Neben TMEM16A erhöht auch TMEM16K die Ca^{2+}-abhängige intestinale Ionensekretion. Abgesehen von der Unterstützung der Anionensekretion werden auch grundlegende zelluläre Funktionen wie die Volumenregulation und die Apoptose durch TMEM16K unterstützt. Mutationen in TMEM16K verursachten zelluläre Defekte und genetische Störungen durch dysfunktionale lokale Ca^{2+}-Signale. Weiterhin zeigen die Ergebnisse, dass intrazelluläre Ca^{2+}-Signale, welche durch TMEM16A und TMEM16F verstärkt werden, die ATP-abhängige konstitutive Schleimsekretion in den Luftwegen und im Darm unterstützen. shRNA-Knockdown in der

Sammelrohr-Zelllinie M1, sowie Knockdown von *Pkd1* oder *Pkd2* in Tubuluszellen der Maus induzierten einen zystischen Phänotyp, ähnlich wie bei ADPKD. Zellen ohne *Pkd1* oder *Pkd2* weisen eine erhöhte konstitutive und ATP-stimulierte Cl^- Sekretion auf, die wesentlich durch die Hochregulierung von CFTR und TMEM16A bedingt ist. Die betroffenen Zellen zeigen eine Zunahme der Proliferation. Wir konnten nachweisen, dass die Zunahme der TMEM16A-Aktivität die Ca^{2+} Füllung des endoplasmatischen Retikulums und die Rezeptor-vermittelte Ca^{2+}-Freisetzung erhöht.

Die hier vorgestellten Ergebnisse könnten ein neuartiges therapeutisches Konzept darstellen, einerseits für die Behandlung von Luftwegserkrankungen wie auch zur Unterdrückung der Zystenbildung bei polyzystischer Nierendysplasie. Die Untersuchungen konnten zeigen, dass die Hemmung von TMEM16A durch die zugelassenen Medikamente Niklosamid und Benzbromaron, die Entzündung der Atemwege reduziert, die Schleimsekretion dämpft und die Weitstellung der Bronchien fördert. Die gleichen Inhibitoren unterdrücken ebenfalls die Zystenbildung in einem Mausmodell für ADPKD, indem sie pathologisch verstärkte Ca^{2+}-Signale normalisierten und die Cl^--Sekretion sowie die Zellproliferation hemmten. Die therapeutische Hemmung der TMEM16-Paraloge legt somit den Grundstein für eine neuartige Behandlung von entzündlichen Atemwegserkrankung und der polyzystischen Nierendysplasie.

PREFACE

The present thesis is composed of articles which were published as results of my work during my PhD project. Therefore, the reader may encounter some variations in the style of writing which are due to the different journal guidelines. The chapters of the present thesis are based on the following manuscripts:

Chapter 2: **Cabrita I.**, Benedetto R., Fonseca A., Wanitchakool P., Sirianant L., Skryabin B.V., Schenk L.K., Pavenstadt H., Schreiber R., Kunzelmann K. Differential effects of anoctamins on intracellular calcium signals. *FASEB J.* 2017 May; 31(5): 2123-2134.

Chapter 3: Wanitchakool P., Ousingsawat J., Sirianant L., **Cabrita I.**, Faria D., Schreiber R., Kunzelmann K. Cellular Defects by Deletion of ANO10 are due deregulated local Calcium Signaling. *Cell Signal.* 2016 Nov 30:41-49.

Chapter 4: **Cabrita I.**, Benedetto R., Schreiber R., Kunzelmann K. Niclosamide repurposed for the treatment of inflammatory airway disease. *JCI Insight*. 2019 Aug 8;4(15).

Chapter 5: **Cabrita I.**, Buchholz B., Schreiber R., Kunzelmann K. TMEM16A drives renal cyst growth by augmenting Ca^{2+} signaling in M1 cells. *J Mol Med (Berl)* 2020 Mar 18 98, 659–671.

Chapter 6: **Cabrita I.**, Kraus A., Schreiber R., Kunzelmann K., Buchholz B. Cyst growth in ADPKD requires Ca^{2+} dependent chloride secretion and is prevented by pharmacological inhibition of TMEM16A *in vivo*. (under revision).

INDEX

LIST OF FIGURES

LIST OF TABLES

CHAPTER 1 | INTRODUCTION

TMEM16 PROTEINS

TMEM16 constitutes a family of ten homologous channels (TMEM16A-K; ANO1-10) characterized by their highly conserved sequence, mostly around the putative pore-forming region [1,2]. Although these proteins are broadly expressed and although they are present in almost every cell type [3], their cellular functions are not well defined: some members are calcium-activated chloride channels (CaCCs), while others are described as phospholipid scramblases, that also conduct ions [2]. These proteins fulfill various physiological functions such as maintaining hemostasis, chloride (Cl^-) secretion by glands, muscle contraction, volume regulation, neuronal excitability, and many more [4]. Defects in TMEM16 proteins cause a wide range of diverse health problems, like bleeding disorders, bone malformation, muscular dystrophy, or anxiety [1]. Overexpression or enhanced function of TMEM16 proteins cause ataxia, cancer or asthma [1]. Recently, the structure of TMEM16 proteins has been identified [1,5,6]. The most accurate structure of TMEM16A (anoctamin 1; ANO1) was determined for mouse TMEM16A. mTMEM16A forms a stable dimer with both N- and C-*termini* located on the cytoplasmatic side of the plasma membrane. Each subunit contains ten transmembrane domains, an extracellular domain and an ion conductive pore with two calcium (Ca^{2+}) binding sites [7]. TMEM16A is activated by Ca^{2+} through stimulation of G-protein-coupled receptors, like those for angiotensin II or adenosine triphosphate (ATP) (Fig. 1.1A) [8-11]. Paulino *et al.* [6] data showed that Ca^{2+} binding is the essential gating mechanism for TMEM16A. Ca^{2+} binding in the transmembrane domains α7 and α8 alters the electrostatic properties of the ion channel and triggers structural rearrangement of TMEM16A. This event leads to a conformational rearrangement of α6 domain with the bound ligands, directly coupling Ca^{2+} binding to pore opening. TMEM16A is upregulated in various types of cancer, such as head and neck squamous cell carcinoma (HNSCC) and colonic cancer. It is generally linked to cell hyperproliferation, migration, and apoptosis.

TMEM16F (anoctamin 6; ANO6) is a Ca^{2+}-activated phospholipid scramblase of the plasma membrane lipid bilayer [12], and also a Ca^{2+}-activated ion channel [13,14] (Fig. 1.1B). TMEM16F is expressed at high levels in bone cells, immune cells and platelets [15,16]. During phospholipid scrambling, TMEM16F translocates phospholipids in both directions across the plasma membrane bilayer, which leads to a transient or, in case of apoptotic scrambling, to a sustained collapse of the membrane asymmetry [17,18]. Ion transport and scrambling by TMEM16F are activated simultaneously upon a large increase in intracellular Ca^{2+} [19,20]. The structural characterization of nhTMEM16, a TMEM16F homologue from the fungus *Nectria hematococca*, revealed the presence of a partially hydrophilic environment within the

conductive pore required for both phospholipid scrambling and ion transport [19]. Subsequent structural determination by cryo-electron microscopy demonstrated that human TMEM16F operates as nhTMEM16 [6,21]. While TMEM16A forms a narrow pore and only conducts Cl^- ions, TMEM16F has an open hydrophilic cleft that faces the lipid bilayer and therefore facilitates translocation of phospholipid between membrane leaflets together with ions [18,22].

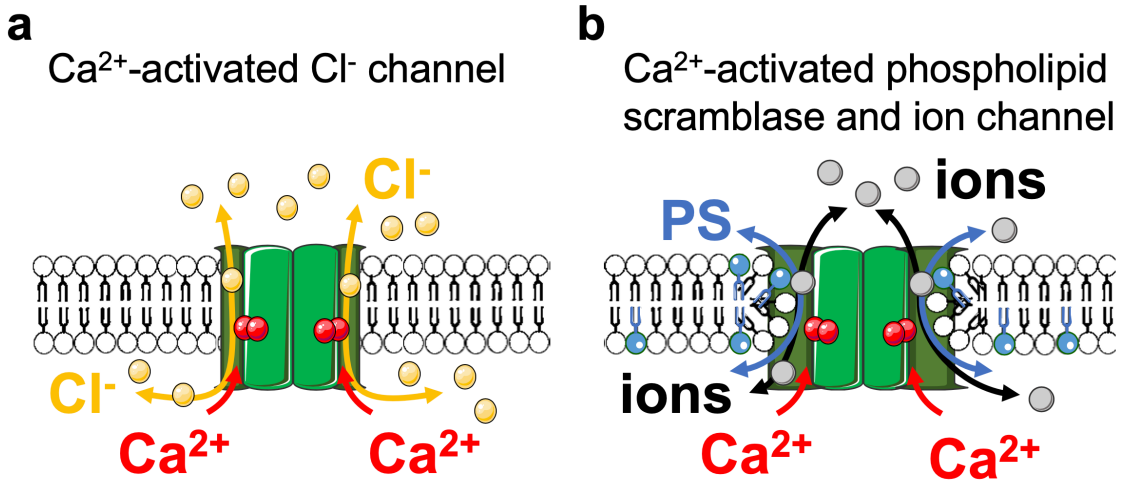

Figure 1.1 | *TMEM16 proteins operate as Ca^{2+}-activated chloride channels **(a)** or as Ca^{2+}-activated phospholipid scramblases that also conduct ions **(b)**.*

TMEM16K (anoctamin 10; ANO10) is an intracellular protein, which is found in various tissues, but is particularly highly expressed in brain frontal cortex, occipital cortex, and cerebellum [11,23,24]. TMEM16K most likely also operates as Ca^{2+}-regulated phospholipid scramblase and ion channel [23]. TMEM16K is found in Purkinje cells of the cerebellum and mutations in TMEM16K are known to cause autosomal-recessive cerebellar ataxia [23,25-28], a rare neurodegenerative disorder related to coenzyme Q10 deficiency [31]. Cerebellar degeneration was associated with dysfunctions in mitochondrial- and DNA-repair. TMEM16K also has a role in schizophrenia [25] while a coding variant of TMEM16K (ANO10-R263H) was shown to affect the immune response against *Borrelia*[27]. TMEM16K is frequently found to be co-expressed with TMEM16A and TMEM16F, especially in neuronal and muscular tissues [23,29]. Furthermore, the *Drosophila* ortholog of TMEM16K, „Axs", has been found to play a role in spindle formation and cell cycle progression, mediating meiotic spindle assembly and chromosome segregation [30].

Calcium-dependent chloride secretion

CaCCs exhibit slow activation, voltage dependence, outward rectification of the steady-state current voltage relationship and an anion permeability sequence of $I^- > Cl^-$. CaCCs are activated by an increase in intracellular Ca^{2+} released from the endoplasmic reticulum (ER)

Ca^{2+} store [31], and by Ca^{2+} entering the cell through store- or receptor-operated ion channels [32]. CaCCs are abundantly expressed in most eukaryotic cells and are associated with many physiological functions, such as epithelial fluid secretion, sensory transduction, control of neuronal and cardiac excitability, regulation of smooth muscle contraction and nociception. In addition, cell proliferation, phospholipid scrambling, and regulation of cell death is affected by TMEM16. The intestinal epithelium secretes Cl^- transiently upon stimulation with carbachol, histamine, and nucleotides, due to transient activation of TMEM16A [33-35]. TMEM16A is predominantly expressed in mouse ileal and colonic epithelium. Ca^{2+}-activated Cl^- transport was found to be absent in tracheal [36] and colonic epithelium [37], as well as hepatocytes and acinar cells from pancreatic and salivary glands of TMEM16A null mice [1,9]. In the renal tubular epithelium, the function of Ca^{2+}-activated chloride channels is to maintain fluid and electrolyte transport as well as acid-base balance [38]. In human or mouse kidney, TMEM16A is mainly expressed in proximal tubular epithelial (PTE) cells, in podocytes, intercalated cells of collecting ducts and in the primary cilium of renal epithelial cells [38,39]. Thus, TMEM16A is important for growth of the primary cilium [39,40]. Faria *et al.* showed that lack of renal TMEM16A leads to proteinuria and accumulation of numerous large reabsorption vesicles in PTE cells [38]. TMEM16A currents were activated by intracellular acidic pH, probably in order to support H^+ secretion by the Vacuolar-type H^+-ATPase (V-ATPase) [38]. In TMEM16A-kidney specific knockout mice, proximal tubular proton secretion was decreased along with endosomal acidification. This caused a defect in proximal tubular albumin reabsorption. Taken together, these results point out that renal TMEM16A has a role in proximal tubular proton secretion and protein reabsorption.

TMEM16A has also been suggested to contribute to apical Cl^- secretion in renal cysts in polycystic kidney disease [41-43]. Later it was shown that TMEM16A has pro-proliferative function in the cyst lining epithelium [44,45]. In mice, tubular-specific knockout of TMEM16A caused reduced numbers of nephrons, albuminuria and tubular damage [46]. Regarding TMEM16F, it was found to contribute to volume-regulated Cl^- currents and cellular volume regulation [13,47]. In fact, upon high intracellular calcium TMEM16F is activated, leading to a decrease in cell volume due to Cl^- loss and water efflux. Recent studies showed that reactive oxygen species (ROS) also activate TMEM16F [48]. TMEM16F missense mutations have been reported in patients with Scott syndrome, a rare congenital bleeding disorder caused by a defect in platelet aggregation required for blood coagulation [12,49].

Crosstalk between TMEM16A and CFTR

Cystic Fibrosis Transmembrane Conductance Regulator (CFTR) is a Cl^- channel that is regulated by cAMP, produced and inactivated by adenylate cyclase and phosphodiesterase, respectively [50]. It is expressed in the apical membrane of epithelial cells of many organs,

including airways, intestine and kidney. Interestingly, it controls the function of other ion channels such as epithelial sodium channels (ENaC) [51,52], outwardly rectifying Cl^- channels (ORCC) [53] and CaCCs [54]. Mutations in CFTR cause cystic fibrosis (CF), the most common severe autosomal recessive disease among Caucasians. It is characterized by reduced Cl^- and bicarbonate secretion in airways, pancreas, and intestine. This leads to formation of a thick and sticky mucus and a compromised local barrier defense, resulting in frequent airways infections [55]. Protein kinase A (PKA) activated by cAMP phosphorylates CFTR at a number of serine residues in the so-called regulatory (R) domain, which is accompanied by ATP-binding to the cytoplasmic nucleotide-binding domains (NBD). Both modifications lead to a conformational change and opening of the CFTR channel [56,57]. In addition, CFTR is also Ca^{2+}-regulated, as outlined below. In contrast to CFTR, TMEM16A supports Cl^- secretion indirectly by facilitating intracellular Ca^{2+} signaling required for the activation of basolateral K^+ channels and for activation of luminal CFTR [36,37,58] (Fig. 1.3). Due to this regulation, Ca^{2+}-activated Cl^- secretion significantly occurs through TMEM16A-mediated activation of apical CFTR and basolateral SK4. Moreover, there is also a functional coupling of CFTR and TMEM16A through exchange protein directly activated by cAMP (EPAC1) and Ca^{2+}-sensitive adenylate cyclase type 1 (ADCY1) [59]. Purinergic stimulation of Ca^{2+} release from the ER not only activates TMEM16A but also stimulates ADCY1, which has a high relevance for production of cAMP. Activation of ADCYs by forskolin (Fsk) generates cAMP which activates not only CFTR, but also TMEM16A via EPAC1 and protein kinase C [36].

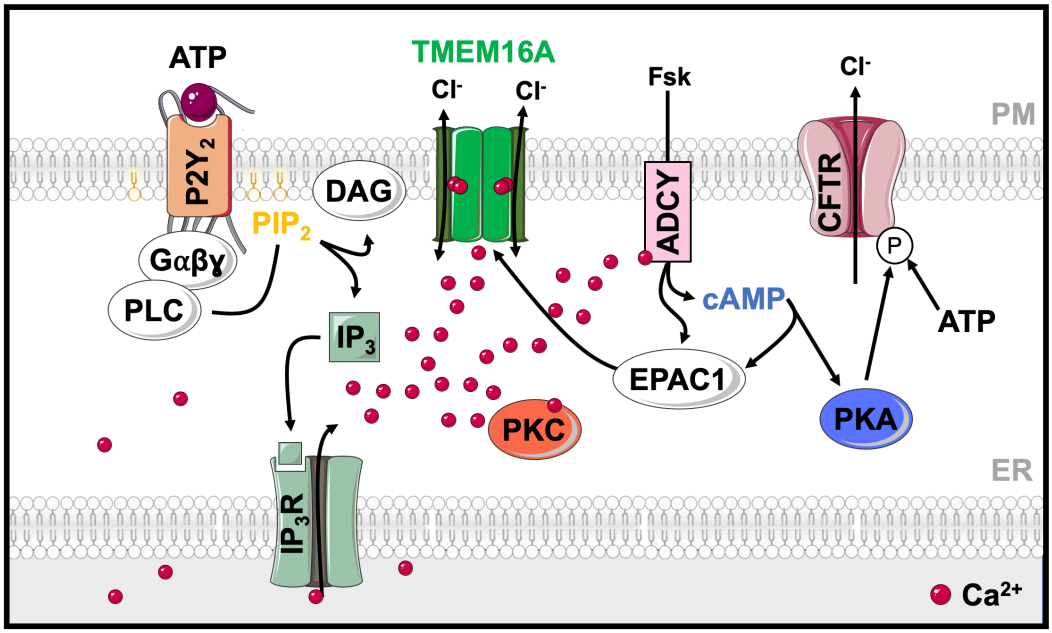

Figure 1.2 | *TMEM16A and CFTR are functionally related and interact through EPAC1 and ADCY1.* Purinergic stimulation increases Ca^{2+}, not only activating TMEM16A but also stimulating ADCY1, which produces cAMP. The intracellular messenger cAMP activates CFTR via protein PKA. Activation of ADCYs by forskolin generates cAMP and activates EPAC1, activating both CFTR and TMEM16A via EPAC1.

It is known that purinergic P2Y receptors are coupled to intracellular second messengers, like Ca^{2+} and cAMP [60]. Intracellular Ca^{2+} controls enzymes responsible for production and degradation of cAMP [61]. Ca^{2+} activates CFTR through inhibition of phosphatases and activation of protein kinase C (PKC) [58,62]. PKC dependent phosphorylation of CFTR enhances subsequent phosphorylation of the channel by PKA [63]. We can conclude that a functional crosstalk between cAMP-activated CFTR and Ca^{2+}-activated TMEM16A takes place [64]. This functional relationship between CFTR and TMEM16A may also occur in the kidney. In patients with ADPKD this may contribute to Cl^- secretion and cyst development.

Cellular Ca^{2+} signaling

Intracellular Ca^{2+} ions regulate a large number of cellular properties and functions. These processes include transcription, cell cycle regulation, differentiation, cell motility/migration, apoptotic cell death, muscle contraction/relaxation and neuronal excitability [65]. Cells are equipped with a sophisticated machinery to precisely control intracellular Ca^{2+} signals, mostly in a spatial and time-dependent manner. Under resting conditions, cells maintain a $[Ca^{2+}]_i$ of ~10^{-7} M, while the extracellular free Ca^{2+} concentration is around 1.2 mM and thus 10.000 times higher. Stimulation of cells, for example by excitation-induced depolarization, mechanical deformation or hormonal activation, increases the cytosolic Ca^{2+} concentration up to 1-2 µM [65]. However, in subcellular compartments the cytosolic Ca^{2+} concentration may reach much higher values. Precise regulation of intracellular Ca^{2+} concentrations requires a sophisticated machinery, consisting of various types of Ca^{2+} stores such as the ER, acidic endolysosomal stores, and mitochondria, along with a number of transport proteins such as Ca^{2+}-permeable ion channels, Ca^{2+} pumps and the Na^+/Ca^{2+} exchanger (Fig. 1.2). Ca^{2+} signaling is triggered by hormonal or electrical stimuli, which generate Ca^{2+}-mobilizing signals to release Ca^{2+} from internal stores and activate Ca^{2+} influx. Inositol-1,4,5-triphosphate receptors (IP_3R) and ryanodine receptors (RyR) are Ca^{2+} release channels that allow exit of Ca^{2+} from the ER or from the sarcoplasmic reticulum (SR) in muscle cells. RyR are activated by entry of extracellular Ca^{2+} upon depolarization of the plasma membrane, a process called Ca^{2+}-induced Ca^{2+} release, or by direct interaction of L-type Ca^{2+} channels with RyR. In contrast, IP_3R are activated by inositol-1,4,5-triphosphate (IP_3) [66]. When agonists bind to G-protein-coupled receptors (GPCR), like adenosine triphosphate (ATP) binding to purinergic receptors ($P2Y_2$), or acetylcholine (ACh) binding to muscarinic acetylcholine receptors (M1-5) [67], heterotrimeric G protein alpha subunits (Gα) bind to phospholipase C (PLC). PLC activation results in cleavage of phosphatidylinositol 4,5-bisphosphate (PIP_2) into IP_3 and diacylglycerol (DAG). IP_3 binding to IP_3R triggers release of Ca^{2+} from the ER into the cytoplasm [68].

There are different types of plasma membrane channels which allow increase of intracellular Ca^{2+} by entry of Ca^{2+} from the extracellular space. We can discriminate voltage-operated (VOCC) Ca^{2+} channels from receptor-operated (ROCC) and store-operated (SOCC) Ca^{2+} channels[65]. Store-operated Ca^{2+} entry (SOCE) results from depletion of Ca^{2+} within the ER. This, in turn, activates Ca^{2+} channels in the plasma membrane such as calcium release-activated calcium channel protein 1 (Orai1) and transient receptor potential (TRP) channels. Orai1 interacts with stromal-interacting molecule 1 (STIM1), which is the ER Ca^{2+} sensor, leading to opening of the plasma membrane Ca^{2+} channel [69]. After increasing cytosolic Ca^{2+}, its concentration rapidly returns to basal levels due to Ca^{2+} pumps and Na^{+}/Ca^{2+}-exchangers. While Na^{+}/Ca^{2+} exchangers and plasma membrane Ca^{2+} ATPases (PMCA) transport Ca^{2+} out of the cell into the extracellular space, the sarco-endoplasmic reticulum Ca^{2+} ATPase (SERCA) pumps Ca^{2+} back into the ER [70,71].

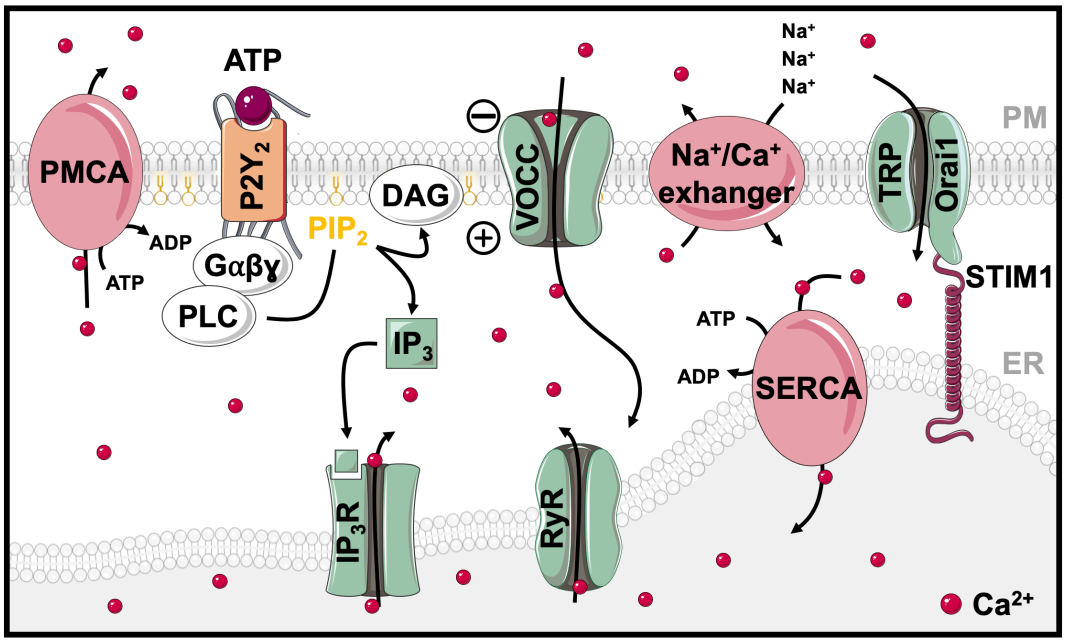

Figure 1.3 | *Elements of the Ca^{2+} signaling toolkit.*

Cells possess an extensive Ca^{2+} signaling toolkit, shown above are some examples relevant to the present project.

Modulation of Calcium signaling by TMEM16 proteins

Several studies suggest that TMEM16 proteins affect intracellular Ca^{2+} signaling, either by operating as Ca^{2+} channels or by controlling Ca^{2+} release from intracellular ER stores [14,37,38,72]. Schreiber *et al.* showed that TMEM16A supports mouse intestinal Cl^- secretion by three possible mechanisms [37]: (1) TMEM16A may be localized in the ER and facilitate Ca^{2+} release through IP_3R, by operating as counterion channels; (2) TMEM16A may control Ca^{2+} influx by operating as a plasma membrane localized Cl^- bypass channel; (3) TMEM16A may tether the ER to the PM thereby enhancing local sub-membranous Ca^{2+} signaling. In case of intestinal epithelial TMEM16A, its predominant basolateral location will enhance

predominantly basolateral Ca^{2+} signals to facilitate activation of basolateral Ca^{2+}-activated potassium (K^+) channels. Activation of basolateral K^+ channels provides the driving force for apical Cl^- secretion by CFTR. Moreover, apical TMEM16A may contribute to activation of CFTR by increasing local Ca^{2+} concentrations, leading to Ca^{2+}-dependent inhibition of protein phosphatases, Ca^{2+}-dependent activation of protein kinase C (PKC), and stimulation of ADCY1 [37]. Similarly, overexpression of TMEM16K resulted in upregulated intracellular Ca^{2+} signaling which supports the function of volume-regulated Cl^- channels [11,27]. The *Drosophila melanogaster* ortholog of TMEM16H/K (Aberrant X segregation "Axs"), is an intracellular transmembrane protein located in the ER that was also shown to affect cytosolic Ca^{2+} signals [73,74]. This suggests that Axs and TMEM16K may share similar properties [27]. Remarkably, mutations in TMEM16K lead to impaired Ca^{2+} signaling in Purkinje cells [23,25,26,75]. These properties of TMEM16K explain why tissue specific knockout of TMEM16K in intestinal epithelial cells leads to a compromised Ca^{2+}-dependent intestinal Cl^- secretion [37].

TMEM16A as tethering protein in lipid rafts

The yeast protein Ist2, a TMEM16A homologue, was described as tethering protein that maintains PM–ER junctions. Due to this property intracellular signaling components associate with the plasma membrane and are concentrated in lipid rafts. Lipid rafts are plasma membrane structures that are known as platforms for cellular signaling [76,77]. Ist2 is located in the ER membrane extending its C-terminus to the cytosol. A poly-basic domain at the end of the Ist2 C-terminus acts as an anchor that attaches to the PM, forming a junction with the ER. Among the anoctamins, TMEM16K shows the highest degree of homology with Ist2. Jin *et al.* reported a similar role of TMEM16A in small nociceptive dorsal root ganglia neurons [78,79]. According to their findings, TMEM16A is part of a signaling complex that also harbors GPCRs. They showed that TMEM16A is selectively activated by GPCR-induced release of Ca^{2+} from ER stores, but not by Ca^{2+} influx through voltage-gated Ca^{2+} channels. Selective Ca^{2+} signaling is accomplished by direct interaction of TMEM16A with IP_3R. Moreover, TMEM16A was found to interact with ERLIN1, a protein found in the ER and in lipid rafts, that associates dynamically with IP_3R. Taken together, these results along with other recent findings concerning the role of TMEM16A in neuronal ganglia [80], validate the role of TMEM16A in cellular Ca^{2+} signaling [80].

Modulation of Exocytosis by TMEM16 proteins

Exocytosis of intracellular vesicles is due to fusion of the vesicular membrane with the plasma membrane. This leads to release of the vesicular content into the extracellular space, which regulates various biological events such as neurotransmission, hormonal regulation, and inflammation. Moreover, exocytosis also delivers proteins and lipids to the plasma membrane, and is required for cell repair, growth, migration, and regulation of cell signaling

[81-85]. During exocytosis two membrane lipid bilayers merge into one by shielding the negative charge on the bilayer surface, thus diminishing the electrostatic repulsion force which overcomes the hydration barrier [86]. TMEM16F-mediated lipid scrambling was shown to support membrane trafficking in several cell types. For example, TMEM16F is involved in microvesicular release from platelets and neutrophils [87]. Human and mouse cells lacking expression of TMEM16F demonstrate a defect in generation of microvesicles [88,89,49,87,90]. These are a subset of extracellular vesicles (EVs) that are also referred to as "microparticles" or "ectosomes". They shed from the plasma membrane in a Ca^{2+}-dependent manner [91,92]. Mice lacking expression of TMEM16F also show deficits in bone development [93], a process that requires release of microvesicles from osteoblasts [94]. In macrophages, TMEM16F is necessary for phagocytosis stimulated by the purinergic receptor $P2X_7$ [16], while microglia lacking TMEM16F show defects in branch motility and phagocytosis [95]. Moreover, TMEM16F-dependent release of EVs have also been implicated in the anti-inflammatory properties of neutrophils during joint inflammation [87]. This vesiculation depends on TMEM16F-mediated lipid scrambling as vesicle formation begins after initiation of phosphatidylserine (PS) exposure [96].

A study conducted by Bricogne *et al.* provided initial evidence that TMEM16F-dependent plasma membrane expansion leads to extensive shedding of plasma membrane vesicles and production of ectosomes [97]. Moreover, TMEM16F-null erythrocytes do not produce vesicles in response to intracellular Ca^{2+} signal [98]. TMEM16F requires very high intracellular Ca^{2+} concentrations for its activation [14,18]. Membrane trafficking triggered by high Ca^{2+} levels occur during the repair of the plasma membrane. Thus, an important function of TMEM16F and Ca^{2+}-stimulated exocytosis could be repair of the plasma membrane. Repair of the plasma membrane occurs physiologically in skeletal muscle due to ongoing mechanical stress [99]. Notably, deficiency in TMEM16E, a close paralog of TMEM16F, causes muscular dystrophy that is caused by defective membrane fusion and repair [100]. It remains to be established whether TMEM16F is equally involved in membrane repair in other cell types.

A novel function of TMEM16 proteins for mucus secretion

Organs such as airways, stomach and intestine are covered by a mucus layer. In the stomach and colon, mucus is composed of two layers, an adherent layer that is impermeable to bacteria, and a non-adherent layer which traps bacteria [101,102]. Similarly, in the airway mucus forms a barrier against bacteria, traps inhaled particles and prevents dehydration [103]. Mucus is produced and secreted by specialized cells, called goblet cells. They acquired their name from their characteristic "wine glass goblet" shape, which is created by mucin granules accumulating in the apical region. The major component of intestinal mucus is the mucin MUC2 [104,105], while the lungs produce MUC5AC and MUC5AB [103]. MUCs are heavily

glycosylated large proteins that reach very high molecular weights and provide mucus with its elastic and gel-forming properties. Mucins consist of oligosaccharide chains, linked to a protein backbone with a high number of threonine/serine and proline-rich tandem repeats (TRs). The protein backbone of the mucins determines the class to which they belong [103]. Mucins are synthesized and densely packed intracellularly in secretory vesicles of goblet cells [106]. This condensed form is achieved due to the low vesicular pH and high calcium content [107]. Upon exocytosis, the dense mucins expand more than 1000-fold. This process depends on HCO_3^-, required for precipitation of Ca^{2+}, and an increase in pH [108,109]. The negative core of mucins is then exposed and will force the compacted mucins into open, soluble and easily transportable strings [107,108].

In the early steps of exocytosis, the GTPase Rab3/27 localizes to secretory granules (SG) membranes and binds to myosin V via the anchoring protein melanophilin, thereby allowing the granule transition from microtubules to the cortical actin network [110-112]. Upon stimulation of secretion, myristoylated alanine-rich C kinase substrate (MARCKS) binds to the mucin granules together with the Vesicle-associated membrane protein 8 (VAMP8) and the Cysteine String Protein (CSP) [113,114]. This interaction helps to position granules for secretion, from microtubules-kinesin-dependent to actin-myosin-dependent transport at the cell periphery [115]. Consecutively, the SGs are tethered and docked to the plasma membrane via interaction of the soluble N-ethylmaleimide sensitive factor attachment receptor (SNARE) proteins that are present on secretory vesicles (v-SNAREs, such as VAMP8) and their target membranes (t-SNAREs, such as Syntaxin and SNAP-23). The v- and t-SNAREs contain-helical domains that interact to form a tightly coiled four-helix bundle (the core complex) that brings together the opposing membranes [81,116]. In addition, this event requires accessory components, such as the Munc proteins. In particular Munc18 and Munc13-2/4 promote the interaction of the core complex and syntaxins [81]. Munc18 opens the Syntaxin structure and permits its interaction with the SNARE proteins. Munc13-2/4 interacts with Syntaxin in close proximity with Munc18 and dissociates their binding, thus allowing the assembly of the core complex [81,117].

Secretion of mucins can take place in at least two ways, as constitutive secretion or as compound exocytosis. Both events are Ca^{2+}-dependent, following agonistic stimulation of P2Y purinoceptor 2 ($P2Y_2$) receptors (via ATP or UTP), A3 adenosine receptors, muscarinic receptors (via carbachol or muscarinic acetylcholine) or protease-activated receptors [118]. Constitutive exocytosis results from low-level stimulation of $P2Y_2$ and A3 adenosine receptors, due to paracrine release of ATP and adenosine. This process includes the fusion of single vesicles with the plasma membrane, mediated by typical exocytic proteins like syntaxins, munc18, VAMP, and SNAP proteins [119]. On the other hand, high levels of these

ligands or cholinergic agonists as well as inflammatory mediators lead to a dramatic form of mucus secretion, called compound exocytosis [120]. Ca^{2+} signaling is involved in both the maturation of the vesicles prior to fusion [121] and in the fusion of the secretory vesicles with the plasma membrane [122] (Fig. 1.4).

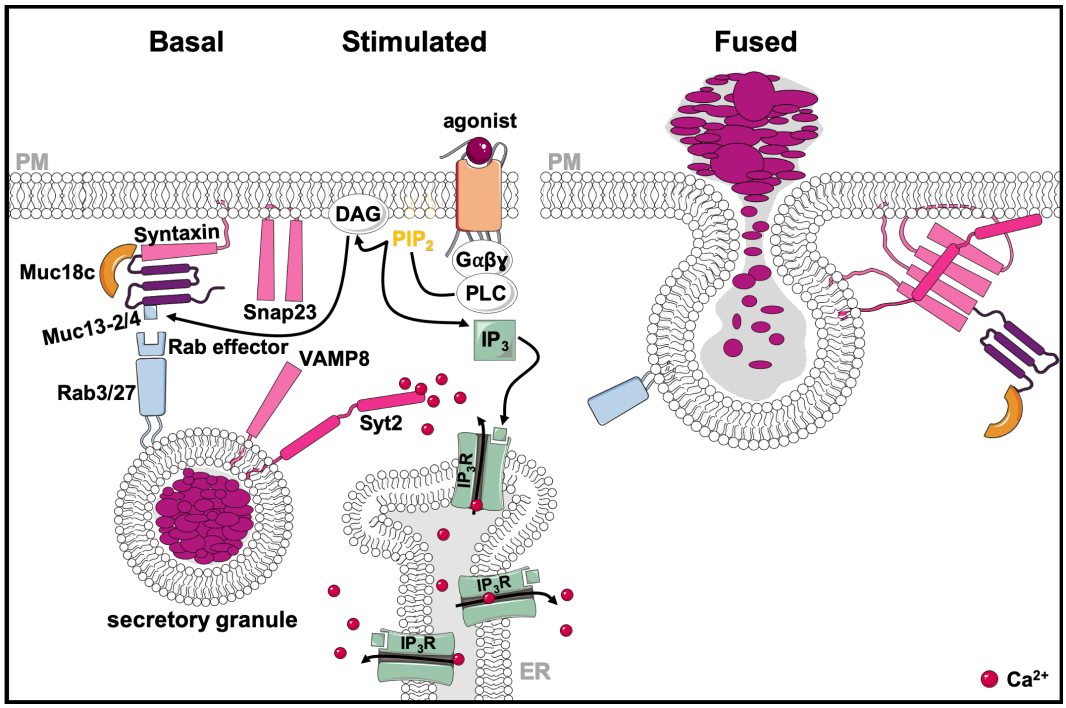

Figure 1.4 | *Regulated mucin secretion.*

Left In the basal state, mucin granules become tethered to the plasma membrane by Rab proteins and effectors that have not yet been identified. They exist in the vicinity of components of the exocytic machinery. **Center** Activation of heptahelical receptors such as those for ATP ($P2Y_2$), leads to activation of Gαβγ, and PLC, resulting in generation of the second messengers DAG and IP_3. DAG activates the priming protein Munc13-2/4, and IP_3 induces the release of Ca^{2+} from apical ER to activate Synaptotagmin-2 (Syt2). Munc13-2/4 also participates in granule priming, and an unknown high affinity calcium sensor likely functions in basal secretion rather than Syt2. **Right** Activation of the regulatory Munc13-2/4 and Syt2 proteins leads to full coiling of the SNARE proteins to induce fusion of the granule and plasma membranes. The interactions of the SNARE proteins take place on a scaffold provided by Munc18c. Exocytic syntaxins contain four hydrophobic coiled-coil domains that must be opened to initiate secretion (left panel), and during fusion the associated Munc18c protein remains associated only by an interaction at the Syntaxin N-terminus (right panel).

In small intestine of CF patients lacking functional CFTR channel [108], mucins remain anchored as levels of local bicarbonate is insufficient to remove calcium ions from the mucins to allow MUC2 unfolding [123]. The immune modulator prostaglandin E2 (PGE_2) has been shown to induce both fluid and bicarbonate secretion in the human colon [124]. In mice and humans, a non-functional CFTR channel causes bacterial overgrowth, distal intestinal obstruction syndrome (DIOS) and sometimes meconium ileus. New insights in mucin

production and exocytosis could improve our efforts to reduce overproduction and hypersecretion of mucins in many diseases in the future. TMEM16A is expressed in intestinal goblet cells. Studies on intestinal goblet cells lacking expression of TMEM16A demonstrated a direct role for TMEM16A in exocytosis and mucus release (Fig. 1.5). We observed in an intestinal-specific TMEM16A knockout mouse enhanced intracellular mucus content in goblet cells [125]. This mucus accumulation suggested a defect in mucus secretion. TMEM16A is also found in mucus producing cells of airways. TMEM16A is strongly upregulated under inflammatory conditions such as CF and asthma [125-130]. Under normal conditions, mucins are continuously synthesized and released from goblet cells. In contrast, the airway-specific knockout for TMEM16A led to accumulation of mucus in goblet cells [125].

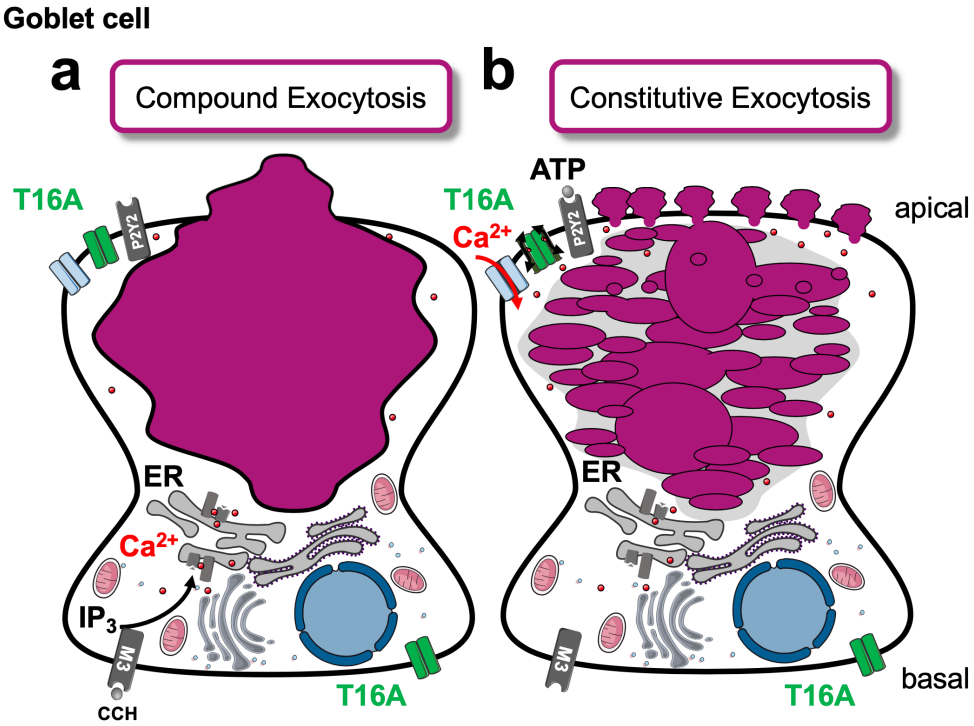

Figure 1.5 | *TMEM16A mediates ATP-dependent constitutive exocytosis at the apical pole of goblet cells.*

a Colinergic (carbachol; CCH) mediated compound exocytosis occurs independently of TMEM16A from the basolateral side, while **b** purinergic (ATP) constitutive exocytosis of mucus in single granules on the apical side is mediated by TMEM16A-localized Ca^{2+} increase.

Increase in Cellular Proliferation via TMEM16 proteins

Changes in $[Ca^{2+}]_i$ are associated with progression through the cell cycle. Both extracellular [131,132] and intracellular Ca^{2+} signals [133] are required for cell proliferation. Ca^{2+} acts both as ubiquitous allosteric activator and inhibitor of intracellular enzymes in the cytosol, organelles, and nucleus. The best known Ca^{2+}-binding protein is calmodulin (CaM). The complex Ca^{2+}/calmodulin regulates numerous intracellular enzymes including phosphodiesterases, adenylyl cyclases, ion channels, protein kinases, and protein phosphatases (i.e., calcium-

calmodulin dependent kinase type II (CaMKII) and the CaM-dependent phosphatase calcineurin). The G1/S transition, the progression from G2 to M and the metaphase/anaphase transition are specific points of intervention of CaMKII [134,135]. Activated CaM-kinase promotes phosphorylation of proteins, such as Ras (a cytosolic Ca^{2+} responsive transcription factor) and Ca^{2+}/cAMP response element (CRE) binding protein (CREB, a nuclear Ca^{2+}- responsive transcription factor), that are required for initiating and maintaining the cell cycle [136]. Additionally, CaM-kinase and calcineurin-regulating nuclear factors are involved in the DNA division machinery, such as cyclin-dependent kinases (cdk4) and cyclins (cyclin D1) [134,135].

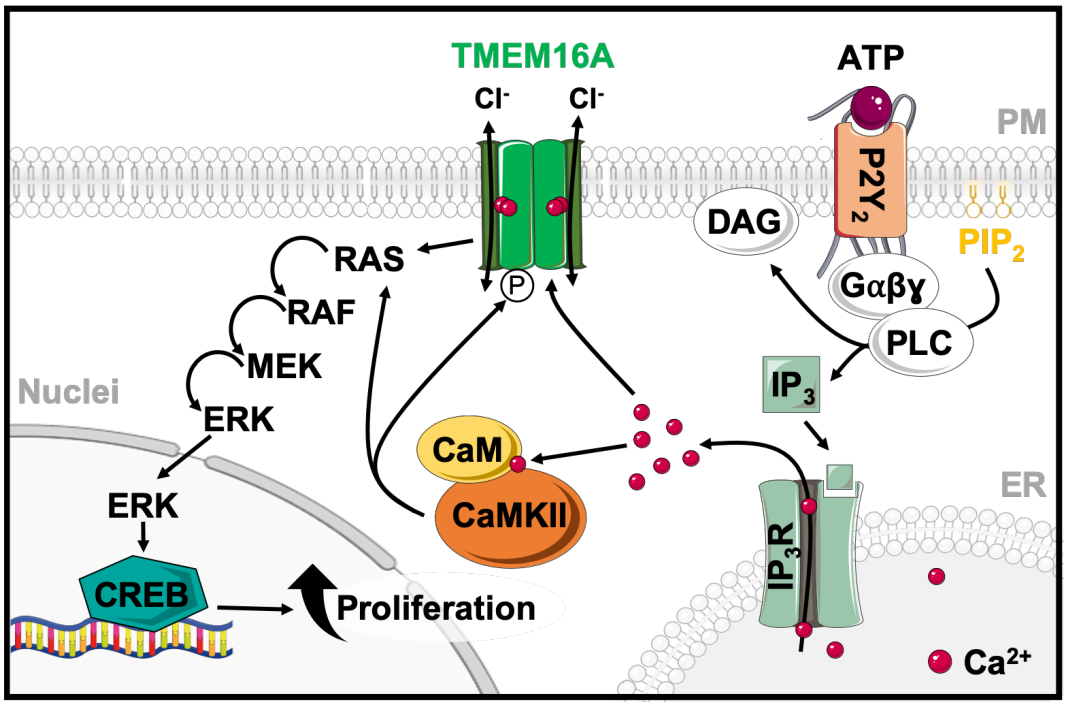

Figure 1.6 | *Proposed schematic representation of TMEM16A and CaMKII proliferative activity.*

As intracellular Ca^{2+} levels rise, TMEM16A is activated by Ca^{2+} and modulated by phosphorylation involving CaMKII. TMEM16A and CaMKII activate RAS-RAF-MEK-ERK pathway, which promotes the expression of genes for cell proliferation.

The function of TMEM16A as a regulator of proliferation and cancer growth is well known [137,138]. Upregulation of TMEM16A was also found in polycystic kidney disease [44]. TMEM16A is known to activate the RAS-RAF-MEK-ERK pathway [139]. Moreover, CaMKII is reported to regulate Ca^{2+}-activated Cl^- currents in rabbit arterial and portal vein smooth muscle cells [140]. Wang *et al*. [141] found that inhibiting CaMKII activity can lead to an increase of CaCC currents in basal smooth muscle cells (BASMCs) of the angiotensin II-induced hypertensive rats. This promotes proliferation of BASMCs and contributes to cerebral vascular remodeling. These and other data suggest that TMEM16A is modulated by CAMKII, thereby participating in cell proliferation (Fig. 1.6). Apart from TMEM16A, other members of the anoctamin family have also been implicated in regulation of cell proliferation and cancer development, like TMEM16E (ANO5), TMEM16G (ANO7) and TMEM16J (ANO9) [142]. TMEM16E is now known

for its role in myoblast proliferation and muscle repair [143,144]. Similar to TMEM16E, TMEM16F was reported to control myoblast proliferation [145]. TMEM16G was shown to be a marker for prostate cancer [146,147]. For TMEM16J an inverse correlation of expression and progression of colorectal cancer was described [148], while it may also promote pancreatic cancer [149].

AUTOSOMAL DOMINANT POLYCYSTIC KIDNEY DISEASE

Polycystic kidney diseases (PKDs) comprise a number of inherited disorders in which renal tubules become structurally and functionally abnormal, resulting in kidney cyst development and growth [150]. The most common form, autosomal dominant polycystic kidney disease (ADPKD), affects 1 in 400-1000 individuals and is characterized by an acute and bilateral development of multiple renal cysts over time. This disease results in the displacement and destruction of the adjacent renal parenchyma, progressive organ enlargement and, ultimately, loss of renal function, being the cause of 10% of end-stage renal disease (ESRD) cases worldwide, which demands renal replacement therapy [151,152]. Extrarenal manifestations also comprise cysts in other epithelial organs including the liver and pancreas [153].

ADPKD is a genetically heterogeneous disease caused by a germline mutation in one of two genes: Polycystic Kidney disease 1 (PKD1) or Polycystic Kidney disease 2 (PKD2) [154,155]. Mutations in PKD1 (located on chromosome 16p13.3) lead to cysts development in 85% of the patients and cause a more serious clinical progression. The remaining 15% of the cases are due to PKD2 mutations (located on chromosome 4q 21-23) [156] and present a milder phenotype with later onset, longer renal survival and fewer complications [157]. Even though ADPKD is a dominant disease, it behaves recessively at the cellular level. The human kidney is constituted of approximately a million nephrons. Nevertheless, microdissection studies indicated that cysts in ADPKD patients arise from about 1000 nephrons [158]. All cells from the patient possess a germline mutation in either *PKD1* or *PKD2* but not all develop cysts, which indicates that the germline mutation alone cannot cause cystogenesis. A second-hit model was proposed to explain this phenomenon. This model states that every cyst emerges as a product of an individual somatic mutation event in addition to the germline mutation in either PKD1 or PKD2 alleles, leading to total loss of function of the polycystins [159,160]. This hypothesis can explain the slow advance of the pathology over several decades. Recent studies show that late inactivation of the Pkd1 gene in adult mice kidneys resulted in a slow onset of cystogenesis [156,161,162]. The authors reported that the slow onset of the disease could not be explained by the previous hypothesis and suggested a third hit theory. This hypothesis states that a cell is not necessarily cystogenic just by having a germline mutation (first hit) and a somatic inactivation of the second allele (second hit) [163,164], but by having an additional event that leads to cell proliferation and cyst growth (such as renal injury) [165]. Although

disease-causing mutations are known, the complex mechanisms of cyst development and cyst growth are still poorly understood [166,167].

Regulation of Calcium signaling by Polycystins

Polycystin-1 (PC1), encoded by the *PKD1* gene, is an integral membrane protein and is composed of eleven transmembrane domains, an extensive extracellular N-terminal domain, and a shorter C-terminal cytosolic domain [156]. The N-terminus of PC1 contains well-recognized motifs involved in protein-protein, protein-saccharide, and protein-ligand interactions. Thus, PC1 is generally thought to function as a cell surface receptor and it is critical for cell-cell or cell-matrix interactions [152,168-172]. It is mainly expressed in epithelial cells of developing and mature renal tubules. PC1 expression is regulated over time showing higher levels in foetal tissues and decreased presence in adult tissues [173]. PC1 is localized on the plasma membrane, adhesion complexes in polarized epithelial cells and on the primary cilium, a single hair-like organelle that protrudes from the surface of most mammalian cells, implicated in many cystic diseases [174,175].

Polycystin-2 (PC2) or TRPP2, encoded by the *PKD2* gene, is a membrane-associated protein that belongs to the TRP family [176]. It has 6 transmembrane domains, two EF-hands (characteristic of Ca^{2+} binding domains that allow the protein to sense changes in Ca^{2+}), an ER retention signal and cytoplasmic N- and C-terminal domains [155,177]. PC2 forms homotetramers in the absence of PC1 [178-180], which works as a nonselective cation channel with high affinity to Ca^{2+}, being also permeable to Na^{+} and K^{+} ions [181-184]. Although PC2 is found on the primary cilium and plasma membrane, where it mediates Ca^{2+} entry into the cytoplasm, most of its pool is located in intracellular compartments, such as the ER and the Golgi complex, acting as Ca^{2+} release channel[183,185]. PC2 regulates intracellular Ca^{2+} on the plasma membrane and primary cilium by interacting with other members of TRP superfamily, namely TRPC1 and TRPV4, to form an heteromeric channel [186-188].

The most significant partner of PC1 is PC2 [189], interacting through their C-terminal coiled-coil domains [152,169]. Biochemical and biophysical studies found that the PC1/PC2 complex contains one PC1 and three PC2 subunits [190-192]. Several studies suggested that PC1 and PC2 reciprocally affect the cellular location of each other, and defects in one of the proteins lead to a mislocalization of the other one, however the precise mechanism of this interdependence has not yet been elucidated [193]. It is thought that the PC1/PC2 interaction is critical for creation of a functional ion channel, yet, details remain unknown. It was shown that both PC1 and PC2 play a key role in intracellular Ca^{2+} homeostasis regulation, not only in the primary cilium, but also at the plasma membrane level and in intracellular compartments [194]. In the ER, polycystins are known to interact with the IP_3R [195,196]. PC2 can

enhance Ca^{2+} release from the ER by stimulating the activity of this receptor [197], whilst PC1 suppresses this mechanism by a decrease on PC2-IP_3R interaction involving STIM1 [198]. PC2 is also known to regulate the RyR [199]. Consequently, it has been suggested that both PC1 and PC2 might regulate Ca^{2+} signaling in different intracellular compartments, and their dysregulation is responsible for the activation of aberrant pathways present in ADPKD, such as the abnormal fluid secretion events. However, the precise nature of these regulatory events remains to be fully elucidated.

Lack of PKD2 may also affect mitochondrial dynamics [200]. Deficiency of PKD2 has been reported to be accompanied by changes in mitochondrial morphology and dynamics, with prolonged ER-mitochondria Ca^{2+} communication and increased Ca^{2+} mitochondrial uptake. As mentioned before, the so-called primary cilium is a single antenna-like protrusion of the plasma membrane containing receptors, ion channels and signal proteins [201]. PC1 and PC2 form a mechano- and/or chemosensory complex that transduces tubular stimuli to tubular epithelial cells [166]. Primary cilia also form a signaling platform during vertebrate development, including hedgehog signaling. This requires proper distribution of phosphatidylinositol phospholipids [202]. Mechanical, chemical and receptor-mediated signals increase intracellular Ca^{2+} within the cilium and possibly in the cytosol, although this is still a subject of discussion [203,204]. Nevertheless, primary cilia can be regarded as specialized Ca^{2+} signaling compartments, with PC1 and PC2 forming a receptor/Ca^{2+} influx-channels complex [205]. Notably, formation of the primary cilium is cell cycle-dependent, being disassembled upon re-entering the cycle [206,207]. There is an accumulation of TMEM16A, as well as TMEM16F and TMEM16K, in the primary cilium [39,208,209] and TMEM16A was suggested to be essential for its maintenance. Thus, TMEM16A and hedgehog signaling are simultaneously active during development and in cancer cells [210].

Cyst development as a consequence of enhanced proliferation and fluid secretion

Continuous dilation of the tubules through increased cell proliferation, defects in the extracellular matrix, transepithelial fluid secretion and, ultimately, separation from the parental tubule lead to the formation of cysts in ADPKD [211,212]. It is still unclear if cysts specifically arise from a determined nephron segment. Some studies report a generalized pattern [213]. Chloride secretion by renal collecting ducts is regulated by circulating hormones and paracrine factors binding to GPCRs and modulation of intracellular cAMP and Ca^{2+} levels. Arginine Vasopressin (AVP) is the central hormone involved in the regulation of plasma osmolality by modulating water permeability of the collecting duct. AVP binding to V2 receptors (V2R) on the distal nephron and collecting ducts stimulates the production of intracellular cAMP by activation of adenylyl cyclase 6 (AC6) [214,215]. In cystic epithelial cells, AVP maintains cAMP at elevated levels, activating pathways involved in cell proliferation

and chloride−dependent fluid secretion [216,217]. cAMP promotes the membrane insertion and activation of aquaporin-2 water channels to the apical membrane, leading to increased water absorption. AVP has also been shown to stimulate Cl^- secretion through cAMP-dependent protein-kinase A (PKA) phosphorylation and activation of CFTR Cl^- channels and subsequent increase in sodium–potassium–chloride cotransporter (NKCC1) activity [218-222]. AVP can also induce the release of autocrine factors by collecting duct cells, including ATP [223] and prostaglandin E2 (PGE2), which may further augment Cl^- secretion.

ATP leads to the stimulation of Cl^- secretion via apically localized CaCCs in collecting duct cells [224-226]. Inhibition of purinergic receptors by suramin abrogates this ATP-mediated rise in intracellular Ca^{2+} and CaCC activation [226-228]. ATP has also been shown to augment fluid secretion induced by cAMP in three-dimensional “cyst” models of Madin-Darby Canine Kidney (MDCK) cells [229]. Knockdown of TMEM16A decreased ATP-induced Cl^- secretion in M1 cells, despite an elevation in intracellular Ca^{2+} levels [228]. Inhibition or knock-down of TMEM16A, reduced fluid secretion and cyst-growth in MDCK cysts, as well as mouse metanephric kidneys treated with forskolin *in vitro* [44]. Furthermore, ATP and β2-AR agonists contribute to Cl^- secretion by ADPKD cells [230,231]. Prostaglandin E2 (PGE2) is a paracrine factor produced by collecting duct cells in response to ATP activation of $P2Y_2$ receptors [232,233]. PGE2 inhibits aldosterone induced, ENaC-mediated Na^+ reabsorption within the renal medulla [234]. Moreover, it activates cAMP-induced Cl^- secretion [220,235-237] and causes PKA activation and stimulation of Cl^- secretion via CaCC [237]. Remarkably, part of the PGE2 activation of CFTR seemed to be modulated by an increase in intracellular Ca^{2+}, dependent in CaCC-mediated currents [237]. In PKD1-deficient inner medullary collecting duct (IMCD) cells, PGE2 was shown to induce Cl^- secretion to a greater level, compared to wild-type cells [43].

As mentioned above, one of the major causes of the cystic fluid secretion is the apical Cl^- transport stimulated by cyclic adenosine monophosphate (cAMP) [219,238,239]. In ADPKD, cAMP activates apical CFTR Cl^- channels and the subsequent Cl^- efflux from the cell that causes indirect activation of basolateral NKCC1, driving Cl^- entry [216,218]. cAMP enhancers increase fluid secretion towards the cyst lumen therefore increasing its electronegativity [216]. Comparisons between cystic epithelium and other secretory epithelia, in conjunction with the use of CFTR specific inhibitors, suggest that CFTR could be responsible for the cAMP-stimulated Cl^- secretion in ADPKD. Indeed, inhibition of CFTR prevents cAMP-dependent anion secretion across human ADPKD cell monolayers [240], slowed cyst-like dilations in embryonic kidneys [241] and delayed disease progression in PKD mice [242]. Correctors of CFTR also seem to decrease the cysts in mouse PKD models [243]. Several studies have reported CFTR expression in all tubular segments of the human kidney [244,245]. Moreover, cultures of ADPKD primary cells and ADPKD kidneys have also shown expression of this protein within

the apical membrane [246]. It is remarkable that some CFTR mutations result in a less severe form of ADPK and liver disease [247], while others do not improve the phenotype [248].

However, other Cl^- channels might also be involved in fluid secretion [229,243]. CFTR activity requires a functional interaction with TMEM16A [36]. Buchholz and colleagues demonstrated that formation of cysts by MDCK cells depends on the synergy of cAMP- and ATP, i.e. Ca^{2+}-mediated fluid secretion [229]. There is good evidence that TMEM16A plays a critical role in cyst formation [44,249]. Studies have shown that nephron segments can release ATP into the lumen, which leads to autocrine and paracrine signaling via the purinergic receptors expressed in the apical membrane of these cells [250]. Cyst enlargement occurs through ATP-binding to $P2Y_2$ receptors, which activates TMEM16A [41,42,251]. TMEM16A is also upregulated and appears to be responsible for glucose-induced cyst growth [252]. In contrast, TMEM16F is highly expressed in apoptotic cyst epithelial cells of human polycystic kidneys and is required to form a cyst lumen [209]. Water channels were suggested to play a role in ADPKD impaired fluid transport [253]. Aquaporins (AQP) constitute the molecular pore for water transport in the cell membrane [254]. Most of the cysts express either Aquaporin-1 (AQP1) or Aquaporin-2 (AQP2) [255]. These two proteins are located on the proximal tubules and principal cells of the collecting ducts, respectively [256]. Thus, the type of AQP expressed in each cyst may shed a light towards its origin. In response to the osmotic gradient (driven by the upregulated Cl^- secretion as explained below) water moves across the apical side of the epithelium towards the cystic lumen, where it accumulates, leading to cyst enlargement [257].

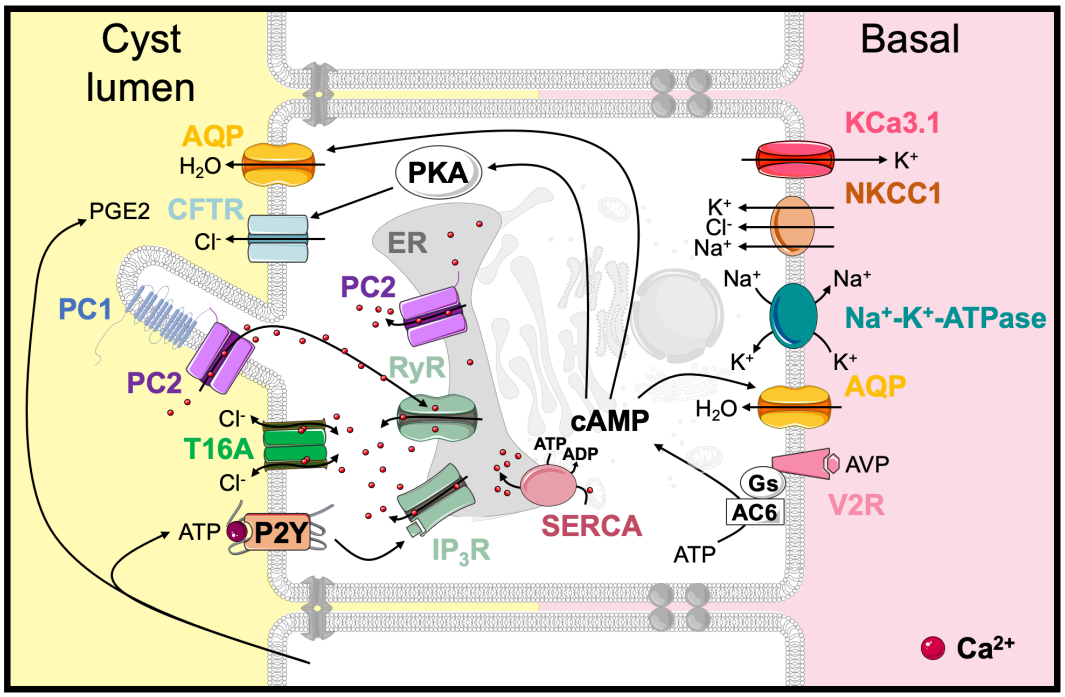

Figure 1.7 | *Model of the mechanisms involved in fluid accumulation in ADPKD.*

Several transporters and channels are implicated in fluid accumulation in ADPKD cysts. Apical

transepithelial Cl^- secretion through cAMP-stimulation (CFTR) and ATP-stimulation (TMEM16A), is supported by the basolateral cotransporter NKCC1, which requires basolateral K^+ (via KCa3.1) and Na^+ (via Na^+-K^+-ATPase) recycling. CFTR is stimulated by increased cAMP concentrations and stimulation of VR2 pathway. Apical TMEM16A is stimulated by an autocrine/paracrine purinergic signaling mediated by purinergic receptors. Net secretion of Cl^- drives Na^+ and water movement into the cyst facilitated by Aquaporins. The complex formed by PC1 and PC2 is involved in Ca^{2+} signaling, both in the primary cilium and intracellular stores.

Basolateral Cl^- uptake was shown to be an important event in cyst lining cells [258]. Bumetanide is a loop diuretic that specifically inhibits the NKCC1 and NKCC2 family of co-transporters (responsible for electroneutral transport of Na^+, K^+, and Cl^-) [259]. NKCC1 is expressed on the basolateral membrane of secreting epithelia [260] and several studies detected its expression on cystic cultured epithelial cells and kidneys [260,261]. Using bumetanide a reduction of luminal electronegativity and a decrease of fluid secretion were observed [258], meaning that this transporter may be an important pathway for basolateral Cl^- entrance into the cell [262]. The Na^+/K^+-ATPase and KCa3.1 work as functional partners of NKCC1 at the basolateral membrane, recycling Na^+ and K^+, respectively [263,264]. The Na^+/K^+-ATPase also plays a role in the formation of intracellular negative membrane potential, providing the electrochemical driving force for apical Cl^- secretion [264]. A better understanding of the players that promote cAMP- and Ca^{2+}-mediated Cl^- secretion will allow the development of targeted therapies to reduce fluid accumulation and proliferation levels within renal cysts (Fig. 1.7).

AIM OF THE STUDY

According to recent studies TMEM16 proteins seem to regulate calcium signaling. My project was focused on understanding this regulation and its mechanistic consequences. Therefore, the role of TMEM16 proteins as modulators of intracellular Ca^{2+} signaling was investigated which is outlined in Chapter 2. In Chapter 3, the effect of TMEM16K on local calcium signaling is shown to control various cellular functions that explain TMEM16K-linked genetic disorders. A novel therapeutic strategy for the treatment of CF lung and intestinal disease is proposed in Chapter 4, based on the FDA-approved drug and TMEM16A/F inhibitor, niclosamide. The work identified TMEM16A and TMEM16F as major players in membrane exocytosis and mucus production/secretion through calcium-dependent regulation. In Chapter 5, experiments were aimed to understand the function of TMEM16A in epithelial transport and proliferation during cyst formation *in vitro*. Using inducible and renal-specific $Pkd1^{-/-}$ knockout mice, the impact of TMEM16A on calcium signaling and cyst formation was verified in Chapter 6. In this chapter, a new therapeutic approach is presented. Using the FDA-approved drugs niclosamide and benzbromarone as potent TMEM16A inhibitors, I demonstrate that treatment of the renal-specific $Pkd1^{-/-}$ knockout mice with these compounds successfully reduces cyst development.

CHAPTER 2 | DIFFERENTIAL EFFECTS OF ANOCTAMINS ON INTRACELLULAR CALCIUM SIGNALS

Abstract

The Ca^{2+} activated Cl^- channel TMEM16A (Anoctamin 1 / ANO1) is homologous to yeast Ist2 and has been shown to tether the cortical endoplasmic reticulum (ER) to the plasma membrane. We therefore examined whether ANO1 and other members of the Anoctamin family affect intracellular Ca^{2+} signals. It is shown that expression of ANO1 augments Ca^{2+} store release upon stimulation of G-protein coupled receptors (GPCR), while knockdown of ANO1, or lack of Ano1 expression in $Ano1^{-/-}$ animals as shown in an earlier report, inhibits Ca^{2+} release. ANO 5, 6, 10 show similar effects, while expression of ANO4, 8, 9 attenuate filling of the ER store. The impact of ANO1 and ANO4 were examined in more detail. ANO1 colocalized and interacted with IP_3R, while ANO4 colocalized with SERCA Ca^{2+} pumps and interacted with ORAI1 channels, respectively. ANO1 chloride currents were rapidly activated exclusively through Ca^{2+} store release and remained untouched by influx of extracellular Ca^{2+}. In contrast expression of ANO4 caused a delayed activation of membrane localized ANO6 channels, solely through store operated Ca^{2+} entry (SOCE) via ORAI. Ca^{2+} signals were inhibited by knocking down expression of endogenous ANO1, 5, 6, 10, and were also reduced in epithelial cells from Ano10 null mice. The data suggest that anoctamins affect intracellular compartmentalized Ca^{2+} signals, which may explain some of the cellular defects related to Anoctamin mutations.

Keywords: TMEM16A, TMEM16D, TMEM16F, Anoctamin 1, Anoctamin 4, Anoctamin 6, Ca^{2+} signaling, Ca^{2+} store, store operated Ca^{2+} influx, SOCE, ORAI, SERCA

Published in: Inês Cabrita, Roberta Benedetto, Ana Fonseca, Podchanart Wanitchakool, Lalida Sirianant, Boris V. Skryabin, Laura K Schenk, Hermann Pavenstädt, Rainer Schreiber, Karl Kunzelmann. Differential effects of anoctamins on intracellular calcium signals. *Faseb j*. 2017 May;31(5): 2123-2134.
Own experimental contribution: Immunocytochemistry, Measurement of $[Ca^{2+}]_i$.

Own written contribution: Methods, Results.

Other contributions: Designed experiments and analyzed data.

Introduction

Anoctamins form phospholipid scramblases and ion channels [1,8,11,12,14,265]. They are expressed and functional in all types of tissues and have a central role in many different diseases [1]. ANO1 is essential for chloride transport in epithelial tissues, controls smooth muscles contraction and arterial blood pressure and has various functions in neuronal and sensory cells [1,266-269]. Many cellular functions of anoctamins, like effects on proliferation, tissue repair, bone mineralization and immunological processes are only poorly understood [27,39,100,139,270,271].

Recent studies suggest a role of anoctamins in controlling compartmentalized Ca^{2+} signals elicited by activation of G-protein coupled receptors (GPCRs): i) The yeast ANO1 homologue Ist2 tethers the endoplasmic reticulum (ER) to the plasma membrane, by means of anchoring in the ER membrane and binding of its polybasic C-terminus to the plasma membrane [272]. ii) In dorsal root ganglia, ANO1 has been shown to be activated exclusively by Ca^{2+} released from the ER. This is achieved by tethering of ANO1-containing plasma membrane to the ER membrane via ANO1/IP_3R interaction [78]. iii) Mid-range Ca2+ signaling requires coupling between store-operated Ca^{2+} entry (SOCE) and IP3-dependent store release [273]. iv) Freshly isolated intestinal crypt cells from mice lacking Ano1 expression demonstrated abrogated GPCR-triggered Ca^{2+} signals [37]. v) Anoctamin-homologous transmembrane channel-like protein 8 (TMC8, EVER2) controls GPCR-induced intracellular Ca^{2+} signaling [274]. Here we identified a differential role of anoctamins in GPCR-induced Ca^{2+} signaling: They affect Ca^{2+} release via IP_3R as well as the Ca^{2+} store content, possibly by operating as leakage channels or by controlling ORAI or the sarcoplasmic/endoplasmic reticulum Ca^{2+} ATPase (SERCA). These results may help to explain the ever growing number of anoctamin-related cellular defects and diseases.

Materials and Methods

Animals, cells, cDNA, RT-PCR, siRNA. Generation of animals with a floxed Ano10 allele has been described in an earlier report [37]. Tissue specific renal tubular knockout was achieved by crossbreeding $ANO10^{loxp/loxp}$ and $Pax8Cre^{+}$ or $Six2Cre^{+}$ mice. Offsprings were genotyped and tubular ANO10 knockout was verified by RT-PCR and Western blot analysis in isolated proximal tubular epithelial cells. All animal experiments were approved by the local ethics commission of the University of Regensburg and the University Münster, and were conducted according to the guidelines of the American Physiological Society and the German law for welfare of animals. For isolation of renal proximal tubular epithelial cells, kidneys were removed and kept in ice cold PAN, PO4-41250 medium. Cortices were cut off, cells were isolated using collagenase type 2 (Worthington, S9H11286) and passed through a sieve. After washing, centrifugation and resuspension, cells were run though a percoll gradient (45% percoll, 55% 2X PBS-Glucose). Cells were resuspended in media and kept

on ice until use.

HEK293 were grown in DMEM-F12 (GIBCO, Karlsruhe, Germany) supplemented with 10% fetal bovine serum at 37°C in the absence of antibiotics in a humidified atmosphere with 5% CO_2. HeLa cells were grown as described earlier [11]. For expression of anoctamins, cells were plated on fibronectin- and collagen-coated 18 cm diameter coverslips and co-transfected with cDNA encoding either hTMEM16A, D, E, F, G, H, J, K, or empty pcDNA3.1 vector (mock) along with $P2Y_2$ receptor and CD8.Transfected cells were detected by binding of anti-CD8 labelled beads. Construction of expression plasmids has been described earlier [3]. RT-PCR analyses were performed using standard conditions and appropriate primers as described earlier [3]. For s*emi-quantitative RT-PCR t*otal RNA (1 µg) was isolated from HeLa, reverse-transcribed using a random primer and M-MLV reverse transcriptase (Promega, Mannheim, Germany). The RT-PCR reaction contained sense and antisense primers [3]. Knockdown of anoctamins by siRNA was reported in our previous study [275]. All experiments were performed 48 h after the transfection.

Immunocytochemistry. Transfected HeLa cells were fixed for 10 minutes with 4% (w/v) PFA at RT. Bovine serum albumin (BSA) was added and left for 30 min at RT. Cells were incubated for 1 h with primary goat anti-GFP antibody (1:200; Rockland, Philadelphia, USA), rabbit anti-IP3R or mouse anti-SERCA (all 1:200; Abcam, UK) in PBS supplemented with 1% BSA at 4°C. Cells were washed three times with cold PBS and incubated with the secondary antibody Alexa Fluor 488 conjugated Donkey Anti-Goat IgG (1:500; Molecular Probes, Invitrogen, Germany) and 0,1 µg/ml Hoechst 33342 (1:200; Aplichem, Darmstadt, Germany) for 1 h. Actin was labeled by Alexa Fluor 647-phalloidin (1:100; Molecular Probes, Invitrogen, Germany) and Fluor 555-conjugated donkey anti-rabbit IgG (1:500) or Alexa Fluor 546 conjugated donkey anti-mouse IgG (1:500; Molecular Probes). Cover slips were mounted with fluorescence mounting medium (DAKO Cytomation, Hamburg, Germany). For quantitative assays ANO1-GFP and ANO4-GFP transfected HeLa cells were fixed with 4% paraformaldehyde in PBS for 10 min, permeabilized with 0,1% Triton X-100 for 10 min at RT and incubated with primary antibodies goat anti-GFP, rabbit anti-human IP3 receptor (Abcam, UK), or mouse anti-SERCA (Abcam, UK) at 4°C overnight. Secondary antibodies were Alexa Fluor 488 goat anti rabbit IgG, Alexa Fluor 555 conjugated donkey anti- rabbit IgG or Alexa Fluor 546 conjugated donkey anti- mouse IgG (Molecular Probes, Invitrogen, Germany). Nuclei were counterstained with Hoechst 33342 (Sigma-Aldrich, Taufkirchen, Germany). Immunofluorescence was detected using an Axiovert 200 microscope equipped with an ApoTome and analyzed with the profile measurement tool of Carl Zeiss AxioVision software AxioVs40 V4.8.2.0 (Zeiss, Jena, Germany).

COIP and Western blotting. HeLa cells overexpressing ANO4-GFP or ANO1-GFP were collected using 1% CHAPs lysis buffer. 500 µg protein was incubated with antibody at 4°C for 1h by spinning on a rotator, followed by incubation with pre-cleaned protein G agarose

(60 µl) at 4°C. Afterward, beads were centrifuged and washed three times with 1% CHAPs lysis buffer containing 1X proteinase inhibitor (Roche). Immune complexes were eluted by 2x sample buffer. IP samples were analyzed by Western blotting. Samples were separated by 8.5% and 12.5% SDS-PAGE and transferred onto PVDF membrane. Membrane was blocked with 5%NFM/TBS-T or 5%NFM/PBS-T for 1h at RT and incubated overnight at 4°C with rabbit anti-ORAI1 (1:1000 in 0.25% BSA/TBS-T), rabbit anti-IP3R (1:1000 in 1% BSA/TBS-T), rabbit anti-DOG1 (1:500 in 1% NFM/TBS-T) (Novus,USA), goat anti-GFP (1:1000 in 1% NFM/TBS-T), mouse anti-SERCa^2 (1:1000 in 0.25% BSA/TBS-T) and mouse anti-actin (1:750 in 5% NFM/PBS-T) (Santa Cruz, USA). The membrane was incubated with HRP-conjugated goat anti-rabbit IgG (1:10,000 in 1% NFM/TBS-T) for 2 hrs, HRP-conjugated donkey anti-goat IgG (1:2,000 in 3% NFM/TBS-T) for 1 h and HRP-conjugated goat anti-mouse IgG (1:5,000 in 1% NFM/TBS-T or PBS-T) for 2 hrs at RT. Signals were detected using SuperSignal West Pico chemiluminescence substrate (Pierce, USA). Experiments were performed in triplicates.

Measurement of [Ca^{2+}]i. The plasma membrane bound calcium sensor GCAMP2 was modified by the addition of a N-terminal signal peptide (20 aa) from Neuromodulin (Pl-G-CaMP2 [276]). Addition of this peptide results in posttranslational palmitoylation of the protein, which facilitates anchoring of the protein to the plasma membrane [277]. HEK293 cells were transfected on coated glass cover slips with pcDNA31 Pl-G-CaMP2, and were mounted in a perfusion chamber 48 hrs after transfection. ER Ca^{2+} signals were detected after expression of the Ca^{2+} sensor ER-LAR-GECO1. Cells were perfused with ringer solution at a rate of 8 ml/min at 37˚C. Cell fluorescence measurements was measured continuously with an inverted microscope Axiovert S100 (Zeiss) using a x40 objective (Fluar 40x/1.3 Oil, Zeiss) and a high speed polychromator system (VisiChrome, Visitron, Puchheim, Germany). Pl-G-CaMP2 was excited at 485 nm and 405 nm. Emission was recorded between 520 and 550 nm using a CCD-camera (CoolSnap HQ, Visitron). Control of experiments, imaging acquisition, and data analysis were done with the software package Meta-Fluor (Universal imaging, New York, USA). Alternatively cells were loaded with Fura2 and intracellular Ca^{2+} concentrations were determined as described earlier [93].

Patch Clamping. Cells were seeded and patch clamped on glass cover slips. If not indicated otherwise, patch pipettes were filled with a cytosolic-like solution containing (in mM): KCl 30, K-gluconate 95, NaH_2PO_4 1.2, Na_2HPO_4 4.8, EGTA 1, Ca-gluconate 0.758, MgCl2 1.03, D - glucose 5, ATP 3, pH 7.2. The Ca^{2+} activity was 0.1 µM. Cells were perfused with a bicarbonate free Ringer bath solution (in mM; NaCl 145, KH_2PO_4 0.4, K_2HPO_4 1.6, D-glucose 6, MgCl2 1, Ca-gluconate 1.3, pH 7.4). Coverslips were mounted in a perfused bath chamber on the stage of an inverted microscope (IM35, Zeiss) and kept at 37 °C. The bath was perfused continuously with Ringer solution at a rate of 8 ml/min. Patch clamp experiments were performed in the fast whole cell configuration. Patch pipettes had an input resistance

of 2–4 MΩ when filled with the cytosolic like (physiological) solution. Currents were corrected for serial resistance. The access conductance was measured continuously and was 60–140 nS. Currents (voltage clamp) and voltages (current clamp) were recorded using a patch clamp amplifier (EPC 7, List Medical Electronics, Darmstadt, Germany), a LIH1600 interface and PULSE software (HEKA, Lambrecht, Germany) as well as Chart software (AD Instruments, Spechbach, Germany). Data were stored continuously on a computer hard disc and analyzed using PULSE software. In regular intervals, membrane voltage (Vc) was clamped in steps of 20 mV from -100 to +100 mV. Current density was calculated by dividing whole cell currents by cell capacitance.

Materials and statistical analysis. All compounds used were of highest available grade of purity and were from Sigma, Tocris Bioscience, or Merck. Mouse monoclonal anti-calreticulin and rabbit anti- actin were from Abcam and Sigma-Aldrich, respectively. Anti-ORAI1 was a generous gift from Prof. Dr. Veit Flockerzi (Institute for pharmacology, University of Saarlandes). Osmolarity of all solutions was measured using an osmometer. Data are reported as mean ± SEM. Student's t-test for unpaired samples or ANOVA were used for statistical analysis. A p-value < 0.05 was accepted as significant difference.

Results

Cl^- transport affects GPCR-controlled local Ca^{2+} increase. The Ca^{2+} sensitive dye Fura-2 detects global Ca^{2+} signals throughout the cell. Activation of the purinergic receptors ($P2Y_2$) by ATP induced the typical intracellular Ca^{2+} peak and plateau increase, indicating a fast release of Ca^{2+} from the ER (peak), followed by Ca^{2+} influx through store operated Ca^{2+} influx channels (SOCE) (Fig 2.1a). Fura-2 detects both parts of receptor triggered Ca^{2+} signals, as it distributes more or less homogenously through the cytosol. In contrast, the Ca^{2+} sensor Pl-G-CaMP2 binds to the plasma membrane and detects preferentially Ca^{2+} signals in close proximity of the cell membrane. We found that Pl-G-CaMP2 detects Ca^{2+} release from IP3-sensitive ER stores (peak), but not Ca^{2+} influx (SOCE; plateau) (Fig 2.1a). Using GCAMP2 as Ca^{2+} monitor, we did not detect any Ca^{2+} rise in the ER store depletion protocol after adding CPA or after re-adding Ca^{2+} in the presence of CPA (Fig 2.1b,c). Interestingly, a negative transient peak was detected by GCAMP2 upon re-addition of extracellular Ca^{2+} indicating a transient dip in the local Ca^{2+} concentration in close proximity to the store release site (IP_3 receptor). This transient peak may somehow reflect refilling of the store, although the mechanisms remain currently obscure.

ANO1 is a membrane localized ion channel that probably accumulates in specific cholesterol-rich membrane compartments, called lipid rafts [79,278]. As ANO1 is preferentially, if not exclusively, activated through ER store release [78], and because store release (but not SOCE) is picked up well by Pl-G-CaMP2, Pl-G-CaMP2 is probably colocalized together with ANO1 in a raft compartment that does not contain elements of the SOCE. Thus there is a

spatial separation between Ca^{2+} release and activation of ANO1, and SOCE influx pathways, as nicely demonstrated in an earlier report by Courjaret and Machaca [273]. In the present experiments maximal store release was achieved at 100 µM ATP (Fig. 2.1d).

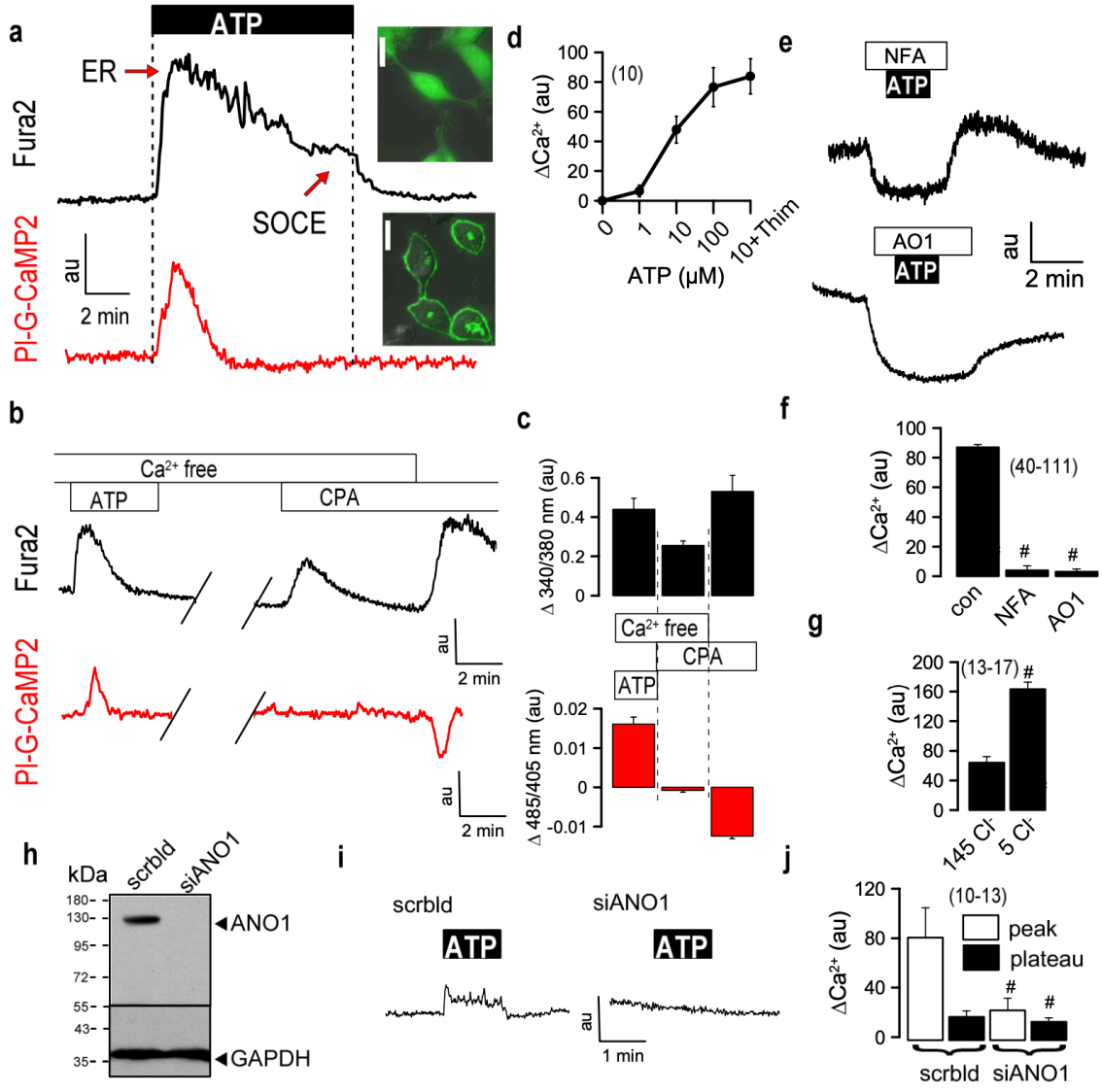

Figure 2.1 | *Receptor-mediated increase in intracellular Ca^{2+} is Cl^- dependent.*

a Increase in intracellular Ca^{2+} in HeLa cells by stimulation with ATP (100 µM) was detected by Fura-2 or by the membrane bound Ca^{2+} sensor PI-G-CaMP2, fused to a N-terminal signal peptide from neuromodulin. While Fura-2 detects Ca^{2+} release from ER (peak) and Ca^{2+} influx through store operated Ca^{2+} entry (SOCE; plateau), GCAMP2 detects only ER store release Ca^{2+}, indicating local separation of store release and Ca^{2+} influx. **b,c** Ca^{2+} store release/depletion by stimulation with ATP (100 µM) and cyclopiazonic acid (CPA; 10 µM), as detected by Fura-2 (upper panels) or by PI-G-CAMP2 (lower panels). **d** Concentration dependent increase in intracellular Ca^{2+} (arbitrary units; au) by ATP. Thimerosal (100 µM), a sensitizer of IP_3 receptors was enclosed to detect maximal store release. **e,f** Anoctamin inhibitors Niflumic acid (NFA) and CaCCinhAO1 (AO1; both 20 µM) inhibited baseline Ca^{2+} and abolished ATP-induced Ca^{2+} release (ΔCa^{2+}). **g** Summary of ATP-induce Ca^{2+} increase in the presence of physiological extracellular Cl^- concentration (145 mM) or low (5 mM) extracellular Cl^-. H) Western blot indicating knockdown of endogenous expression of ANO1 in CAL27

cells. **I** ATP induced Ca^{2+} signal (measured by PI-G-CAMP2), which was abolished by knockdown of ANO1. **J** Summary of Ca^{2+} peak and plateau induced by ATP in CAL27 cells. Mean ± SEM (number of cells). #significant inhibition by NFA and AO1, and augmented Ca^{2+} release in the presence of 5 Cl^- (ANOVA).

Blockers of anoctamins such as NFA or AO1 strongly reduced baseline Ca^{2+} concentrations and completely abolished Ca^{2+} store release, suggesting a role of Cl^- transport through anoctamins for Ca^{2+} signaling (Fig. 1e,f). Cl^- dependence was further supported by the finding that ATP-induced Ca^{2+} increase was augmented in the presence of a low (5 mM; 5Cl^-) extracellular Cl^- concentration (Fig. 2.1g). Possible artefacts of these inhibitors and of 5Cl^- on intracellular pH, fluorescence intensity or absorbance were excluded in control experiments. Moreover, both NFA and AO1 slightly hyperpolarized (11.2 ± 1.6 mV (n=13; NFA) and 12.2 ± 1.9 mV (n=9; AO1) the membrane voltage. Hyperpolarization of Vm is generally augmenting GPCR-mediated Ca^{2+} signaling, but in our experiments NFA and AO1 inhibited Ca^{2+} signaling, suggesting a role of Cl^- conductance for ATP induced Ca^{2+} transients. 5Cl^- depolarized Vm by 13.4 ± 1.8 mV (n=11). Depolarization of Vm is generally inhibitory on GPCR-mediated Ca^{2+} signaling [279]. However, in our experiments 5Cl^- augmented Ca^{2+} increase (Fig. 2.1g), arguing against an artefact, but supporting the role of Cl^- / Cl^- conductance for ATP induced Ca^{2+} transients. We observed that siRNA-knockdown of endogenous expression of ANO1 in the head and neck cancer cell line CAL27, inhibited GPCR-mediated Ca^{2+} increase (Fig. 2.1h-j). We therefore examined in detail the impact of ANO1 and other anoctamins on intracellular Ca^{2+} signaling.

Anoctamins affect compartmentalized Ca^{2+} signals. We analyzed if anoctamins affect compartmentalized Ca^{2+} signals triggered by GPCRs in HeLa cells. We found that expression of some anoctamins (ANO1, 5, 6, 10; green) augmented Ca^{2+} store release detected by PI-G-CaMP2, while others (ANO4, 8, 9; red) largely reduced Ca^{2+} signals (Fig. 2.2a,b). ANO4, 6, 8, and 10 were found to be expressed endogenously in HeLa cells (not shown). When endogenous Ca^{2+}-enhancing ANO6 and ANO10 were knocked down by siRNA, ATP-induced Ca^{2+} signals were strongly attenuated (Fig. 2.2c). Effects of anoctamins on ATP-induced Ca^{2+} signals or ionomycin induced ER Ca^{2+} store depletion were only partially detected when Fura2 was used as a global cytosolic Ca^{2+} sensor (data not shown). It appears unlikely that ANO1 affects hydrolysis of PIP_2 and generation of IP_3, when examining fluorescence changes during ATP stimulation of cells expressing GFP-tagged PLCδ1PH [280] (Supplementary Fig. 2.1a,b).

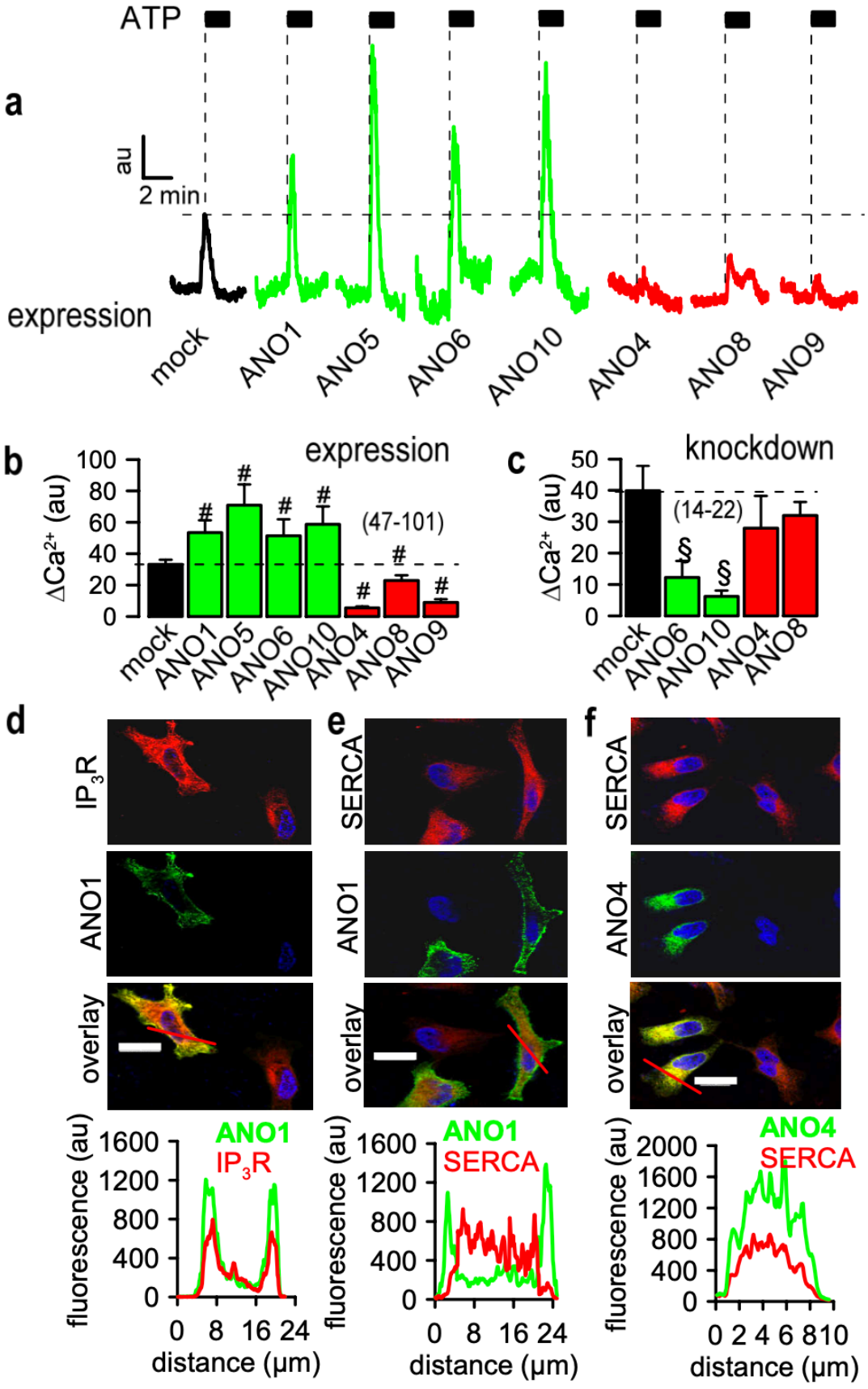

Figure 2.2 | *Anoctamins affect intracellular Ca^{2+} signals.*

a Ca^{2+} store release detected by PI-G-CaMP2 fluorescence in HeLa cells overexpressing different anoctamins. **b** Summary of ATP (100 μM) induced Ca^{2+} signals (arbitrary units; au) in the presence

of different anoctamins, which augmented (ANO1, 5, 6,19; green) or reduced (ANO4, 8, 9; red) Ca^{2+} store release. **c** Summary of Ca^{2+} signals in cells treated with scrambled RNA or after knockdown of different endogenous anoctamins, which abolished (arbitrary units; au) enhancing (ANO6, ANO10) and inhibitory (ANO4, ANO8) effects of anoctamins on Ca^{2+} signals. Successful knockdown of anoctamins by siRNA is shown in Supplementary Fig 2.1f. **d-f** Immunofluorescence of IP_3 receptor, SERCA, ANO1 and ANO4 in HeLa cells (upper panels). Scanning of fluorescence intensities (arbitrary units, lowest panels) indicated colocalization of cortical IP_3R (red) and ANO1 (green) close to the plasma membrane (D), but lack of colocalization of SERCA and ANO1 (F). ANO4 was found to be colocalized with SERCA (F). Mean ± SEM (number of cells). #significant increase (ANO1,5,6,10; green) and inhibition (ANO4,8,9; red) of Ca^{2+} signals by overexpression of anoctamins (ANOVA). §significant inhibition of Ca^{2+} signals and mRNA expression by siRNA-knockdown of anoctamins (ANOVA).

Immunofluorescence labelling of IP_3 receptors (IP_3R) and overexpressed ANO1 suggested colocalization of ANO1/IP_3R in close proximity to the plasma membrane (Fig. 2.2d). In contrast SERCA colocalized with ANO4 in a cytosolic compartment, but did not co-localize with ANO1 (Fig. 2.2e,f). Colocalization of proteins is supported by scanning red (IP_3R, SERCA) and green fluorescence (ANO1, ANO4) (Fig. 2.2d-f, lowest panels). Moreover, fluorescence labelling of the ER protein calreticulin suggested the presence of cortical ER close to ANO1, which is located in the plasma membrane, while most ANO4 localized to intracellular calreticulin (Supplementary Fig. 2.1c,d). Compounds known to deplete biological membranes of cholesterol and to disrupt lipid rafts like methyl-ß-cyclodextrin (MβCD) [281] or filipin [282], abolished the inhibitory effects of ANO4 on Ca^{2+} signaling (Supplementary Fig. 2.1e). As ORAI1 was detected as the main isoform, ANO4 may be co-localized with ORAI1 in a raft population separate from the one containing ANO1.

Differential interaction of ANO1 and ANO4 with IP_3R and ORAI. ANO1 augmented but ANO4 strongly inhibited ATP-induced currents. While ANO1 is strictly plasma membrane localized, ANO4 is expressed intracellularly in an ER compartment. We therefore decided to examine the cellular functions of these anoctamins in more detail. Immunocytochemistry may suggest a differential molecular interaction of ANO1 with IP_3R and ANO4 with ORAI or SERCA [78]. This assumption was supported by coimmunoprecipitation of ANO1 and IP_3R in overexpressing HeLa cells (Fig. 2.3a). In contrast, SERCA (or ORAI; data not shown) could not be coimmunoprecipitated with ANO1 (Fig. 2.3b). Moreover, while ANO4 and ORAI coimmunoprecipitated (Fig. 2.3c), no evidence was found for an interaction of ANO4 with IP_3R or ANO4 with SERCA (data not shown). This result indeed suggests a differential interaction of ANO1 and ANO4 with IP_3R/ORAI, and suggests that ANO1 and ANO4 may control different Ca^{2+} sources. ANO1 may be activated only by store release Ca^{2+}, but not by SOCE, while ANO4 is activated by SOCE, and not by store release. Remarkably, and in contrast to Fura2, store release induced by CPA or Ca^{2+} influx through SOCE after re-adding extracellular Ca^{2+} was not at all detected by GCAMP2 targeted to the IP_3R/ANO1

compartment (not shown). Thus the data strongly suggest that in mammalian cells Ca^{2+} pools (store release Ca^{2+} and SOCE) are spatially separated, as demonstrated recently in experiments in *Xenopus* oocytes [273].

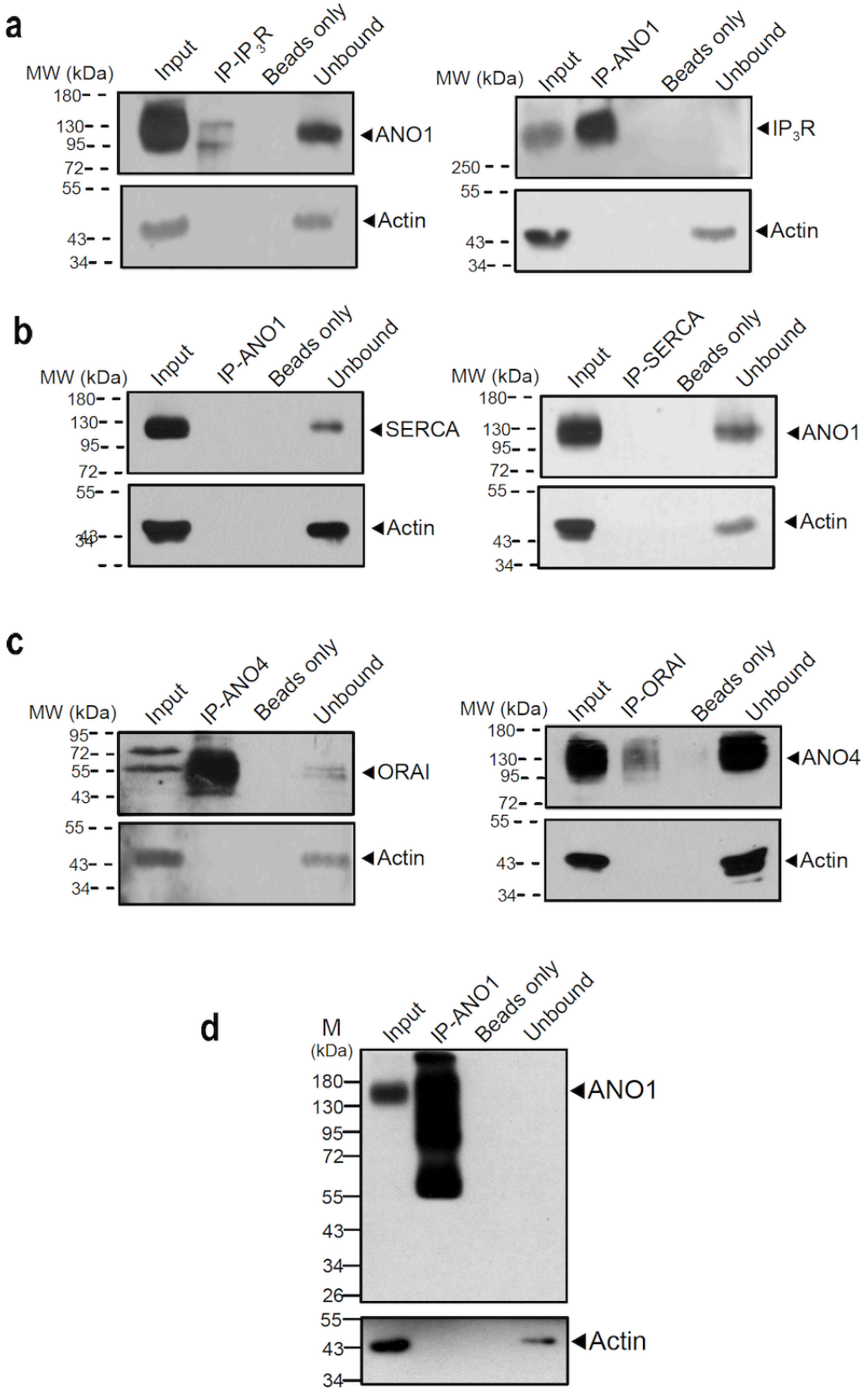

Figure 2.3 | *Coimmunoprecipitation of ANO1 and ANO4 with IP₃ receptor and SERCA in HeLa cells.* **a** ANO1 was coimmunoprecipitated with IP_3R, while IP_3R was pulled down with ANO1. **b**

Immunoprecipitation of ANO1 did not pull down SERCA, and no pull down of ANO4 was seen by immunoprecipitation of SERCA. **c** ORAI was coimmunoprecipitated with ANO4, while immunoprecipitation of ORAI pulled down ANO4. **d** Control experiment in which ANO1 was pulled down and the pulled down protein was detected by ANO1 Western blotting. Experiments were performed in triplicates.

We demonstrated earlier that ANO4, similar to ANO1, induces Ca^{2+} activated Cl^- currents when overexpressed in HEK293 cells [11]. Also in the present study we found that whole cell currents were activated by ATP in ANO1 and in ANO4 expressing HEK293 cells, but not in mock transfected cells (Fig. 2.4a-d,i,j). Currents were strongly inhibited by removal of extracellular Cl^- indicating activation of Cl^- currents. Remarkably, ATP-induced Ca^{2+} increase activated ANO1 instantaneously (fast Ca^{2+} store release), while activation of ANO4 slow (delayed SOCE). This suggests an exclusive crosstalk of store release Ca^{2+} and ANO1 (Fig. 2.4e). But how is it possible that expression of ANO4 leads to delayed-activated whole cell Cl^- currents although ANO4 is expressed in an intracellular compartment? It is known from earlier studies that ANO6 is expressed in the plasma membrane and produces delayed Ca^{2+} activated Cl^- currents [283,284]. ANO6 has also been shown to be activated through Ca^{2+} influx [284]. We therefore speculated that ANO4 may facilitate activation of ANO6 by emptying the ER store or by inhibiting filling of the ER store and thereby enhancing Ca^{2+} influx (SOCE), which activates ANO6. We examined mock transfected cells or ANO4-expressing cells without or with simultaneous siRNA-knockdown of endogenous ANO6. In mock transfected cells (no ANO4), ATP did not activate a current and simultaneous siRNA-knockdown of ANO6 had only a minor effect. In ANO4-overexpressing cells, a whole cell current was activated by ATP, which was largely suppressed by simultaneous knockdown of ANO6. The data indicate that expression of ANO4 (intracellular) induces a ATP-induced whole cell current that requires plasma membrane localized ANO6 (Supplementary Fig. 2.1d,f,g,h).

ANO6 is obviously activated by SOCE, while ANO1 is activated by IP_3R-mediated Ca^{2+} release. In fact, removal of extracellular Ca^{2+} did not compromise activation of ANO1, but completely abolished activation of ANO6 (in ANO4 expressing cells) (Fig. 2.4f). Vice versa, inhibition of IP_3R with Xestospongin C [285] (IP_3R-inhibitor A in Fig. 2.4g) or low molecular weight heparin (IP_3R-inhibitor B in Fig. 2.4g) [286] blocked activation of ANO1, but had no effect on ANO4-induced currents (Fig. 2.4g). Finally, inhibition of ORAI by YM8483 (ORAI-inh. A)[287] or GSK-7975A (ORAI-inh. B) [288] completely blocked ANO4 activation, without affecting ANO1. These results were validated by performing comparable experiments in HeLa cells, which produced essentially identical results (Supplementary Fig. 2.2a-d). Taken together, these results strongly suggest differential coupling of ANO1 and ANO6 to IP_3R and ORAI, respectively (Fig. 2.4g).

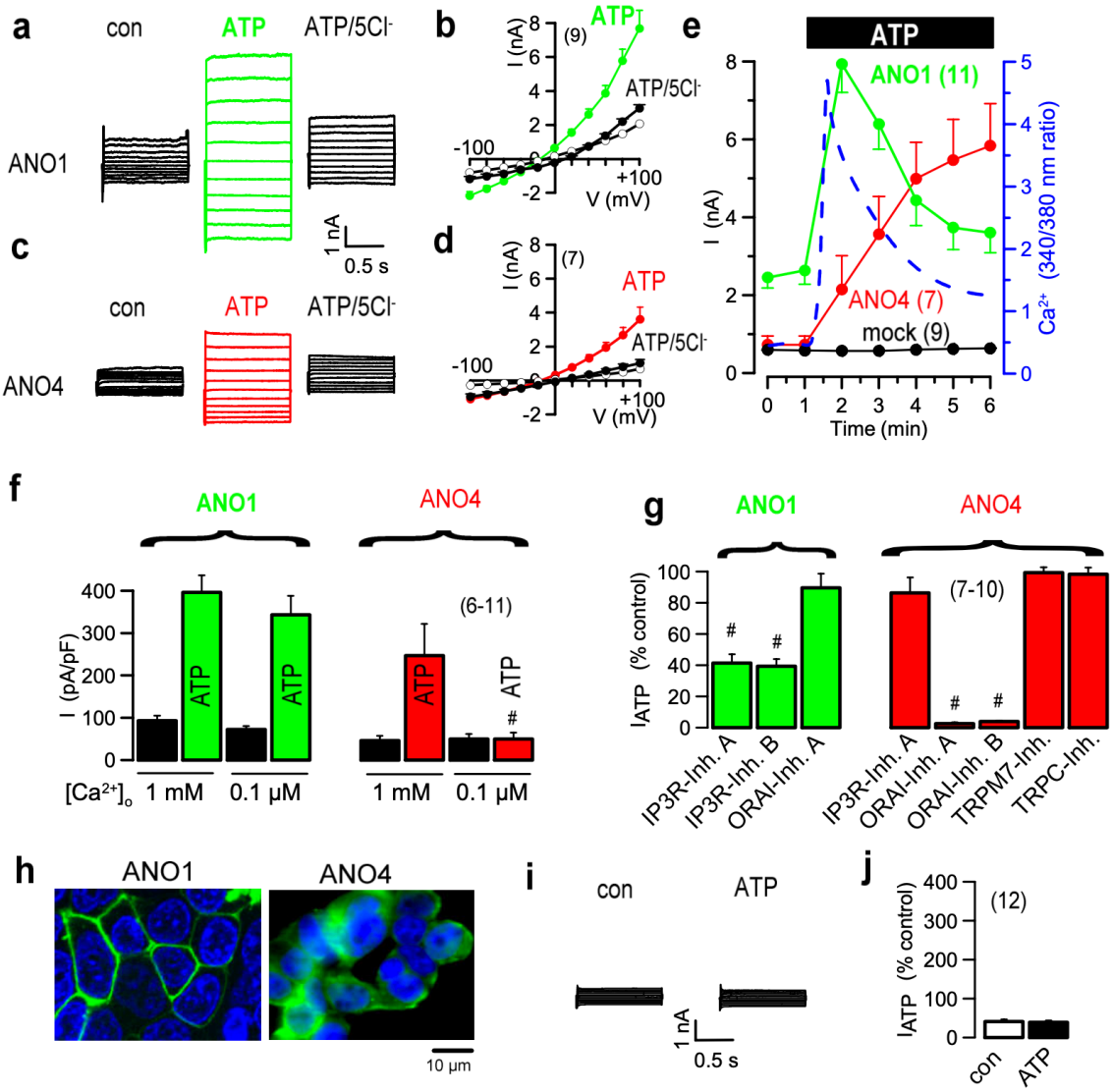

Figure 2.4 | *ANO1 and ANO4 Cl^- currents are activated by different Ca^{2+} sources.*

a Patch clamp recording of ATP (100 µM) activated whole cell currents in an ANO1-expressing HEK293 cells. Inhibition of currents by removal of extracellular Cl^- ($5Cl^-$). **b** Corresponding current/voltage relationships. **c** Patch clamp recording of ATP activated whole cell currents in an ANO4-expressing HEK293 cell. Inhibition of currents by removal of extracellular Cl^- ($5Cl^-$). **d** Corresponding current/voltage relationships. **e** Current activation during Ca^{2+} peak and plateau. Time course for ATP-activation of whole cell currents: Fast activation of ANO1, but delayed activation of ANO4. **f** Activation of whole cell currents by ATP in ANO1 and ANO4 expressing cells, in the presence of high (1 mM) or low (0.1 µM) extracellular Ca^{2+} concentration. Activation of ANO4 requires influx of extracellular Ca^{2+} while activation of ANO1 is independent of the extracellular Ca^{2+} concentration. **g** Effects of compounds inhibiting Ca^{2+} signaling and activation of ANO1 and ANO4. Activation of ANO1 is suppressed by inhibition of IP3R with xestospongin C (1 µM/30 min; IP3R-Inh. A) and low molecular weight heparin (1 mM/30 min; IP3R-Inh. B), but not by the ORAI inhibitor YM8483 (5 µM; ORAI-Inh. A). In contrast activation of ANO6 (in ANO4-expressing cells) is abolished with YM8483 and GSK-7975A (5 µM; ORAI-Inh. B), but not by Xestospongin C. The TRPM7 inhibitor NS8593 (10 µM) and the TRPC inhibitor SKF-96365 (100 µM) had no effects on activation of ANO4. ORAI inhibitors, NS8593, and SKF-96365 were applied acutely, cells were pre-incubated with Xestospongin C and

heparin for 10 min. **h** Demonstration of expression of ANO1 (plasma membrane) and ANO4 (intracellular) in HEK293 cells. **i,j** Control experiments in mock transfected cells. ATP did not activate any whole cell currents. Mean ± SEM (number of cells). #significant inhibition by low extracellular Ca^{2+} and inhibitors, respectively (unpaired t-test and ANOVA).

ANO4, 8, 9 probably lower filling of the ER Ca^{2+} store. ATP-induced Ca^{2+} peaks and plateau were larger in ANO1-expressing cells, but were small and very transient in ANO4 expressing cells, which might be due to reduced store Ca^{2+} in ANO4 expressing cells (Supplementary Fig. 2.2e). In the presence of extracellular Ca^{2+} free solution, the SERCA inhibitor CPA emptied ER Ca^{2+} stores, leading to a transient Ca^{2+} increase. The results from this store release protocol suggested that expression of ANO4, 8 and 9 lowered Ca^{2+} store content, as Ca^{2+} release was small and quickly collapsing, while expression of ANO1, 5, 6 and 10 did not affect store content (Supplementary Fig. 2.2f,g). These results are supported by several additional Ca^{2+} store release protocols described above. Taken together, the results suggest that ANO1, 5, 6, 10 facilitate local ER Ca^{2+} release in close proximity to the plasma membrane. In contrast ANO4, 8, and 9 seem to lower the Ca^{2+} store content. It is likely that localization of ANO4 (and maybe ANO8, 9) in the ER membrane leads to a Ca^{2+} leakage out of the ER, thereby reducing ER store content. In fact ANO4 (and other anoctamins) have been described as leaky Cl^- channels that are also permeable for cations such as Ca^{2+} [11,289]. Remarkably, augmented ATP-induced Ca^{2+} signals in ANO1-expressing cells, and reduced ATP-induced Ca^{2+} signals in ANO4 or ANO9 expressing cells could also be monitored by expression of the Ca^{2+} activated K^+ channel hSK4 (KCNN4). ATP-activated hSK4 currents were strongly attenuated in cells expressing either ANO4 or ANO9, while expression of ANO1 augmented ATP-activation of hSK4 (Supplementary Fig. 2.2h-k).

Ca^{2+} signaling is attenuated in epithelial cells from Ano10$^{-/-}$ mice. It appears essential to demonstrate the role of anoctamins for Ca^{2+} signaling also in original tissues. This has been shown already for Ano1 in intestinal epithelial cells from Ano1 knockout mice [37]. We found a pronounced inhibition of ATP induced Ca^{2+} signals after siRNA knockdown of endogenous ANO10 and, inversely, a strong augmentation of Ca^{2+} signals in ANO10 overexpressing cells (Fig. 2.2). Moreover, our earlier study indicated a role of ANO10 for Ca^{2+} signaling also in macrophages [27]. We therefore further validated the effects of Ano10 on intracellular Ca^{2+} signaling by generating renal tubular specific Ano10 knockout mice (Fig. 2.5a,b). Ano10 was found to be localized in an intracellular compartment below the brush boarder membrane (Fig. 2.5c). This compartment is likely to correspond with the endoplasmic reticulum, as localization of ANO10 in the ER has been demonstrated earlier [27]. Proximal tubular epithelial cells were isolated from Ano10+/+ and Ano10-/- mice, primary cultured and loaded with Fura2. Cells were stimulated with ATP, which induced the typical peak/plateau response. In

Ano10-/- cells, baseline Ca^{2+} as well as ATP-induced peak and plateau responses were attenuated (Fig. 2.5d-f). Despite the changes in Ca^{2+} signaling, we did not observe any overt phenotype in renal Ano10 null mice, and renal serum and urine parameters were not different to wt animals (Supplementary Figs. 2.3, 2.4). However, we noticed an upregulation of ANO6 expression in tubular epithelial cells from Ano10 null mice, which could somehow compensate for the lack of ANO10 (Supplementary Fig. 2.4d).

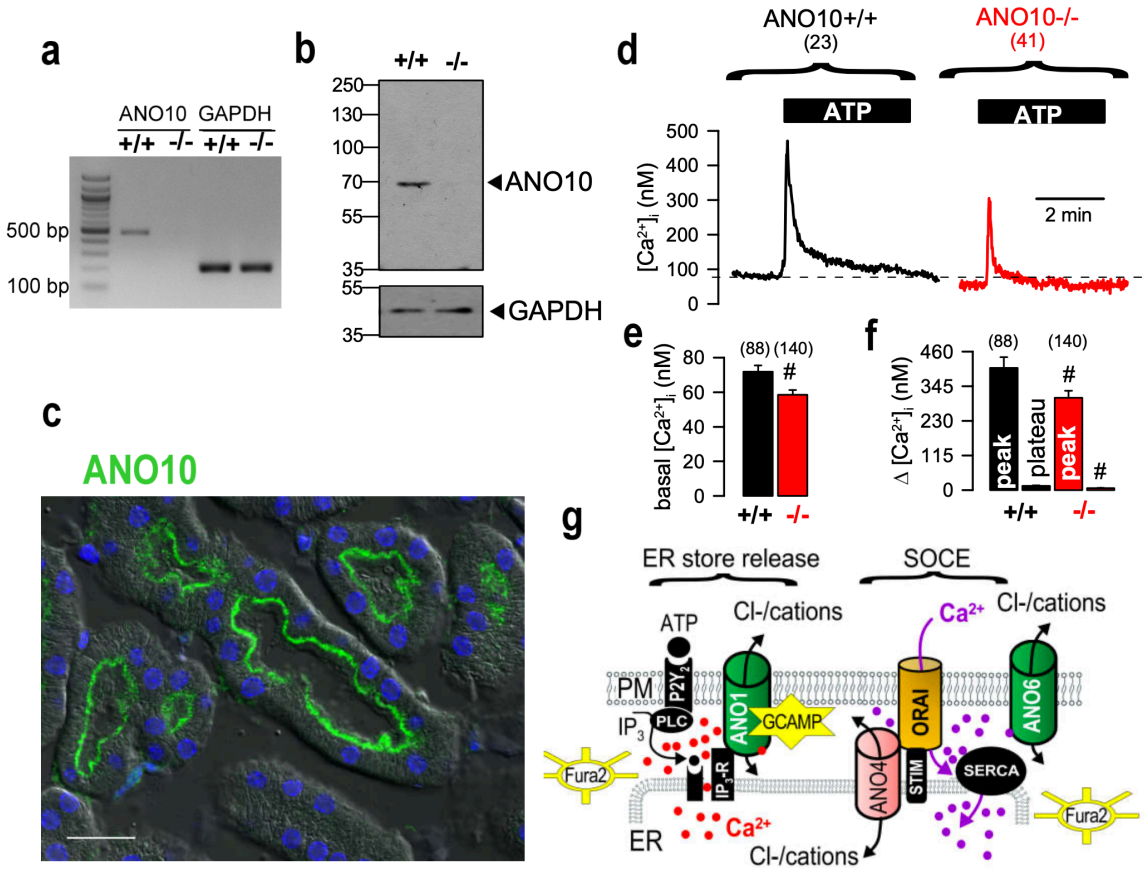

Figure 2.5 | *Attenuated Ca^{2+} signals in isolated epithelial cells from Ano10$^{-/-}$ mice.*

RT-PCR **a** and Western blotting **b** demonstrating lack of expression of Ano10 in proximal tubular epithelial cells from ANO10$^{-/-}$ mice. **c** Immunohistochemistry of Ano10 in proximal tubular epithelial cells. Ano10 is located underneath the brush boarder membrane in a cytosolic compartment. Bar indicates 50 µm. **d** ATP (100 µM) induced Ca^{2+} increase measured by Fura-2 in mouse primary cultured proximal tubular epithelial cells. Summary traces showing reduced basal Ca^{2+} and attenuated ATP-induced Ca^{2+} peak and plateau in cells isolated from Ano10$^{-/-}$ mice. Summaries for basal Ca^{2+} **e** and ATP-induced Ca^{2+} peak and plateau **f** in cells from wt ($^{+/+}$) and Ano10 knockout ($^{-/-}$) mice. $^{\#}$significantly reduced Ca^{2+} plateau and Ca^{2+} increase in Ano10 knockout cells (unpaired t-test). Mean ± SEM (number of cells). **g** Model for the differential effects of ANO1 and ANO4 on receptor operated Ca^{2+} signaling. Two well-separated cytosolic Ca^{2+} pools exist in mammalian cells, caused by store release (red dots) and Ca^{2+} entry (violet dots). Plasma membrane localized ANO1 tethers ER Ca^{2+} stores to raft compartments and augments compartmentalized Ca^{2+} signals and activation of ANO1 (or other Ca^{2+} dependent channels such as SK4). This compartment also contains the Ca^{2+} sensor Pl-G-CaMP2. ER-localized ANO4 possibly operates as a Ca^{2+} leakage channel, thereby reducing

Ca^{2+} store filling which activates/augments ORAI-mediated Ca^{2+} influx. Ca^{2+} entry activates ANO6 whole cell currents. This compartment does not contain the Ca^{2+} sensor PI-G-CaMP2. Fura-2 detects global Ca^{2+} signals throughout the cell.

Discussion

TMEM16A/ANO1 has been reported as a protein that confers receptor-activated calcium-dependent chloride conductance [8]. In their paper the authors showed data indicating that ANO1 is much more activated through phospholipase C coupled GPCRs than through direct large Ca^{2+} rises induced by Ca^{2+} ionophores [8]. These results suggest a cellular compartment containing GPCR, ANO1, and components of intracellular Ca^{2+} signaling that allow efficient activation of ANO1. Notably, an inhibitory role of PIP_2 on TMEM16A encoded calcium-activated chloride channels has been demonstrated in rat pulmonary artery, which further substantiates the functional coupling of Ano1 to GPCRs [290]. This functional coupling leads to augmented Ca^{2+} store release via IP_3R. Apart from the ER-store/plasma membrane tethering function the present data also suggest that chloride transport through ANO1 is crucial for this effect, as suggested by the use of ANO1 inhibitors. Although currently unclear, Cl^- exit and change of local submembranous Cl^- concentrations may determinate store release. As an alternative ANO1 may be partially located in the ER where it may function as a counter ion channel, facilitating electroneutrality during Ca^{2+} exit [291]. Clearly more work will be required to fully understand the effects of ANO1 on Ca^{2+} signaling.

Subsequent reports supported the existence of such functional compartments in *Xenopus* oocytes as well as dorsal root ganglia [78,273,292]. These signaling compartments are essential for efficient activation of ANO1, and may allow local Ca^{2+} concentrations that are much higher than global cytosolic Ca^{2+} levels detected by standard (Fura2) fluorescence techniques [79]. Tethering of the ER to the plasma membrane by means of ANO1/IP_3R interactions is therefore an essential mechanism to concentrate Ca^{2+} signals at the plasma membrane. ER-tethering has also been well described for the yeast ANO1 homologue Ist2 [293]. In contrast to ANO1, the present data support the concept that ANO6 (through expression of ANO4, which lowers ER Ca^{2+} and thereby facilitates capacitive Ca^{2+} entry) is activated by SOCE through ORAI and maybe other Ca^{2+} influx channels [284] (Fig. 2.5g). Moreover, earlier studies showed that ANO6 is only weakly activated through GPCRs, but strongly activated by ionomycin [11].

In intact cells ANO1 requires Ca^{2+} concentrations in the higher µmolar range to be fully activated, because the negative membrane voltage interferes with binding of Ca^{2+} to the channel [79]. These signaling compartments appear to be well shielded, as Ca^{2+} influx through

voltage gated Ca^{2+} channels or store operated channels does not reach these compartments and therefore does not activate ANO1 [78] (also c.f. Fig. 2.4). The present results directly demonstrate the role of ANO1 (and ANO5, 6, 10) for GPCR-activated local Ca^{2+} signaling and suggested a different role for ANO4, 8, 9. ANO4,8,9 lower ER store Ca^{2+}, possibly as Cl^- bypass channels to allow Ca^{2+} leakage out of the ER or by operating directly as ER Ca^{2+} leakage channels, thereby activating Ca^{2+} influx and thus activation of plasma membrane localized Ca^{2+} sensitive Cl^- channels (ANO6) or K^+ channels (SK4) (Supplementary Figs. 2.1f, 2.2, 2.4). Cytosolic Ca^{2+} increase by ATP, CPA or ionomycin-induced ER-store release was reduced in ANO4 expressing cells, while store filling was attenuated when measured by the ER Ca^{2+} sensor ER-LAR-GECO1, pointing to store depletion by ANO4 (and ANO8,9) (data not shown).

The physiological role of ANO1 Cl^- currents in the context of Ca^{2+} signaling has been demonstrated in small nociceptive neurons from rat dorsal root ganglia [294]. Stimulation by the pain-inducing hormone bradykinin activates ANO1, which depolarizes the membrane voltage thus increasing firing of action potentials. In airway and intestinal smooth muscles, ANO1 maintains baseline contraction, muscle tone and coordinated intestinal contraction by very similar mechanisms [127,295-297]. Inhibitors of ANO1 lower airway smooth muscle tone and intracellular calcium, which has a large therapeutic potential in asthma. Pharmacological modulation of ANO1 changes contractile activity and intestinal fluid secretion [298,299]. A functional interaction has been demonstrated between ANO1 and TRPV4 in epithelial cells from the choroid plexus [300]. The microdomains in which Ano1 functionally interacts with Ca^{2+} channels and transporters may be therefore cell specific. E.g., in intestinal epithelial cells ANO1 is predominantly in the basolateral membrane, while in renal proximal tubule, pancreatic and salivary gland acini or in airway epithelial cells, ANO1 is resides in the apical membrane [8,37,266]. Finally, regulation of ANO1 by store operated Ca^{2+} entry in eccrine sweat glands was reported recently [301]. Thus ANO1 may couple to different Ca^{2+} transporting proteins in a tissue specific manner. Notably, attenuated agonist-induced Ca^{2+} signaling has also been demonstrated recently in large intestine of ANO10-/- mice [302].

Notably, in intestinal epithelial cells where ANO1 is expressed on the basolateral side of the epithelium, it augments Ca^{2+} signals that activate Ca^{2+} sensitive hSK4 K^+ channels [37]. These K^+ channels maintain a negative membrane voltage that is required to drive Cl^- secretion at the apical side of the epithelium. Thus ANO1 supports Cl^- secretion not as a secretory Cl^- channel, but indirectly by activating K^+ channels. In airway epithelial cells ANO1 may have a similar role by facilitating Ca^{2+} signals in close proximity of the cystic fibrosis transmembrane conductance regulator (CFTR) Cl^- channel[72]. CFTR is known as protein kinase A and ATP regulated Cl^- channel, but it requires also Ca^{2+} dependent kinases to be fully activated [58]. In fact, most of the apparent Ca^{2+} activated Cl^- secretion may actually occur through CFTR [61]. Thus anoctamins control physiological functions through

compartmentalized Ca^{2+} signaling, which may explain their role in many cellular functions and diseases [72] (Fig. 2.5g).

Acknowledgements

Supported by DFG SFB699-A7/A12, DFG KU756/12-1, and Cystic Fibrosis Trust SRC 003, INOVCF. The excellent technical assistance by Mss. B. Wild, P. Seeberger, and E. Tartler is gratefully acknowledged.

Supplementary material

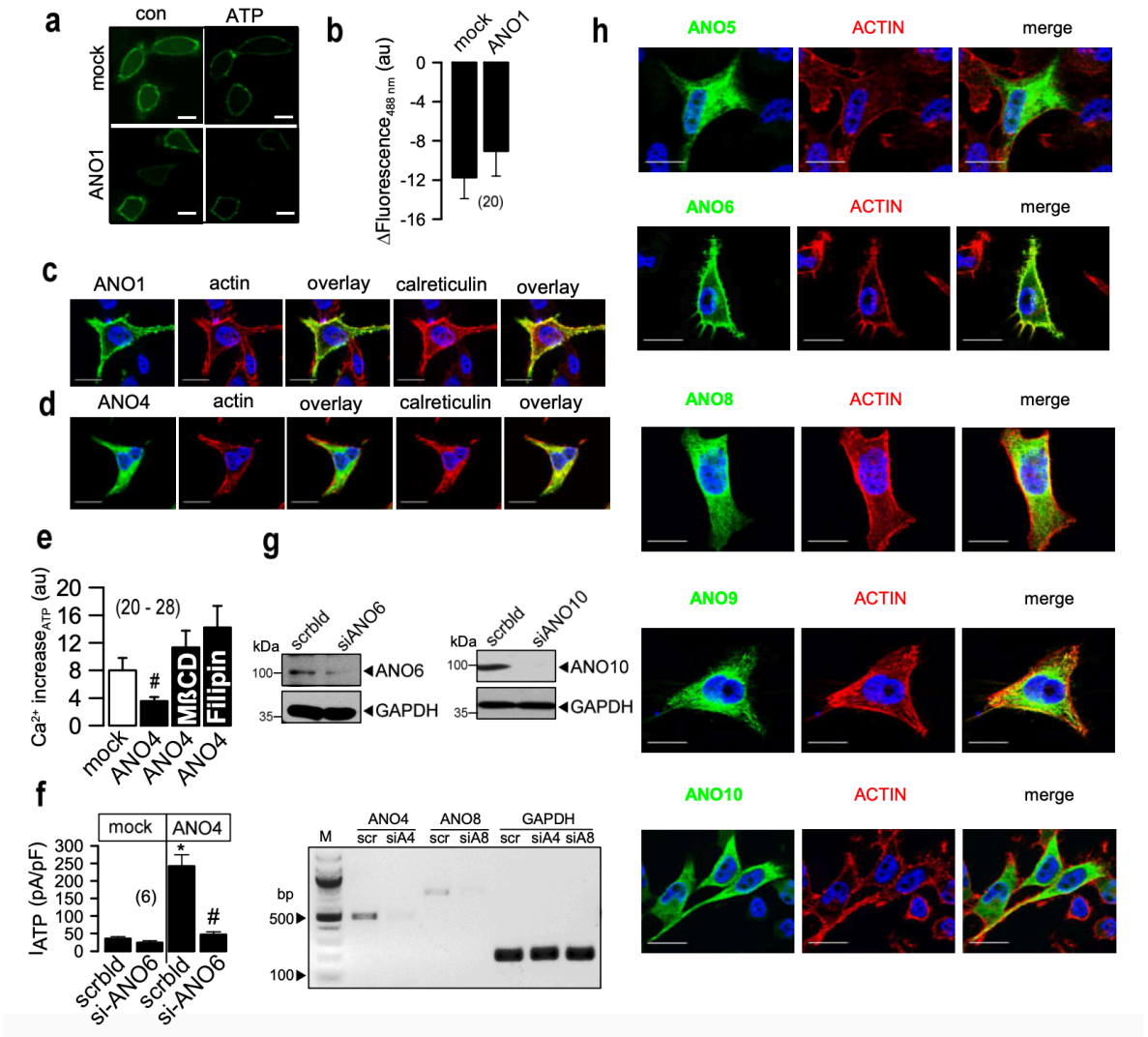

Supplementary Figure 2.1 | *Role of ANO1, ANO4, and ANO6 for Ca^{2+} signaling and whole cell currents.*

a HeLa cells expressing PLCδ1PH-GFP to monitor PIP2 hydrolysis by stimulation with ATP (100 µM, 20 min) in the absence or presence of ANO1. ATP reduced membrane binding of PLCδ1PH-GFP and thus decreased membrane GFP fluorescence by ATP-induced PIP2 hydrolysis. Typical examples out of 20 measured cells are shown. Bar indicates 10 µm. **b** Decrease in membrane fluorescence was comparable in mock transfected and ANO1 expressing cells. **c** Predominant membrane expression of ANO1-GFP in HeLa cells and colocalization with cortical actin. **d** Predominant intracellular expression of ANO4. The endoplasmic reticulum (ER) is demonstrated using the ER marker calreticulin. Bars indicate 10 µm. **e** HeLa cells were incubated with 1 mM methyl-ß-cyclodextrin (MβCD) at 37 °C/2-4 hrs to remove cholesterol from the plasma membrane, or treated with the membrane disrupter filipin (37 °C/30') to dissolve lipid rafts. Summary of the ATP induced Ca^{2+} increase in mock transfected control cells, and ANO4 expressing cells in the absence or presence of MβCD or Filipin. The results suggest that the inhibitory effect of ANO4 on Ca^{2+} signaling requires intact rafts. **f** Whole cell currents in ANO4 expressing cells are due to activation of endogenous ANO6. Activation of whole cell currents by ATP (100 µM) in ANO4 expressing cells was almost abolished by

simultaneous siRNA knockdown of endogenous ANO6. No currents were activated in the absence of ANO4. **g** Western blots indicating knockdown of ANO6 and ANO10 by siRNA. For ANO4 and ANO8 knockdown is shown by quantitative RT-PCR, which was 80.1% ± 7.9 % (n = 8, siANO4) and 74.1 ± 5.3 % (n = 6, siANO8). **H** Expression of GFP-tagged ANO5, 6, 8, 9, and 10 in Hela cells. Bars indicate 10 µm. Mean ± SEM (number of cells). #significant inhibition by ANO4 or siANO6 (ANOVA). *significant increase by ATP (paired t-test).

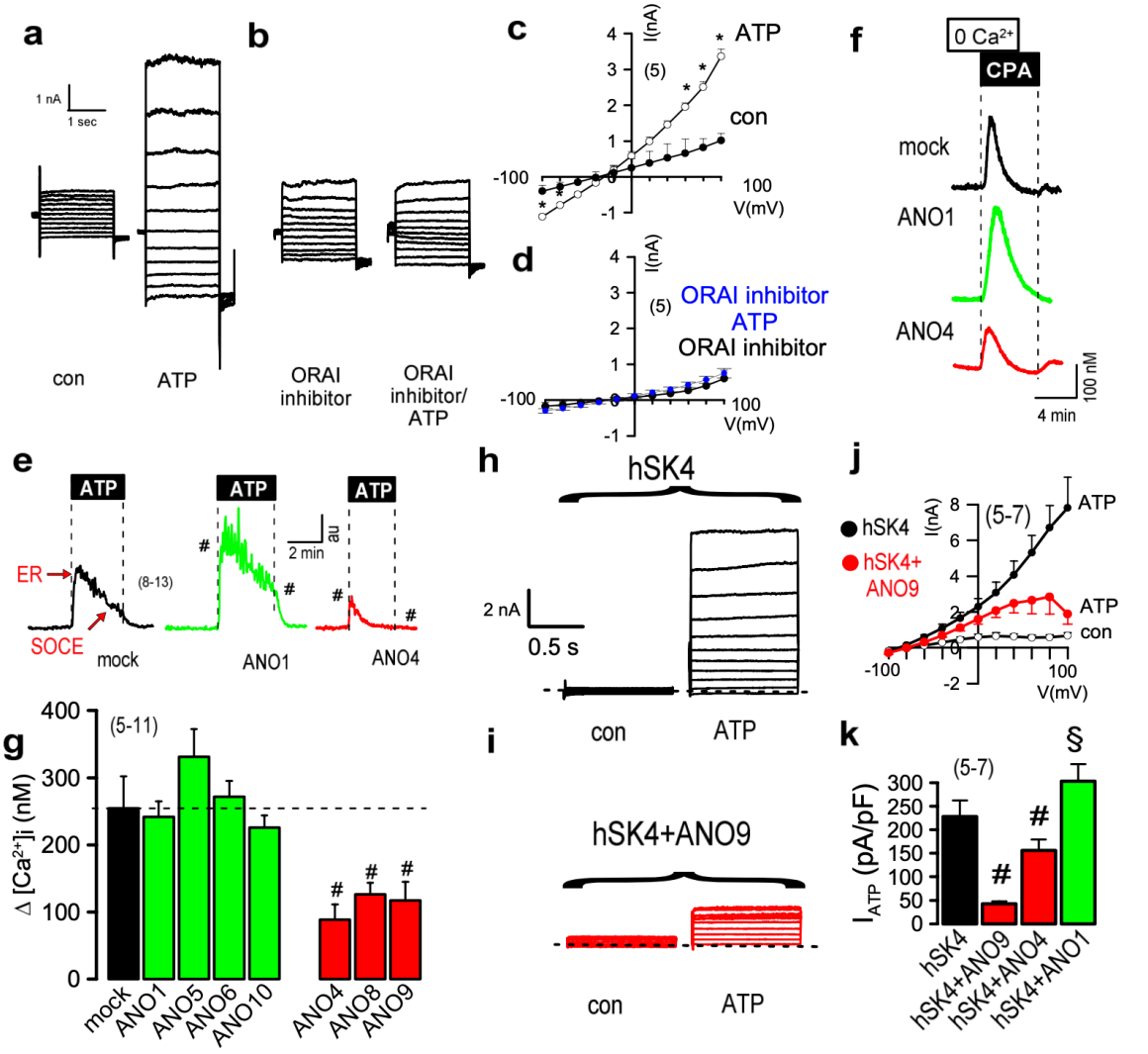

Supplementary Figure 2.2 | *Anoctamins control activation of ion channels through regulation of Ca^{2+} levels.*

a Whole cell currents activated by ATP (100 µM) in ANO4 expressing HeLa cells. **b** Complete suppression of activation of whole cell currents by the ORAI inhibitor YM8483 (5 µM). **c,d** Summary current / voltage relationships of the experiments shown in a,b. **e** ATP (100 µM) induced Ca^{2+} increase measured by Fura-2. Summary recordings for Ca^{2+} store release (ER) and store operated Ca^{2+} entry (SOCE) indicate an increase by ANO1 but decrease by ANO4. **f** Ca^{2+} stores emptying by inhibition of SERCA with cyclopiazonic acid (CPA; 10 µM) in the presence of Ca^{2+} free extracellular buffer. **g** Ca^{2+} store content was not affected by overexpression of ANO1, 5, 6, 10, but was significantly reduced by overexpression of ANO4, 8, 9. **h,i** Whole cell patch clamp currents in HeLa cells overexpressing hSK4 or coexpressing hSK4 with ANO9. Activation of hSK4 by ATP was much reduced in the presence of ANO9. **j** Current voltage relationships indicate reduced activation of hSK4 in cells coexpressing ANO9. **k** Current densities indicating inhibition or amplification of Ba^{2+} sensitive ATP-activated currents, by coexpression of ANO9/ANO4 or ANO1, respectively. Mean ± SEM (number of cells). *significant activation ATP (paired t-test). #significantly different from mock and hSK4 (ANOVA).

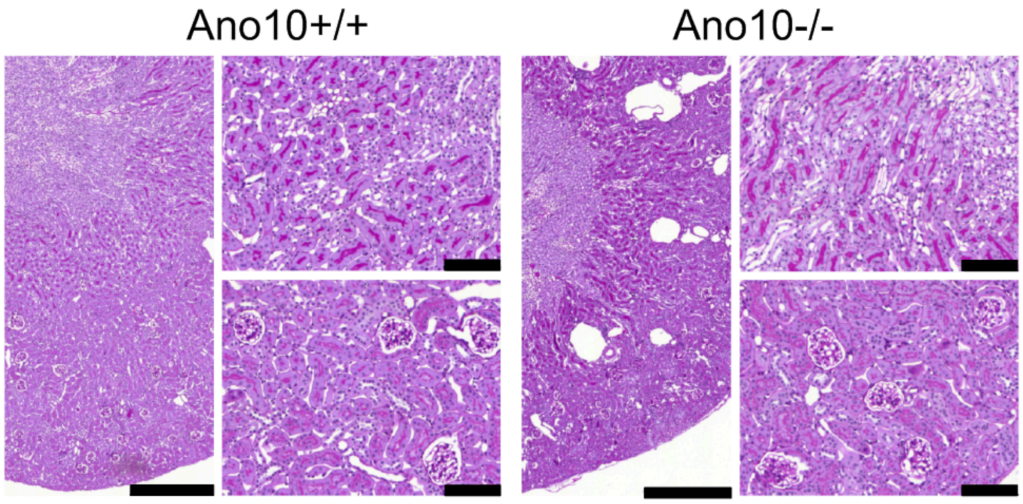

Supplementary Figure 2.3 | *Representative periodic acid-Schiff stainings of kidneys from Ano10$^{+/+}$ and Ano10$^{-/-}$ animals.*

Scale bars indicating 500 µm in overview and 100 µm in detailed view. Mean ± SEM (n = 8-9).

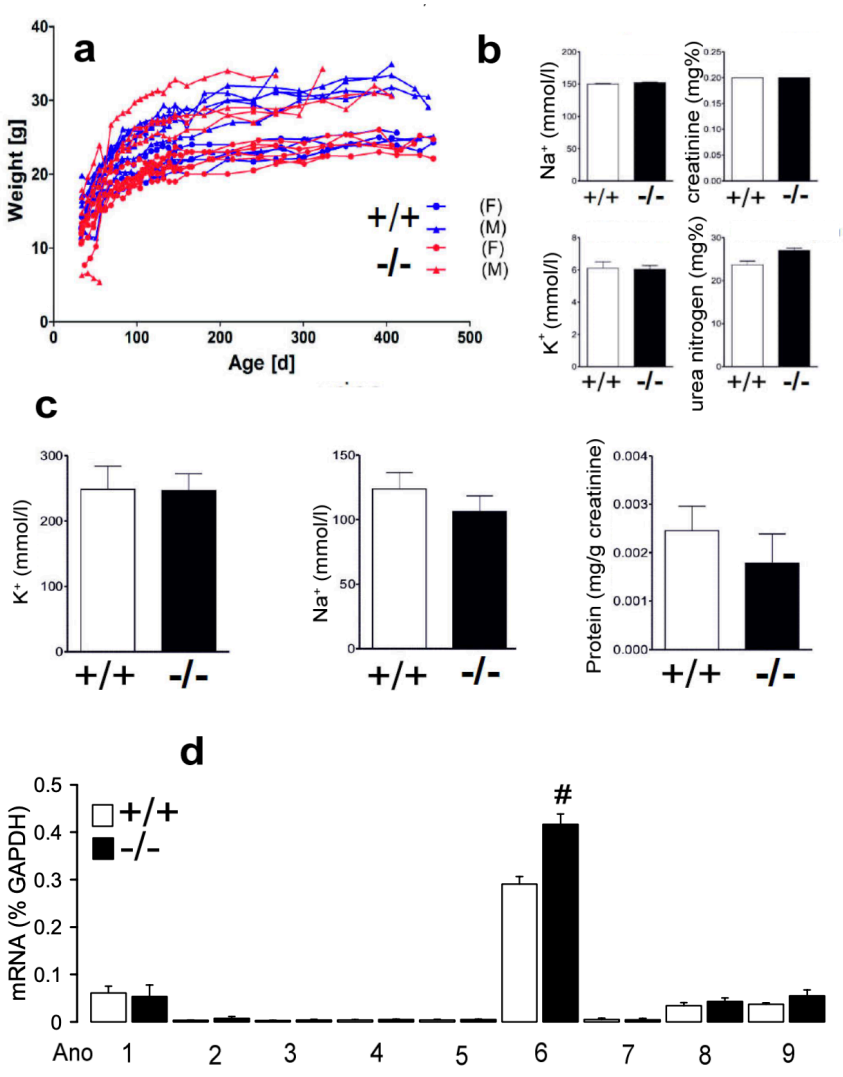

Supplementary Figure 2.4 | *Phenotypic characterization of mice with renal tubular specific Ano10 knockout.*

Nephron-specific knockout was achieved by crossbreeding Ano10$^{loxp/loxp}$ with Six2Cre mice. Knockout

mice ($^{-/-}$) were compared to their Cre-negative littermate controls (+/+). **a** Individual weight gain of $^{+/+}$ (blue) and $^{-/-}$ (red), (circles, female; triangles, male). **b** Serum concentrations for sodium, potassium, creatinine and urea nitrogen (each n = 3). **c** Urine concentrations for potassium, sodium and normalized protein in spontaneous urine (each n = 10). **d** RT-PCR analysis of anoctamin expression in tubular epithelial cells isolated from kidneys of +/+ and -/- animals. Mean ± SEM (n = 8-9), $^{\#}$indicates statistical significance ($p<0.05$).

CHAPTER 3 | CELLULAR DEFECTS BY DELETION OF ANO10 ARE DUE TO DEREGULATED LOCAL CALCIUM SIGNALING

Abstract

TMEM16K (ANO10) belongs to a family of ion channels and phospholipid scramblases. Mutations in ANO10 cause neurological and immunological defects, and abrogated ion transport. Here we show that Ano10 knockout in epithelial cells leads to defective ion transport, attenuated volume regulation and deranged Ca^{2+} signaling. Intestinal epithelial cells from Ano10 null mice are reduced in size and demonstrate an almost abolished spontaneous and TNFα-induced apoptosis. Similar defects were found in mouse peritoneal Ano10 null macrophages and in human THP1 macrophages with reduced ANO10 expression. A cell cycle dependent colocalization of Ano10 with acetylated tubulin, centrioles, and a submembranous tubulin containing compartment was observed in Fisher rat thyroid cells. Axs, the Drosophila ortholog of ANO10 is known for its role in mitotic spindle formation and association with the endoplasmic reticulum and Ca^{2+} signaling. We therefore propose that mutations in ANO10 cause cellular defects and genetic disorders through deranged local Ca^{2+} signaling.

Key words: TMEM16K, Anoctamin 10, ANO10, apoptosis, Ca2+ signaling, ion channels, jejunum, macrophages

Published in: Podchanart Wanitchakool, Jiraporn Ousingsawat, Lalida Sirianant, **Inês Cabrita**, Diana Faria, Rainer Schreiber, Karl Kunzelmann. Cellular Defects by Deletion of ANO10 are due deregulated local Calcium Signaling. Cell Signal. 2016 Nov 30:41-49.
Own experimental contribution: All measurements of $[Ca^{2+}]_i$.
Own written contribution: Methods, Results, Parts of Introduction and Discussion.
Other contributions: Designed experiments and analyzed data.

Introduction

TMEM16K (anoctamin 10; ANO10) is one of 10 members that belongs to a family of proteins that induce Ca^{2+} activated ion currents and membrane phospholipid scrambling [4,8,12,303]. Although Ca^{2+} and volume activated ion currents were found to be upregulated in cells overexpressing ANO10, the cellular role of ANO10 and most of the other anoctamins remains unclear [11,27]. The available data suggest that ANO10 is an intracellular protein that does not operate as a Ca^{2+} dependent phospholipid scramblase [27,265]. Recently, anoctamins have been proposed to control intracellular Ca^{2+} signaling [72]. ANO10 mutations lead to spinocerebellar ataxia [23,25,26] and other genetic disorders [27,28]. Moreover, Ca^{2+} dependent intestinal ion secretion has been shown to be altered in mice with a knockout of Ano10 [37]. Remarkably, the *Drosophila* ortholog of ANO10 Axs is required for meiotic/mitotic spindle formation and associates with an endoplasmic reticulum membrane system that functions in the regulation of cytosolic Ca^{2+} [73,74]. Notably mutations in ANO10 lead to deranged Ca^{2+} signaling in Purkinje cells, which appears to be the most important mechanism causing cerebellar ataxia [23,25,26,75]. The present report presents strong evidence for a role of ANO10 in compartmentalized Ca^{2+} signaling that controls various cellular functions.

Materials and Methods

Animals, isolation of cells. All animal experiments were approved by the local ethics commission of the University of Regensburg and were conducted according to the guidelines of the American Physiological Society and the German law for welfare of animals. Generation of animals with a floxed Ano10 allele has been described in an earlier report [37]. Intestinal epithelial cell specific knockout of ANO10 was achieved by crossbreeding $ANO10^{loxp/loxp}$ with villinCre^{+} mice. Total ANO10 knockouts were produced by crossbreeding $ANO10^{loxp/loxp}$ with pCxCre mice. Results were compared with data obtained from homozygous wild type litter mates. Offsprings were genotyped and tubular ANO10 knockout was verified by RT-PCR and Western blot analysis. To collect mouse intestine, mice were euthanized with CO_2 and immediately followed by cervical dislocation. Mouse intestine was collected from the peritoneal cavity and then washed with ice-cold (Dulbecco's PBS) DPBS. The intestines were stored in ice- cold DPBS for following experiments. Jejunal epithelial cells were isolated using CMF solution containing Ca^{2+} and Mg^{2+} free Hanks balance salt solution (HBSS), 10 mM HEPES, 25 mM $NaHCO_3$, 10% FBS, 1.5 mM EDTA and 0.5 mM dithiothreitol (DTT), pH 7.3. Jejunal segments were cut longitudinally and divided into 4-cm pieces. Tissues were incubated with CMF solution at 37°C for 8 min with gentle agitation (8 times). Cell pellets were centrifuged at 400g for 2 min and washed twice with ice-cold DPBS. Cells were suspended in RPMI1640 medium, supplemented with 10% FBS and kept on ice for further experiments. Peritoneal macrophages were isolated by injection of ice-cold DPBS

into the peritoneal cavity. Cell suspensions were washed once with DPBS and centrifuged at 400g 4°C for 10 min. Cells were resuspended in DPBS, seeded into plates and incubated at 37°C 5% CO_2 incubator for 2h. Attached cells were washed 5 times with DPBS and added RPMI1640 medium, supplemented with 10% FBS, 1% penicillin/streptomycin and 2 mM L-glutamine.

Cells lines, cDNA, RT-PCR. THP1 monocytes were grown in RPMI1640 medium, supplemented with 10% FBS, 1% penicillin/streptomycin as described earlier [16]. Fisher rat TM thyroid (FRT) cells were cultured in Invitrogen's DMEM/F-12-GlutaMAX^{TM}-I medium, supplemented with 5% fetal calf serum and penicillin/streptomycin [3]. HEK293 cells were cultured as described earlier [284]. Generation of cDNAs for ANO10, LRRC8A and AQP3 has been described earlier [3,304,305]. For RT-PCR total RNA was isolated from jejunum and macrophages using NucleoSpin RNA II columns (Macherey-Nagel, Düren, Germany). Total RNA (1 µg / 50 µl reaction) was reverse-transcribed using random primer (Promega, Mannheim, Germany) and M-MLV Reverse Transcriptase RNase H Minus (Promega, Mannheim, Germany). Each RT-PCR reaction contained sense and antisense primer for anoctamins (0.5 µM, see Tables 3.1 and 3.2) or for GAPDH (0.5 µM), 0.5 µl cDNA and GoTaq Polymerase (Promega, Mannheim, Germany). After 2 min at 95°C cDNA was amplified 30 cycles for 30 s at 95°C, 30 s at 57°C and 1 min at 72°C. PCR products were visualized by loading on ethidiumbromide containing agarose gels and analysed using Meta Morph Vers. 6.2 (Molecular Devices, USA).

Table 3.1 | *RT-PCR mouse primer.*

Anoctamin mouse	Primer	Size (bp)
ANO1	Sense: 5'-AGGAATATGAGGGCAACCTG	492
	Antisense: 5'-CGTTGTCACCCTCATAGTCC	
ANO2	Sense: 5'-CCAGAGGAAAGTCGACTATG	544
	Antisense: 5'-GGTAGCATTGTCAAAGAAGG	
ANO3	Sense: 5'-TGATAAAAGAAACACATTTGAAAAGAA	611
	Antisense: 5'-GAGGCTGATGCTTGTACCAC	
ANO4	Sense: 5'-TGGCTTCATTTTTGCTGTTCT	555
	Antisense: 5'-GAAGAGCATGCCTGTGTACC	
ANO5	Sense: 5'-TCCTGAGGAGGCGTCTTATG	548
	Antisense: 5'-CCCAATCTTTTTCTTCCCCTC	
ANO6	Sense: 5'-GTATGAGGCCCAGTGCAATC	519

	Antisense: 5'-TCTTCGCTTCTGTATTTGCC	
ANO7	Sense: 5'-TTGGAATCCGAAATGAGGAG	584
	Antisense: 5'-GTGTGCGGAGGTGAAAGTG	
ANO8	Sense: 5'-CTTGGAGGACCAGCCAATC	682
	Antisense: 5'-CTTCTTGTAGCCCTCAGCAC	
ANO9	Sense: 5'-CAAGATGTTAAAGGACCAGAAG	487
	Antisense: 5'-GAAGATATCATTGGCACTACAG	
ANO10	Sense: 5'-GGACATGAAGCTTTTGCGCC	478
	Antisense: 5'-CCAACACTTTCAGAACGAGATG	
ANO10	Sense: 5'-GGACATGAAGCTTTTGCGCC	WT 522
	Antisense: 5'-GGCAATGTAGAAGAGTGAGGC	KO 648
GAPDH	Sense: 5'-GTATTGGGCGCCTGGTCAC	200
	Antisense: 5'-CTCCTGGAAGATGGTGATGG	

Table 3.2 | *RT-PCR human primer.*

Anoctamin human	Primer	Size (bp)
ANO1	Sense: 5'-CGACTACGTGTACATTTTCCG	445
	Antisense: 5'-GATTCCGATGTCTTTGGCTC	
ANO2	Sense: 5'-GTCTCAAGATGCCAGGTCCC	544
	Antisense: 5'-CTGCCTCCTGCTTTGATCTC	
ANO3	Sense: 5'-CTTCCCTCTTCCAGTCAAC	461
	Antisense: 5'-AAACATGATATCGGGGCTTG	
ANO4	Sense: 5'-CGGAAGATTTACAGGACACCC	503
	Antisense: 5'-GATAACAGAGAGAATTCCAATGC	
ANO5	Sense: 5'-GAATGGGACCTGGTGGAC 713	713
	Antisense: 5'-GAGTTTGTCCGAGCTTTTCG	
ANO6	Sense: 5'-GGAGTTTTGGAAGCGACGC	325
	Antisense: 5'-GTATTTCTGGATTGGGTCTG	
ANO7	Sense: 5'-CTCGGGAGTGACAACCAGG	470

	Antisense: 5'-CAAAGTGGGCACATCTCGAAG	
ANO8	Sense: 5'-GGAGGACCAGCCAATCATC	705
	Antisense: 5'-TCCATGTCATTGAGCCAG	
ANO9	Sense: 5'-GCAGCCAGTTGATGAAATC	472
	Antisense: 5'-GCTGCGTAGGTAGGAGTGC	
ANO10	Sense: 5'-GTGAAGAGGAAGGTGCAGG	769
	Antisense: 5'-GCCACTGCGAAACTGAGAAG	
GAPDH	Sense: 5'-GTATTGGGCGCCTGGTCAC	200
	Antisense: 5'-CTCCTGGAAGATGGTGATGG	

siRNA, solutions, materials and statistical analysis. Cells were transfected with siRNA for ANO10 and scrambled RNA, respectively using lipofectamine (Invitrogen). The sequence of the siRNA for ANO10 was 5'-CGAUGAGUGUUAUAUCUGUtt, and 5'-ACAGAUAUAACACUCAUCGtt. All experiments were performed 48 h after the transfection. For most experiments cells were kept initially in HCO3-free ringer solution (mM): NaCl 145, KH_2PO_4 0.4, K_2HPO_4 1.6, D-glucose 5, $MgCl_2$ 1, calcium gluconate 1.3, pH 7.4. For cell swelling experiments, cells were exposed initially to ringer solution, which was then replaced by an isotonic solution containing (mmol/l) NaCl 95, mannitol 100, KH_2PO_4 0.4, K_2HPO_4 1.6, D-glucose 5, $MgCl_2$ 1, calcium gluconate 1.3, pH 7.4. To induce cell swelling a hypotonic solution (Hypo) (200 mosmol/l) was produced by removal of mannitol. Osmolarity was measured using an osmometer. All compounds (3-Isobutyl-1-methyl xanthine (IBMX), forskolin, carbachol (CCH), TNFα, cisplatin, trichostatin A (TSA), and 5-nitro-2-[(3-phenylpropyl)amino]benzoic acid (NPPB) were of highest available grade of purity and were from Sigma or Merck. NS3728 was a generous gift by NeuroSearch (Ballerup, Denmark). Student's *t* test for unpaired samples was used for statistical analysis. $p < 0.05$ was accepted as significant difference.

Western Blotting, coimmunoprecipitation, biotinylation. Expression of ANO10 in isolated intestinal (jejunal) epithelial cells, THP1 and FRT cells, as well as siRNA-knockdown of endogenous expression of Ano10 was validated by Western blotting. Protein was isolated from transfected cells in a lysis buffer containing 50 mM Tris-HCl, 150 mM NaCl, 50 mM Tris, 100 mM dithiothreitol, 1% Nonidet P-40, 0.5% deoxycholate sodium, and 1% protease inhibitor mixture (Roche), separated by 8.5 % SDS-PAGE and transferred to a polyvinyl membrane (GE Healthcare, Munich, Germany). Membranes were incubated with primary antibodies at a dilution of 1:1000 overnight at 4 °C. Proteins were visualized using horseradish peroxidase-conjugated secondary antibody and ECL detection. Antibodies

against ANO10 and LRRC8A were from Aviva System Biology and Sigma, respectively.

For coimmunoprecipitation of LRRC8A and ANO10. HEK293 cells were transfected with LRRC8A and ANO10-GFP/ANO10L384fs-GFP for 3 days. Protein was collected in 0.5% CHAPs in HEPES lysis buffer containing 1% protease inhibitor mixture. Proteins (300 µg) were pulled down with rabbit anti-LRRC8A (sigma) or goat anti-GFP (Rockland) at 4°C for 2h, followed by adding 60 µl protein G agarose (Thermo Scientific) and further incubated at 4°C for 1h. Pellets were washed twice with CHAPs buffer and centrifuged at 3000 rpm at 4°C for 5 min. Pellets were once washed again with wash buffer and centrifuged at 14,000 rpm at 4°C for 15 min. Protein was eluted by adding 50 µl 2xsample buffer and then analysed by western blotting.

Biotinylation experiments were performed using cell surface biotinylation assay (Thermo Scientific). Cells were washed twice with ice-cold Ca^{2+}/Mg^{2+} PBS and then exposed to Sulfo-NHS-SS-Biotin solution at 4°C for 30 min. The reactions were stopped by quenching solution. Cells were harvested and lysed in 0.5% NP-40 lysis buffer. Proteins were incubated with NeutrAvidin agarose for 1 h at room temperature. The beads were washed five times with wash buffer and eluted by SDS-PAGE sample buffer containing 50 mM DTT. The biotinylation samples were analysed by western blotting.

Immunohistochemistry, TUNEL and HE histology. Mouse intestine was fixed with 4 % paraformaldehyde (PFA) and post-fixed in 0.5 mol/l sucrose, 4 % PFA solution. Cryosections of 5 µm were incubated in 0.1 % SDS for 5 min, washed with PBS, and blocked with 5 % bovine serum albumin (BSA) and 0.04 % Triton X-100 in PBS for 30 min. Sections were incubated with primary antibodies against ANO10 (ARP47389, Aviva System Bio) in 0.5 % BSA and 0.04 % Triton X-100 overnight at 4 °C and with Alexa Fluor 488 labeled donkey anti rabbit IgG (Molecular Probes, ThermoFisher Scientific). Sections were counterstained with Hoe33342 (Sigma-Aldrich). Immunofluorescence was detected using an Axiovert 200 microscope equipped with ApoTome and Axio-Vision (Zeiss, Germany). For HE histology, Terminal deoxynucleotidyl transferase dUTP nick end labeling (TUNEL), staining of Ki67 and acetylated tubulin PFA fixed tissue embedded in paraffin or PFA fixed FRT cells on coverslips were used. Hematoxylin eosin stainings were done be standard technique. Cell area was determined using an Axiovert 200 microscope and Axio-Vision software (Zeiss, Germany). For TUNEL assay the DeadEnd Fluorometrie TUNEL system (Promega, Germany) was used according manufacturer´s instructions. To detected Ki67 positive cells a rat anti-Ki67 antibody from DAKO (M7249, Germany) and a goat anti rat Alexa Fluor 546 antibody (Molecular Probes, ThermoFisher Scientific) were used. Acetylated Tubulin was visualized using a monoclonal anti-acetylated tubulin antibody produced in mouse (T7451, Sigma-Aldrich, Germany). Immunofluorescence was detected using an Axiovert 200 microscope equipped with ApoTome and analysed with Axio-Vision software (Zeiss, Germany).

Caspase assay. Caspase assays were performed using Caspase-Glo® 3/7 assay (Promega,

Madison, WI), according to the manufacturer's protocol. Cells were incubated with luminogenic caspase3/7 substrate for 30 min in room temperature after incubation with 10 ng/ml TNFα for 14 h. The luminescence was measured using a microplate-reading Luminometer (Beckman Coulter).

Assessment of intracellular calcium concentrations in intestinal epithelial cells. Intracellular Ca^{2+} concentrations were assessed in isolated intestinal epithelial cells by Fura2 fluorescence as described earlier [37]. In brief cells were seeded on glass cover slips and loaded with 2 µM Fura-2/AM and 0.02 % Pluronic F-127 (Invitrogen, Darmstadt, Germany) in ringer solution (mmol/l: NaCl 145; KH_2PO_4 0,4; K_2HPO_4 1,6; Glucose 5; $MgCl_2$ 1; Ca^{2+}-Gluconat 1,3) for 1h at room temperature. Fluorescence was detected in cells perfused with Ringer's solution at 37 °C using an inverted microscope (Axiovert S100, Zeiss, Germany) and a high speed polychromator system (VisiChrome, Puchheim, Germany). Fura-2 was excited at 340/380 nm, and emission was recorded between 470 and 550 nm using a CoolSnap camera (CoolSnap HQ, Visitron). $[Ca^{2+}]_i$ was calculated from the 340/380 nm fluorescence ratio after background subtraction. The formula used to calculate $[Ca^{2+}]_i$ was $[Ca^{2+}]_i$ =Kd x (R-Rmin)/(Rmax-R) x (Sf2/Sb2), where R is the observed fluorescence ratio. The values Rmax and Rmin (maximum and minimum ratios) and the constant Sf2/Sb2 (fluorescence of free and Ca^{2+}-bound Fura-2 at 380 nm) were calculated using 1 µM ionomycin (Calbiochem), 5 µM nigericin, 10 µM monensin (Sigma), and 5 mM EGTA to equilibrate intracellular and extracellular Ca^{2+} in intact Fura-2-loaded cells. The dissociation constant for the Fura-2•Ca^{2+} complex was taken as 224 nmol/liter. Control of experiment, imaging acquisition, and data analysis were done with the software package Meta- Fluor (Molecular Devices, USA) and Origin (OriginLab Corporation, USA).

Cell volume measurements by flow cytometry. THP1 and FRT cells were trypsinized, washed and re-dissolved in 10 ml isotonic or hypotonic ringer solution (Hypo) as described above. Cells were analyzed at 37 °C / pH 7.4 using a CASY flow cytometer (Roche Diagnostics, Mannheim, Germany).

Ussing chamber. Mice were killed after exposure to CO_2, and the jejunum, was removed. Stripped intestinal sections were put into ice-cold Ringer bath solution (in mM; NaCl 145, KH_2PO_4 0.4, K_2HPO_4 1.6, D-glucose 6, $MgCl_2$ 1, Ca^{2+}-gluconate 1.3, pH 7.4) containing indomethacin (10 µM). Tissues were mounted into a micro-perfused Ussing chamber with a circular aperture of 0.785 mm^2. Luminal and basolateral sides of the epithelium were perfused continuously at a rate of 5 ml/min. Bath solutions were heated to 37 °C, using a water jacket. Experiments were carried out under open circuit conditions. Data were collected continuously using PowerLab (AD Instruments, Australia). Values for transepithelial voltages (V_{te}) were referred to the serosal side of the epithelium. Transepithelial resistance (R_{te}) was determined by applying short (1 s) current pulses (ΔI=0.5 µA). R_{te} and equivalent short circuit currents (I'SC) were calculated according to

Ohm's law ($R_{te}=\Delta V_{te}/\Delta I$, $I'SC=V_{te}/R_{te}$).

Patch Clamping. For patch clamping, isolated intestinal crypts were immobilized on polylysine- coated cover slips. FRT cells were grown on glass cover slips. Patch pipettes were filled with a cytosolic-like solution containing KCl 30, K -gluconate 95, NaH_2PO_4 1.2, Na_2HPO_4 4.8, EGTA 1, Ca^{2+}-gluconate 0.758, $MgCl_2$ 1.03, D-glucose 5, ATP 3, pH 7.2. The Ca^{2+} activity was 0.1 µM. Coverslips were mounted in a perfused bath chamber on the stage of an inverted microscope (IM35, Zeiss) and kept at 37 °C. The bath was perfused continuously with Ringer solution at a rate of 8 ml/min. For activation of volume dependent Cl^- currents, Ringer bath solution was first changed to Iso and then to Hypo (c.f. above). Patch clamp experiments were performed in the fast whole cell configuration. Patch pipettes had an input resistance of around 4 MΩ when filled with the cytosolic like (physiological) solution. The access conductance was monitored continuously and was 60–140 nS. Currents (voltage clamp) and voltages (current clamp) were recorded using a patch clamp amplifier (EPC 7, List Medical Electronics, Darmstadt, Germany), the LIH1600 interface and PULSE software (HEKA, Lambrecht, Germany) as well as Chart software (AD Instruments, Spechbach, Germany). Data were stored continuously on a computer hard disc and analyzed using PULSE software. In regular intervals, membrane voltage (*Vc*) was clamped from a holding voltage of -100 mV in steps of 20 mV from -100 to +100 mV. Current density was calculated by dividing whole cell currents by cell capacitance.

Double electrode voltage clamping. Oocytes were injected with cRNA encoding aquaporin 3 (0.5 ng), or coinjected with cRNA for AQP3 and Ano10 (5 ng). Water injected oocytes served as controls. 2 – 4 days after injection, oocytes were impaled with two electrodes (Clark Instruments Ltd, Salisbury, UK), which had resistances of < 1 MΩ when filled with 2.7 mol/l KCl. Using two bath electrodes and a virtual-ground head stage, the voltage drop across the serial resistance was effectively zero. Membrane currents were measured by voltage clamping (oocyte clamp amplifier, Warner Instruments LLC, Hamden CT) in intervals from -80 to +60 mV, in steps of 20 mV, each 1 s. The bath was continuously perfused at a rate of 5 ml/min. All experiments were conducted at 22 °C.

Results

Abnormal cell size and volume regulation in intestinal epithelial cells lacking Ano10. Ano10 was knocked out in a tissue specific manner in intestinal epithelial cells [37]. As shown in Fig. 3.1a-c, expression of Ano10 mRNA and Ano10 protein were completely absent in isolated intestinal epithelial cells of Ano10 null mice. Ano6 - 9 were also expressed in epithelial cells and were not different in cells from knockout animals (Fig. 3.1c). We examined expression of Ano10 along the intestinal epithelium and found pronounced expression in cells of the small intestine (particularly jejunum), while in the large intestine only occasionally cells were found to be positive for Ano10 (Fig. 3.1d). No staining was

detected in Ano10 null mice. Analysis of hematoxylin/eosin-stained tissues suggested a reduced size of epithelial cells of the small intestine from Ano10-/- mice (Fig. 3.1e). This this difference was not seen in epithelial cells of the large intestine (not shown). The different cell size of jejunal epithelial cells was validated by analyzing cell area (Fig. 3.1f) and by measuring the volume of isolated intestinal epithelial cells using flow cytometry (Fig. 3.1g). The data clearly indicate much smaller cells in the jejunum of Ano10-/- mice. Moreover, normal swelling and volume regulation (regulatory volume decrease in the presence of an extracellular hypotonic bath solution; Hypo) was absent in the Ano10 null cells. These data suggest a cellular defect caused by lack of Ano10 expression. Surprisingly and despite these defects, Ano10-/- animals developed normally and showed uncompromised weight gain (Fig. 3.1h). No gross abnormalities were detected when inspecting the animals and the intestine appeared normal.

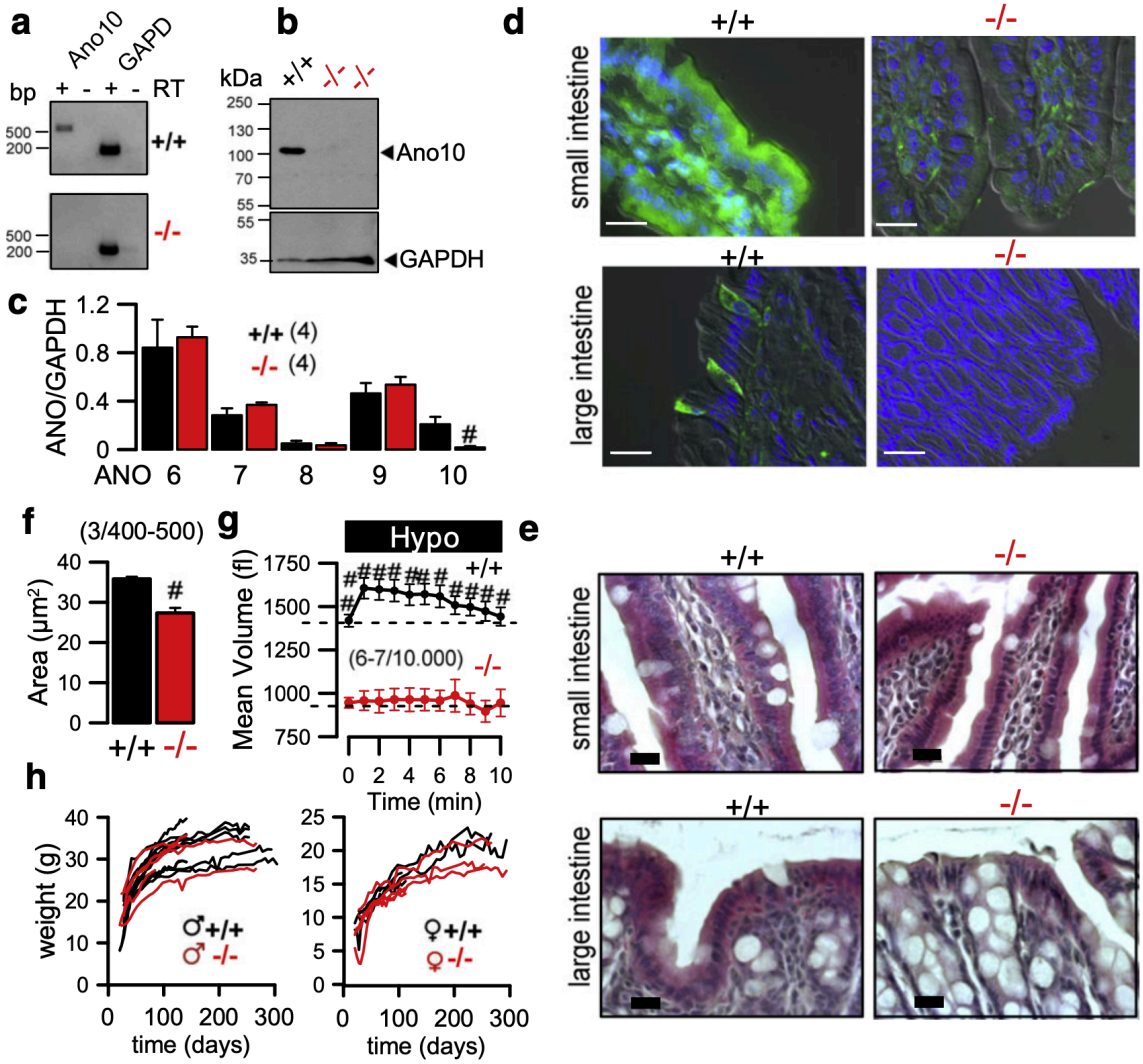

Figure 3.1 | *Cellular abnormalities in jejunum of Ano10-/- mice.*

a,b Analysis of Ano10 expression by RT-PCR (A) and Western blotting (B) in wild type (+/+) and Ano10 knockout (-/-) animals. RT = reverse transcriptase. Blots were performed as replicates. **c**

Semiquantitative analysis of the expression of different anoctamins in mouse jejunum. **d** Immunohistochemistry of Ano10 in jejunum of +/+ and -/- animals. Bars indicate 20 µm. **e** HE staining of jejunal epithelium of Ano10+/+ and -/- animals. Bars indicate 10 µm. **f** Measured area indicates reduced size of epithelial cells from Ano10-/- animals. **g** Largely reduced cell volume and attenuated regulatory volume decrease (RVD) in the presence of hypotonic bath solution (200 mosmol/l) in freshly isolated jejunal epithelial cells from Ano10-/- animals. **h** Weight gain of Ano10+/+ and -/- male and female animals. Mean ± SEM; (n/n) = number of animals/cells per animal measured. #significantly different from +/+ animals (paired *t*-test).

Abnormal cellular functions by deranged Ca^{2+} signaling in intestinal epithelial cells lacking Ano10. Recent studies suggest that anoctamins affect intracellular Ca^{2+} signaling by operating as Ca^{2+} channels or by controlling Ca^{2+} release from intracellular endoplasmic reticulum (ER) stores [14,72]. We compared the ER in jejunal epithelial cells from wt and Ano10-/- animals using calreticulin staining, but did not recognize any obvious difference (Fig. 3.2a). Nevertheless, when measuring intracellular Ca^{2+} levels we found reduced basal Ca^{2+} levels and attenuated agonist-induced Ca^{2+} increase in Ano10-/- cells (Fig. 3.2b-d). In these experiments, ATP was used to stimulate purinergic receptors which led to release of Ca^{2+} from ER stores (peak) and activation of store operated Ca^{2+} influx (plateau). Both components were reduced in Ano10-/- cells (Fig. 3.2b-d). Jejunal mucosa was mounted in perfused micro Ussing chambers to measure transepithelial potentials under open circuit conditions, indicative for epithelial transport [37]. We found that activation of ion transport by stimulation of basolateral muscarinic receptors by carbachol (CCH), or by exposure to hypotonic bath solution (Hypo), were largely attenuated in Ano10-/- mucosa (Fig. 3.2e). Moreover, in whole cell patch clamp recordings form isolated jejunal epithelial cells, currents could be activated by CCH and cell swelling (Hypo) in wild type but not Ano10-/- cells (Fig. 3.2f,g). Notably, ion transport activated by increase in intracellular cAMP was also compromised in Ano10-/- cells, which was probably due to altered Ca^{2+}-dependent activation of basolateral KCNN4 K^+ channels that are necessary for maintaining the driving force for Cl- secretion [306] (data not shown). As both CCH-induced and swelling (Hypo) activated whole cell currents require intracellular Ca^{2+} to be activated, these data suggest compromised Ca^{2+} signaling in the absence of Ano10.

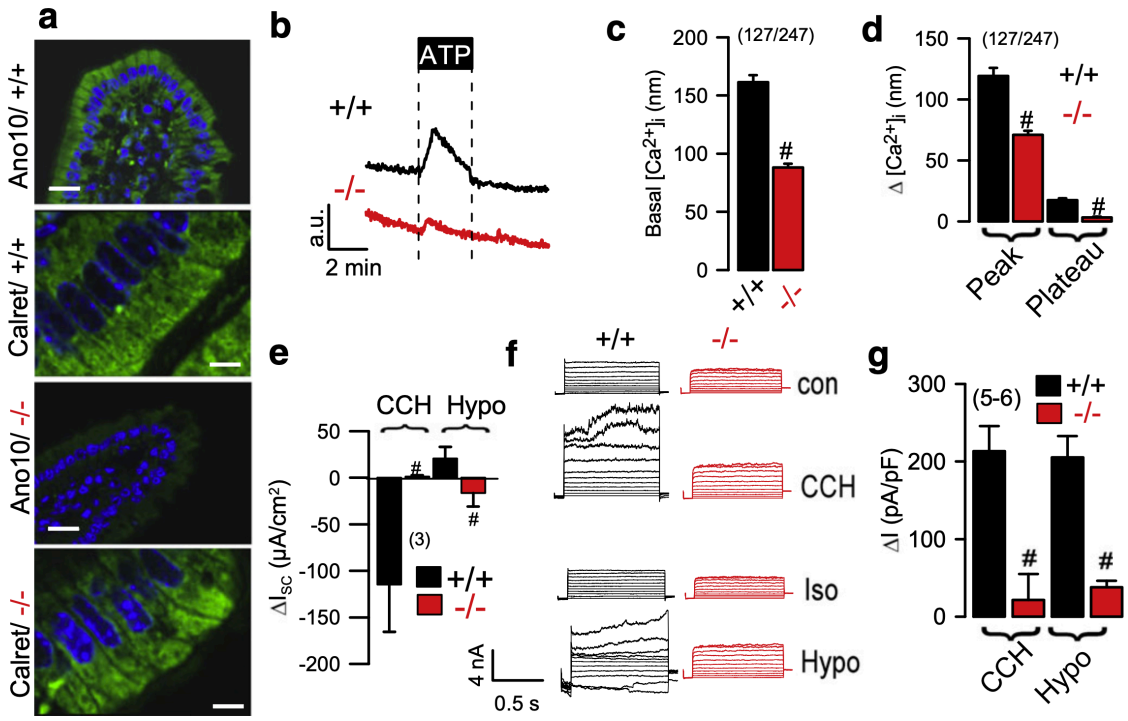

Figure 3.2 | *Ca^{2+} signals and ion transport in jejunum of Ano10-/- mice.*

a Ano10, ER and acetylated tubulin in jejunal epithelial cells from wild type animals and Ano10 KO animals. **b** Recording of intracellular Ca^{2+} (Fura2; 340/380 ratio) upon stimulation by the purinergic agonist ATP (100 µM) in freshly isolated jejunal epithelial cells of +/+ and -/- animals. **C** Summary of intracellular Ca2+ concentrations assessed under control conditions (basal Ca^{2+}) in freshly isolated jejunal epithelial cells of +/+ and -/- animals. **d** Summary of ATP-induced peak and plateau Ca^{2+} in +/+ and -/- cells. **e** Summary of equivalent short circuit currents activated by carbachol /CCH; 100 µM), and hypotonic bath solution (Hypo; 200 mosmol/l), respectively, in jejunum of +/+ and -/- animals. **f** Whole cell patch clamp recordings from freshly isolated jejunal epithelial cells of +/+ and -/- animals. **g** Summary of whole cell currents (current density) activated by carbachol and hypotonic bath solutions, respectively. Mean ± SEM; (n) = number of cells and tissues, which were obtained from 3-5 different animals. #Significantly different from +/+ animals (paired *t*-test).

Ano10 is essential for apoptosis. Intracellular Ca^{2+} levels are a crucial for cell growth and for regulated cell death as in apoptosis [307]. We therefore examined proliferation using the marker Ki67 and assessed apoptosis using TUNEL assays. While proliferation was undisturbed in Ano10-/- jejunum, the number of apoptotic cells was largely reduced (Fig. 3.3a-c). Moreover, TNFα-induced caspase-3 activity was strongly attenuated in isolated jejunal epithelial cells from Ano10-/- mice (Fig. 3.3d). To determine whether Ano10 is relevant for extrinsic apoptosis also in other mouse tissues, we generated Ano10-knockout macrophages by crossbreeding mice with a floxed Ano10 allele with pCxCre mice (Fig. 3.3e). Indeed, freshly isolated peritoneal Ano10-/- macrophages demonstrated almost abolished TNFα-induced caspase-3 activity (Fig. 3.3f). Notably, Ano10 was found to be strictly

colocalized with acetylated tubulin in mouse macrophages, similar to colocalization of the Drosophila ortholog of Ano10, Axs with acetylated tubulin [74] (Fig. 3.3g).

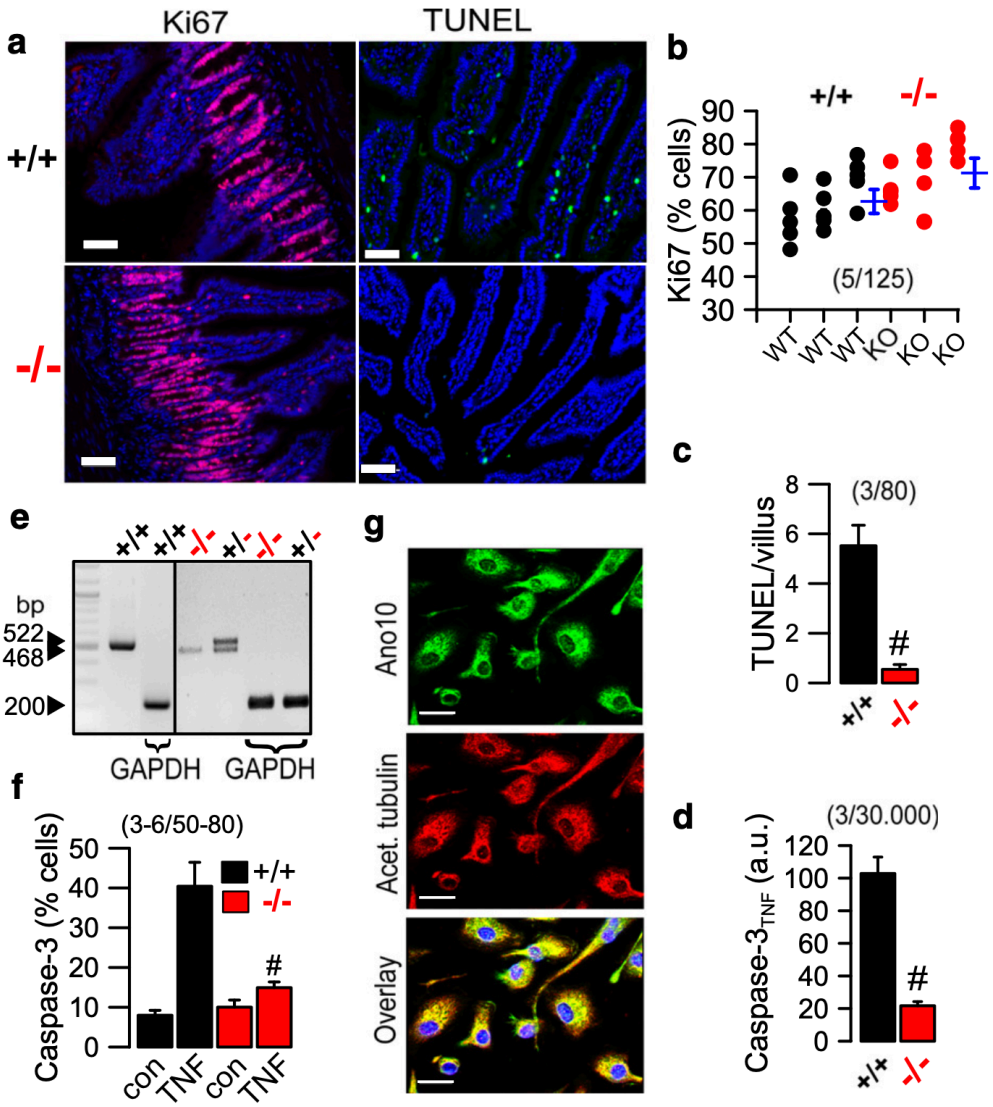

Figure 3.3 | *Abnormal apoptosis in jejunal epithelial cells and macrophages of Ano10 knockout animals.*

a Immunohistochemistry of the proliferation marker Ki67 and terminal deoxynucleotidyl transferase dUTP nick and labeling (TUNEL) in jejunal epithelium of +/+ and -/- mice. Bars indicate 50 µm. **b** Percentage of Ki67 positive cells per crypt of +/+ and -/- mice. Each dot indicates one section with 25 crypts being analysed. **c** Number of TUNEL positive cells per villus. 80 villi have been examined in each of 3 +/+ and 3 -/- animals. **d** Number of caspase-3 positive jejunal epithelial cells upon treatment with TNFα (10 ng/ml 14 h). Experiments were performed in triplicates with each 30.000 cells. **e** Genotyping of Ano10 null mice be crossbreeding $Ano10^{lox/loxp}$ with pCxCre mice. **f** Caspase 3 positive peritoneal macrophages from +/+ and -/- animals, upon stimulation with TNFα (100 ng/ml 6 h). Macrophages were isolated from 3 to 6 animals and between 100 and 150 macrophages were analysed per image. **g** Immunocytochemistry of Ano10 and acetylated tubulin in freshly isolated mouse macrophages. Bars indicate 20 µm. Mean ± SEM. #Significantly different from +/+ animals

(paired *t*-test). Blots were performed as replicates.

The role of ANO10 for apoptotic cell death was further elucidated in human THP1 monocytes/macrophages. The in vivo life spans for monocytes and macrophages differ remarkably, ranging from a few days for monocytes up to several years for macrophages [308]. THP1 monocytes (MC) can be transdifferentiated into macrophages (MP) by treatment with phorbolesters. Interestingly the expression level of ANO10 dropped largely upon differentiation to macrophages (Fig. 3.4a,b,g). The change from MC to MP and loss of ANO10 expression was paralleled by a loss in TNFα-induced caspase-3 activity (Fig. 3.4c). Moreover, regulatory volume decrease (RVD) in the presence of hypotonic bath solution was significantly attenuated in MP (Fig. 3.4d). The link between high/low ANO10 expression and high/low rate of apoptosis in MC/MP was further corroborated by siRNA-knockdown of ANO10 in MC, which significantly inhibited TNFα-induced caspase-3 activity (Fig. 3.4f). In contrast, TNFα-induced caspase-3 activity was partially recovered in MP by overexpression of ANO10 (Fig. 3.4f). These data clearly indicate that ANO10 is a protein crucial for apoptotic cell death.

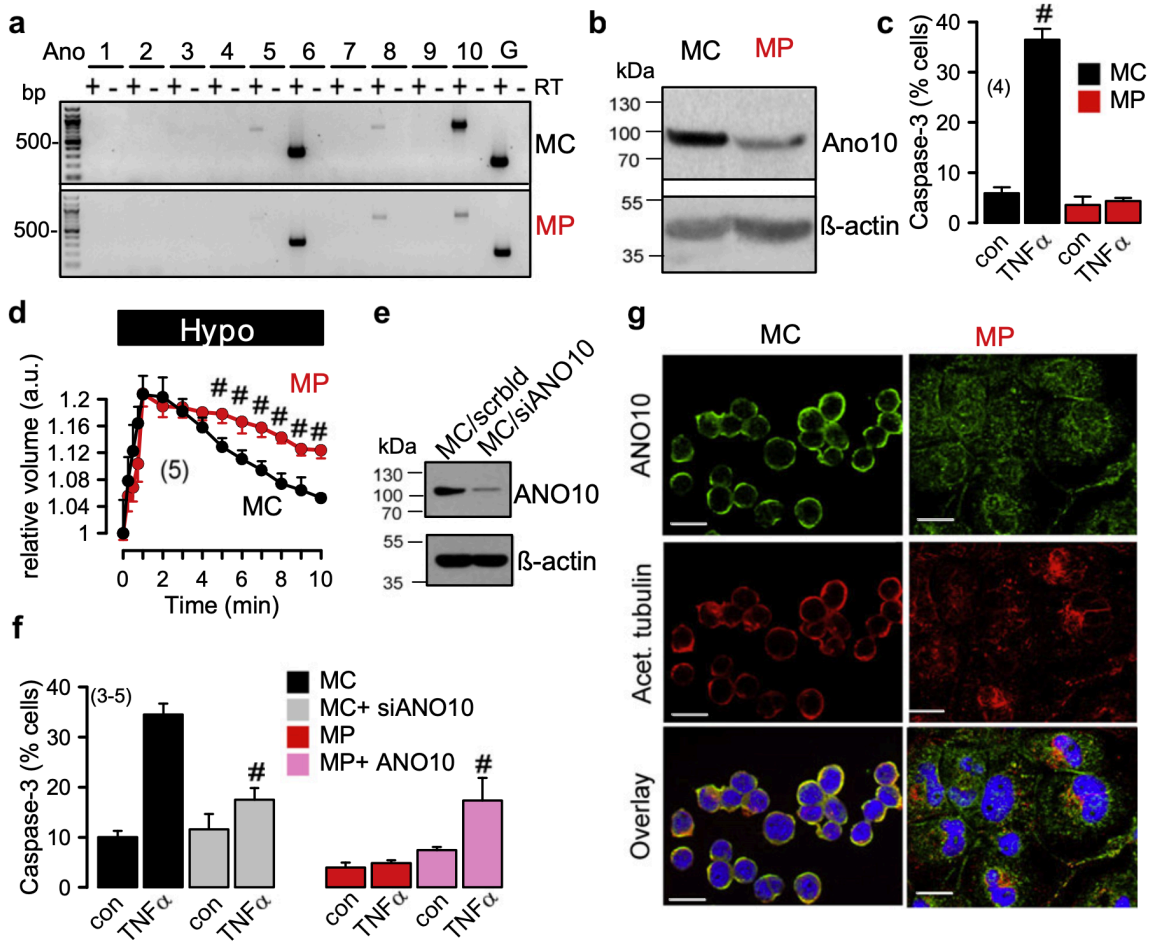

Figure 3.4 | *Reduced expression of Ano10 in TPH1 macrophages attenuates regulatory volume decrease and caspase 3 activity.*

a Analysis of expression of anoctamin 1-10 in THP1 monocytes (MC) and THP1 macrophages (transdifferentiated by culturing in 100 nM phorbol-12-myristat-13-acetat; PMA) (MP). **b** Expression of ANO10 in THP1-MC and THP1-MP, as detected by Western blotting. **c** Caspase 3 positivity of THP1-MC and THP1-MP upon stimulation with TNFα (100 ng/ml 6 h). About 500 cells were counted in quadruplicates. **d** Attenuated regulatory volume decrease (RVD) in THP1-MP when compared to THP1-MP, in the presence of hypotonic bath solution (200 mosmol/l). **e** Western blotting of ANO10 indicating knockdown of expression by siRNA-ANO10. Blots were performed as replicates. **f** Percentage of caspase-3 positive cells after treatment with TNFα (100 ng/ml 6 h). Knockdown of ANO10 inhibited TNFα-induced cell death of THP1-MC, while overexpression of ANO10 in THP1-MP enabled TNFα-induced cell death. **g** Immunocytochemistry of ANO10 and acetylated tubulin in freshly THP1-MC and THP1-MP. About 500 cells were counted in 4-5 repeats. Mean ± SEM. #Significantly different from +/+ animals (paired *t*-test). Blots were performed as replicates. Bars indicate 20 µm.

Loss of ANO10 leads to loss of apoptotic cell death and compromised volume regulation. Cisplatin is a common anticancer drug that induces apoptotic cell death in cancer cells [309]. It has been shown earlier that cancer cells which become resistant towards cisplatin, lose their ability to shrink upon apoptotic stimulation (loss of apoptotic volume decrease; AVD). AVD is known as a basic requirement for apoptotic cells death [310-313]. Typically loss of AVD is paralleled by attenuated regulatory volume decrease (RVD) and both types of volume changes (AVD, RVD) require the activity of volume activated Cl^- channels (VRAC), which have now been identified as LRRC8 [314,315]. LRRC8 channels take up cisplatin and induce cell shrinkage [316]. We exposed Fisher rat thyroid (FTR) cells to cisplatin, which induced apoptotic cell death.

Surviving cisplatin resistant cells demonstrated a complete loss of Ano10 expression (Fig. 3.5a), and showed largely abrogated volume regulation (RVD; Fig. 3.5b), and strongly reduced VRAC currents (Fig. 3.5c,d). To further demonstrate the role of Ano10 for activation of VRAC, we knocked down Ano10 in FRT cells by siRNA, which largely inhibited VRAC (I_{Hypo}; Fig. 3.5e,f). Moreover the inhibitor of histone deacetylase trichostatin A (TSA), which has been shown earlier to recover VRAC [311,317], partially recovered expression of Ano10, VRAC, and RVD in FRT cells (Fig. 3.5a,f,g). Thus, apoptotic cell shrinkage and RVD require Ano10, which explains defective volume regulation in intestinal cells, macrophages and FRT cells lacking Ano10 expression. Further support for a role of ANO10 in volume regulation came from experiments in ANO10- expressing Xenopus oocytes (Supplementary Fig. 3.1).

Cell growth dependent expression of ANO10. Our data indicate colocalization of Ano10 with acetylated tubulin, suggesting a functional link between Ano10 and tubulin (Figs. 3.3-4). We found that Ano10 was upregulated in proliferating cells, particularly during mitosis where it was found to be colocalized in close proximity with the spindle apparatus and the

centrosome (Fig. 3.5h,i). In contrast, in non-proliferating FRT monolayers (kept under serum free conditions), expression of Ano10 was downregulated and was restricted to plasma membrane and centrioles (Fig. 3.5j). Additional data from membrane biotinylation confirmed that ANO10 is indeed an intracellular protein located underneath the plasma membrane (Supplementary Fig. 3.2).

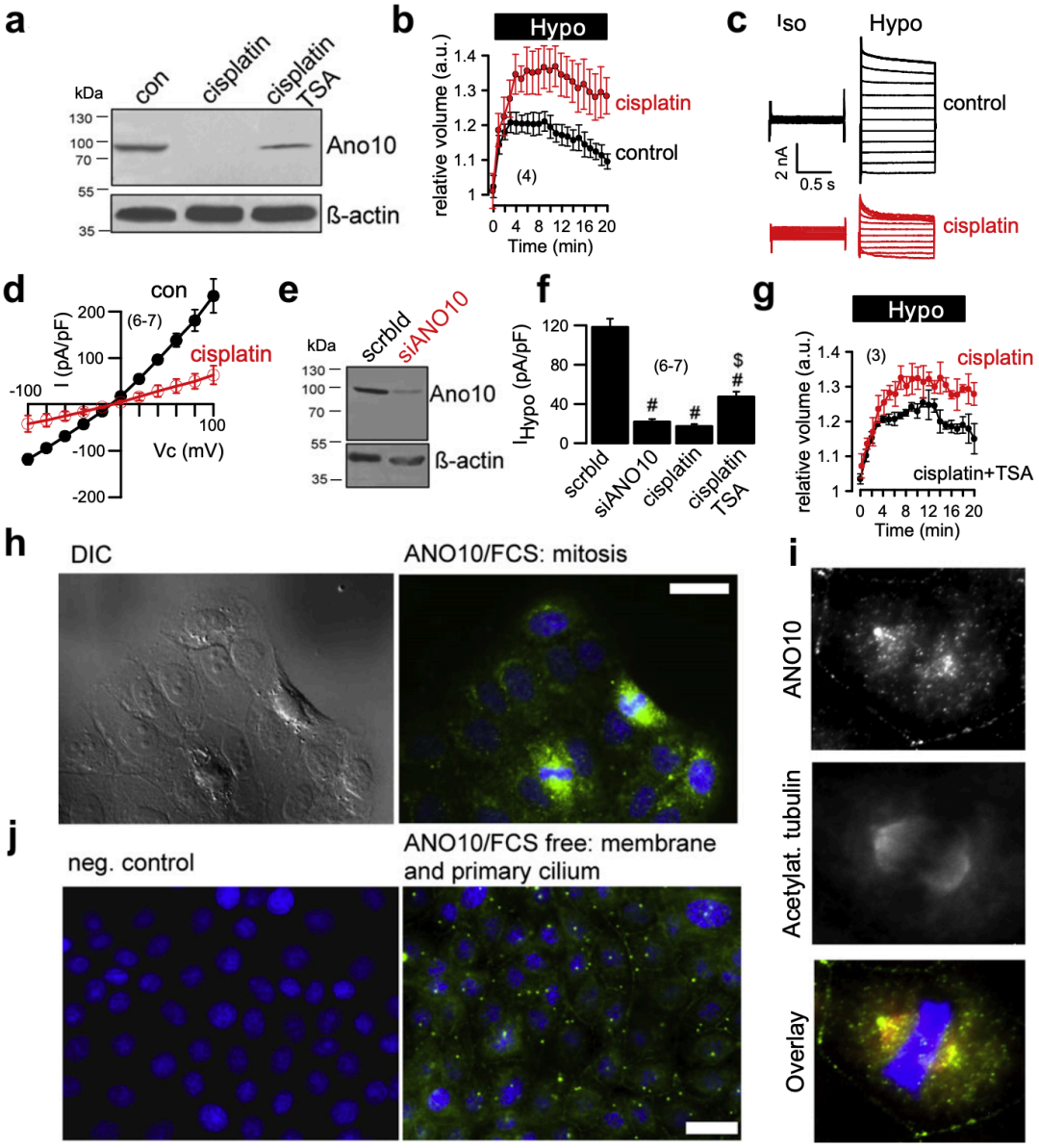

Figure 3.5 | *Cellular localization and role of Ano10 in FRT cells.*

a Western blotting indicating inhibition of Ano10-expression in cells resistant to the cytostatic compound cisplatin. Cisplatin resistant FRT cells were selected by long term culturing (2 months) of FRT cells in the presence of 20 µM cisplatin. Treatment of cisplatin-resistant cells for 24 h with the inhibitor of histone acetylase, trichostatin A (TSA; 100 nM) partially regained expression of Ano10. **b** Changes in cell volume in control cells and cisplatin resistant cells as assessed by flow cytometry. Exposure to hypotonic bath solution (Hypo; 200 mosmol/l) induced cell swelling with subsequent regulatory volume decrease (RVD). **c** Whole cell currents activated by Hypo were largely reduced in cisplatin resistant cells. **d** Current/voltage relationships of whole cell currents measured in control

cells and cisplatin resistant cells. **e** Western blotting indicating inhibition of endogenous expression of Ano10 in FRT cells by siRNA. **f** Summary of swelling induced current densities in control FRT cells treated with scrambled RNA (scrbld) or siRNA for ANO10 and in cisplatin resistant cells in the absence or presence of TSA. **g** Volume regulation of cisplatin-resistant cells and cisplatin resistant cells treated with TSA. Mean ± SEM, (n) = number of experiments. **h** Differential interference contrast (DIC) image of FRT cells and immunocytochemistry of Ano10. Note the upregulation of Ano10 expression in mitotic cells. **i** Ano10 localization in densely grown FRT cells in the absence of fetal calf serum. Note the scarce expression and localization of Ano10 close to the centriole and the plasma membrane. Bars indicate 20 µm. **j** Immunocytochemistry of Ano10 and acetylated tubulin in mitotic FRT cells. Bars indicate 8 µm. ANO10 is detected in the centrosome, close to the spindle apparatus, and close to the plasma membrane.

Discussion

The present study examines the cellular function of ANO10, a poorly characterized member of the anoctamin family of Ca^{2+} activated Cl^- channels and phospholipid scramblases. The data shown here demonstrate ANO10 as an intracellular protein. Intracellular location of ANO10 has also been suggested earlier [3,27]. Additional support for an intracellular localization of ANO10 is provided through a lack of biotinylation of ANO10 in overexpressing cells (Supplementary Fig. 3.2). Although being an intracellular protein, we detected Ca^{2+} activated Cl^- currents in cells overexpressing ANO10 [11]. How can ANO10 induce ion currents when localized in intracellular compartments? The present data suggest that, instead of operating as a plasma membrane Cl^- channel, ANO10 augments intracellular Ca^{2+} signals, thereby facilitating activation of endogenous Ca^{2+} activated Cl^- channels such as ANO6 [16]. Evidence was provided in intestinal epithelial cells (Fig. 3.2b), and previously in macrophages and overexpressing HEK293 cells [27]. Moreover, enhanced Ca^{2+} signaling by ANO10 improved volume regulation and activation of VRAC (Figs. 3.2f,g; 3.4d; 3.5b; Supplementary Fig. 3.1) [27]. Cell swelling was shown to induce local Ca^{2+} rises that are required for proper activation of VRAC [284]. Because intracellular Ca^{2+} signals are rather compartmentalized [72], these results suggest a colocalization of ANO10 and VRAC (LRRC8). Indeed, in additional experiments ANO10 and LRRC8A could be coimmunoprecipitated (Supplementary Fig. 3.3).

Reduced VRAC activity in the absence of ANO10 may also explain the lower rate of apoptosis as observed in various cell types in this present report (Fig. 3.3-5). Indeed VRAC is essential for both regulatory and apoptotic cell shrinkage [316]. Interestingly, we observed an inverse correlation between expression of ANO10 and LRRC8A: Monocytes express high levels of ANO10 but very little LRRC8A, while macrophages express little ANO10 but upregulate expression of LRRC8A (Fig. 3.4b, Supplementary Fig. 3.3b). This may reflect some sort of feedback control. One may speculate that the shorter life time of monocytes and their ability to change their shape during penetration of narrow endothelial gaps when

leaving the blood stream, is related to the higher level of ANO10 expression [308]. Nevertheless, it may be surprising that no further abnormalities such as tumor formation or cancer were detected in the intestinal epithelium of ANO10-/- mice. This may be due to the fact that apoptosis is not essentially required for cell turnover in the gut [318].

ANO10 mutations were found to be associated with cerebellar ataxia [23,25,26]. Interestingly the Drosophila ortholog of Ano8/10, called Axs, is necessary for normal spindle formation and progression through the cell cycle. It was shown that Axs colocalizes with the ER, and is recruited to microtubules during mitosis and meiosis [74], indicating that Axs and ANO10 share similar properties (Fig. 3.3g, 3.5h-j) [27]. Moreover, the present data demonstrate dynamic changes in the intracellular localization of ANO10, depending on cell cycle and other factors such as polarization and cell density. Notably, dominant mutations in Axs cause abnormal segregation of chromosomes due to defects in spindle formation, [74].

An intraspindle ER membrane system has been detected in spermatocytes and oocytes that has a role in the regulation of cytosolic Ca^{2+} during meiosis and probably also during mitosis [73,319]. Although Ca^{2+} signals cannot always be detected in cells undergoing mitosis due to compartmentalized signaling in Ca^{2+} microdomains, there is general agreement that Ca^{2+} is essential for cycle progression [320]. We found that receptor-activated Ca^{2+} signals were augmented in HeLa cells overexpressing ANO10 (in addition to endogenous ANO10), a result corresponding well to those shown in Fig. 3.2b-d and earlier [27]. Moreover expression of two different types of ataxia causing ANO10 mutants, caused larger Ca^{2+} increases upon stimulation with ATP than expression of wt ANO10 (Supplementary Fig. 3.4a), which supports the concept that mutations in ANO10 cause ataxia by deranged, i.e. enhanced Ca^{2+} signaling [23]. Also interesting, an ataxia causing frame shift mutant of ANO10 (ANO10-L384fs) could not be coimmunoprecipitated with LRRC8A, in contrast to wild type ANO10 (Supplementary Fig. 3.3a, 3.4b). Probably the major cellular mechanism leading to cerebellar ataxia is deranged Ca^{2+} signaling in Purkinje cells [75,321-325]. Deranged Ca^{2+} signals are caused by mutations of several ataxia-associated genes encoding proteins that regulated intracellular Ca^{2+} signals [23]. It is therefore tempting to speculate that ANO10 mutations causes ataxia by deregulated Ca^{2+} signaling.

Ataxia is also known to be the most common clinical phenotype associated with coenzyme CoQ10 deficiency. CoQ10 deficiency has also been detected in two ataxia patients carrying ANO10 mutations [271]. Idebenone is a synthetic analog of coenzyme Q10, which is used as a therapeutic drug for the treatment of ataxia [326]. Remarkably, idebenone was shown to potently inhibit ANO1, another member of the anoctamin family [327]. It is very likely that idebenone/CoQ10 are also inhibitors of ANO10, as currently available anoctamin inhibitors are rather nonspecific among anoctamin paralogs. Thus idebenone may inhibit enhanced intracellular Ca^{2+} levels caused by ataxia causing mutants of ANO10 [23,25]. Finally, it is entirely possible that other cellular abnormalities caused by mutations in ANO10 are due to due to

dysregulated intracellular Ca^{2+} levels and diminished coenzyme Q10 levels. Taken together our data demonstrate that ANO10 is required for proper compartmentalized Ca^{2+} signaling, through which ANO10 controls various cellular functions like ion secretion, cell cycling as well as activation of VRAC and apoptosis. These ANO10-induced cellular effects are likely to be related to ANO10-linked genetic disorders.

Acknowledgments

Supported by DFG KU757/12-1, SFB699/A7, SFB699/A12 and Cystic Fibrosis Trust SRC003. The excellent technical assistance by B. Wild, E. Tartler and P. Seeberger is gratefully acknowledged.

Supplementary material

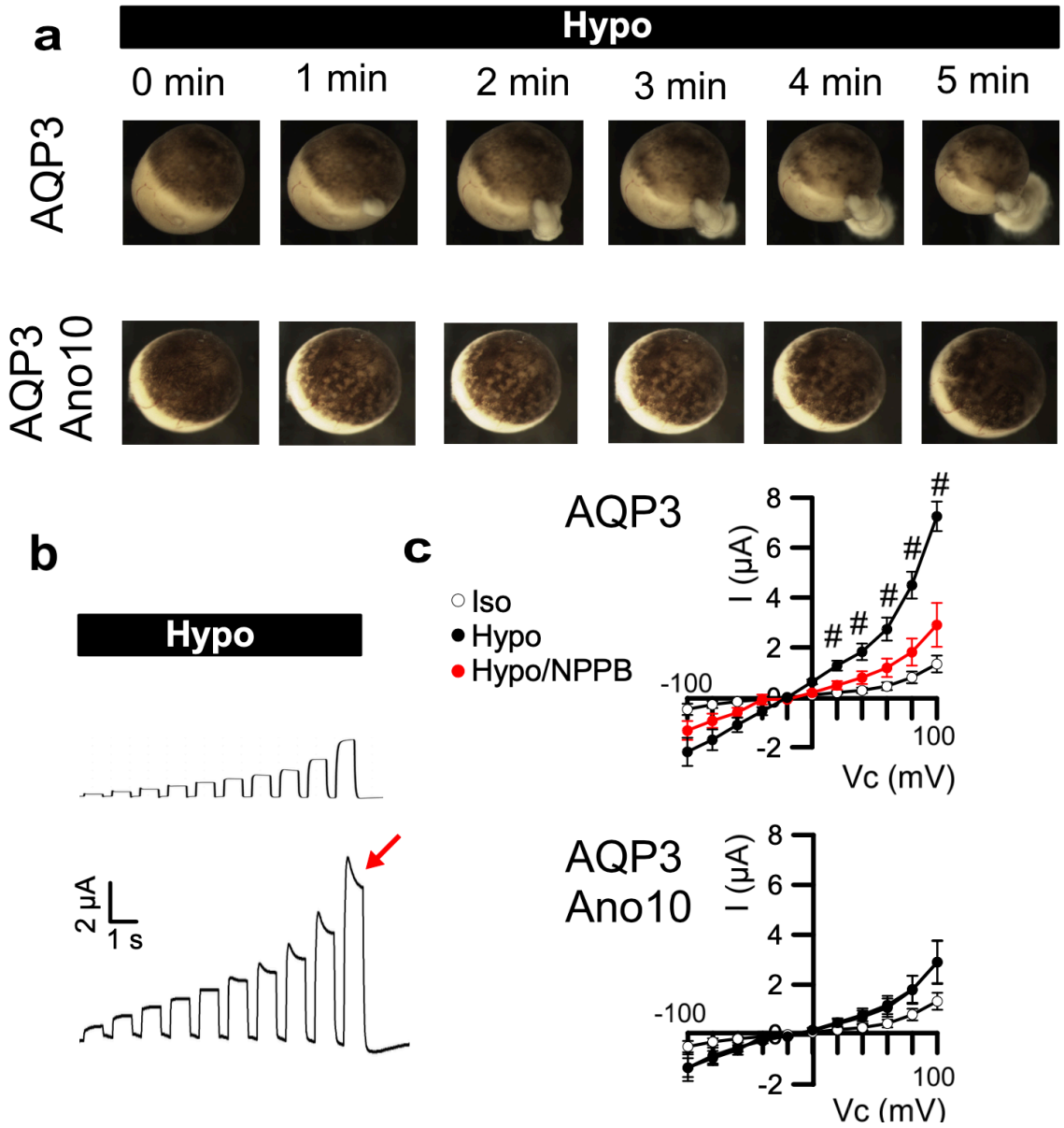

Supplementary Figure 3.1 | *Activation of VRAC by expression of ANO10 in Xenopus oocytes.*

a Aquaporin 3 (AQP3) or AQP3 together with ANO10, respectively, were expressed in *Xenopus* oocytes to induce hypotonic cell swelling. Exposure to hypotonic bath solution (Hypo; 100 mosmol/l) typically induced cell swelling and rupture of the cell membrane with leakage of yolk out of the cell (in about 85 %). Membrane rupture was much rarer in cells coexpressing AQP3 and ANO10 (in about 28 %). **b** Whole cell currents in voltage clamped oocytes (stepwise increase in clamp voltage from -100 to +100 mV in steps of 20 mV from a holding voltage of -100 mV). The whole cell current was larger in ANO10 expressing oocytes, and showed inactivation at strongly depolarizing clamp voltages, characteristic for volume regulated anion currents (VRAC; red arrow). **c** Current / voltage relationships indicating larger currents in ANO10 expressing oocytes and current inhibition by the anoctamin inhibitor NPPB (20 µM). Mean ± SEM, (n) = number of experiments.

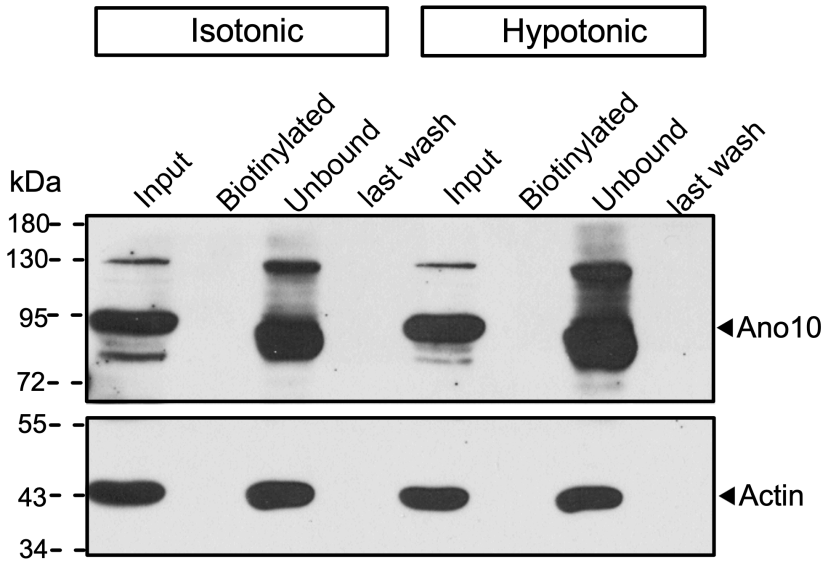

Supplementary Figure 3.2 | *Intracellular localization of ANO10.*

Biotinylation of human BHY cells expressing endogenous ANO10. ANO10 was not biotinylated independent of the presence of extracellular isotonic or hypotonic (cell swelling) bath solution, suggesting lack of membrane expression of ANO10. Cells were cultured in serum free media. Blots were performed in replicates.

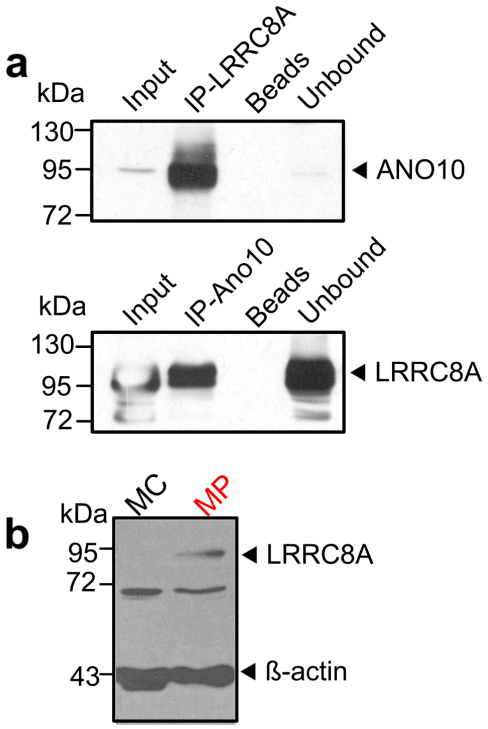

Supplementary Figure 3.3 | *Relationship between ANO10 and VRAC/LRRC8A.*

a Coimmunoprecipitation of ANO10 and LRRC8A. 50 µg protein were loaded as input, 20 µg of immunoprecipitated protein was loaded as IP. **b** THP1 monocytes (MC) express very low or even undetectable levels of the volume regulated anion channel (VRAC) subunit LRRC8A, while THP macrophages (MP) show upregulation of LRRC8A. 20 µg protein was loaded in each lane. Experiments were performed in replicates.

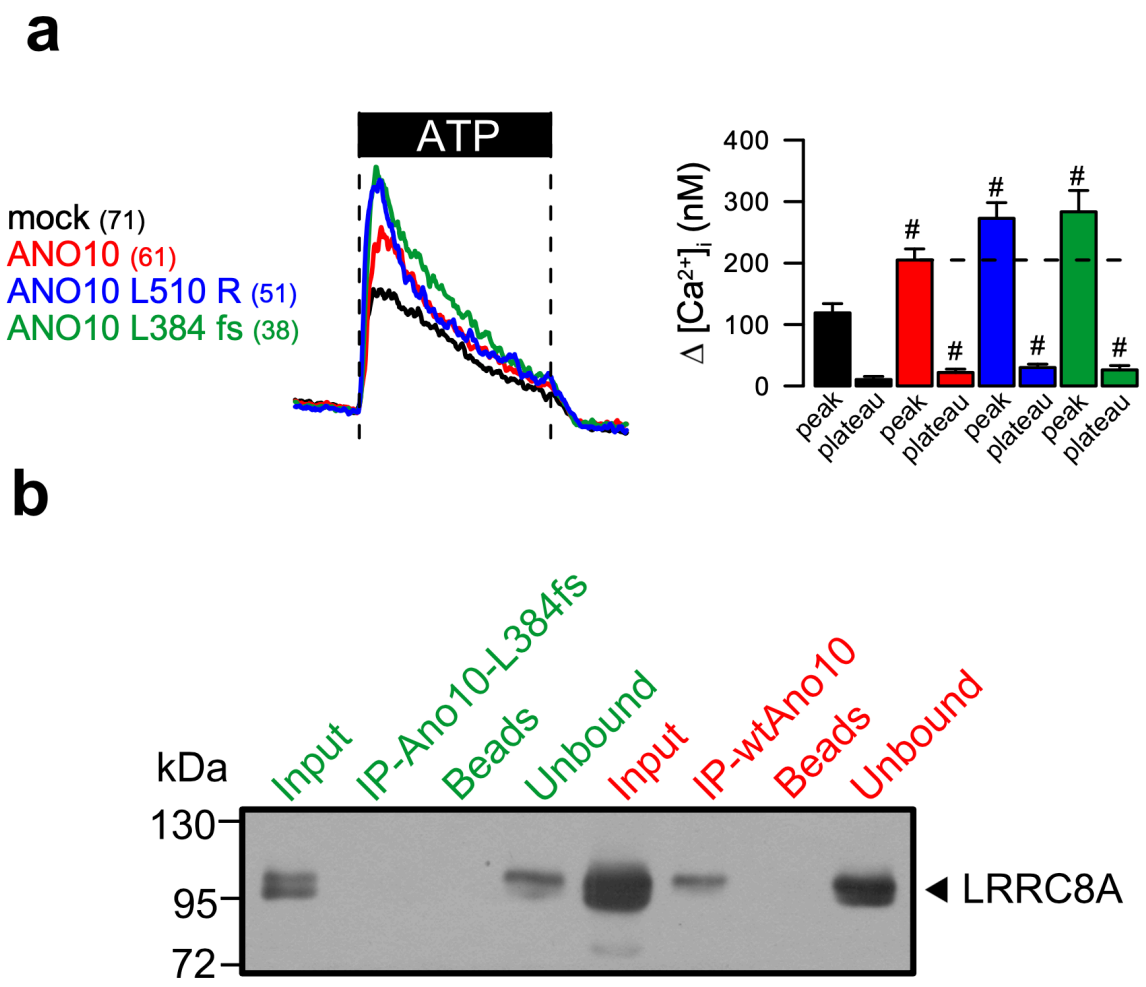

Supplementary Figure 3.4 | *ANO10 ataxia mutations may compromise functional interaction of ANO10 with the VRAC subunit LRRC8A.*

a Ca^{2+} signaling in cells overexpressing wild type (wt) ANO10 or two mutant forms of ANO10 occurring in autosomal-recessive cerebellar ataxia. **b** Immunoprecipitation of LRRC8A with wild type (wt) ANO10, but not with a mutant from of ANO10 (ANO10-L384fs) detected in patients with autosomal-recessive cerebellar ataxia. Experiments were performed in replicates. Mean ± SEM, (n) = number of experiments.

CHAPTER 4 | NICLOSAMIDE REPURPOSED FOR THE TREATMENT OF INFLAMMATORY AIRWAY DISEASE

Abstract

Inflammatory airway diseases such as asthma, cystic fibrosis (CF) and COPD are characterized by mucus hypersecretion and airway plugging. In both CF and asthma, enhanced expression of the Ca^{2+} activated Cl^- channel TMEM16A is detected in mucus producing club/goblet cells and airway smooth muscle. TMEM16A contributes to mucus hypersecretion and bronchoconstriction, which is both inhibited by blockers of TMEM16A such as niflumic acid (NFA). Here we demonstrate that the FDA-approved drug niclosamide, a potent inhibitor of TMEM16A identified by high throughput screening, is an inhibitor of both TMEM16A and TMEM16F. In asthmatic mice, niclosamide reduced mucus production and secretion, as well as bronchoconstriction, and showed additional anti-inflammatory effects. Using transgenic asthmatic mice, we found evidence that TMEM16A and TMEM16F are required for normal mucus production/secretion, which may be due to their effects on intracellular Ca^{2+} signaling. TMEM16A/F support exocytic release of mucus and inflammatory mediators, both being blocked by niclosamide. Thus, inhibition of mucus and cytokine release, bronchorelaxation, along with reported antibacterial effects make niclosamide a potentially suitable drug for the treatment of inflammatory airway diseases, such as cystic fibrosis, asthma, and COPD.

Key words: Niclosamide, TMEM16A; TMEM16F; anoctamin 1; anoctamin 6; mucus, Cystic Fibrosis, asthma, COPD, Ca^{2+} signaling, repurposing

Published in: Inês Cabrita, Roberta Benedetto, Rainer Schreiber, Karl Kunzelmann. Niclosamide repurposed for the treatment of inflammatory airway disease. JCI Insight. 2019 Aug 8;4(15).

Own experimental contribution: Crypt isolation, *In vitro* perfusion of intestine, Intestinal histology, mucus staining by PAS and quantification, Measurements of intracellular Ca^{2+} concentration.

Own written contribution: Methods, Results, Parts of Introduction and Discussion.

Other contributions: Designed experiments and analyzed data.

Introduction

Inflammatory airway diseases such as cystic fibrosis (CF) [328,329], asthma and COPD are characterized by airway obstruction due to mucus hypersecretion, mucus plugging and bronchoconstriction [126-130,330]. The cystic fibrosis transmembrane conductance regulator (CFTR) chloride channel is dysfunctional in CF, leading to attenuated fluid and bicarbonate secretion. Along with Na^+ hyperabsorption and dehydration of the airway surface liquid (periciliary fluid layer; ASL) covering the airway epithelium, this will lead to an inflammatory airway disease [328,331]. While low ASL pH and airway mucus plugging is believed to cause chronic inflammation in CF, mucus hypersecretion in allergic asthma is due to proinflammatory $CD4^+$ Th2-dependent IL-4/IL-13 signaling [332-334]. Additional local hypoxia, neutrophilic infiltration, accumulation of reactive oxygen species and bacterial superinfection cause a destructive pulmonary inflammation. It is important to note that asthma-like airway hyper-responsiveness, cough, wheeze and airway obstruction is also observed in more than 50% of CF patients, and an inflammation-induced β-adrenergic hyporesponsiveness is likely to contribute to airway dysfunction in CF [335-337]. It is therefore of vital importance to identify novel strategies which limit both mucus production and bronchoconstriction in inflammatory airway disease.

A recent study on adult mice with airway epithelial knockout provided rather surprising results: Mice lacking airway epithelial expression of TMEM16A exhibit neither Ca^{2+} activated TMEM16A nor cAMP-activated CFTR Cl^- currents. Yet, the animals did not develop a CF-like phenotype, and did not show attenuated mucociliary clearance [36]. Normal mouse and human lungs express low levels of TMEM16A. TMEM16A is upregulated in CF and asthma, in both goblet cells and airway smooth muscle. Expression of TMEM16A is also enhanced in arterial smooth muscles in pulmonary arterial hypertension (PAH) [125-130,330,338-340]. This provides evidence for TMEM16A being important for basal mucus secretion as well as for bronchoconstriction in asthma and CF, and for PAH [125,339,341-344].

A similar regulatory effect of TMEM16A was found for mucus secretion by intestinal goblet cells, and we described a novel ATP-driven pathway for intestinal mucus secretion [125]. TMEM16A supports intestinal fluid secretion and membrane expression of CFTR. Quite surprisingly, the function of TMEM16A in small intestinal epithelial cells, which show very low expression of TMEM16A, seemed to be replaced by expression of TMEM16F [125]. Taken together, TMEM16A mediates a number of adverse events in inflammatory airway disease, suggesting inhibition rather than activation of TMEM16A as therapy in asthma and CF. Using airway and intestinal specific knockout mice, we examined the contribution of TMEM16A and the coexpressed homologue TMEM16F to mucus secretion. We found positive effects of niclosamide, a common FDA-approved drug and potent inhibitor of TMEM16A [344], on various lung parameters. These effects consist in inhibition of mucus release, suppression

of inflammation, and airway relaxation, as well as intestinal mucus release. The data propose inhibition of TMEM16A and TMEM16F by niclosamide as a novel therapy in inflammatory lung disease.

Materials and methods

Animals, OVA-induced asthma. All animal experiments complied with the ARRIVE guidelines and were carried out in accordance with the U.K. Animals Act, 1986 and associated guidelines, EU Directive 2010/63/EU for animal experiments. Mice (C57BL/6) with a floxed TMEM16A allele and FOXJ1-Cre mice were kindly provided by Prof. Jason R. Rock (Boston University School of Medicine) and Prof. Michael J. Holtzman and Dr. Y. Zhang (Washington University School of Medicine), respectively. Adult mice aging 8 to 12 weeks were used for the experiments. Knockout of TMEM16A in ciliated airway epithelial cells (*TMEM16A$^{flox/flox}$FoxJ1Cre*) has been described elsewhere [36]. Generation of mice with a floxed TMEM16F allele was described in [345]. For knockout of TMEM16F in ciliated epithelial and intestinal epithelial cells, *TMEM16F$^{flox/flox}$* mice were crossed with *FoxJ1-Cre* and *Vil1-Cre* mice to obtained *TMEM16F$^{flox/flox}$FoxJ1Cre* and *TMEM16A$^{flox/flox}$Vil1Cre*, respectively. Mice were sensitized to ovalbumin (OVA, Sigma-Aldrich, Germany) by intraperitoneal (ip) injection of 100 µg OVA with 1 mg aluminum hydroxide gel (Sigma) on days 0 and 14. At days 21, 22 and 23, mice were anaesthetized and challenged to OVA by intratracheal instillation of 50 µg OVA in 100 µl saline. Control mice were sham sensitized with saline and aluminum hydroxide gel (Sigma-Aldrich, Germany) and challenged to 100 µl saline by intratracheal instillation [346]. NFA (0.5 mg/kg/day for three days, dissolved in Corn Oil (Sigma-Aldrich, Germany)) and Niclosamide (13 mg/kg/day for three days, dissolved in Corn Oil) were administered via ip injections. In addition, Niclosamide (13mg/kg/day, dissolved in Corn Oil) was received via gavage. For control treatment vehicle were used.

Cells culture, crypt isolation. HEK293 cells were cultured in DMEM media (GIBCO, Germany) supplemented with 10% FBS (Capricorn, Germany). Calu3 cells were grown in DMEM-F12 media (GIBCO, Germany) supplemented with 1% HEPES, 1% L-glutamine, 10% FBS (Capricorn, Germany). Cell lines have been obtained originally from ATCC (Manassas, VA, USA) and were grown at 37ºC in the absence of antibiotics in a humidified atmosphere with 5% CO_2. For experiments, cells were grown on lass cover slips and subsequently mounted into a perfused bath on the stage of an inverted microscope (Zeiss, Axiovert 200, München, Germany). Animals were euthanized by CO_2 inhalation. Crypts were isolated from mouse colon by incubation of the resected colon in chelating buffer on ice, washed afterwards and mechanically agitated. Crypt-rich supernatant was collected, centrifuged, kept on ice and used immediately in Ca^{2+} measurements.

RT-PCR, siRNA. RT-PCR has been performed using RNA isolated from lungs of wt and TMEM16A and TMEM16F KO mice using NucleoSpin RNA columns (Macherey-Nagel,

Germany). Total RNA (1 µg/50 µl reaction) was reverse-transcribed using random primer (Promega, Germany) and M-MLV Reverse Transcriptase RNase H Minus (Promega, Germany). Each RT-PCR reaction contained sense and antisense primer (Table 4.1), 0.5 µl cDNA, and GoTaq Polymerase (Promega, Germany). After 2 min at 95 °C cDNA was amplified for 30 cycles for 30 s at 95 °C, 30 s at 57 °C and 1 min at 72 °C, followed by 10 min at 72°. PCR products were visualized by loading on peqGREEN (Peqlab,VWR, Germany) containing agarose gels and were analyzed using ImageJ. TMEM16F was downregulated by human siRNA transfection into Calu3 cells using standard methods (Lipofectamine, Invitrogen, Germany).

Table 4.1 | *Primers used for RT-PCR.*

	Acc.No.	Primer
Tmem16a	NM_178642.5	for: 5´-GTGACAAGACCTGCAGCTAC rev: 5´-GCTGCAGCTGTGGAGATTC
Tmem16f lung	NM_001253813.1	for: 5´- ATGCAGATGATGACTAGGAAGG rev: 5´- CGGAGGACCTTGGTGAACC
Tmem16f intestine	NM_001253813.1	for: 5´- CATACGAATCTAACCTTATCTGC rev: 5´- CATTCTCTGTACAGGAGGTAAC
P2rY2	NM_008773.4	for: 5´- GGAACCCTGGAATAGCACC rev: 5´- CTGGTGGTGACGAAGTAGAG
Chrm3	NM_033269.4	for: 5´- CTTTTCTATTACCAGGCCACTC rev: 5´- GCTTGAGTACAATGGAATAGATG
Gapdh	NM_001289726.1	for: 5´- GTATTGGGCGCCTGGTCAC rev: 5´- CTCCTGGAAGATGGTGATGG

Western blotting. Cells were collected and lysed in 1% NP40 lysis buffer containing protease inhibitor cocktail and DTT (Sigma-Aldrich, Germany). Protein (30–50 µg) was separated by 8.5% SDS-PAGE and transferred to nitrocellulose membranes. Membranes were blocked with 5% NFM/TBST at RT for 1 h and were incubated overnight at 4 °C with rabbit polyclonal anti-TMEM16F (diluted 1:5000 in 5% NFM/TBST, Thermo Fisher Scientific, USA) or rabbit polyclonal anti-actin (diluted 1:10,000 in 5% NFM/TBST, Sigma-Aldrich, Germany). Subsequently, membranes were incubated with secondary antibody at RT for 2 h. Immunoreactive signals were visualized using supersignal chemiluminescence substrate detection kit (Pierce Biotechonology, USA).

IL-8 assay. To measure secretion of the cytokine IL-8 (Peprotech, Germany), Calu3 cells were rinsed twice with PBS (Capricorn, Germany), placed in OPTIMEM (GIBCO, Germany) and exposed to LPS (10 µg/ml48h). After 48 hours, the conditioned medium was collected and used to quantify IL-8 using Quantikine ELISA kits (R&D systems, Germany) according to the manufacturer's instructions.

In vitro perfusion of intestine. Mice were sacrificed by cervical dislocation and excised intestines were placed immediately in ice-cold Ringer solution and carefully flushed to

remove residual luminal contents. The intestinal segments were mounted and perfused vertically in a custom-designed perfusion chamber with a constant temperature, similar to [125,347]. After mounting, the serosal side was exposed to Ringer solution (NaCl 120 mM, KH2PO4 0.4 mM, K2HPO4 1.6 mM, D-glucose 5 mM, MgSO4 1 mM, Ca2+-gluconate 1.5 mM and NaHCO3 25 mM, pH 7.4 , continuously gassed with 95% O_2 and 5% CO_2) and perfused luminally with glucose-free mannitol-replaced Ringer. Perfusates were collected at a rate of 0.5 ml/min at 3 min intervals for an additional 27 min. Tissues were stimulated with methacholine (MCh; 100 µM) or ATP (100 µM) for 9 min, always in the presence of 1 µM Prostaglandin E2 (PGE2) if not mentioned otherwise. In luminal Ca^{2+} free solution, Ca^{2+} was substituted with equimolar EGTA. The amount of mucus secretion was analyzed using a periodic acid-Schiff (PAS) assay (Sigma-Aldrich, Germany). In brief, 50 mM dithiothreitol was pipetted into each sample and incubated for 1h at 37º under continuous shaking. 0.2 ml periodic acid (0.1%) was added, incubated for 2 hours at 37°C, and additional 30 min at 20°C after adding 0.2 ml Schiff´s reagent (Sigma-Aldrich, Germany). Samples were centrifuged at 500 g/5 min and OD of the resulting solution was measured at 540 nm. The amount of mucus per tissue and minute was calculated using a calibration curve from defined pig gastric mucin (Sigma-Aldrich, Germany).

Histology, mucus staining by alcian blue and PAS, quantification. Mice were sacrificed by cervical dislocation. Small and large intestine were removed and cut in two sections. One section was kept in Ringer solution, the other section was exposed to 100 µM ATP (ROTH, Germany) or 100 µM carbachol (Sigma-Aldrich, Germany). Before and after each experiment, intestinal sections were fixed for further histological analyses. Mouse airways were fixed by transcardial fixation and were embedded in paraffin or frozen in liquid N_2. For paraffin sections, tissues were fixed in 4% paraformaldehyde (PFA), 0.2% picric acid and 3.4% sucrose in PBS, and were washed in methanol before embedding in paraffin. For mucus analysis sections were stained according to standard Periodic acid-Schiff (PAS) or Alcian Blue methods and examined by light microscopy. A minimum of nine random images for each embedded tissue were acquired from a minimum of three animals (*TMEM16A$^{flox/flox}$*, *TMEM16F$^{flox/flox}$*, *TMEM16A$^{flox/flox}$FoxJ1Cre*, *TMEM16F$^{flox/flox}$FoxJ1Cre*, *TMEM16F$^{flox/flox}$Vil1Cre*). Sections were analyzed using an Axiovert 200 microscope equipped with AxioCam ICc 1 and ApoTome (Zeiss, Germany) and amalysedusing AxioVision (Zeiss, Germany).

Patch Clamping. Crypts from jejunum and distal colon were isolated in Ca^{2+}-free Ringer solution and immobilized on polylysine coated glass cover slips. HEK293 cells were grown on glass-coated cover slips and were mounted on the stage of an inverted microscope (Zeiss, Germany). Experimental procedures are described in detail in [36].

Measurement of intracellular Ca^{2+} concentration. All measurements of intracellular Ca^{2+} concentration ([Ca^{2+}]) of cell lines and isolated goblet cells have been performed using the

Ca^{2+} sensitive dye Fura2-AM (TOCRIS, Germany), as described earlier [348].

YFP-Quencing. Quenching of the intracellular fluorescence generated by the iodide-sensitive enhanced yellow fluorescent protein (YFP) was used to measure anion conductance. YFP fluorescence was excited at 490 nm using a semi-automatic Novostar plate reader (BMG-Labtech, Offenburg, Germany). I^- influx was induced by replacing 20 mM extracellular Cl^- with 20 mM I^- in the presence of 1µM Ionomycin (Enzo Life Science). Background fluorescence was subtracted and autofluorescence was negligible. Changes in fluorescence induced by I^- are expressed as initial rates of fluorescence decrease (arbitrary units/sec) and analyzed using MARS data analyzing program (BMG-Labtech, Offenburg, Germany).

Materials and statistical analysis. All compounds used were of highest available grade of purity: Niclosamide, Eact, OVA, MCh, NFA, Dichlorophene, (Sigma-Aldrich, Taufkirchen, Germany). Niclosamide-ETHO, Nitazoxanide, tizoxanide (Caymann-Chemicals, Michigan, USA), CaCCinhAO1 (Tocris; Wiesbaden, Germany) IL-8, IL-13 (Peprotech, Hamburg, Germany). Antibodies were purchased from Thermo Fisher Scientific (Darmstadt, Germany; TMEM16F; PA5-35240), Bioss (Woburn, USA; MUC5AC; bs-7166R) and Novus (Wiesbaden, Germany; MUC5B;6F10-E4). All gene symbols are consistent with Entrez Gene nomenclature, are italicized, and are capitalized according to biological species. Data are reported as mean ± s.e.m. Two-tailed student's t-test (for paired or unpaired samples as appropriate) or ANOVA were used for statistical analysis. A p-value < 0.05 was accepted as significant difference.

Results

Niflumic acid (NFA) is an inhibitor of TMEM16A/F and blocks airway mucus secretion. OVA-induced allergic asthma in mice caused airway goblet cell metaplasia (Fig. 4.1a). Exposure of asthmatic mice to aerosolized carbachol (CCH) induced release of intracellular mucus as well as airway contraction (Fig. 4.1a-c). Pretreatment of OVA-sensitized animals for three days with the TMEM16A inhibitor niflumic acid (NFA; ip and tracheal instillation) before application of CCH, abolished mucus production. Thus, there was no intracellular mucus left to be released by CCH. Moreover, airway contraction was largely inhibited, as judged from airway cross sections. We found that the two main TMEM16 paralogs coexpressed in airway epithelial and smooth muscle cells [349], TMEM16A and TMEM16F are inhibited by NFA, when overexpressed and activated by ionomycin in HEK293 cells (Fig. 4.1d-f). The data suggest a role of both TMEM16A and TMEM16F for mucus production and contraction of airway smooth muscle (ASM). Although it is entirely possible that NFA also acts via additional cellular mechanisms, it may be beneficial to inhibit both TMEM16 paralogues, as a treatment of inflammatory airway diseases such as asthma, CF, and COPD [344].

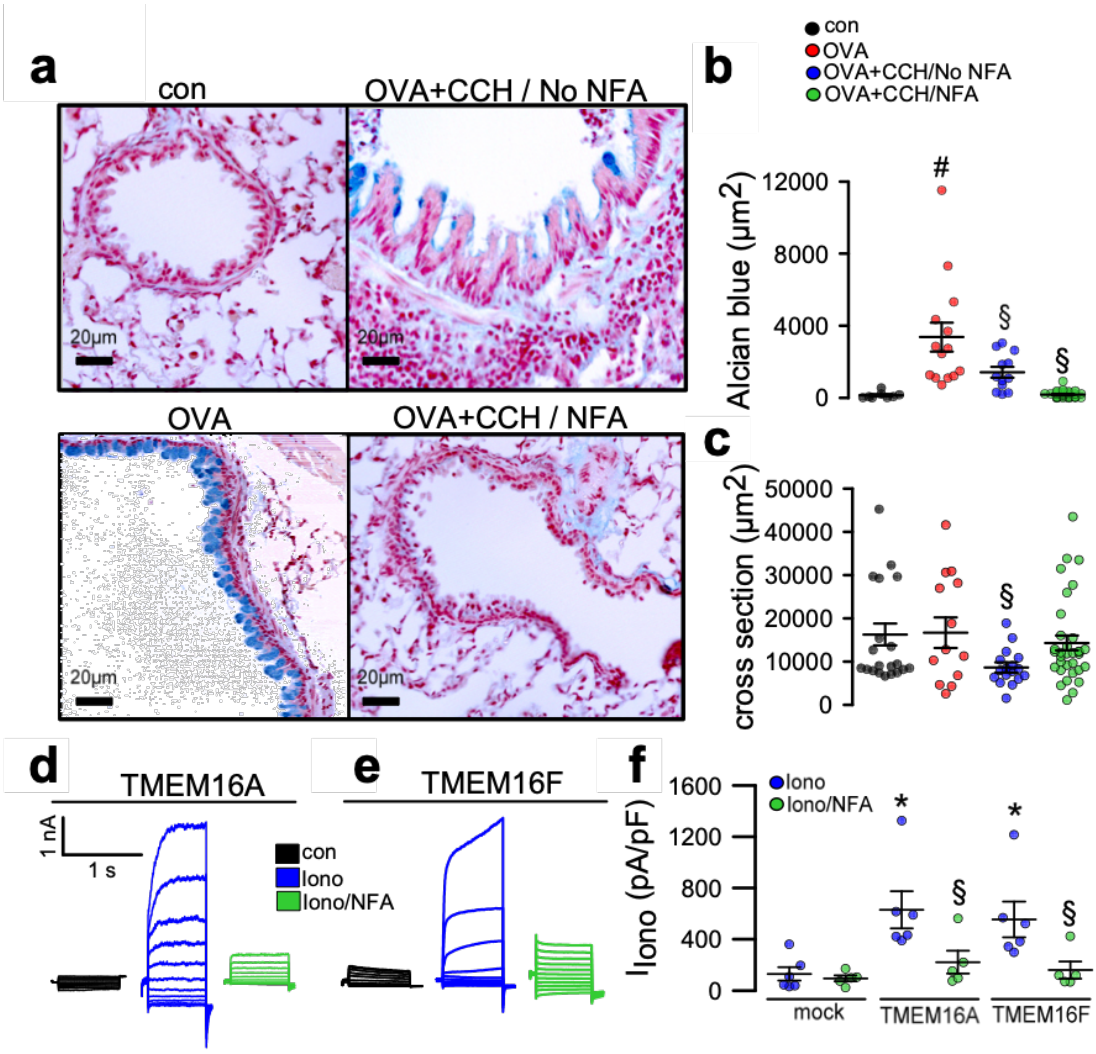

Figure 4.1 | *The TMEM16-inhibitor niflumic acid attenuates inflammatory airway disease.*

a,b OVA-sensitization induced goblet cell metaplasia as indicated by alcian blue positivity. Exposure to carbachol (CCH, 25 mg/ml, nebulizer) induced release of mucus and airway contraction (3 mice/8-20 airway sections). Bars 20 µm. Pre-exposure to the TMEM16A-inhibitor niflumic acid (NFA, 0.5 mg/kg/day; intratracheal application for three days), strongly attenuated mucus production and CCH-induced airway contraction (A-C). **c** Cross section of airways indicating airway relaxation by NFA (3 mice/8-13 airway sections). **d-f** Whole cell currents obtained in patch clamp experiments with HEK293 cells expressing TMEM16A or TMEM16F. Currents were activated by 1 µM ionomycin (Iono), and inhibited by NFA (20 µM) (n = 5-6 cells). Bars indicate 20 µm. Mean ± SEM; #significant increase compared to control ($p<0.05$; unpaired *t*-test); §significant inhibition ($p<0.05$; unpaired t-test); *significant activation ($p<0.05$; paired t-test).

Previous studies demonstrated that expression of TMEM16 proteins augments intracellular Ca^{2+} signals, while the TMEM16-inhibitors CaCCinhAO1 and NFA inhibited intracellular Ca^{2+} signals [348]. Here we demonstrate in different cell types that niclosamide also blocks Ca^{2+} increase elicited by ATP, or by the TMEM16-activator Eact [299] (Supplementary Fig. 4.2).

According to previous studies, TMEM16A augments intracellular Ca^{2+} signals by increasing filling of the ER Ca^{2+} store, and by augmenting IP_3-induced Ca^{2+} release an store-operated Ca^{2+} influx [348]. Importantly, niclosamide inhibited Ca^{2+} signals in freshly isolated goblet cells, which may explain its inhibitory effects on mucus secretion [125] (Supplementary Fig. 4.2c,d). Niclosamide inhibited ATP-induced ER Ca^{2+} store release (Ca^{2+} peak) and eliminated Ca^{2+} influx (Ca^{2+} plateau). In Ca^{2+} free solution ATP-induced store release was fully maintained, while the plateau is eliminated. Niclosamide still attenuated store release but had no further effect on Ca^{2+} influx in Ca^{2+} free solution (Supplementary Fig. 4.3).

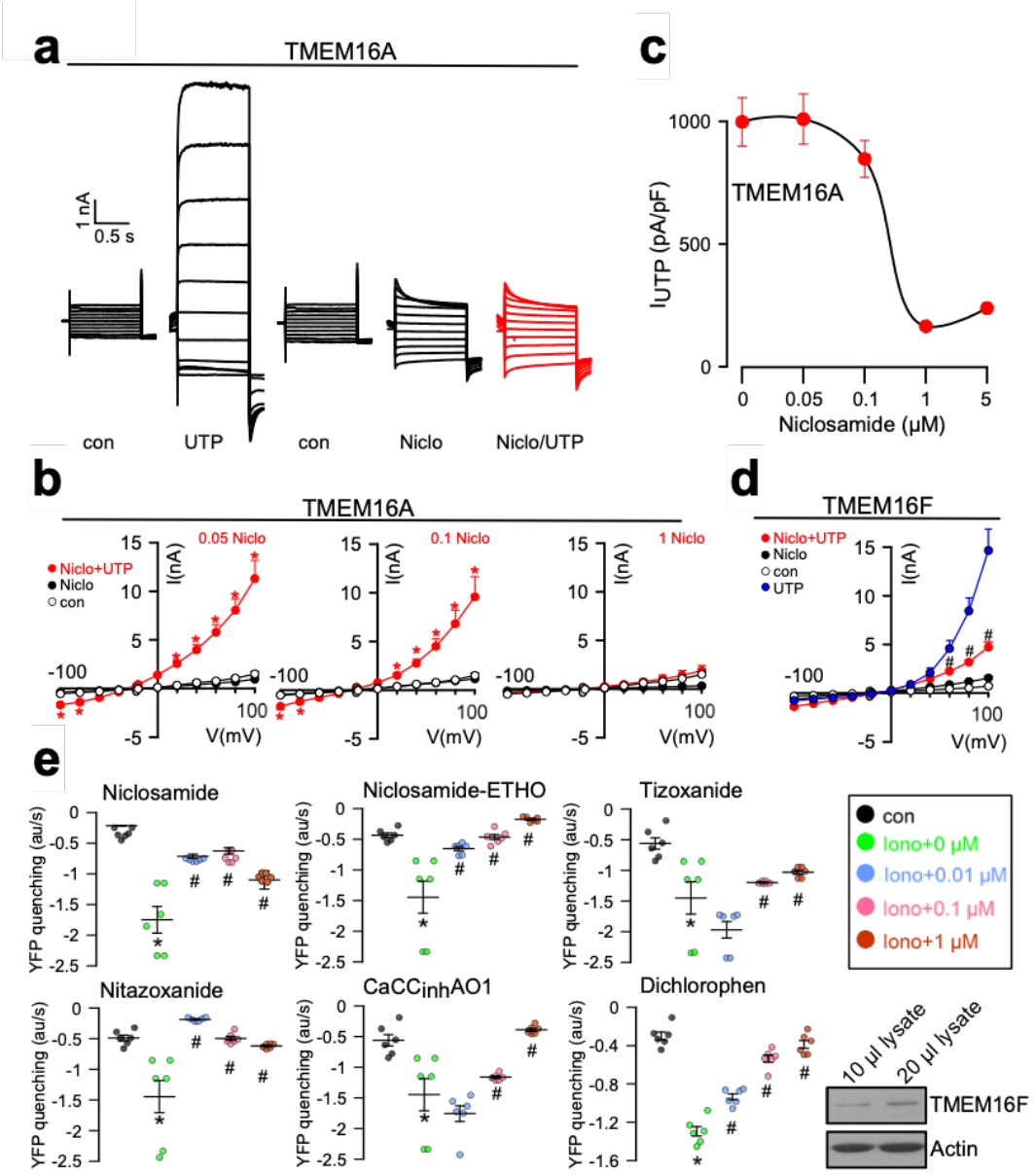

Figure 4.2 | *Inhibition of TMEM16A and TMEM16F by niclosamide.*

a TMEM16A whole cell currents in TMEM16A-overexpressing HEK293 cells. The purinergic agonist UTP (100 μM) was used to activate TMEM16A. UTP-induced currents were inhibited by niclosamide (Niclo, 1 μM). **b,c** Concentration-dependent inhibition of TMEM16A by Niclo (n=5-7 cells). **d**

Current/voltage relationship showing inhibition of TMEM16F expressed in HEK293 cells by Niclo (n=5 cells each). **e** Inhibition of endogenous TMEM16A/F expressed in HT_{29} cells examined by iodide quenching. Rate of YFP quenching (arbitrary units (au/second), when applying 20 mM iodide to the extracellular bath solution. HT_{29} cells stably overexpressing YFP were stimulated with 1 µM ionomycin (Iono). 100.000 cells were seeded per well (n=6-8 wells each concentration). Mean ± SEM; *significant activation ($p<0.05$; paired *t*-test); #significant inhibition ($p<0.05$; unpaired *t*-test). Inset: Western blot indicating expression of TMEM16F in HT29 cells.

Niclosamide inhibits mucus production and mucus secretion, ASM contraction, and inflammation. Intracellular mucus in asthmatic mice was reduced by both NFA and niclosamide (Fig. 4.3a,b). We reported earlier that knockout of TMEM16A inhibits basal mucus secretion in airways and intestine, which results in accumulation of intracellular mucus under control (non-inflammatory) conditions [125]. According to these earlier studies, TMEM16A/F are expressed in mucus-producing cells, where they exert their positive effects on compartmentalized apical intracellular Ca^{2+} levels. This supports fusion of mucus-filled granules with the apical membrane, thereby facilitating exocytosis.

However, goblet cells metaplasia and intracellular mucus accumulation under inflammatory (OVA) conditions occurred in both wild type (*TMEM16A*$^{flox/flox}$) mice and mice with airway epithelial knockout of TMEM16A (TMEM16A$^{flox/flox}$FoxJ1Cre) (Fig. 4.3c). Intracellular mucus was released and airways were contracted after application of CCH (OVA/CCH; Fig. 4.3c,g). In contrast, when mice were treated with niclosamide for three days, intracellular mucus was nearly abolished and airway contraction by CCH was attenuated (OVA/CCH/Niclo; Fig. 4.3c-e). We speculate that niclosamide-inhibition of TMEM16A or TMEM16F contribute to inhibition of intracellular mucus production. Notably, the two main TMEM16 paralogs expressed in mouse airway epithelial cells, TMEM16A and TMEM16F, along with intracellular TMEM16K [349], were upregulated in OVA-sensitized (asthmatic) mice. Thus, TMEM16A and TMEM16F and possibly TMEM16K may participate in Th2-driven goblet cell metaplasia (Fig. 4.3f, Table 4.2).

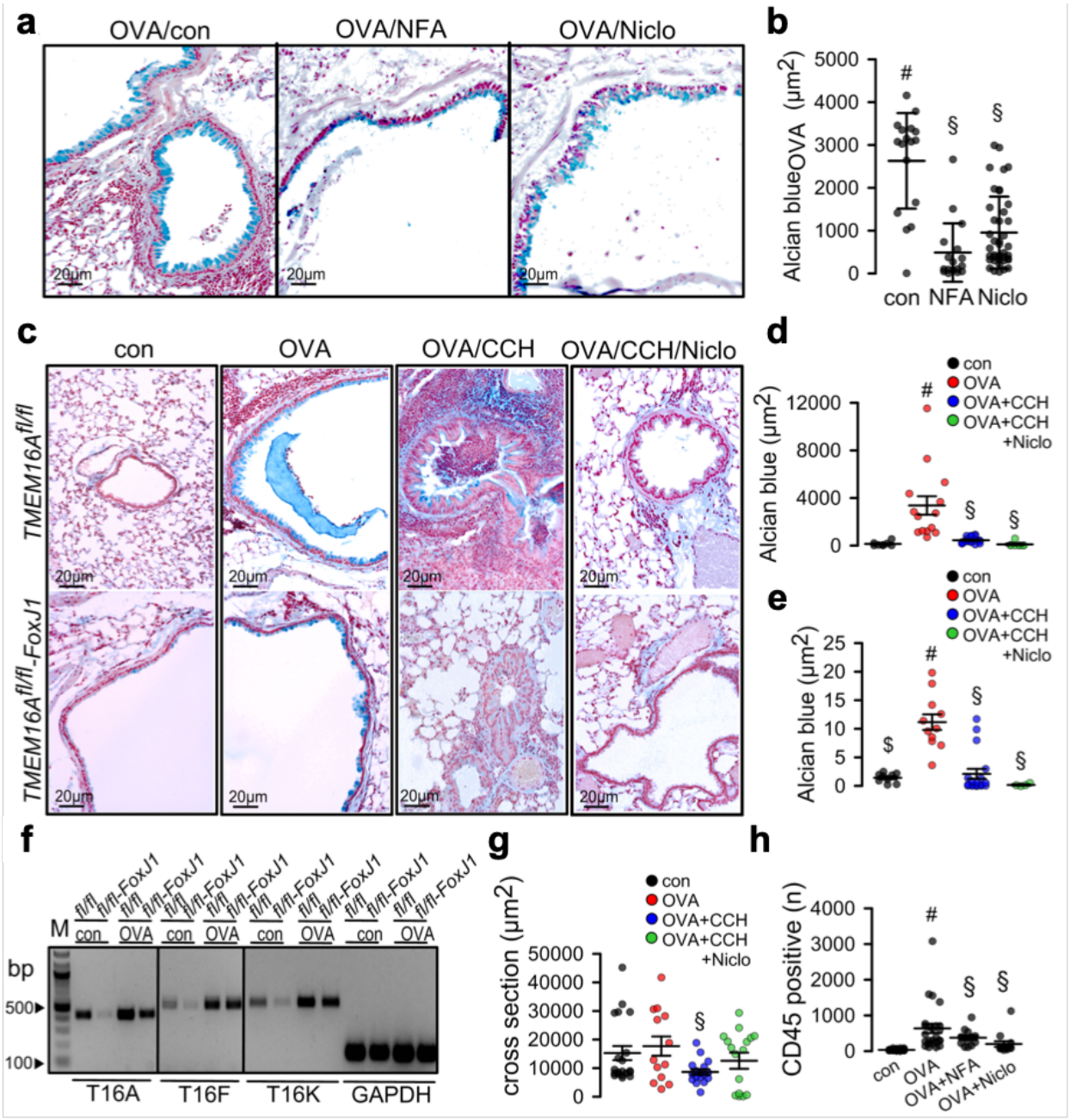

Figure 4.3 | *Niclosamide attenuates inflammatory airway disease.*

a,b Goblet cell metaplasia in OVA-sensitized mice detected by alcian blue. Tracheal instillation of niflumic acid (NFA; 0.5 mg/kg/day) or niclosamide (Niclo; 13 mg/kg/day) significantly reduced mucus production (n=3 mice/17-40 airway sections). Bar = 15 µm. **c-e** OVA-sensitization of *TMEM16A*$^{flox/flox}$ (*fl/fl*) and *TMEM16A*$^{flox/flox}$*FoxJ1Cre* (*fl/fl-FoxJ1*) mice induced goblet cell metaplasia. Exposure of *fl/fl* and *fl/fl-FoxJ1* mice to carbachol (CCH, 25 mg/ml, nebulizer) induced mucus release and airway contraction. Pre-exposure to Niclo by intratracheal application for three days attenuates mucus production and CCH-induced airway contraction (n = 3 mice analyzed/ 4-19 airway sections examined). Bar = 20 µm. **f** Semiquantitative RT-PCR analysis of expression of the three main TMEM16 paralogs (A,F,K) in mouse airways, before and after OVA-sensitization. TMEM16A, F, and K have been knocked out in ciliated (fl/fl-FoxJ1) airway epithelial cells. Wild type littermates are shown for control (fl/fl). Induction of asthma by ovalbumin treatment causes goblet cell metaplasia and

upregulation of transcription of TMEM16A, F, and K in mucus producing cells. Lanes were run on the same gel but were noncontiguous. Primers used are listed in Table 4.1. Quantification is provided in Table 2. **g** Airway cross section indicating airway contraction by muscarinic stimulation (aerosol) and inhibition of contraction by niclosamide (n = 3 mice analyzed/ 13-20 airways sections examined). **h** Number of CD45 positive cells (airways) under different conditions (n=3 mice/19-20 airway sections). Bars indicate 20 µm. Mean ± SEM; #significant increase by OVA ($p<0.05$; unpaired *t*-test); §significant effect of NFA, Niclo, or CCH ($p<0.05$; ANOVA). Fig. 4.1b-c and Fig. 4.3d-e share the same control groups (control, OVA).

Table 4.2 | *Upregulation of expression of TMEM16A,F,K in airways of asthmatic mice.*

Summary from semiquantitative RT-PCR shown in Fig. 4.3f. The three main TMEM16 paralogs expressed airway epithelial cells are TMEM16A, TMEM16F and TMEM16K. Data from mice with knockout of TMEM16A in ciliated epithelial cells (fl/fl-FoxJ1) and wt littermates (fl/fl). Expression was analyzed in control mice and in OVA-sensitized (asthmatic) mice. Expression of TMEM16A, TMEM16F and TMEM16K was upregulated in asthmatic mice (n=4 reactions each). Bands for TMEM16 and internal GAPDH-standard were analyzed densitometrically and the ratio was calculated. Mean ± SEM; #significant upregulation in asthmatic mice ($p<0.05$; unpaired t-test).

TMEM16	Mouse	Relative expression	
		Control	Asthmatic
TMEM16A	fl/fl	0.61 ± 0.06	1.09 ± 0.11#
	fl/fl-FoxJ1	0.07 ± 0.03	0.51 ± 0.04#
TMEM16F	fl/fl	0.26 ± 0.01	0.50 ± 0.04#
	fl/fl-FoxJ1	0.16 ± 0.02	0.49 ± 0.07#
TMEM16K	fl/fl	0.40 ± 0.02	0.77 ± 0.09#
	fl/fl-FoxJ1	0.17 ± 0.01	0.67 ± 0.08#

Niclosamide not only reduced mucus production but also cholinergic airway contraction, when analyzing airway cross sectional area (Fig. 4.3c,g). Potent bronchodilation by niclosamide occurs particularly in cytokine-exposed pre-contracted airways, which typically show defective ß-adrenergic relaxation [344]. Because many CF-patients suffer from asthma-like airway hyperresponsiveness [336], niclosamide could also serve as a novel therapeutic tool in CF lung disease. Peribronchial immune cell infiltration observed in allergic airways of OVA-treated animals was strongly reduced by niclosamide and by anti-inflammatory NFA (Fig. 4.3h). This result suggests an anti-inflammatory effect of niclosamide, which corresponds well to inhibition of allergic lung inflammation by the TMEM16A-inhibitor benzbromarone [127,129].

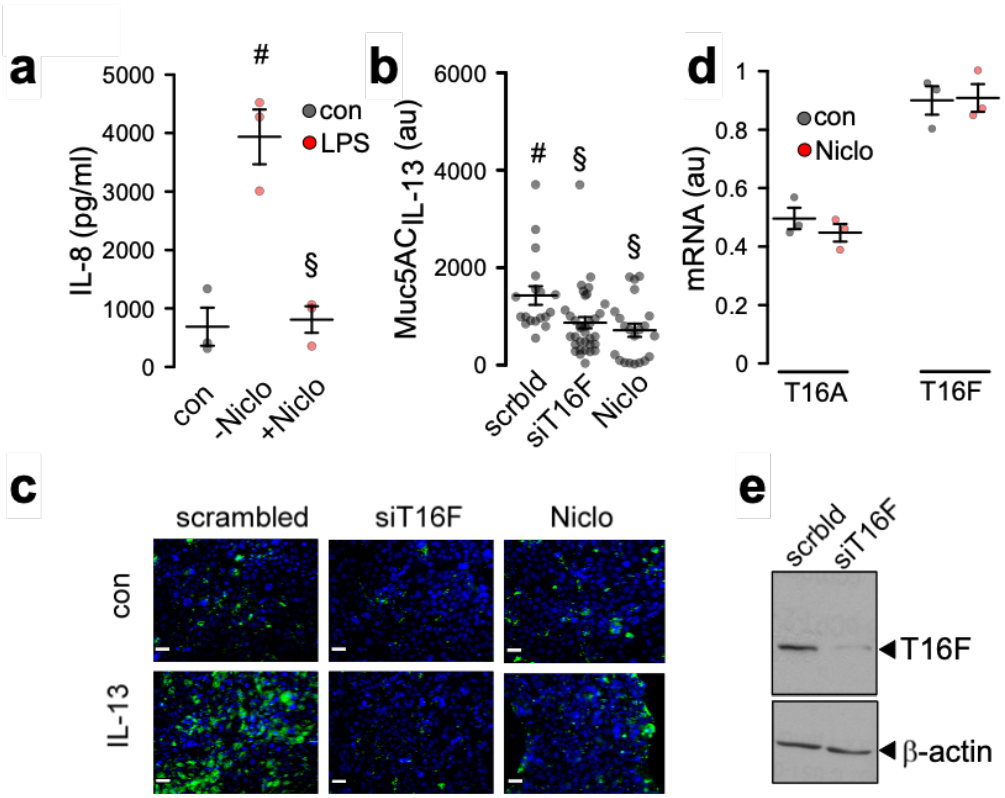

Figure 4.4 | *Niclosamide attenuates inflammatory airway response.*

a Effect of niclosamide (1 µM) on LPS (10 µg/ml) - induced release of IL-8 in Calu3 cells (n=3). **b,c** IL-13 – induced MUC5AC release and inhibition by siRNA-TMEM16F and niclosamide (1 µM) (n=19-34 sections). Bar = 15 µm. **d** Effect of niclosamide on mRNA-expression for TMEM16A and TMEM16F (semiquantitative RT-PCR) (n=3). **e** Western blot indicating knockdown of TMEM16F by siRNA. The knockdown was 91 ± 4.2 % (n=3). Bars indicate 20 µm. Mean ± SEM; #significant increase (ANOVA). §significant inhibition (ANOVA).

Niclosamide inhibits inflammation of synoviocytes from patients with rheumatoid arthritis and a number of other tissues [350]. Here, we exposed Calu3 airway epithelial cells to LPS for 48 hrs and measured release of the neutrophil attractor interleukin 8 (IL-8). LPS-induced release of IL-8 was inhibited in the presence of niclosamide (Fig. 4.4a). Upon stimulation with the Th2 cytokine IL-13, Calu3 cells produced MUC5AC (Fig. 4.4b,c). IL-13-induced synthesis of Muc5AC was suppressed by knockdown of TMEM16F or treatment of the cells with niclosamide, while niclosamide did not affect expression of TMEM16A or TMEM16F (Fig. 4.4b-e). Expression of MUC5B was not detected in Calu3 cells. Moreover, we found that knockdown of both TMEM16A and TMEM16F reduced expression of MUC5AC, and simultaneous knockdown almost abolished MUC5AC expression. Notably, knockdown of TMEM16K also exerted some inhibitory effects on MUC5AC expression (Supplementary Fig. 4.4). The data suggest Th2/IL-13-dependent upregulation of TMEM16A, F, K in airways of asthmatic mice. While it is likely that niclosamide has additional cellular effects, inhibition of

mucus production, bronchoconstriction and airway inflammation may occur through blockade of TMEM16 paralogs expressed in airway epithelial cells.

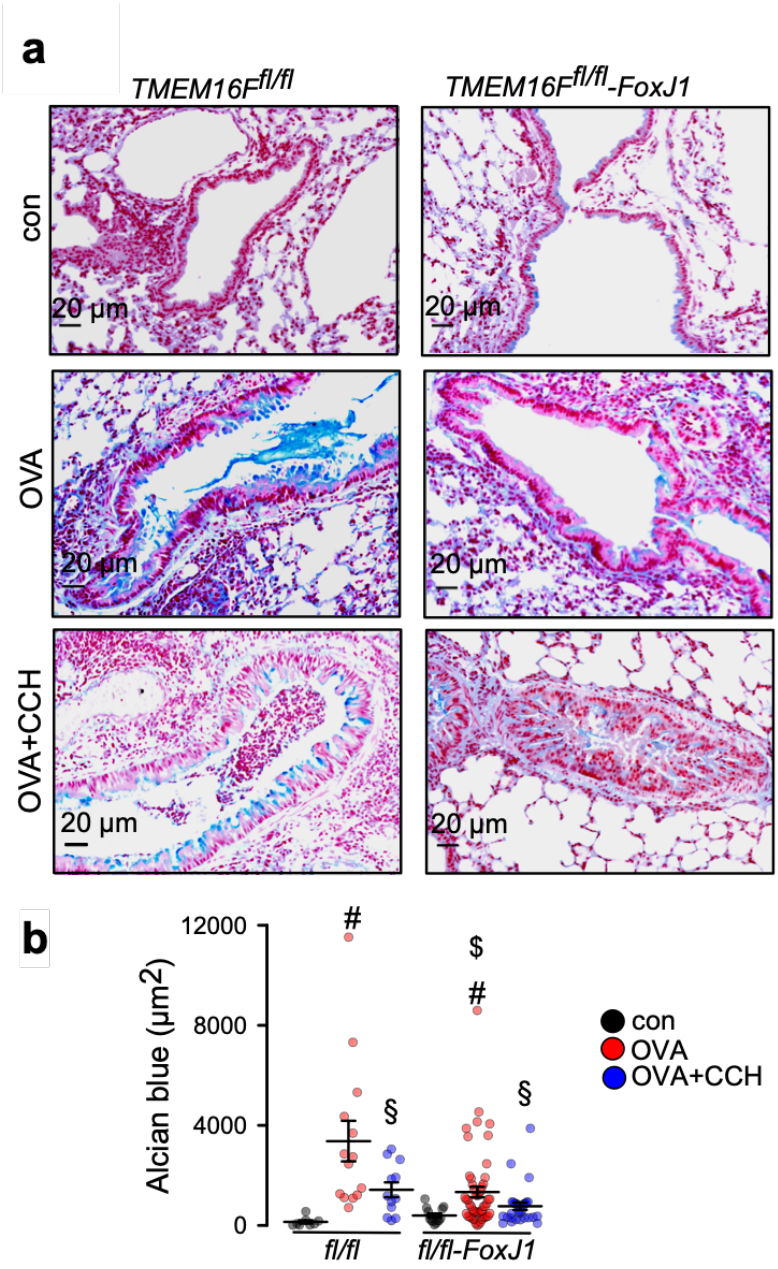

Figure 4.5 | *TMEM16F controls mucus production.*

a Mucus in *TMEM16F*$^{flox/flox}$ (*fl/fl*) and *TMEM16F*$^{flox/flox}$*FoxJ1Cre* (*fl/fl-FoxJ1*) airways under control conditions, after OVA sensitization and after exposure to carbachol (CCH, 25 mg/ml, nebulizer). Bars indicate 20 µm. **b** Summary alcian blue staining in *fl/fl* and *fl/fl-FoxJ1* animals (n = 3 mice/ 8-52 airway sections analyzed). Mean ± SEM; $^{\#}$significant increase by OVA (ANOVA); §significant decrease by CCH (ANOVA); $^{\$}$significant difference to *fl/fl* (ANOVA).

Airway epithelial knockout of TMEM16F attenuates mucus production. The data suggest that TMEM16F is relevant for mucus production. In a previous study, we found that knockout of TMEM16A in FoxJ1-positive cells leads to an accumulation of mucus due to a

lack of mucus release by secretory cells, probably through a paracrine loop [125]. Knockout of TMEM16A may compromise release of IL-6 and/or other cytokines that stimulate mucus production [351]. However, TMEM16A is also directly involved in mucus secretion by airway epithelial and intestinal goblet cells [125]. We generated an airway specific knockout of TMEM16F *(TMEM16F$^{flox/flox}$FoxJ1Cre)* and found accumulation of mucus, similar to *TMEM16A* airway knockout mice [125] (Fig. 4.5). OVA-sensitization induced goblet cell metaplasia and intracellular mucus was attenuated in *TMEM16F$^{flox/flox}$FoxJ1Cre* mice, while cholinergic release of mucus appeared uncompromised (Fig. 4.5).

TMEM16F is required for acute ATP-induced mucus secretion in the intestine. We examined whether TMEM16F has a role for acutely stimulated intestinal mucus secretion, similar to that reported recently for TMEM16A [125]. We induced acute mucus release in *ex vivo* perfused colon of mice with intestinal knockout of TMEM16F (*TMEM16F$^{flox/flox}$Vil1Cre* mice) and wt mice (*TMEM16F$^{flox/flox}$*), as described previously [125]. Acute application of methacholine (MCh) induced mucus release in both wt and TMEM16F-knockout intestine, as shown by attenuated PAS staining of intracellular mucus after MCh (Fig. 4.6). Mucus release induced by luminal ATP was somewhat reduced in intestine from TMEM16F-knockout mice (Fig. 4.6). We noticed elongated crypts in knockout animals. After ATP-induced mucus release, the empty granules appeared expanded. These changes could be related to the partial secretory defect, but may also due to the lack of volume regulatory properties of TMEM16F [284]. Notably, in mice with an intestinal epithelial knockout of TMEM16K we also noticed a change in tissue architecture [302].

Niclosamide blocks acute intestinal mucus secretion and inhibits Ca^{2+} signaling. We examined whether niclosamide inhibits intestinal mucus secretion using *in vitro* perfused intestinal segments, as described earlier [125]. We collected mucus released upon stimulation with MCh or luminal ATP. Intestinal mucus release was quantified in the absence or presence of niclosamide. The amount of mucus released by MCh was not affected by niclosamide, while ATP-released mucus was attenuated (Fig. 4.7a). Niclosamide was also applied *in vivo* for three days by intraperitoneal (ip) injection or per gavage. Both ip and oral application of niclosamide abolished ATP-induced release of mucus. Although ATP released no mucus, mucus accumulation in intestinal goblet cells was not observed, which may suggest inhibition of both production and secretion of mucus by niclosamide (Fig. 4.7b-e).

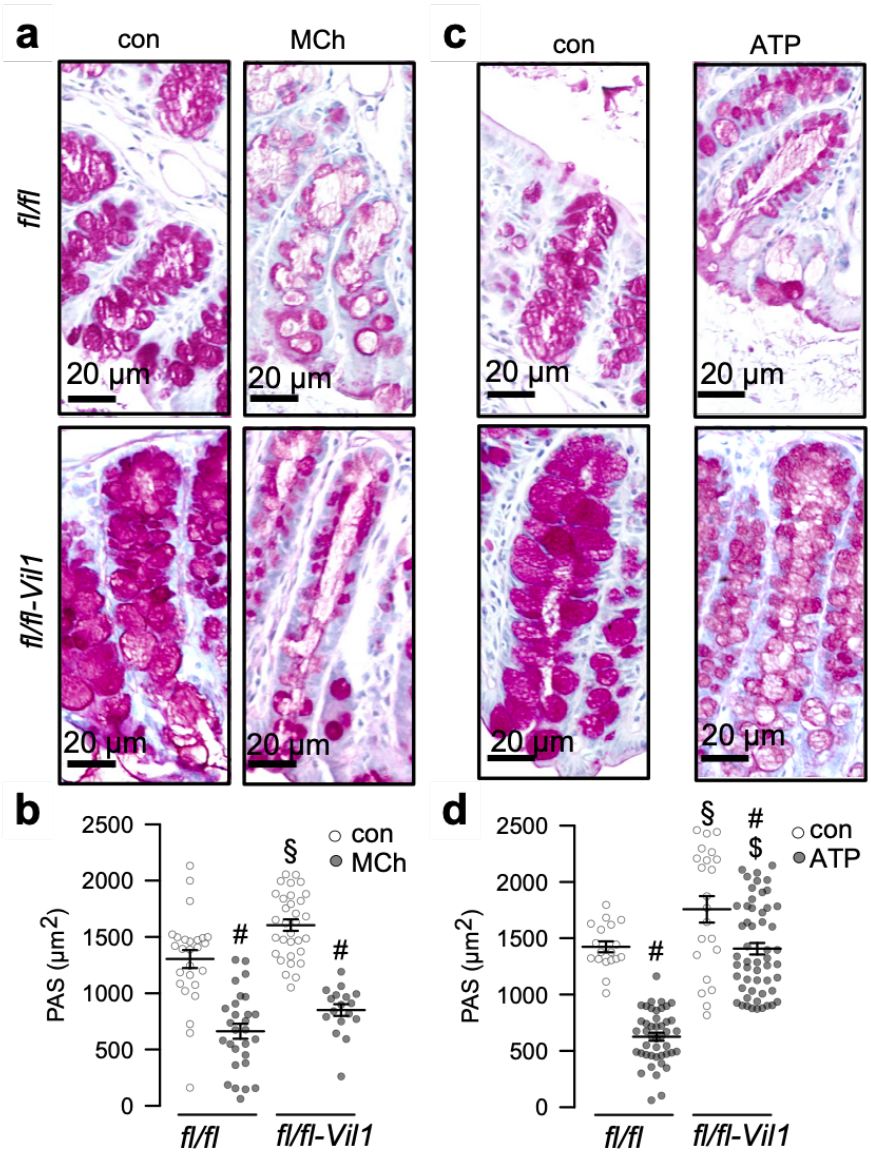

Figure 4.6 | *Production of mucus but not release is affected in TMEM16F$^{flox/flox}$CreVil1 intestine.*

PAS staining of proximal colon before and after stimulation with methacholine (MCh; 100 µM) **a,b** (n=3 mice/17-32 sections) or ATP (100 µM) (n=3 mice/28-85 sections) **c,d**. Bars indicate 20 µm. Mean ± SEM; $^{\#}$significant decrease (ANOVA). §significant increase in *fl/fl-Vil1* (ANOVA). $^{\$}$significant difference to *fl/fl* (ANOVA).

It is rather likely that inhibition of mucus by niclosamide is due to inhibition of TMEM16F: i) niflumic acid, CaCCinhAO1, and niclosamide block all TMEM16F and mucus production. ii) Knockout of TMEM16F (TMEM16F$^{flox/flox}$FoxJ1Cre) resulted in reduced mucus in asthmatic mice (Fig. 4.5). iii) In Calu-3 human airway epithelial cells knockout of TMEM16F strongly reduced IL-13-induced mucus production (Fig. 4.3; Supplementary Fig. 4.4). iv) After inhibition of mucus production by knockdown of TMEM16F, niclosamide has no further effect on IL-13-induced mucus production.

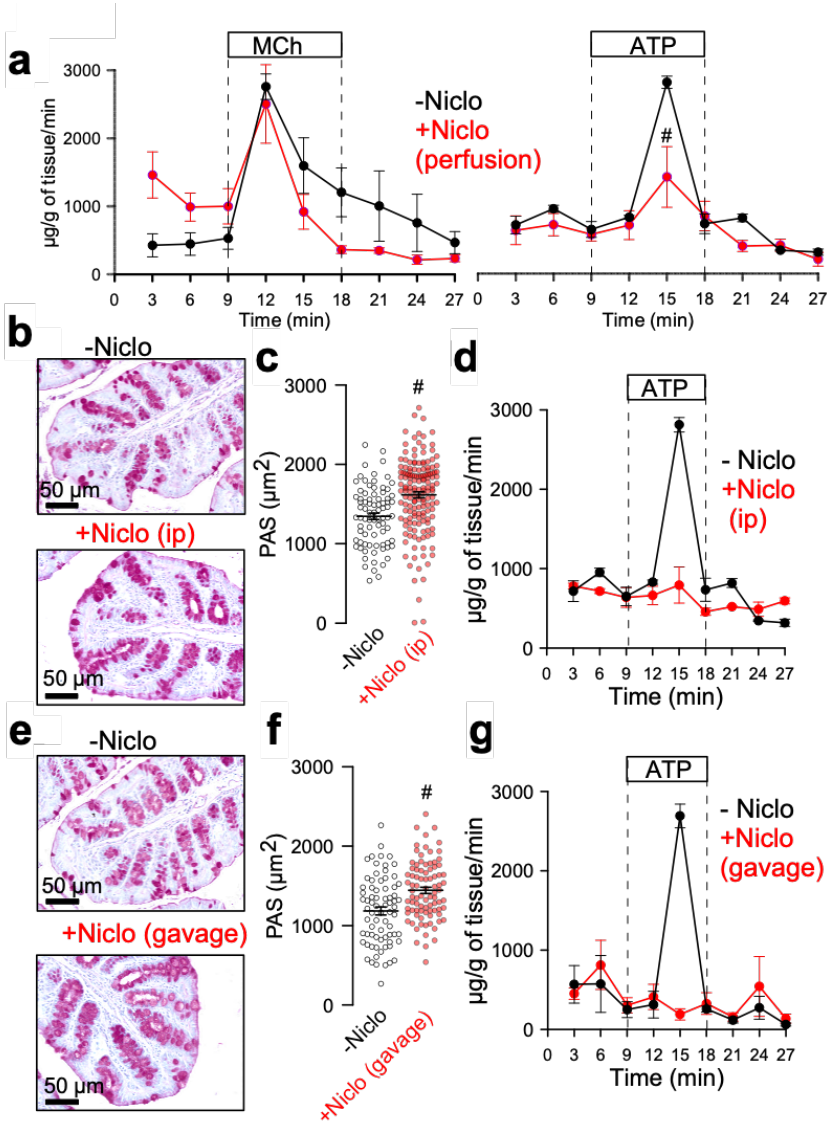

Figure 4.7 | *Effect of niclosamide on intestinal mucus release.*

a Acute mucus secretion in excised wt colon activated by methacholine (MCh) or ATP, respectively, and inhibition by acute perfusion with niclosamide (Niclo; 10 µM) (n=3-5 mice). **b-d** Effect of intraperitoneal injection of Niclo (10 mM stock dissolved in DMSO) at a concentration of 13 mg/kg/day (dissolved in corn oil, total volume 100 µl) on PAS staining (n=3 mice/81-156 sections) (b,c) and acute mucus discharge induced by perfusion with 100 µM ATP (n=3 mice/74-87 sections) (d). **e-g** Effect of application of niclosamide by gavage (13 mg/kg/day) on PAS staining (e,f) and acute mucus discharge induced by perfusion with 100 µM ATP (g) (n=3-5 mice). Bars indicate 50 µm. Mean ± SEM; #significant difference when compared to Niclo (unpaired *t*-test).

We earlier reported the role of TMEM16F for intracellular Ca^{2+} signaling [348]. In the present study, we confirm these earlier findings as we found reduced Ca^{2+} increase upon ATP-stimulation of freshly isolated crypt cells from *TMEM16F*$^{flox/flox}$*Vil1Cre* mice (Supplementary Fig. 4.5a-c). In contrast, CCH-induced Ca^{2+} rise was not affected (Supplementary Fig. 4.5d,g). Niclosamide also inhibited ATP-induced Ca^{2+} increase (Supplementary Fig. 4.5e).

Comparable results were obtained in goblet cells from small and large intestine. The fluorescence dye FM4-64 can be used to demonstrate acute membrane exocytosis [97,125]}. We found that stimulation of purinergic receptors by ATP in P2Y2R/TMEM16F-coexpressing cells augmented exocytosis, while cholinergic signaling (CCH in M3R/TMEM16F-coexpressing cells) did not. This result may indicate functional coupling of TMEM16F with purinergic, but not with cholinergic receptors (Supplementary Fig. 4.6). Taken together, TMEM16A/F support airway and intestinal mucus production and secretion. Niclosamide is an inhibitor of both TMEM16 paralogs. By blocking TMEM16A/F and possibly by additional cellular effects, niclosamide inhibits mucus production/secretion, release of cytokines and bronchoconstriction.

Discussion

Role of TMEM16A/F in inflammatory airway diseases. The present paper discusses the importance of TMEM16A/F for mucus production and secretion, and identifies TMEM16A/F as targets of the anthelmintic drug niclosamide [344]. Nevertheless, it is entirely possible that niclosamide acts via additional mechanisms, which are independent of TMEM16A/F [142,352]. We recently provided evidence that TMEM16A and TMEM16F can replace each other concerning their pro-exocytic effects [125]. Unlike TMEM16F, TMEM16A does not transport phospholipids and operates as a Cl^- selective ion channel [1]. Yet, both paralogs support intracellular compartmentalized Ca^{2+} signals [348], and a similar role has been found recently for TMEM16H [353]. To further rule out additional effects of niclosamide, a double knockout of TMEM16A/F in mouse would have been very useful. However, as described earlier, intestinal specific double knockout for TMEM16A/F appears to be developmentally lethal [125]. Taken together, we propose niclosamide to be repurposed as a novel pharmacological tool to treat diseases with excessive mucus secretion, such CF, asthma, and COPD. Notably, anti-inflammatory talniflumate, a phthalidyl ester of the TMEM16A/F-inhibitor NFA, was shown to improve survival in a CF mouse model of DIOS [354].

Mucus hypersecretion in airways results in mucus plugging, causing reduced mucociliary clearance, the predominant problem in CF lung disease [330]. Pronounced upregulation of TMEM16A, particularly in secretory cells, is observed in asthma and CF, but the role of TMEM16A is still unclear [338,339,344,355,356]. The present and previous data present evidence that both TMEM16A and TMEM16F are upregulated during airway inflammation and support mucus secretion, probably by augmenting intracellular Ca^{2+} signals. Given the potential role of TMEM16A for mucociliary clearance, it may be possible that inhibition by niclosamide reduces mucociliary clearance. However, in preliminary experiments we did not detect a negative effect of niclosamide on stroke amplitude or particle transport in excised mouse tracheas (not shown).

Using T16Ainh-AO1 inhibitor, regulation of MUC5AC-expression by TMEM16A via

STAT6/Erk1,2 has been proposed [357]. However, TMEM16A inhibitors, including T16AinhAO1, are not specific for TMEM16A, and inhibit other TMEM16 proteins as well [284,344]. The data shown here suggest a role of TMEM16F for mucus production in airways and intestine. Like TMEM16A, also TMEM16F is upregulated during Th2-dependent goblet cell metaplasia, along with TMEM16K (Fig. 4.3f). They are the main TMEM16-paralogs expressed in human and mouse airway epithelium [3,349] and are inhibited by common TMEM16A inhibitors like NPPB, NS3728, T16inhAO1, or NFA [27,284].

TMEM16A/F control intracellular Ca^{2+} signals and exocytosis. TMEM16A, F, K augment intracellular Ca^{2+} signals induced by stimulation of G-protein coupled receptors. This is shown in airways, intestine and kidney, as well as macrophages, sensory neurons, goblet cells and different cell lines [16,36,72,78,302,348,358]. TMEM16 proteins enhance GPCR-induced Ca^{2+} signals by tethering the ER to the plasma membrane, by Ca^{2+} influx through TMEM16F, and by refilling the ER Ca^{2+} store [14,348]. ER tethering has also been shown for TMEM16H [353]. TMEM16 paralogs may also enhance Ca^{2+} signals by increasing phosphatidylinositol-4,5-bisphosphate (PIP_2) in the plasma membrane [40]. Increase in intracellular Ca^{2+} causes exocytosis of mucus from secretory cells, and supports membrane insertion and activation of CFTR [36,40,125].

Inhibition of TMEM16 may improve CF lung disease. Pharmacological activation of TMEM16A and induction of Cl^- secretion is thought to improve CF lung disease [359]. However, it is worth considering that in CF, activation of Cl^- secretion through stimulation of TMEM16A might be ineffective. Maturation/function of TMEM16A in ciliated cells is compromised in CF [36,360], and purinergic continuous Cl^- secretion is essentially through CFTR and not through transient TMEM16A currents [36,58,361]. Along this line, earlier trials using stabilized purinergic ligands (denufosol) to restore Ca^{2+} dependent Cl^- secretion, failed to demonstrate any benefit in CF [362,363].

Using niclosamide as a potent inhibitor of TMEM16A/F may have a number of beneficial effects in CF: i) It is a potent inhibitor of excessive mucus secretion as shown in the present study. ii) It relaxes airways and thereby reduces bronchoconstriction [344] (and present study). iii) It is a commonly used FDA-approved drug, which is well tolerated [352]. iv) It was shown to inhibit *Pseudomonas aeruginosa* quorum sensing [364]. v) Inhalable formulations of niclosamide have been developed for the treatment of *Pseudomonas* lung infections [365]. vi) It was shown to have broad antimicrobial effects directed against hospital-acquired bacterial infections [366]. vii) It is anti-inflammatory [367] (and present study). viii) It has additional anti-cancer effects [368]. Because niclosamide inhibits mucus release and mucus production, it could be beneficial in interrupting a status asthmaticus or acute CF exacerbation. Taken together these reported positive effects, additional preclinical studies and subsequent

clinical pilot studies appear indicated.

Acknowledgements

Supported by Cystic Fibrosis Trust SRC 013, Gilead Stiftung, DFG KU756/14-1. The excellent technical assistance by Miss. B. Wild, P. Seeberger, E. Tartler, is gratefully acknowledged. We gratefully acknowledge the supply of mice with a floxed *TMEM16A* allele by Prof. Jason R. Rock (Boston University School of Medicine), and the FOXJ1-Cre mice by Prof. Michael J. Holtzman and Dr. Y. Zhang (Washington University School of Medicine).

Supplementary material

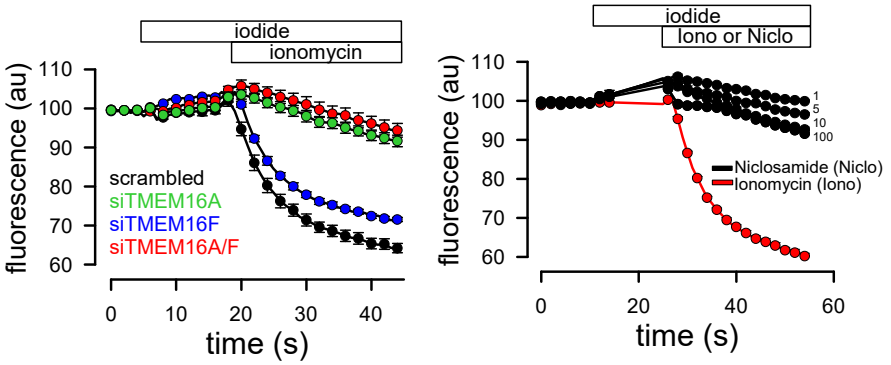

Supplementary Figure 4.1 | *Role of TMEM16A and TMEM16F for ionomycin-induced quenching in HT29 cells.*

YFP quenching by 20 mM extracellular iodide upon stimulation with ionomycin (1 µM). **a** siTMEM16A and siTMEM16F inhibited ionomycin-induced quenching. **b** Niclosamide itself did not exert any significant effect on YFP quenching, when applied at different concentrations (µM). Mean ± SEM. n=6 repeats for each condition.

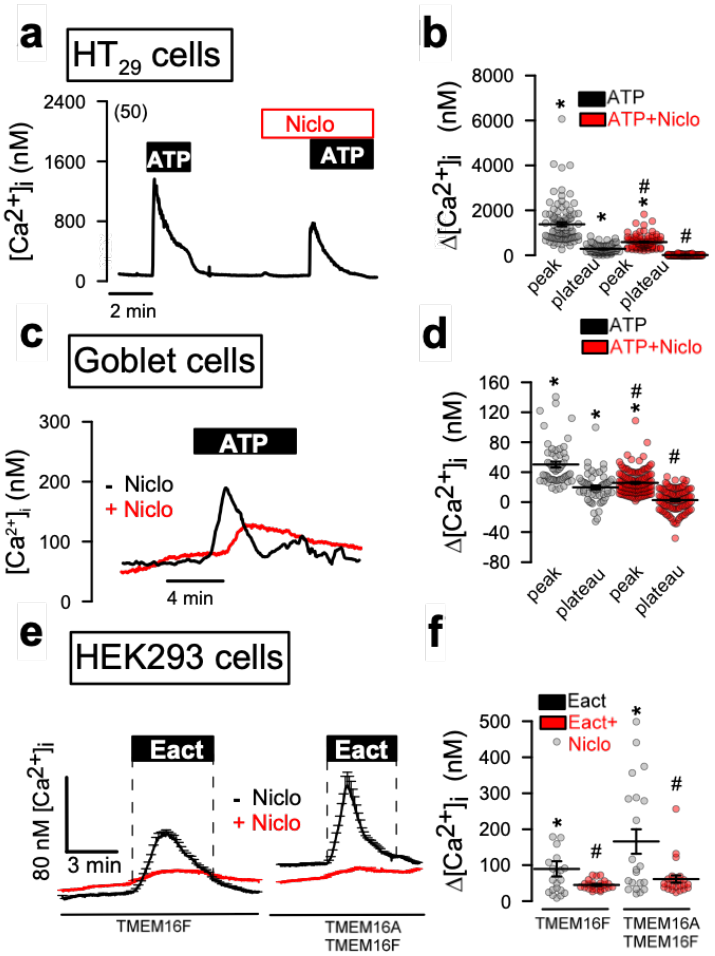

Supplementary Figure 4.2 | *Inhibition of Ca^{2+} signaling by niclosamide in different cell types.*

a,b HT29 cells were loaded with the Ca^{2+}-sensitive dye Fura2 (5 µM/30 min). 10 µM ATP was applied to stimulate purinergic receptors, which increased intracellular Ca^{2+} and activated TMEM16A.

Activation of TMEM16A was inhibited in the presence of niclosamide (Niclo, 5 µM), which also inhibited ATP-induced Ca^{2+}-release from the endoplasmic reticulum (peak) and blocked store operated Ca^{2+} influx (plateau) (n=50 cells). **c** ATP-induced Ca^{2+} increase in goblet cells of freshly isolated colonic crypts. ATP (100 µM) was applied in the absence (black curve) or presence (red curve) of Niclo (100 nM). **d** Summary of ATP-induced Ca^{2+} changes in goblet cells, indicating inhibition of peak and plateau Ca^{2+} increase by Niclo (n=55- 132 cells). **e,f** Ca^{2+} increase in HEK293 cells expressing endogenous TMEM16F only, or overexpressing TMEM16A together with endogenous TMEM16F. Ca^{2+}-rise by the activator of TMEM16A, Eact (50 µM), was inhibited by Niclo (1 µM; n=21-24 cells). Mean ± SEM; *significant increase (p<0.05; pairedt-test). #significant inhibition by Niclo (p<0.05; unpairedt-test).

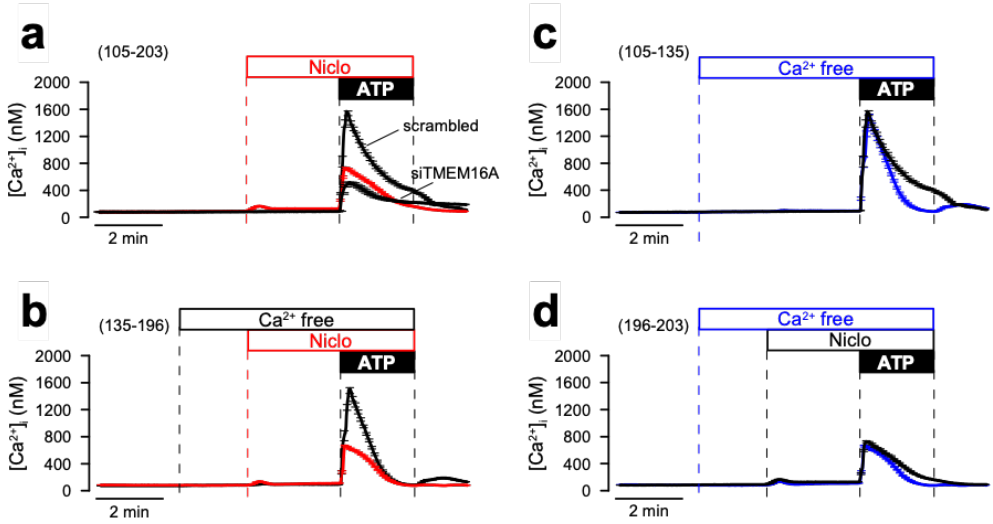

Supplementary Figure 4.3 | *Inhibition of Ca^{2+} signaling by niclosamide in the presence and absence of extracellular Ca^{2+}.*

a Niclosamide (1 µM) inhibits the agonist induced ER Ca^{2+} store release (Ca^{2+} peak) and eliminates the Ca^{2+} influx (Ca^{2+} plateau) (red tracing). Black tracing was obtained in the absence of niclosamide, before (scrambled) and after siRNA-knockout of TMEM16A (siTMEM16A). The inhibitory effect of niclosamide and siTMEM16A on ATP-induced store release were comparable. **b** In Ca^{2+} free solution, ATP-induced store release is fully maintained, but the plateau is eliminated (black tracing). Niclosamide in Ca^{2+} free solution still blocks store release (red tracing). Additional effects of niclosamide on Ca^{2+} plateau cannot be detected in Ca^{2+} free buffer. **c,d** Both peak and plateau are inhibited in the presence of niclosamide and in extracellular free Ca^{2+} (blue tracing was obtained in extracellular free buffer). n=105-203 cells analyzed.

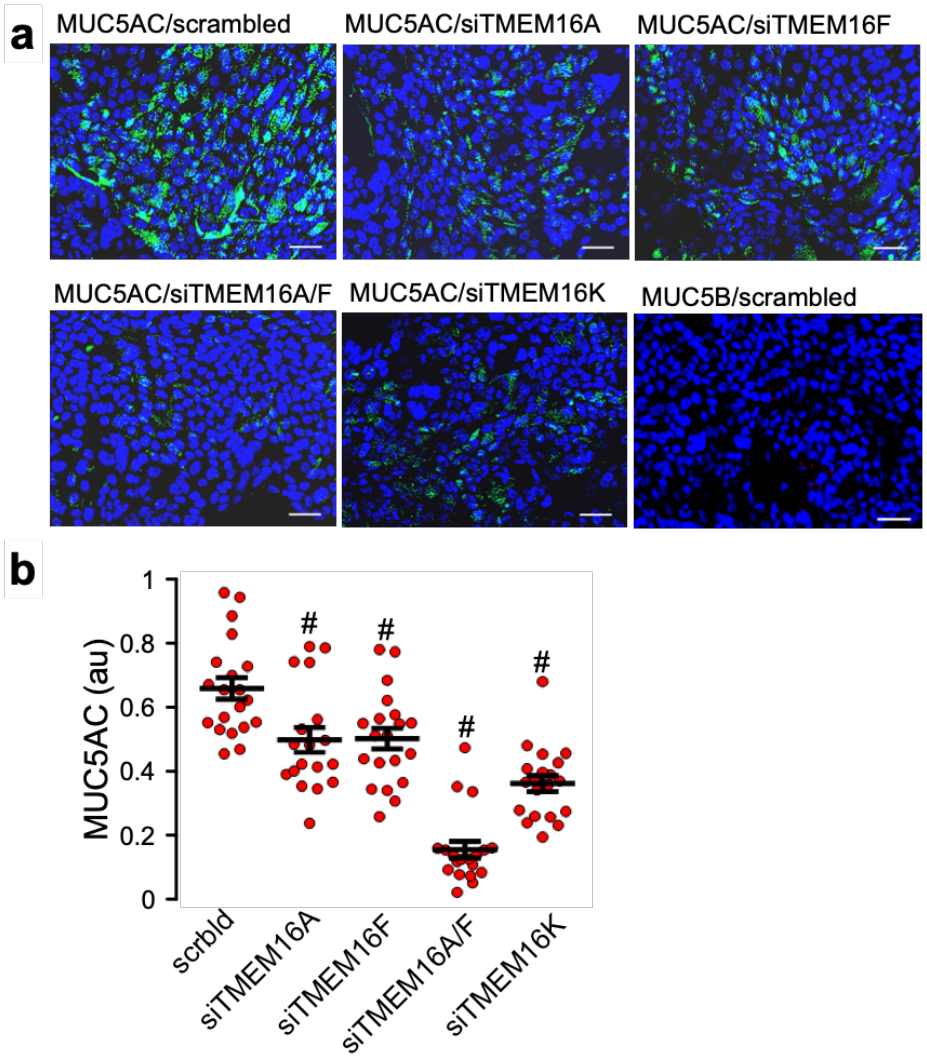

Supplementary Figure 4.4 | *Role of TMEM16A, TMEM16F and TMEM16K for mucus production in Calu3 cells.*

a IL-13 (20 ng/ml; 72 hrs) induced expression of MUC5AC but not MUC5B in Calu3 cells. siRNA for TMEM16A, TMEM16F, and TMEM16K suppressed expression of MUC5AC. **b** Inhibition of MUC5AC expression by knockdown of TMEM16 proteins. (n=19-21 images analyzed for each). Mean ± SEM; #significant inhibition ($p<0.05$; ANOVA).

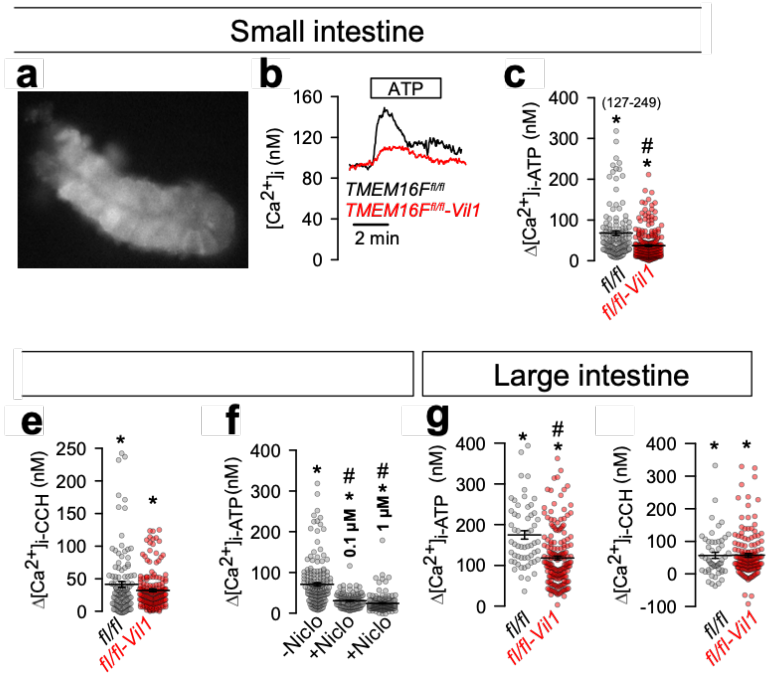

Supplementary Figure 4.5 | *Inhibition of intestinal Ca^{2+} signals in the absence of TMEM16F, and by niclosamide.*

a Crypt from small intestine (jejunum) loaded with the Ca^{2+} dye Fura2 (5 µM/30 min). **b** ATP (100 µM) induced Ca^{2+} signals in crypt cells from TMEM16F$^{flox/flox}$ (fl/fl) and TMEM16F$^{flox/flox}$ Vil1Cre (fl/fl-Vil1) littermates. **c,d** Summary of ATP (100 µM) and carbachol (CCH, 100 µM) induced Ca^{2+} peaks, respectively (n=118-249 cells). **E** Inhibition of ATP-induced Ca^{2+} increase by two different concentrations of niclosamide (Niclo; n=175-195 cells). **f,g** Summary of ATP (100 µM) and carbachol (CCH, 100 µM) induced Ca^{2+} peaks in colonic crypt cells from fl/fl and fl/fl-Vil1 littermates (n=53-183 cells). Mean ± SEM; *significant activation (p<0.05; paired t-test). #significant difference when compared to fl/fl or –niclo, respectively (p<0.05; unpaired t-test).

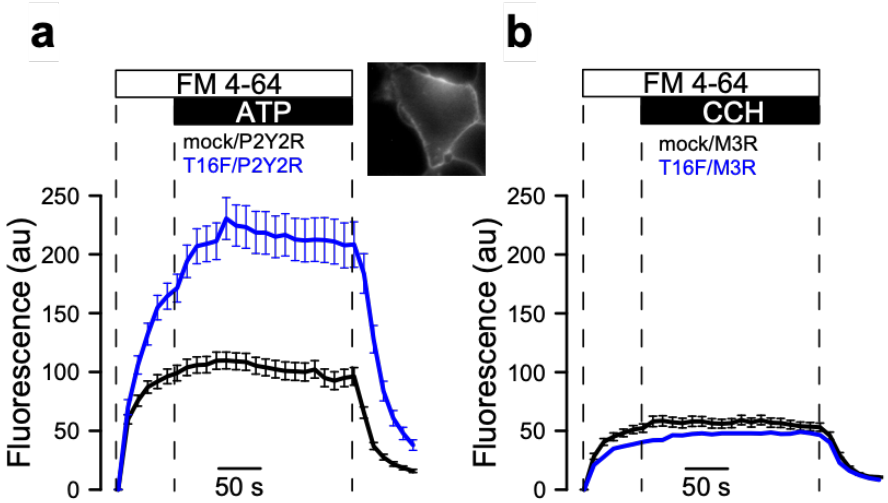

Supplementary Figure 4.6 | *Coupling of P2Y2 receptors but not muscarinic M3 receptors with TMEM16F.*

a Effect of ATP (100 µM) on plasma membrane insertion of the lipid dye FM4-64, present in the

extracellular bath solution. Increase in FM4-64 fluorescence in the plasma membrane of HEK293 cells can be taken as a measure for endosomal recycling/exocytosis. Cells expressing TMEM16F in addition to $P2Y_2$ receptors, show stronger basal FM4-64 fluorescence, which is further enhanced by stimulation with ATP. Inset: FM4-64 labeled HEK293 cell. **b** Effect of CCH (carbachol; 100 μM) on FM4-64 insertion and staining of the plasma membrane in HEK293 cells expressing mock/M3R or TMEM16F/M3R. Lower basal FM6-64 fluorescence and lack of muscarinic stimulation of membrane exocytosis was observed in these cells. Mean ± SEM; n = 30 cells for each experimental series.

CHAPTER 5 | TMEM16A DRIVES RENAL CYST GROWTH BY AUGMENTING CA^{2+} SIGNALING IN M1 CELLS

Abstract

Polycystic kidney disease (PKD) leads to continuous decline of renal function by growth of renal cysts. Enhanced proliferation and transepithelial chloride secretion through cystic fibrosis transmembrane conductance regulator (CFTR) and Ca^{2+} activated TMEM16A Cl^- channels is thought to cause an increase in cyst volume. Recent work shows the pro-proliferative role of the Ca^{2+} activated Cl^- channel TMEM16A (anoctamin 1) and demonstrates the essential contribution of TMEM16A to CFTR-dependent Cl^- secretion. The present data now demonstrate an increase in intracellular Ca^{2+} ($[Ca^{2+}]i$) signals and Cl^- secretion by TMEM16A, in renal collecting duct principle cells from dog (MDCK) and mouse (M1) as well as primary tubular epithelial cells from PKD1-/- knockout mice. M1 organoids proliferated, increased expression of TMEM16A and secreted Cl^- upon knockdown of endogenous polycystin 1 or 2 (PKD1,2) by retroviral transfection with shPKD1 and shPKD2, respectively. Knockdown of PKD1 or PKD2 increased basal intracellular Ca^{2+} levels and enhanced purinergic Ca^{2+} release from endoplasmic reticulum. In contrast, ryanodine receptors were found not to be expressed and caffeine had no effects on $[Ca^{2+}]i$. Ca^{2+} signals, proliferation and Cl^- secretion were largely reduced by knockdown or blockade of TMEM16A. TMEM16A may therefore be important for enhanced Ca^{2+} release from IP_3-sensitive Ca^{2+} stores in polycystic kidney disease.

Key words: ADPKD, renal cysts, TMEM16A, anoctamin 1, Ca^{2+} activated Cl^- channel

Submitted for publication: Inês Cabrita, Björn Buchholz, Rainer Schreiber, Karl Kunzelmann. TMEM16A drives renal cyst growth by augmenting Ca^{2+} signaling. J. Mol. Med 2020 March 18; 98, 659–671.

Own experimental contribution: Viral transfection, Western blotting, M1 organoid model, Immunocytochemistry, Cell proliferation assay, Ussing Chamber experiments, Measurement of intracellular Ca^{2+}.

Own written contribution: Methods, Results, Parts of Introduction and Discussion.

Other contributions: Designed experiments and analyzed data.

Introduction

Frequent autosomal dominant polycystic kidney disease (ADPKD) accounts for 5 –10 % of end-stage renal disease [369]. ADPKD is characterized by continuous cyst enlargement over time, leading to compression of adjacent healthy parenchyma [152]. ADPKD is caused by mutations in PKD1 (polycystin 1) or PKD2 (polycystin 2), but the underlying complex molecular events leading to continuous cyst growth are still poorly understood [166]. In normal renal epithelial cells, PKD1 and PKD2 appear to be located in the primary cilium, a single antenna-like protrusion of the plasma membrane, where they form a complex of receptor and Ca^{2+} influx channel [201]. Ca^{2+} ions are more concentrated within the primary cilium compared to the cytoplasm, however, Ca^{2+} signals generated within the cilium may occur independent of cytoplasmic Ca^{2+} signaling [205]. Loss of the primary cilium or loss of PKD1 /PKD2 function leads to relocalization of the polycystins to plasma membrane and endoplasmic reticulum, with the consequence of disturbed intracellular Ca^{2+} signaling [370].
We reported earlier an upregulation of the Ca^{2+} activated chloride channel TMEM16A (anoctamin 1) in polycystic kidney disease. TMEM16A enables calcium-activated chloride secretion that supports expansion of renal cysts and probably proliferation of the cyst–forming epithelium [44]. Remarkably, primary cilia present in terminally differentiated naïve cells or in non-proliferating cells in culture, contain TMEM16A as well as the paralogous proteins TMEM16F and TMEM16K [39,209,371]. Loss of expression of TMEM16A was shown to compromise ciliary genesis and decreased length of the primary cilium and of motile cilia [39,40,142].
In the presence of TMEM16A basal and agonist-induced Ca^{2+} levels are increased [78,348]. TMEM16A was shown to couple to inositol 1,4,5-trisphosphate (IP_3) receptors [78,348] and different TRP Ca^{2+} influx channels [372]. TMEM16A enhances ER Ca^{2+} store release by tethering the ER to the membrane localized receptor signaling complex. As a result, transmembrane signaling, fluid secretion or general cellular properties like proliferation, migration or volume regulation are affected. We examined in the present study, whether TMEM16A contributes to disturbed Ca^{2+} signaling observed in ADPKD. We further asked whether TMEM16A-related changes in Ca^{2+} signaling affect proliferation and fluid secretion. We found upregulation of TMEM16A with the loss of PKD1 or PKD2 expression. TMEM16A supported Ca^{2+} store release, cell proliferation and fluid secretion and thereby contributes to cyst growth.

Materials and Methods

Cells, animals, virus production RT-PCR, cDNA. MDCK M2 and C7 cell lines were cultured in DMEM supplemented with 10% Fetal Bovine Serum (FBS). M1 cells were cultured DMEM/F12 medium supplemented with 5% (v/v) fetal bovine serum (FBS), 1% Insulin-

Transferrin-Selenium 100x (ITS), and 1% L-Glutamine 200mM (all from Capricorn Scientific GmbH, Ebsdorfergrund, Germany) at 37°C in a humidified incubator in 5% (v/v) CO_2. M1 cells were transduced to downregulate Pkd1 and Pkd2. Mice with a floxed PKD1 allele were generously provided by Prof. Dr. Dorien J.M. Peters (Department of Human Genetics, Leiden University Medical Center, Leiden, The Netherlands) [161]. Experiments were approved by the local Ethics Committee of the Government of Unterfranken/Wuerzburg (AZ: 55.2-2532-2-328). Animals were euthanized between week 8-12, medullary tubular epithelial cells were isolated and were kept as primary culture. M1 cells were infected with lentiviral recombinant vectors containing the shRNAs of mouse Pkd1 (5´-GAATATCGGTGGGAGATAT) and Pkd2 (5´-GCATCTTGACCTACGGCATGA) with YFP_{I152L}, as previously described [373,374]. Stable transfected M1 cells were maintained in the presence of 5 µg/ml of Puromycin (Thermo Fisher Scientific, Darmstadt, Germany).

For semi-quantitative RT-PCR total RNA from M1 cells, MDCK cells and murine kidney were isolated using NucleoSpin RNA II columns (Macherey-Nagel, Düren, Germany). Total RNA (1 µg / 50 µl reaction) was reverse-transcribed using random primer (Promega, Mannheim, Germany) and M-MLV Reverse Transcriptase RNase H Minus (Promega, Mannheim, Germany). Each RT-PCR reaction contained sense (0.5 µM) and antisense primer (0.5 µM) (Table 5.1), 0.5 µl cDNA and GoTaq Polymerase (Promega, Mannheim, Germany). After 2 min at 95°C cDNA was amplified (30 cycles) for 30 s at 95°C, 30 s at 57°C and 1 min at 72°C. Realtime PCR of cDNA samples was performed in a LightCycler 480 device (Roche, Basel, Switzerland) using specific, intron-spanning primers (Table 5.2) and a SYBR® Green mastermix (Takyon, Eurogentec, Belgium). Target gene expression levels were quantified relative to beta-actin expression under consideration of PCR efficiencies calculated on the basis of standard dilution curves. The specificity of PCR amplifications was verified by agarose electrophoresis and melting curve analysis. PCR products were visualized by loading on peqGREEN (Peqlab; Düsseldorf, Germany) containing agarose gels and analysed using ImageJ.

Table 5.1 | *RT-PCR Primer (mouse).*

Tmem16a (mouse)	forward: 5´- GTGACAAGACCTGCAGCTAC reverse: 5´- GCTGCAGCTGTGGAGATTC	406 bp
Tmem16a (dog)	forward: 5´- CTATAAGCTCCAGTCCCTAC reverse: 5´- CGACCCCGTGAATTTTAGTG	513 bp
Tmem16f (mouse)	forward: 5´- CATACGAATCTAACCTTATCTGC reverse: 5´- CATTCTCTGTACAGGAGGTAAC	520 bp
Cftr (mouse)	forward: 5´- GAATCCCCAGCTTATCCACG reverse: 5´- CTTCACCATCATCTTCCCTAG	544 bp
αEnac (Scnn1a, mouse)	forward: 5´- CCTTGACCTAGACCTTGACG reverse: 5´- CGAATTGAGGTTGATGTTGAG	409 bp
βEnac (Scnn1b, mouse)	forward: 5´- CAATAACACCAACACCCACG	588 bp

	reverse: 5´- GAGAAGATGTTGGTGGCCTG	
γEnac (Scnn1g, mouse)	forward: 5´- GCACCGACCATTAAGGACC reverse: 5´- GCCTTTCCCTTCTCGTTCTC	464 bp
Nkcc1(Slc12a2, mouse)	forward: 5´- GCGAGAAGGTGCACAATAC reverse: 5´- CTGTACGGCTCGATCATGTC	747 bp
Pkd1 (mouse)	forward: 5´- GTGGAAAGCAGGTCGGAAG reverse: 5´- TCGTCTCGTTCAGCACCAG	236 bp
Pkd2 (mouse)	forward: 5´- GTGGATGTACACAAGTGAGAAGGAGC reverse: 5´- CACGACAATCACAACATCCAGACA	454 bp
Ptch1 (mouse)	forward: 5´- GTCTTGGGGGTTCTCAATGGACTGG reverse: 5´- ATGGCGGTGGACGTTGGGTTCC	590 bp
Ptch2 (mouse)	forward: 5´- GTGTGATCCTCACCCCGCTTGACTG reverse: 5´- CGCTCCAGCCGATGTCATGTGTC	487 bp
Gapdh (dog, mouse)	forward: 5´- GTATTGGGCGCCTGGTCAC reverse: 5´- CTCCTGGAAGATGGTGATGG	200 bp

Table 5.2 | *Primers for real time PCR.*

mouse Tmem16a	forward: 5´-AGGAATATGAGGGCAACCTG reverse: 5´-CGACACCATGGATTTTGGTA	75
mouse Pkd1	forward: 5´-CATAGTGTGGAAAGCAGGTC reverse: 5´-CAGTGACCCTCCAAGTACAC	159
mouse Pkd2	forward: 5´-CTCAGGAGGAACTTCTGG reverse: 5´-GAAACTGCCAAGAGGGTAC	148
beta-actin	forward: 5´-CAACGGCTCCGGCATGTG reverse: 5´- CTTGCTCTGGGCCTCGTC	151

Western Blotting: Protein was isolated from cells using a sample buffer containing 25 mM Tris-HCl, 150 mM NaCl, 100 mM dithiothreitol, 5.5% Nonidet P-40, 5% glycerol, 1 mM EDTA and 1% protease inhibitor mixture (Roche, Mannheim, Germany). Proteins were separated by 7 % sodium dodecyl sulfate (SDS) polyacrylamide gel and transferred to a polyvinylidene difluoride membrane (GE Healthcare Europe GmbH, Munich, Germany) or 4-20% Mini-PROTEAN TGX Stain-Free (Bio-Rad) using a semi-dry transfer unit (Bio-Rad). Membranes were incubated with primary anti-Tmem16a rabbit polyclonal antibody (Davids Biotech, Regensburg, Germany; 1:1000), anti-PKD1 (Polycystin-1 (7E12), Santa Cruz; 1:500) mouse antibody or anti-PKD2 (Polycystin-2 (D-3), Santa Cruz; 1:500) mouse antibody, overnight at 4 °C. Proteins were visualized using horseradish peroxidase-conjugated secondary antibody and ECL detection. Actin was used as a loading control.

M1 organoid model. M1 cells were resuspended as a single-cell suspension in 50/50% Matrigel/ type I collagen and transferred into 24-well plates (30×10^3 cells/well, four wells per condition) for 9 days. Medium was changed every 3 days. Every 3 days thirty random visual fields per well were photographed with an Axiovert 200 microscope (Zeiss, Germany). Cyst area of the lumina (~30–150 cysts per condition and single experimental procedure) were measured with AxioVision (Zeiss, Germany). Cyst volume was then estimated using

the formula for the volume of a sphere, $4/3\pi r^3$.

Immunocytochemistry. M1 cells grown under confluent conditions for 4 days on glass coverslips and M1 organoids grown for 6 days were fixed for 10 min with methanol at -20 °C. Organoids were isolated with ice cold 5 mM EDTA in PBS and seeded in poly-L-lysine coated coverslips. After seeded, cells were fixed for 10 min with methanol at -20 ºC. After washing, the cells were permeabilized with 0.5% (v/v, PBS) Triton X-100 for 10 min and blocked with 1% (w/v, PBS) bovine serum albumin for 1 h at room temperature. The cells were incubated overnight with primary antibodies (1:100) against rabbit anti-TMEM16A [37] (Davids Biotechnologie, Regensburg, Germany), rat anti-Ki-67 (DAKO, M7249, Germany), anti-mouse CFTR antibody ACL-006 (Alomone labs, Jerusalem, Israel), or mouse anti-acetylated tubulin (T7451, Sigma-Aldrich, Germany). Binding of the primary antibody was visualized by incubation with appropriate secondary antibodies conjugated with Alexa Fluor 488 or Alexa Fluor 546 (1:300, Molecular Probes, Invitrogen). Nuclei were stained with Hoe33342 (0.1 g/ml PBS, AppliChem, Darmstadt, Germany). Glass coverslips were mounted on glass slides with fluorescent mounting medium (DakoCytomation, Hamburg, Germany) and examined with an ApoTome Axiovert 200M fluorescence microscope (Zeiss, Germany).

Cell proliferation assay. M1 cells were plated in 96-well plates at a density of 2×10^3 cells per well for the time duration as indicated (0, 3, 6 and 9 days). Medium was changed every 3 days. Cells were incubated for 2 h in 100 µl of fresh media containing 0.5 mg/ml of the tetrazolium salt MTT. The dark blue formazan product was dissolved with DMSO and measured the absorbance at 595 nm.

Ussing Chamber. MDCK or M1 cells were grown as polarized monolayers on permeable supports (Millipore MA, Germany) for 8 days. Cells were mounted into a perfused micro-Ussing chamber, and the luminal and basolateral surfaces of the epithelium were perfused continuously with Ringer's solution (mmol/l: NaCl 145; KH_2PO_4 0.4; K_2HPO_4 1.6; glucose 5; $MgCl_2$ 1; Ca^{2+} gluconate 1.3) at a rate of 5 ml/min (chamber volume 2 ml). Bath solutions were heated to 37 °C, using a water jacket. Experiments were carried out under open circuit conditions. In addition, 100 µM ATP/UTP were added on the apical or basolateral side, or 100 µM 3-isobutyl-1-methylxanthine and 2 µM Forskolin (I/F) were added on the basolateral side, or 2 µM Ionomycin were added on the apical side, as indicated in the figure. Data were collected continuously using PowerLab (AD Instruments, Australia). Values for transepithelial voltages (V_{te}) were referred to the basolateral side of the epithelium. Transepithelial resistance (R_{te}) was determined by applying short (1 s) current pulses (ΔI = 0.5 µA). R_{te} and equivalent short circuit currents (I'_{SC}) were calculated according to Ohm's law ($R_{te} = \Delta V_{te} / \Delta I$, $I'_{SC} = V_{te} / R_{te}$).

Measurement of $[Ca^{2+}]_i$. Primary cilium and membrane Ca^{2+} signals were detected after MDCK M2 and C7 cell were transfected with 5HT6-mCherry-GECO1.0 (5HT6-GECO ,

Addgene, Cambridge, MA, USA; [375]. Cells were grown to confluence in glass coverslips and serum starved for 4-6 days to induce cilium formation. Afterwards, the cells were mounted and perfused in Ringer's solution. The mCherry fluorescence of the indicator was used to localize the Ca^{2+} sensor. Therefore, before each experiment, a photo was taken exciting the 5HT6-GECO at 560 nm, and the emission was recorded between 620±30 nm using a CCD-camera (CoolSnap HQ, Visitron Systems, Germany). To measure the ciliary Ca^{2+} changes, 5HT6-GECO was excited at 485/405 nm, and the emission was recorded between 535±12,5 nm. The results for $[Ca^{2+}]$cilium and $[Ca^{2+}]$cyt were obtained at 485/405 nm changes and given in ratio. Measurement of the global cytosolic Ca^{2+} changes were performed as described recently [16]. In brief, cells were loaded with 5 µM Fura-2, AM (Molecular Probes) in OptiMEM (Invitogen) with 0.02% pluronic (Molecular Probes) for 1h at RT and 30 min at 37°C. Fura-2 was excited at 340/380 nm, and the emission was recorded between 470 and 550 nm using a CCD-camera (CoolSnap HQ, Visitron Systems, Germany). Control of experiment, imaging acquisition, and data analysis were done with the software package Meta-Fluor (Universal imaging, USA). $[Ca^{2+}]_i$ was calculated from the 340/380 nm fluorescence ratio after background subtraction. The formula used to calculate $[Ca^{2+}]_i$ was $[Ca^{2+}]_i = Kd \times (R-R_{min})/(R_{max}-R) \times (S_{f2}/S_{b2})$, where R is the observed fluorescence ratio. The values R_{max} and R_{min} (maximum and minimum ratios) and the constant S_{f2}/S_{b2} (fluorescence of free and Ca^{2+}-bound Fura-2 at 380 nm) were calculated using 1 µmol/liter ionomycin (Calbiochem), 5 µmol/liter nigericin, 10 µmol/liter monensin (Sigma), and 5 mmol/liter EGTA to equilibrate intracellular and extracellular Ca^{2+} in intact Fura-2-loaded cells. The dissociation constant for the Fura-2•Ca^{2+} complex was taken as 224 nmol/liter. ER Ca^{2+} signals were detected in Ca^{2+} sensor ER-LAR-GECO1 (Addgene, Cambridge, MA, USA, [376] expressing M1 cells. Cells were excited at 560 nm and emission was recorded between 620±30 nm.

Materials and statistical analysis: All compounds used were of highest available grade of purity. The number of experiments is provided for each single experiment. Statistical differences between samples were examined using paired and unpaired Student's t-tests, with significance assumed when $p<0.05$, after variances homogeneity of the samples were tested by F-test. Differences between more than two means were tested by using one-Way ANOVA with a Bonferroni-Holm multiple comparisons test (post-hoc test) with significance assumed when $P<0.05$.

Results

TMEM16A augments fluid secretion by increase in intracellular Ca^{2+}. We demonstrated earlier the impact of TMEM16A on fluid secretion and cyst growth in a MDCK cyst model and in embryonic kidney cultures [44]. MDCK cells derived from dog principle cells exist as a MDCK-C7 clone expressing TMEM16A, and as a MDCK-M2 clone, lacking expression of

TMEM16A (Fig. 5.1a). The Ca^{2+} sensor Fura2 showed a remarkable increase in intracellular Ca^{2+} when C7 cells were stimulated with the purinergic agonists ATP or UTP (Fig. 5.1b-d). In contrast, M2 cells lacking expression of TMEM16A showed a much reduced Ca^{2+} response upon purinergic stimulation. In TMEM16A-expressing C7 cells a pronounced Cl^- secretion was activated by ATP/UTP, which was potently inhibited by siRNA-knockout of TMEM16A (Fig. 5.1e) [44]. In contrast, Cl^- secretion is largely reduced in M2 cells, as reported earlier [209]. Moreover, because siRNA-knockdown of TMEM16F did not affect Ca^{2+} activated Cl^- currents, the data suggest that TMEM16A is the Ca^{2+} activated Cl^- channel in MDCK cells, similar to other tissues (Fig. 5.1f,g) [209].

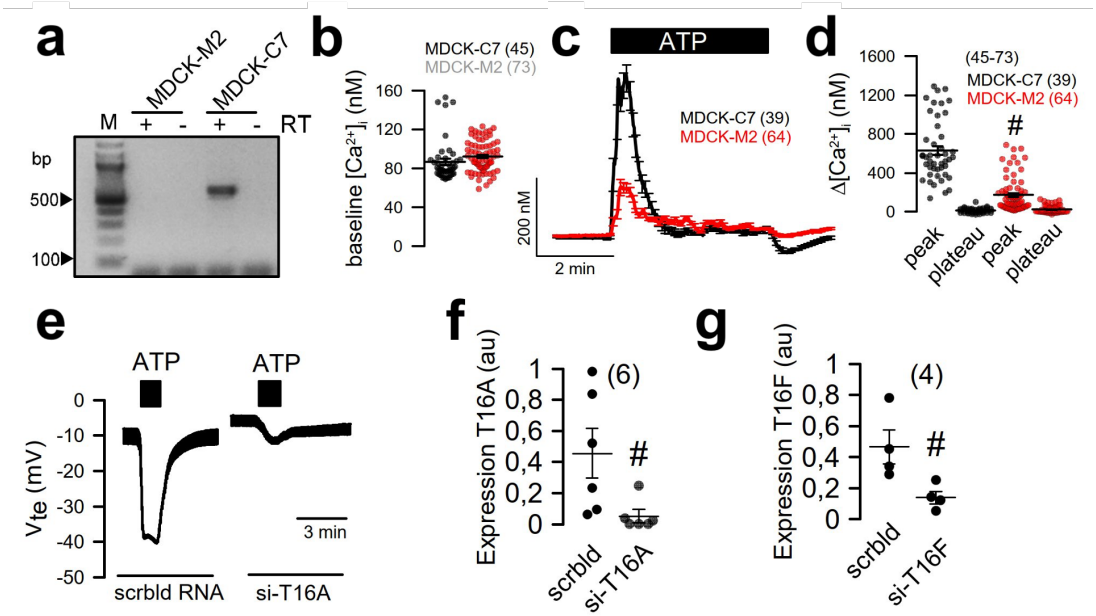

Figure 5.1 | *TMEM16A augments Ca^{2+} signaling and ion transport in MDCK cells.*

a RT-PCR indicating expression of TMEM16A in MDCK-C7 cells but not in MDCK-M2 cells. **b** Summary of basal Ca^{2+} levels in MDCK-C7 and MDCK-M2 cells. **c,d** Assessment of intracellular Ca^{2+} using the Ca^{2+} sensor Fura2. ATP or UTP (both 100 µM) increased intracellular peak and plateau Ca^{2+} in MDCK-C7 and MDCK-M2 cells. **e** Original recordings and summary of ATP or UTP induced transepithelial voltages in MDCK-C7 cells and effect of TMEM16A-knockout. **f,g** Effect of siRNA on expression of TMEM16A and TMEM16F, respectively, as assessed by quantitative RT-PCR. Mean ± SEM (number of cells measured). #significant difference when compared to C7 and scrambled, respectively.

TMEM16A was found to be expressed in plasma membrane and primary cilium of MDCK and naïve renal tubular epithelial cells [39,371] (Fig. 5.2a). Ca^{2+} changes in primary cilium and near the plasma membrane were measured using 5-HT6-G-GECO1 (kindly provided by Prof. Takanari Inoue, Johns Hopkins University, Baltimore, USA; Fig. 5.2b). A Ca^{2+} rise in both cilium and near plasma membrane was detected upon purinergic stimulation with ATP or UTP (Fig. 5.2c-e). Importantly, peak increase in $[Ca^{2+}]_i$ (store release) was similar in

plasma membrane and cilium also in the absence of extracellular Ca^{2+} (Fig. 5.2f,g). Purinergic Ca^{2+} rise was larger in the primary cilium than close to the plasma membrane, but otherwise qualitatively similar. It was attenuated in MDCK-M2 cells lacking expression of TMEM16A (Fig. 5.2h,i). Moreover, overexpression of TMEM16A in MDCK-M2 increased the ATP-induced Ca^{2+} signal in both cilium and plasma membrane. These results are in line with the previously reported role of TMEM16 proteins in Ca^{2+} signaling [348].

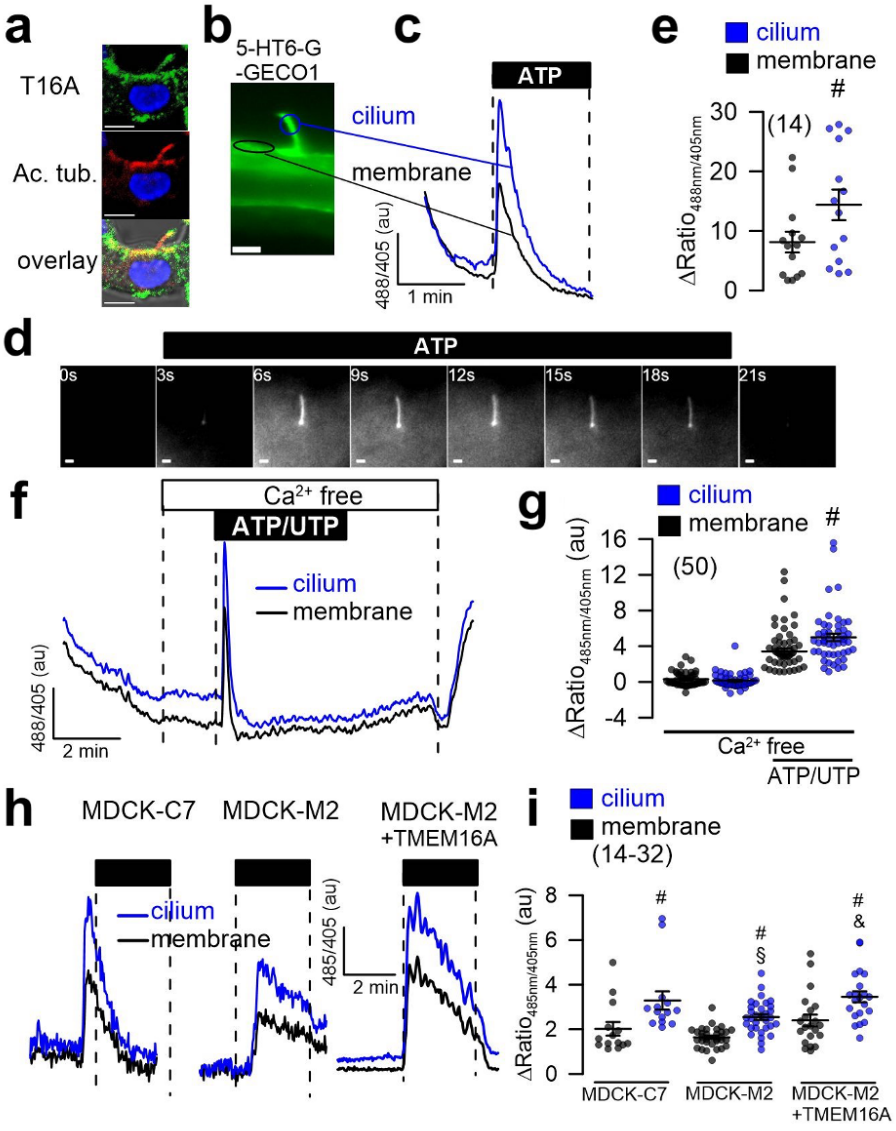

Figure 5.2 | *Role of TMEM16A in plasma membrane and primary cilium of MDCK cells.*

a TMEM16A (green), acetylated tubulin (red) and overlay showing expression of TMEM16A in primary cilium and plasma membrane of a naïve renal epithelial cell. **b** Ca^{2+} sensor 5-HT6-G-GECO1 expressed in the primary cilium and near plasma membrane allowing measurement of Ca^{2+} in both compartments. **c-e** Original recordings and summary of Ca^{2+} signals elicited by stimulation with ATP or UTP (both 100 µM) in primary cilium and near plasma membrane. Bars = 1 µm. **f,g** Increase of intracellular Ca^{2+} in the absence of extracellular Ca^{2+}. **h,i** Comparison of purinergic Ca^{2+} increase in MDCK-C7 (expressing TMEM16A) and MDCK-M2 (not expressing TMEM16A). Expression of TMEM16A in the M2 clone increased the ATP-induced Ca^{2+} signal in both cilium and plasma

membrane. Bars = 2 µm. Mean ± SEM (number of cells measured). #significant difference when compared to membrane ($p<0.05$; unpaired t-test). §significant difference when compared to MDCK-C7 ($p<0.05$; unpaired t-test).

Loss of PKD1 or PKD2 induces Cl^- secretion in M1 renal organoids. We further examined the role of TMEM16A and other PKD-associated proteins for cyst growth, cell proliferation and Ca^{2+} signaling using a 3D culture model. To that end M1 mouse collecting duct cells were analyzed for expression of the relevant proteins polycystin (PKD1, PKD2), TMEM16A, TMEM16F, CFTR, NKCC1, and αβγENaC (Fig. 5.3a). Cells were grown in a collagen/Matrigel matrix and readily formed spherical renal organoids (Fig. 5.3b,c). The cells appeared highly differentiated and produced primary cilia (Fig. 5.3d,e).

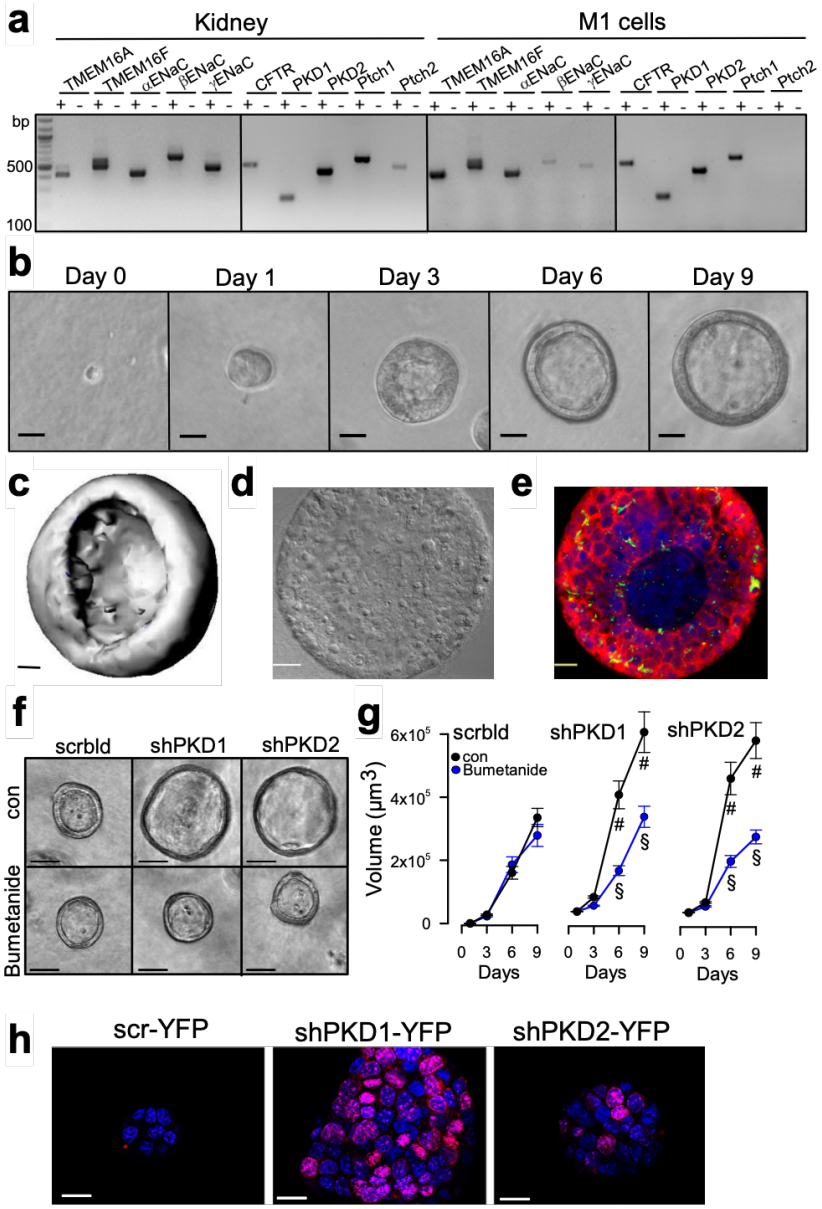

Figure 5.3 | *M1 renal organoid and cyst model.*

a RT-PCR analysis of mRNA expression of ion channels and receptors in mouse kidney and M1

collecting duct cells: TMEM16A, TMEM16F, αβγ-ENaC, NKCC1, PKD1, PKD2, and the receptors patched 1,2 (Ptch1,2). Similar expression patterns were found in mouse kidney and M1 cells. +/- indicate presence/absence of reverse transcriptase. **b** Time-dependent development of renal organoids in Matrigel (n = 20). Bars = 20 µm. **c** Reconstructed 3D image from a renal M1 organoid with a view inside the organoid. Bar = 20 µm. **d,e** Differential interference contrast (DIC) image and immunocytochemistry of a cross-section of an organoid. Green, primary cilia; red, CFTR; blue, DAPI. Bars = 20 µm. **f,g** Increase of the volume of M1 organoids by shRNA-knockdown of PKD1 or PKD2. The presence of the NKCC1-inhibitor bumetanide (100 µM) did not change the size of control organoids (treated with scrambled RNA; scrbld), but inhibited further enlargement by shRNA-knockdown of PKD1 or PKD2, indicating fluid secretion upon knockdown of PKD1,2. Bars = 50 µm. **h** Increase of proliferative activity in shPKD1/shPKD2 organoids as indicated by Ki-67 staining. Bars = 20 µm. Mean ± SEM (number of organoids measured). $^{\#}$significant difference when compared with scrambled ($p<0.05$; unpaired t-test). §significant difference when compared to absence of bumetanide ($p<0.05$; unpaired t-test).

Enhanced secretion and proliferation in PKD require TMEM16A. A hallmark of renal cysts is the upregulation of proliferation [377]. TMEM16A is well known to cause cell proliferation and Cl^- secretion and proliferation. The proliferation marker Ki-67 demonstrated a strong upregulation of proliferation of M1 renal organoids upon knockdown of PKD1 or PKD2 (Fig. 5.4a). The effect of shRNA-PKD1 and shRNA-PKD2 was analyzed by Western blotting/densitometry and indicated a knockdown by 61 % and 92 %, respectively. In addition, significant suppression of mRNA for PKD1 and PKD2 was demonstrated by semiquantitative RT-PCR (Fig. 5.4b,c). Attenuation of expression of PKD1 or PKD2 and consecutive rise in cell proliferation was paralleled by a strong increase in TMEM16A expression (Fig. 5.4a, green staining). The increase in cell proliferation and enhanced TMEM16A-dependent secretion further enhanced the volume of M1 organoids (Fig. 5.4a,d). In contrast, organoid volume was significantly reduced in the presence of benzbromarone CaCCinhAO1, and Ani9, potent inhibitors of TMEM16A (Fig. 5.4d, Supplementary Fig. 5.1). Moreover, both inhibitors blocked proliferation of M1 cells as measured in proliferation assays (Fig. 5.4e).

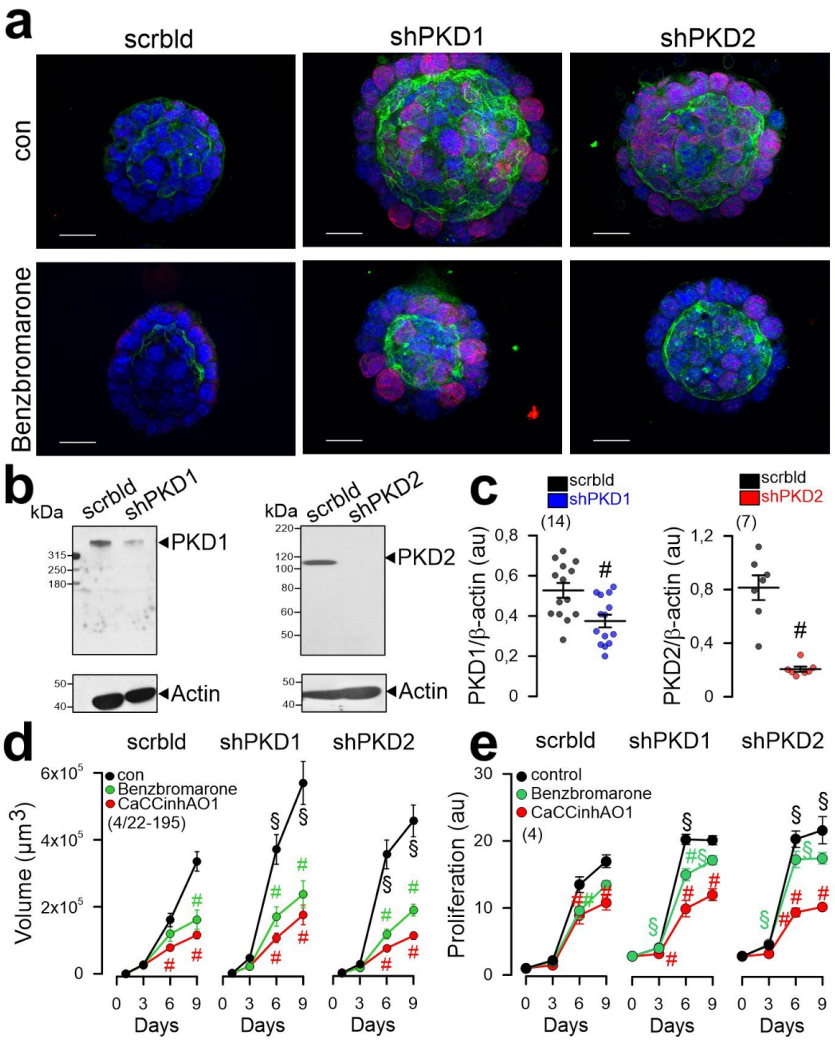

Figure 5.4 | *Increased expression of TMEM16A, proliferation and organoid growth by knockdown of PKD1 or PKD2.*

a Knockdown of both PKD1 or PKD2 induced cell proliferation (Ki-67 staining; red), enhanced expression of TMEM16A (green) and growth of M1 organoids. **b,c** Western blot and quantification of mRNA by semiquantitative RT-PCR indicates significant knockdown of PKD1 and PKD2 by small hairpin (sh) RNA. Western blots were performed in replicates and indicated a knockdown by 61 % and 92 %, respectively. **d,e** Increase in cyst volume and proliferation upon knockdown of PKD1/PKD2, and inhibition by 5 µM benzbromarone or CaCCinh172 [378]. Bars = 20 µm. Ki67 was quantified by measuring fluorescence intensity. Mean ± SEM (number of organoids measured). #significant difference when compared control ($p<0.05$; ANOVA). §significant difference when compared to scrambled ($p<0.05$; ANOVA).

M1 cells were grown as 2D cultures on permeable supports. Knockdown of PKD1 or PKD2 caused enhanced Cl^- secretion when stimulated by the Ca^{2+} dependent purinergic agonist ATP (Fig. 5.5a,c). Also, cAMP-dependent transport activated by IBMX and forskolin (IF) was augmented with knockdown of PKD1 or PKD2 (Fig. 5.5b,d). The data suggest that both Ca^{2+}-activated TMEM16A and cAMP-dependent CFTR Cl^- channels contribute to renal cyst development. Co-staining of TMEM16A (green) and calreticulin (red) indicate upregulation

of TMEM16A in plasma membrane and cytosol with knockdown of PKD1 or PKD2, while colocalization of TMEM16A with calreticulin was not observed (Fig. 5.5e,f).

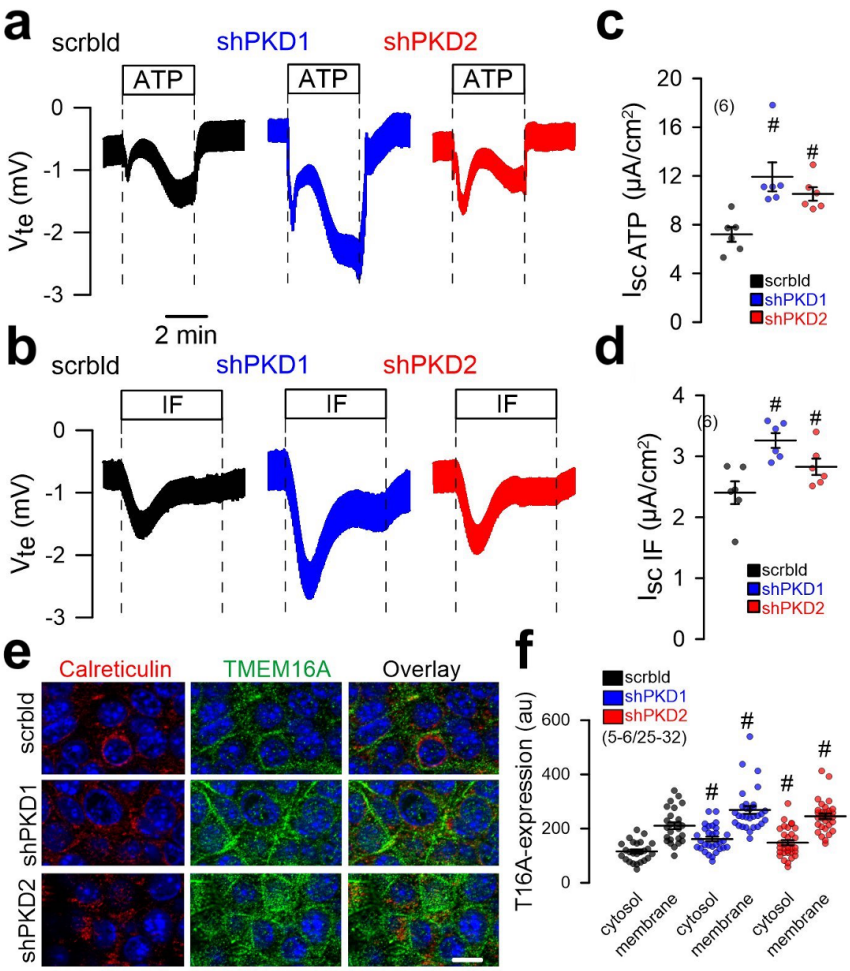

Figure 5.5 | *Induction of Cl^- secretion by knockdown of PKD1 or PKD2.*

a,c Original Ussing chamber recordings of polarized M1 cells grown permeable supports (2D culture). Enhanced Cl^- secretion by luminal stimulation with ATP (100 µM) or IF (100 µM IBMX and 2 µM forskolin) upon shRNA-knockdown of PKD1 or PKD2. **b,d** Summaries for calculated equivalent basal short circuit currents (I_{sc}) and I_{sc} activated by ATP and forskolin/IBMX, respectively. **e,f** Co-staining of TMEM16A (green) and calreticulin. Knockdown of PKD1 or PKD2 upregulated TMEM16A in plasma membrane and cytosol. No colocalization with calreticulin was observed. Bar = 20 µm. Mean ± SEM (number of organoids measured). #significant difference when compared scrambled ($p<0.05$; ANOVA).

Disturbed Ca^{2+} signaling in PKD relies on TMEM16A. Abrogated Ca^{2+} signaling in ADPKD has been intensely examined, but controversial results have been reported [370]. We reported a role of TMEM16A in Ca^{2+} signaling, i.e. enhanced agonist-induced Ca^{2+}-store release by TMEM16A [348]. Here we examined the role of TMEM16A for ER Ca^{2+}-store release through IP_3R and ryanodine receptors (RyR) upon knockdown of PKD1 and PKD2. shRNA-knockdown of PKD1 or PKD2 upregulated expression of TMEM16A (Fig. 5.6a).

Densiometric analysis indicates an upregulation of TMEM16A by 1.6 (shPKD1) and 1.8 (shPKD) fold. Knockdown of PKD1 or PKD2 enhanced basal $[Ca^{2+}]_i$ and augmented ATP-induced store release (Fig. 5.6b-d). The enhanced Ca^{2+} signals observed in the absence of PKD1 or PKD2 required the presence of TMEM16A, as both basal Ca^{2+} levels and ATP-induced store release were strongly attenuated by siRNA-knockdown of TMEM16A, which was 49 ± 3.8 % (n=5) (Fig. 5.6a,c-f). Successful knockdown of TMEM16A was further validated by real time RT-PCR and was 91 ± 8.5 % (n=3). Expression of TMEM16A is found in primary cilium and plasma membrane of polarized grown renal epithelial cells (Fig. 5.6g, upper panel). Similar to M1-organoids, also M1-monolayers increase expression of TMEM16A upon knockout of PKD1 or PKD2 (Fig. 5.6g, lower panel). Using the ER Ca^{2+} sensor ER-LAR-GECO1, we found higher basal ER Ca^{2+} levels and enhanced ATP-induced Ca^{2+} release in cells lacking expression of PKD1 or PKD2 (Fig. 5.6h-j). In contrast, knockdown of TMEM16A (Fig. 5.6a) strongly reduced store filling and ATP-induced Ca^{2+}-release (Fig. 5.6k).

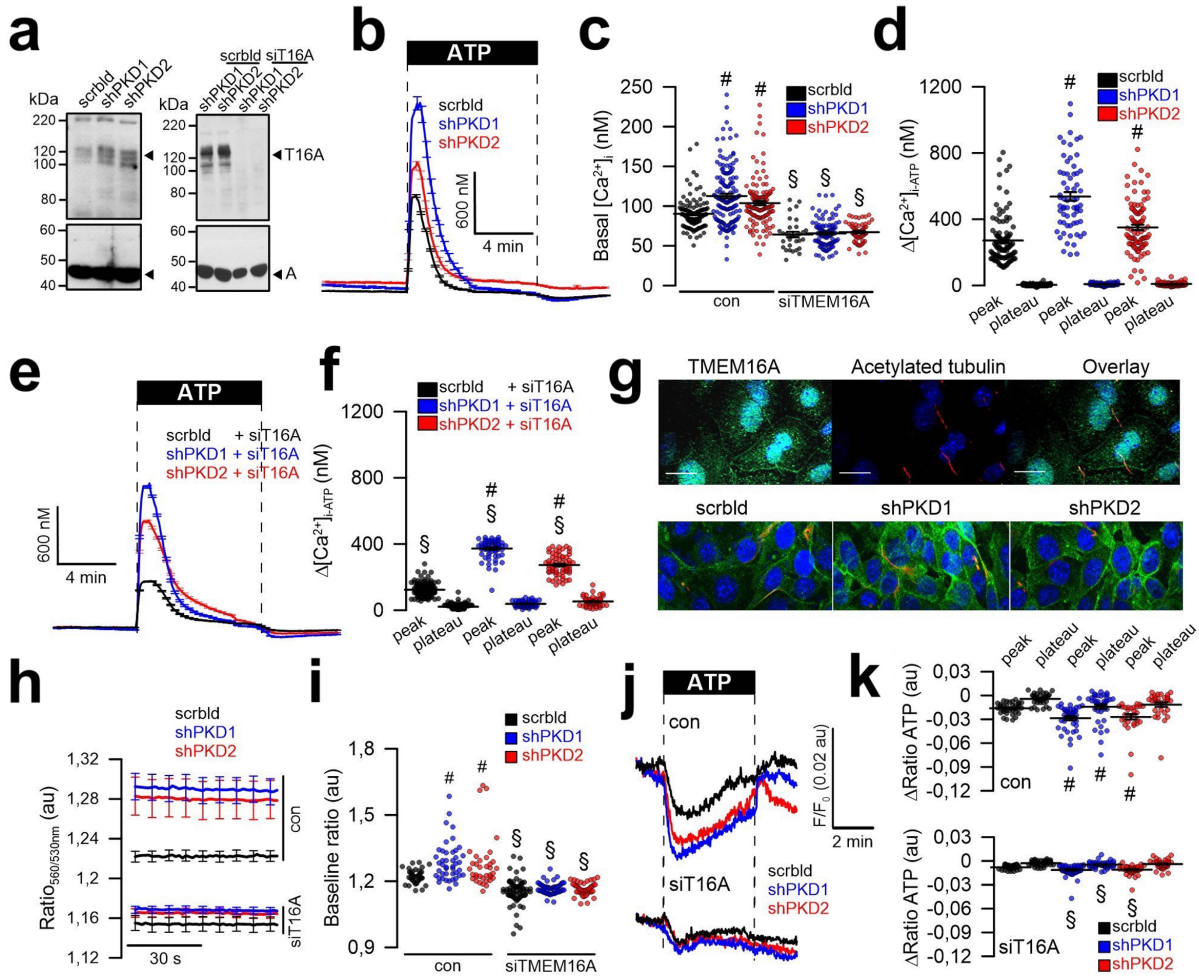

Figure 5.6 | *Upregulation of TMEM16A is essential for enhanced Ca^{2+} signaling upon knockdown of PKD1 and PKD2.*

a Left: Western blot indicating upregulation of TMEM16A by shRNA-knockdown of PKD1 or PKD2.

Blots were performed as replicates, Densiometric analysis indicates an upregulation of TMEM16A by 1.6 (shPKD1) and 1.8 (shPKD) fold. Right: siRNA-knockdown of TMEM16A upregulated by shRNA-knockdown of PKD1 or PKD2. Blots were performed in replicates. siRNA-knockdown of TMEM16A protein was 49 ± 3.8 % (n=5; Western blotting) and 91 ± 8.5 % (n=3, real time PCR). **b-d** Original recordings and summaries of basal Ca^{2+} and ATP (100 µM) induced Ca^{2+} increase (Fura2) in control cells (scrbld), and cells with a knockdown of PKD1 or PKD2, respectively. **e,f** Original recordings and summaries of ATP-induced Ca^{2+} increase in cells lacking expression of TMEM16A (siT16A). **g** Expression of TMEM16A in M1 control cells (scrbld) and cells lacking expression of PKD1 or PKD2. **h-j** Original recordings and summaries of the effect of ATP on ER Ca^{2+} levels in control cells and cells lacking expression of PKD1 or PKD2. **k** Attenuated ATP-induced Ca^{2+} release after knockdown of TMEM16A. Bars = 20µm. Mean ± SEM (number of monolayers measured). $^{\#}$significant difference when compared scrbld ($p<0.05$; ANOVA). §significant difference when compared to control ($p<0.05$; ANOVA).

Upregulated TMEM16A causes enhanced ER store release and store refill in ADPKD. Ryanodine receptors were claimed to have a role in flow-induced Ca^{2+} increase in mouse kidney [166]. However, the activator of RyR, caffeine, did not increase intracellular Ca^{2+}. Moreover, we did not detect expression of RyR1-3 in primary tubular epithelial cells from wild type or PKD1-/- knockout animals, of M1 collecting duct cells (Fig. 5.7a,b). In contrast, signals for RyR1-3 were clearly present in skeletal muscle, heart muscle, and brain, respectively (not shown). Lack of PKD1 or PKD2 increased store emptying induced by inhibition of SERCA with cyclopiazonic acid (CPA). Moreover, store operated Ca^{2+} entry (SOCE) was also enhanced by knockdown of PKD1/PKD2 (Fig. 5.7c,d). Enhanced store release and enhanced SOCE was strongly reduced in the absence of TMEM16A (Fig. 5.7e,f). Moreover, the inhibitor of transient receptor potential (TRP) channels SK&F96365 and the ORAI inhibitor YM58483 inhibited enhanced Ca^{2+} entry in PKD1/PKD2 knockout cells and abolished enhanced CPA-induced store release (Fig. 5.7g-j).

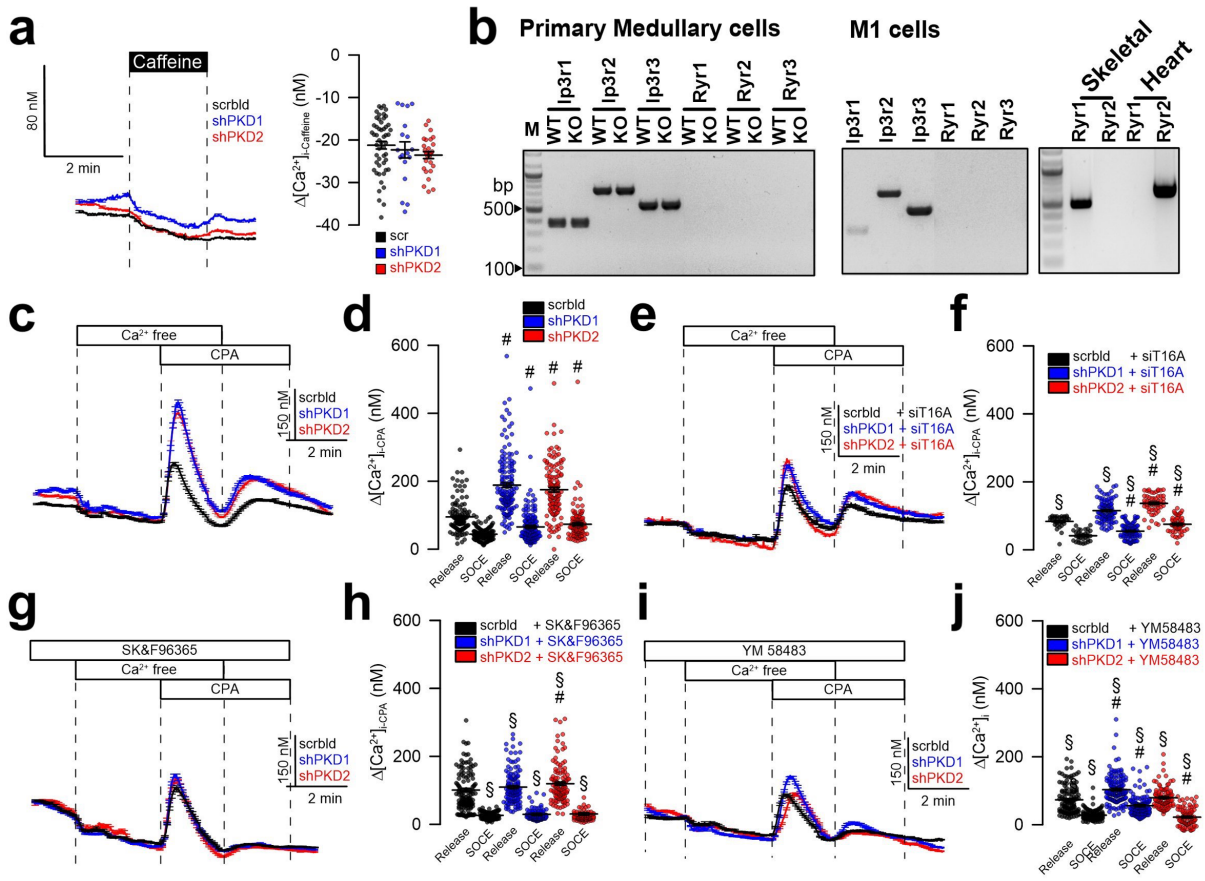

Figure 5.7 | *TMEM16A is essential for enhanced Ca^{2+} store release by knockdown of PKD1 and PKD2.*

a,b Lack of effects of caffeine on intracellular Ca^{2+} and lack of expression of RyR1-3 in mouse primary renal medullary and M1 collecting duct cells. c,d CPA (10 µM) induced store release in the presence or absence PKD1/PKD2. e,f CPA-induced store release was strongly attenuated by siRNA-knockdown of TMEM16A. g-j Original recordings and summaries of CPA-induced Ca^{2+} store release and SOCE in the presence of SK&F96365 and YM58483 (both 5 µM). Mean ± SEM (number of monolayers measured). #significant difference when compared scrbld ($p<0.05$; ANOVA). §significant difference when compared to absence of siT16A or SK&F96365/YM58483, repectively ($p<0.05$; ANOVA).

Finally, to confirm the present results in M1 cells we compared primary renal tubular epithelial cells from $PKD^{+/+}$ and $PKD1^{-/-}$ mice. We found enhanced ATP-induced Ca^{2+} store release, with a consecutive enhancement of store operated Ca^{2+} influx (SOCE) in cells from PKD-/- animals, almost identical to the results obtained in M1 cells (Fig. 5.8). Taken together the present data demonstrate augmented Ca^{2+} signals in the absence of either PKD1 or PKD2. These enhanced Ca^{2+} signals require upregulation of TMEM16A Cl^- channels.

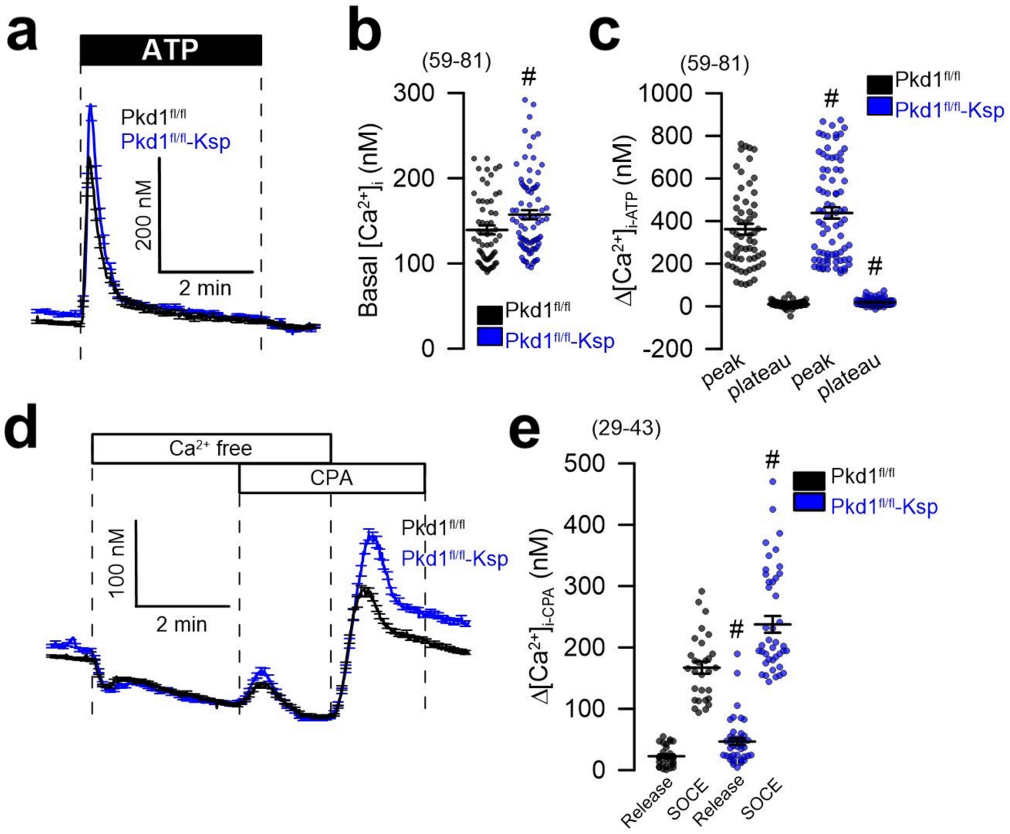

Figure 5.8 | *Enhanced Ca^{2+} signaling in primary renal tubular epithelial cells from PKD-/- mice.*

a-c Original recordings and summaries of basal Ca^{2+} and ATP (100 µM) induced Ca^{2+} increase (Fura2) in primary renal epithelial cells isolated from wild type mice ($PKD^{fl/fl}$) and from mice with a renal tubular knockout of PKD1 ($PKD^{fl/fl}$-KspCre). **d,e** Original recordings and summaries of Ca^{2+} increase induced by inhibition of SERCA with CPA (10 µM). Store release and store operated Ca^{2+} influx (SOCE) was augmented in $PKD^{-/-}$ cells. Mean ± SEM (number of cells measured). #significant difference when compared to wt ($p<0.05$; ANOVA).

Discussion

Aberrant intracellular Ca^{2+} signaling, enhanced cell proliferation and fluid secretion are essential factors that drive growth of renal cysts [152]. Disturbed flow sensing and mechanical activation of Ca^{2+} influx into primary cilia were proposed as major mechanisms in ADPKD, a concept that has been questioned recently [204]. In the present paper, we found ATP-induced Ca^{2+} increase in both the primary cilium as well as in the cytosol near the plasma membrane of MDCK cells (Fig. 5.2). Although ciliary Ca^{2+} increase by ATP was larger, the responses in the cilium and cytoplasm were similar. Both PKD1 and PKD2 are required for cellular trafficking and proper colocalization in the primary cilium of differentiated renal epithelial cells [166,379]. Mutations or lack of expression of PKD2 may lead to compromised trafficking and accumulation of PKD1 in the ER, while defective or missing PKD1, loss of the primary cilium or overexpression of PKD2 leads to enhanced density of PKD2 in the apical membrane and

in the ER membrane [196]. Apart from localization within the primary cilium, both PKD1 and PKD2 have been detected at different subcellular locations (reviewed in [370]). In fact, most studies report an intracellular ER-localization of PKD2. However, many studies have been performed in cultured cells under non-differentiated conditions, and it is notoriously difficult to obtain specific immunocytochemistry signals for both proteins in the kidney.

Inhibition of the IP_3 receptors by PKD1 with attenuation of Ca^{2+} release from IP_3-sensitive stores has been reported earlier [195]. Accordingly, receptor mediated Ca^{2+} release will be enhanced with the loss of PKD1, as also observed in the present study. After proteolytic cleavage, a PKD1 fragment has been proposed to interact with the ER Ca^{2+} -sensor STIM1 to inhibit store operated calcium entry [380]. Lack of PKD1 therefore is likely to augment store operated calcium entry, which was detected in our study (Fig. 5.7). Enhanced Ca^{2+} entry was blocked by the inhibitor of receptor-mediated Ca^{2+} entry SK&F96365, and by the inhibitor of store operated Orai1 Ca^{2+} influx channels, YM58483 (Fig. 5.7). Enhanced (and mislocalized) expression of PKD2 in the ER in the absence of PKD1 is likely to operate as a Ca^{2+} activated ER Ca^{2+} leakage channel, which will contribute to enhanced Ca^{2+} release from IP_3-sensitive (IP_3R) stores (Fig. 5.8). Notably, abnormal Ca^{2+} permeability of the ER membrane in ADPKD may account for both change in apoptotic activity and increased proliferation [377].

The present data are in line with the role of TMEM16A for intracellular Ca^{2+} signaling, which we reported earlier in cell models and transgenic animals [348]. TMEM16A channels enhance ER-Ca^{2+} store release by sequestering the ER and IP3 receptors to Ca^{2+} signaling compartments near the plasma membrane. In contrast to earlier reports [166], we were unable to detect a contribution of RyR channels in mouse primary renal epithelial cells or M1 cells (Fig. 5.7i,j).

The role of CFTR-dependent Cl^- secretion for growth of renal cysts has been implicated for long. We showed earlier that formation of cysts by principal-like MDCK cells is due to a synergism between cAMP and Ca^{2+} mediated fluid secretion [229]. The relevance of Ca^{2+} activated TMEM16A Cl^- channels became evident through our recent work [44,249,251]. Notably, STAT6-dependent transcription is upregulated in ADPKD [381]. Because expression of TMEM16A is upregulated through activation of STAT6 (and STAT3), this could explain upregulation of TMEM16A in M1 cysts observed in the present study (Fig. 5.4a). It is now clear that TMEM16A supports proliferation, cell migration and development of cancer by recruiting a number of intracellular signaling pathways [382]. Although the contribution of TMEM16A to ADPKD is not yet fully understood, the present data provide evidence for its pronounced impact on disturbed intracellular Ca^{2+} signaling, caused by elimination of PKD1 or PKD2. As a number of potent inhibitors for TMEM16A are already available, TMEM16A may represent a novel drug target in the therapeutic regimen of polycystic kidney disease.

Disclosure

All authors declared no competing interests

Acknowledgements

We are grateful to Prof. Dr. Dorien J.M. Peters (Department of Human Genetics, Leiden University Medical Center, Leiden, The Netherlands) for providing us with animals with a floxed PKD1 allele. The 5HT6-G-GECO1.0 was kindly provided by Prof. Takanari Inoue at Johns Hopkins University School of Medicine, Baltimore, USA, and was obtained through addgene (Watertown, MA, USA).

Funding

Supported by Supported by Deutsche Forschungsgemeinschaft (DFG) – project number A3, 387509280 – SFB 1350.

Supplementary material

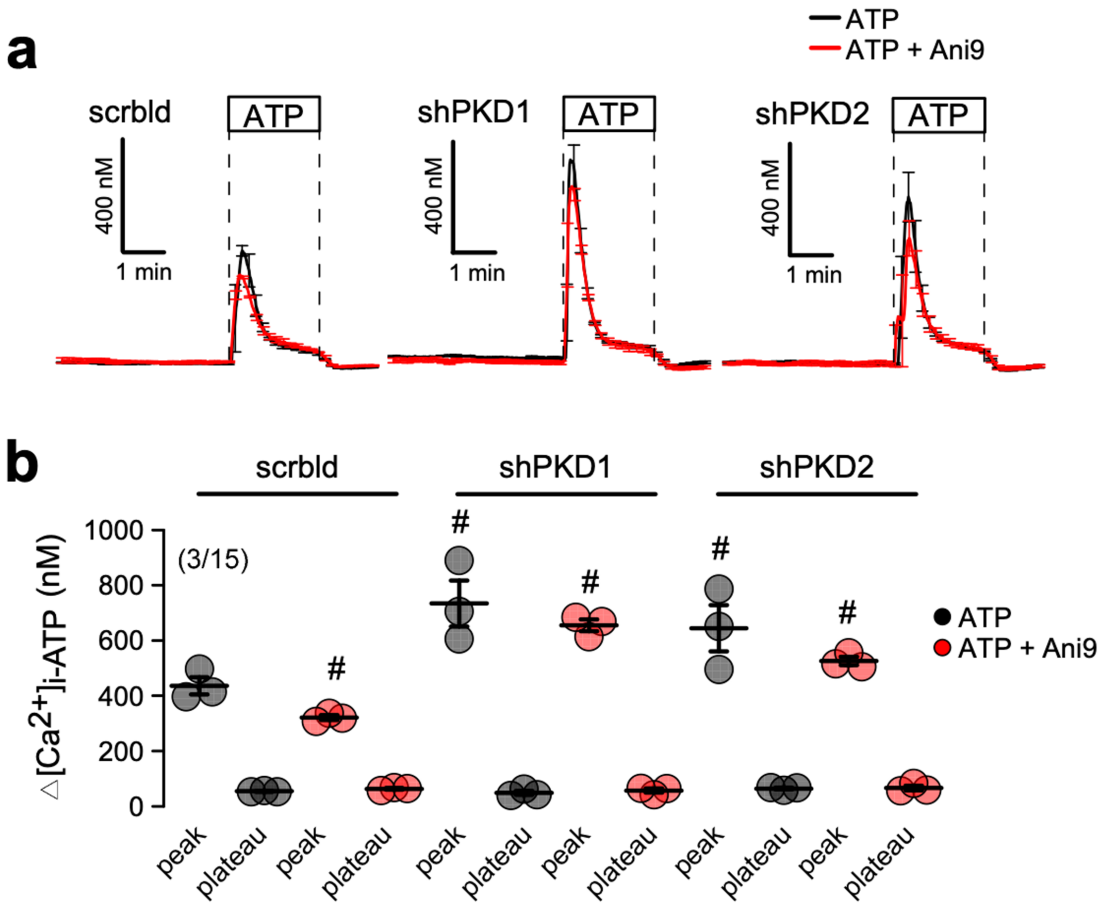

Supplmentary Figure 5.1 | *Inhibition of ATP-induced Ca^{2+} store release by Ani9.*

a Original recordings of intracellular Ca^{2+} as measured by Fura2. ATP (100 µM) induced Ca^{2+} store release in M1 cells treated with shRNA for PKD1, shRNA for PKD2 or treated with scrambled RNA. Inhibition of store release by the TMEM16A inhibitor Ani9. **b** Summary of store release and store operated Ca^{2+} influx. Mean ± SEM (number of cover slips/cells measured per cover slip). #significant difference compared to scrambled or absence of Ani9, respectively ($p<0.5$; ANOVA).

CHAPTER 6 | CYST GROWTH IN ADPKD REQUIRES CA^{2+} DEPENDENT CHLORIDE SECRETION AND IS PREVENTED BY PHARMACOLOGICAL INHIBITION OF TMEM16A *IN VIVO*

Abstract

In polycystic kidney disease (PKD) multiple bilateral renal cysts gradually enlarge leading to decline in renal function. Transepithelial chloride secretion through cystic fibrosis transmembrane conductance regulator (CFTR) and TMEM16A (anoctamin 1) are known to drive cyst enlargement. Here we demonstrate that loss of Pkd1 increased expression of Tmem16a and cftr in murine kidneys, which both largely contributed to cyst formation. Upregulated Tmem16a enhanced intracellular Ca^{2+} signaling and proliferation in Pkd1-deficient renal epithelial cells, while increase in Ca^{2+} signaling and cftr expression was not observed in Pkd1/Tmem16a double knockout mice. Knockout of Tmem16a or inhibition of Tmem16a *in vivo* by the FDA-approved drugs niclosamide and benzbromarone largely reduced abnormal proliferation and cyst formation. These data provide a novel therapeutic concept for the treatment of PKD.

Key words: ADPKD, renal cysts, TMEM16A, anoctamin 1, Ca^{2+} activated Cl^- channel

Submitted for publication: Inês Cabrita, Andre Kraus, Rainer Schreiber, Karl Kunzelmann, Björn Buchholz. Cyst growth in ADPKD requires Ca^{2+} dependent chloride secretion and is prevented by pharmacological inhibition of TMEM16A *in vivo*. (Submitted for publication)

Own experimental contribution: Animal treatment, Isolation of renal medullary and cortical primary cells, Immunohistochemistry, Quantification of immunohistochemical and fluorescent signals, Morphological analysis, Ussing Chamber experiments, YFP-quenching assay, Measurement of intracellular Ca^{2+}.

Own written contribution: Methods, Results, Parts of Introduction and Discussion.

Other contributions: Designed experiments and analyzed data.

Introduction

Polycystic kidney diseases (PKDs) comprise a number of inherited disorders that lead to bilateral renal cyst development. The most common form, autosomal dominant polycystic kidney disease (ADPKD), affects 1 in 500–1000, and accounts for 5%–10% of end-stage renal disease. ADPKD is characterized by continuous cyst enlargement over time, leading to compression of adjacent healthy parenchyma [152]. Disease causing mutations are known such as those in polycystin-1 (PKD1) and polycystin-2 (PKD2), but the complex mechanisms of cyst development and cyst growth are still poorly understood [166,205,369]. Cell proliferation and fluid secretion are two essential characteristics of cyst development. Cystic Fibrosis Transmembrane conductance regulator (CFTR) is the anion channel essential for fluid secretion in renal cysts and other epithelia [242,383]. To be fully activated CFTR requires TMEM16A, which was shown to act synergistically on fluid secretion into renal cysts *in vitro* [36,44,229,384]. Cyst enlargement is promoted by purinergic signaling and lipid peroxidation, which both activate TMEM16A [251,358].

Here we used *in vitro* and *in vivo* models for ADPKD, which unmasked the upregulation of expression of TMEM16A and CFTR in Pkd1-knockout MDCK cells and kidneys of Pkd1-knockout mice. Increased expression of TMEM16A and CFTR caused enhanced intracellular Ca^{2+} signaling and induced cyst growth, both being normalized by additional knockdown of TMEM16A. The results suggest TMEM16A as a novel pharmacological target to inhibit cyst growth in ADPKD. This is fully supported by an impressive inhibition of the cystic phenotype using the two TMEM16A inhibitors niclosamide or benzbromarone [344,385].

Materials and methods

Animals. Animal experiments were approved by the local institutional review board and all animal experiments complied with the with the United Kingdom Animals Act, 1986, and associated guidelines, EU Directive 2010/63/EU for animal experiments. Experiments were approved by the local Ethics Committee of the Government of Unterfranken/Wuerzburg (AZ: 55.2-2532-2-328). Animals were hosted on a 12:12 hours light:dark cycle under constant temperature (24 ± 1 C°) in standard cages. They were fed a standard diet with free access to tap water. Generation of mice with a tamoxifen-inducible, kidney epithelium-specific Pkd1-deletion were described recently [386]. Mice carrying loxP-flanked conditional alleles of Pkd1 were crossed with KSP-Cre mice in a C57BL/6 background ($KspCreER^{T2}$;$Pkd1^{lox;lox}$; abbreviated as $Pkd1^{-/-}$). Mice carrying loxP-flanked alleles of Tmem16a [38] were crossed to generate $KspCreER^{T2}$;$Pkd1^{lox;lox}$; $Tmem16a^{lox;lox}$ double knockout mice (abbreviated as $Pkd1^{-/-}$/$T16a^{-/-}$). Primers for genotyping are listed in Table 6.1.

Table 6.1 | *Genotyping primer sequences.*

Primer	Gene	Sequence 5‘- 3‘
mPKD1 loxPF	Pkd1	ACCCTTCCCTGAGCCTCCAC
mPKD1 loxPR	Pkd1	CCACAGGGGAAGCCATCATA
F427 Va	Ksp	CATTCTCTCCCACTGAATGGA
F427 Vb	Ksp	ACAGAGTGGGGTTTGTGTCTG
inv	Ksp	AACTGTCCCCTTGTCATACCC
16aCKOf	Tmem16a	GGCTCTATCAATGTTCTGTTC
16aCKOr1	Tmem16a	CTCAAGTCCTCAAGTCCCAGTC

Animal treatment. Conditional knockout was induced in $Pkd1^{-/-}$ (n = 12) and $Pkd1^{-/-}$/$T16a^{-/-}$ (n = 12) mice by administrating tamoxifen (2 mg/kg body weight) dissolved in 5 % ethanol and 95 % neutral oil, daily at postnatal days PN 20 - 22. Non-induced $Pkd1^{-/-}$ (n = 9) served as controls. Induced $Pkd1^{-/-}$ mice were fed with maintenance diet 1320 (Altromin, Lage, Germany) (n = 3) or with Altromin supplemented with 0.2 % niclosamide (n = 3). All animals were sacrificed 10 weeks after induction with tamoxifen and kidneys were analyzed. Alternatively, $Pkd1^{-/-}$ mice were maintained for 30 days and subsequently treated with benzbromarone (1 mg/kg/day) dissolved in corn oil or corn oil/DMSO (50 µl) by intraperitoneal injection for 30 days (n = 5). Mice were monitored twice a day by trained staff.
Isolation of renal medullary and cortical primary cells. Mice were killed by cervical dislocation after exposure to CO_2. Kidneys were removed and kept in ice-cold DMEM/F12 medium (Thermo Fisher Scientific, Darmstadt, Germany). The renal capsule was removed under germ-free conditions. Cortex and medulla were separated and chopped into smaller pieces of tissue using a sharp razor blade (Heinz Herenz, Hamburg, Germany). Tissues were incubated in Hanks balanced salt solution/DMEM/F12 (Life Technologies/Gibco®, Karlsruhe, Germany) containing 1 mg/ml collagenase type 2 (Worthington, Lakewood, USA) for 20 min at 37° C. The digested tissue was passed through a 100 µm cell strainer (Merck KGaA, Darmstadt, Germany), transferred to a 50 ml falcon tube and washed with ice cold PBS. After centrifugation at 5100 rpm for 4 min / 4° C, cells were resuspended. After resuspension, the cortical cell pellet was centrifuged at 17500 rpm for 30 min at 4° C through a 45 % Percoll (Ge Healthcare GmbH, Munich, Germany) 55 % 2X PBS-Glucose gradient. After washing with ice-cold PBS, tubular preparations were maintained at 37 °C / 5 % CO_2 in DMEM/F12 supplemented with 1 % FBS, 1 % Pen/Strep, 1 % L-Glutamine (200 mM), 1 % ITS (100x), 50 nM hydrocortisone, 5 nM triiodothyronine, and 5 nM Epidermal Growth Factor (Sigma Taufkirchen, Germany). After 24 hours, primary cells grew out from isolated tubules.
Principal-like MDCK cell cyst model and PKD1 knockout cells. Principal-like MDCK cells were grown at 37 °C, 21 % O_2 and 5 % CO_2 in modified MEM containing Earl’s balanced salt solution supplemented with 2 mM L-glutamine, 10 % heat-inactivated FCS, 50 U/ml

penicillin, and 50 µg/ml streptomycin. *In vitro* cyst assays were performed as described previously [44]. In brief cells were resuspended as a single-cell suspension in type I collagen and transferred to 24-well plates (3 wells per condition). Forskolin (FSK; 10 µM), ATP (10 µM), suramin (Sur; 100 µM), niclosamide ethanolamine (Niclo; 1 µM) and CFTR-inh172 (CFTRi; 10 µM) were added to the medium at day 0, and medium was changed every 2 days. All substances were purchased from Sigma (Taufkirchen, Germany). After 5 days, images were taken from four random visual fields per well using Zeiss Primo Vert microscope and Zeiss Axiocam 105 camera (Zeiss Microscopy GmbH, Jena, Germany). Diameters of all captured spherical cysts were analyzed using ImageJ and spherical cyst volumes were calculated according to 4/3πr3.

A subclone of MDCK cells was used that resembles principal cells of the collecting duct as described earlier [229]. For genome editing pSpCas9(BB)-2A-puro-vectors (PX459) V2.0 (Addgene, Watertown, MA, USA) were used to generate a $PKD^{-/-}$ cell line. The guide RNA was designed according to the algorithms provided by the Zhang laboratory (http://crispr.mit.edu/), which provided a quality score of 92. After ligation of the DNA-oligonucleotides with the vectors, 10^6 cells were transfected using 10 µl polyethylenimine and 4 µg of the vector. After 24 h, cells were incubated with puromycine (3.5 µg/ml) for 48 h. Clones of cells were generated by dilution. For mutation screens, genomic DNA of single-cell clones was isolated and the CRISPR/Cas9 target region was amplified by PCR. Products were resolved by polyacrylamide gel electrophoresis. Genomic DNA of potential cell clones was amplified by PCR and cloned into pGL3 vector (Promega, Madison, WI, USA) and subjected to Sanger sequencing (eurofins, Nuernberg, Germany). The two main potential off-targets in DNA regions were tested for off-target effects by PCR amplification and polyacrylamide gel electrophoresis analysis. No off-target effects were detected.

cAMP measurements. MDCK cells were grown in a pre-coated assay capture plate (cAMP-Screen Direct System P/N 4412186; Applied Biosystems, Foster City, CA, USA) in serum-free medium. Cells were exposed to serum-free control medium or medium supplemented with 10 µM forskolin. cAMP measurements were performed by the use of the GloMax-Multi Detection System (Promega) according to the manufacturer's protocol.

Western Blotting. Protein was isolated from MDCK and renal primary cells using a sample buffer containing 25 mM Tris-HCl, 150 mM NaCl, 100 mM dithiothreitol, 5.5% Nonidet P-40, 5% glycerol, 1 mM EDTA and 1% protease inhibitor mixture (Roche, cOmplete, EDTA-free, Mannheim, Germany). Proteins were separated by 7 % sodium dodecyl sulfate (SDS) polyacrylamide gel and transferred to a polyvinylidene difluoride membrane (GE Healthcare Europe GmbH, Munich, Germany) or 4-20% Mini-PROTEAN TGX Stain-Free (Bio-Rad) using a semi-dry transfer unit (Bio-Rad). Membranes were incubated with primary anti-Tmem16a rabbit polyclonal antibody (Davids Biotech, Regensburg, Germany; 1:1000) or anti-PKD1 (Polycystin-1 (7E12), Santa Cruz; 1:500) mouse antibody overnight at 4 °C.

Proteins were visualized using horseradish peroxidase-conjugated secondary antibody and ECL detection. Beta-Actin was used as a loading control.

Immunohistochemistry and antibodies. Two-micron thick transverse kidney sections were stained. For co-staining of CFTR and TMEM16A, anti-CFTR (rabbit; 1:100; Alomone, Jerusalem, Israel) and anti-TMEM16A (rabbit; 1:200, P80, described previously [44]) antibodies were used. As secondary antibodies, anti-rabbit IgG Alexa Fluor 555 and 488 antibodies (1:1000; Thermo Fisher Scientific, Inc., Erlangen, Germany) were used. Ki-67 staining was performed using a monoclonal anti-ki-67 antibody (rabbit; 1:100, Linaris, Dossenheim, Germany). Signals were amplified by the use of the Vectastain Elite ABC Kit (Vector Laboratories, Burlingame, CA) according to the manufacturer's instructions. Signals were analyzed with a DM6000B fluorescence microscope (Leica, Wetzlar, Germany), and photographs were taken with a Leica DFC 450C camera.

Affinity purified polyclonal antiserum against mouse Tmem16a was produced in rabbits immunized with DPDAECKYGLYFRDGKRKVD (aa 44-63, N-terminus) or NHSPTTHPEAGDGSPVPSYE (aa 957-976, C-terminus), coupled to keyhole limpet hemocyanin (Davids Biotechnologie, Regensburg, Germany). Mouse kidneys were fixed by perfusion with 4% (v/v) paraformaldehyde and post-fixed in 0.5 mol/L sucrose and 4% paraformaldehyde solution. Paraffin sections of 5 µm were blocked with 5% bovine serum albumin (BSA) and 0.04% Triton X-100 in PBS for 30min. Cryo sections of 5 µm were incubated in 0.1% sodium dodecyl sulfate for 5 min and afterwards washed with PBS. Sections were incubated with primary antibodies (1:200) in 0.5% BSA and 0.04% Triton X-100 overnight at 4 ºC. Additional primary antibodies were guinea pig anti-megalin (gift from Dr. F. Theilig, University of Freiburg, Germany), rabbit anti-CFTR (Alomone labs, # ACL-006), goat anti-AQP2 (Santa Cruz Biotechnology, Heidelberg, Germany), mouse anti-calbindin (Swant, Bellinzona, Switzerland), mouse anti-acetylated tubulin (Sigma-Aldrich, Munich, German), and rat anti-mouse Ki67 (Dako Cytomation, Hamburg, Germany). After washing, sections were incubated with appropriate secondary antibodies for 1h at room temperature (Alexa Fluor 488-labeled donkey anti-rabbit IgG (1:300, Invitrogen, Darmstadt, Germany), Alexa Fluor 546-labeled goat anti- mouse IgG (Molecular Probes), Alexa Fluor 546-labeled donkey anti-goat IgG (Molecular Probes), Cy5-labeled donkey anti-guinea pig IgG (Dianova), and Alexa Fluor 546 -labeled goat anti- rat IgG (Molecular Probes). Sections were counterstained with Hoe33342 (1:200, Sigma-Aldrich). Coverslips were mounted with fluorescence mounting medium (Dako Cytomation, Hamburg, Germany). Immunofluorescence was detected using an Axiovert 200 microscope equipped with ApoTome and AxioVision (Zeiss, Germany).

Quantification of immunohistochemistry and fluorescent signals. Ten random photographs were taken from the cortex of each kidney at a magnification of X200. Immunofluorescence (TMEM16A and CFTR) was analyzed as described previously [386]. Briefly, fluorescent signals

were turned into 8-bit images after subtracting background (ImageJ) and a predefined threshold was used for all images to capture signals. Colocalization was visualized in white by use of ImageJ and an algorithm (http://rsb.info.nih.gov/ij/plugins/colocalization-finder.html, Laummonerie and Mutterer, Institut de Biologie Moleculaire des Plantes, Strasbourg, France). For quantification of ki67, the color deconvolution algorithm (ImageJ) was applied to dissect the different signals, followed by binarization and particle analysis to obtain the ratio of the number of positive cells and cortex area (normalized to mm^2 cortex tissue).

Morphological analyses. Photographs from hematoxylin and eosin–stained kidney sections were taken at a magnification of X25 and stitched to obtain single photographs of the whole transverse kidney sections using a Leica DM6000B microscope and a Leica DFC 450C camera. The whole kidney cortex was defined as region of interest using ImageJ and Cinteq 13HD creative pen display (Wacom, Düsseldorf, Germany). Next, we used an algorithm [386] that separates normal tubule space from cystic area by defining diameters of noncystic tubules <50 mm. The whole cortex cyst area was divided by the whole cortex area and defined as the cystic index.

Ussing chamber. Medullary or cortical primary cells were grown as polarized monolayers on permeable supports (Millipore). Filters were mounted into a perfused micro Ussing chamber and the luminal and basolateral surfaces of the epithelium were perfused continuously with ringer solution (in mM: NaCl (145), KH_2PO_4 (0.4), K_2HPO_4 (1.6), Glucose (5), $MgCl_2$ (1) Ca-gluconate (1.3)) at a rate of 6 ml/min (chamber volume 2 ml). All experiments were carried out at 37 C° under open-circuit conditions. Transepithelial resistance (Rte) was determined by applying short (1 s) current pulses (ΔI = 0.5 μA) and the corresponding changes in transepithelial voltage (Vte) were recorded continuously. Values for Vte were referred to the basolateral side of the epithelium. Rte was calculated according to Ohm's law ($Rte = \Delta Vte/\Delta I$). The equivalent short-circuit current (Isc) was calculated according to Ohm's law from Vte and Rte (Isc = Vte / Rte).

YFP-quenching assay. For YFP-quenching assays, primary renal cells were infected with lentiviral vectors to express halide-sensitive YFP_{I152L}, as previously described [3]. Cells were isolated from 4 different mice and for each mouse 40 cells were measured. Quenching of the intracellular fluorescence generated by the iodide sensitive Enhanced Yellow Fluorescent Protein (EYFP-I152L) was used to measure anion conductance. YFP-I152L fluorescence was excited at 500 nm using a polychromatic illumination system for microscopic fluorescence measurement (Visitron Systems, Puchheim, Germany) and the emitted light measured at 535±15 nm with a Coolsnap HQ CCD camera (Roper Scientific). Quenching of YFP-I152L fluorescence by I^- influx was induced by replacing 5 mM extracellular Cl^- with I^-. Cells were grown on cover slips and mounted in a thermostatically controlled imaging chamber maintained at 37°C. Cells were continuously perfused at 8 ml/min with Ringer solution and exposed to I^- concentration of 5 mM by replacing same amount

of NaCl with equimolar NaI. Background fluorescence was subtracted, while auto-fluorescence was negligible. Changes in fluorescence induced by I^- are expressed as initial rates of maximal fluorescence decrease ($\Delta F/\Delta t$). For quantitative analysis, cells with low or excessively high fluorescence were discarded.

Measurement of intracellular Ca^{2+} ($[Ca^{2+}]i$). Renal primary cells were loaded with 2 µM Fura-2/AM and 0.02 % Pluronic F-127 (Invitrogen, Darmstadt, Germany)) in ringer solution (mmol/l: NaCl 145; KH_2PO_4 0,4; K_2HPO_4 1,6; Glucose 5; $MgCl_2$ 1; Ca^{2+}-Gluconat 1,3) for 1h at room temperature. Fluorescence was detected in cells perfused with Ringer's solution at 37 °C using an inverted microscope (Axiovert S100, Zeiss, Germany) and a high speed polychromator system (VisiChrome, Puchheim, Germany). Fura-2 was excited at 340/380 nm, and emission was recorded between 470 and 550 nm using a CoolSnap camera (CoolSnap HQ, Visitron). $[Ca^{2+}]_i$ was calculated from the 340/380 nm fluorescence ratio after background subtraction. The formula used to calculate $[Ca^{2+}]_i$ was $[Ca^{2+}]_i = Kd$ x $(R-R_{min})/(R_{max}-R)$ x (S_{f2}/S_{b2}), where R is the observed fluorescence ratio. The values R_{max} and R_{min} (maximum and minimum ratios) and the constant S_{f2}/S_{b2} (fluorescence of free and Ca^{2+}-bound Fura-2 at 380 nm) were calculated using 1 µmol/liter ionomycin (Calbiochem), 5 µmol/liter nigericin, 10 µmol/liter monensin (Sigma), and 5 mmol/liter EGTA to equilibrate intracellular and extracellular Ca^{2+} in intact Fura-2-loaded cells. The dissociation constant for the Fura-2•Ca^{2+} complex was taken as 224 nmol/liter.

Patch clamping. Patch-clamp experiments were performed in the fast whole-cell configuration. Patch pipettes had an input resistance of 2–4 MΩ, when filled with a solution containing (mM) KCl 30, K-gluconate 95, NaH_2PO_4 1.2, Na_2HPO_4 4.8, EGTA 1, Ca-gluconate 0.758, $MgCl_2$ 1.034, D-glucose 5, ATP 3. pH was 7.2, the Ca^{2+} activity was 0.1 µM. The access conductance was measured continuously and was 30 – 140 nS. Currents (voltage clamp) and voltages (current clamp) were recorded using a patch-clamp amplifier (EPC 7, List Medical Electronics, Darmstadt, Germany), the LIH1600 interface and PULSE software (HEKA, Lambrecht, Germany) as well as Chart software (AD-Instruments, Spechbach, Germany). Data were stored continuously on a computer hard disc and were analyzed using PULSE software. In regular intervals, membrane voltages (V_c) were clamped in steps of 20 mV from -100 to +100 mV relative to resting potential. Membrane conductance G_m was calculated from the measured current (I) and V_c values according to Ohm's law.

Materials and statistical analysis. All compounds used were of highest available grade of purity. Data are reported as mean ± SEM. Student's t-test for unpaired samples and ANOVA were used for statistical analysis. $p < 0.05$ was accepted as significant difference. Data are expressed as mean ± SEM. Differences among groups were analyzed using one-way ANOVA, followed by a Bonferroni test for multiple comparisons. An unpaired t test was applied to compare the differences between two groups. Wilcoxon signed-rank test for columns statistics was used for relative values. $P<0.05$ was considered statistically

significant.

Results

TMEM16A supports cyst growth in PKD1 deficient MDCK cells. We previously demonstrated that blocking of TMEM16A inhibits MDCK cysts grown in a collagen matrix [44,358]. This was further investigated by eliminating expression of Pkd1 in MDCK cells ($PKD1^{-/-}$; clone c7) using CRISPR/Cas9. As shown for one of the clones, knockdown of PKD1 ($Pkd1^{-/-}$) caused spontaneous cyst growth, which was not observed in control cells ($PKD^{+/+}$). Additional stimulation with forskolin further augmented cyst size (Fig. 6.1a,b).

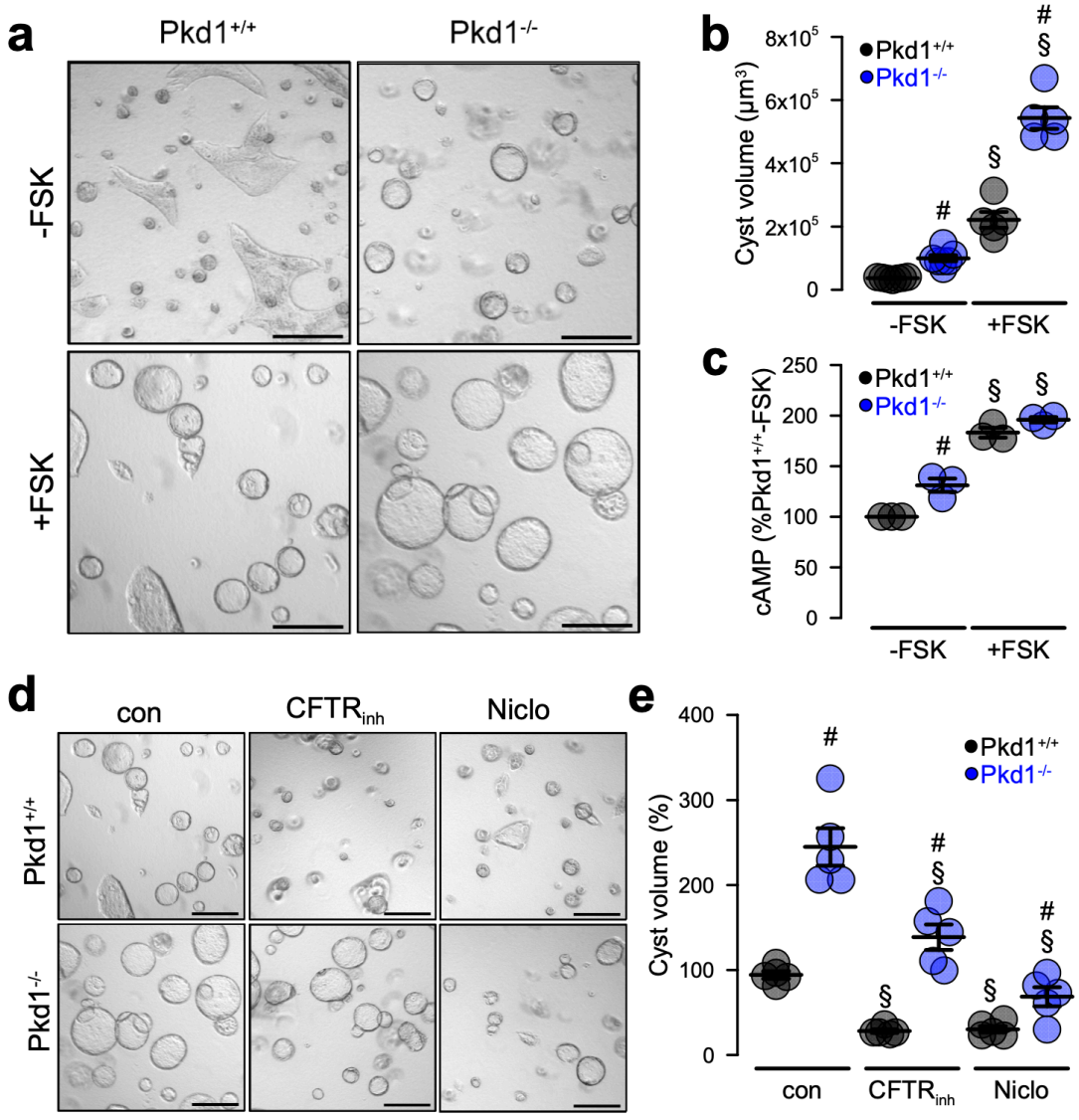

Figure 6.1 | *Cyst growth of Polycystin-1-deficient collecting duct cells depends on cAMP- and Ca^{2+}-activated secretion.*

a Wild type ($Pkd^{+/+}$) and polycystin-1 ($Pkd1^{-/-}$) principal-like (pl) MDCK cells were cultured in a collagen matrix. In the presence but not absence of 10 µM forskolin (-FSK) $PKD^{+/+}$ cells formed small cysts after 5 days, whereas $Pkd1^{-/-}$ cells spontaneously formed cysts without FSK. **b** Volumes of 85 - 105 cysts were analyzed per condition and were significantly enhanced for $Pkd1^{-/-}$ cells. **c** Deletion of

polycystin-1 in plMDCK cells induced an increase in intracellular cAMP concentrations under control conditions (-FSK) and upon stimulation with forskolin (+FSK, n = 3 assays for each condition). cAMP levels in $Pkd1^{+/+}$ cells were set to 100%). **d,e** Cyst volumes were strongly inhibited in both $Pkd1^{+/+}$ and $Pkd1^{-/-}$ cells by CFTRinh172 (CFTRinh; 5 µM) and niclosamide (Niclo; 1 µM). Bars 200 µm. Mean ± SEM. #significant difference when compared to $Pkd1^{+/+}$ ($p<0.05$, unpaired t-test), §significant effects by forskolin or inhibitors ($p<0.05$, unpaired t-test).

Intracellular cAMP levels were enhanced in $Pkd1^{-/-}$ cells (Fig. 6.1c). Cyst growth in the presence of forskolin was strongly attenuated by inhibition of CFTR using CFTRinh172. Inhibition of cyst growth was even more pronounced in the presence of the TMEM16-inhibitor niclosamide (Fig. 6.1d,e). Cyst growth was also inhibited in the presence of the inhibitor of purinergic receptors, suramin (100 µM, not shown). The data suggest upregulation of CFTR and TMEM16A in the absence of PKD1, which drives the cystic phenotype.

Renal tubule specific knockout of Pkd1 upregulates Tmem16a that drives cyst growth. We crossed mice with floxed alleles for Pkd1 [387] with tamoxifen-inducible tam-KspCad-Cre animals to obtain $Pkd1^{fl/fl}$; tam-KspCad-Cre mice. To obtain a renal tubular specific knockout for Pkd1 ($Pkd1^{-/-}$), animals were treated with tamoxifen for 3 days starting at postnatal day 20. Kidneys isolated from 8 weeks old $Pkd1^{-/-}$ mice demonstrated clear knockdown of Pkd1-expression as shown by Western blotting (Fig. 6.2a,b). In contrast, expression of Tmem16a was upregulated in $Pkd1^{-/-}$ kidneys (Fig. 6.2c,d). Knockdown of Pkd1 induced polycystic kidney disease with multiple renal cysts and large kidneys. The calculated cystic index (c.f. Methods) was strongly enhanced (Fig. 6.2e,f). Additional knockout of TMEM16A in Pkd1-/- mice ($Pkd1^{fl/fl}$;$Tmem16a^{fl/fl}$; tam-KspCad-Cre) (Fig. 6.2a-d) dramatically reduced cyst formation and almost abolished the cystic phenotype (Fig. 6.2e,f). The results suggest an essential role of TMEM16A for proliferation of cysts and electrolyte secretion [44,142] (Fig. 6.2e,f).

Knockdown of Pkd1 causes upregulation of tubular expression of CFTR and TMEM16A. Induction of PKD by downregulation of Pkd1 ($Pkd1^{-/-}$) induced an upregulation of Tmem16a expression (Fig. 6.2c). Immunolabelling of TMEM16A and CFTR indicated upregulation of both ion channels in the cyst epithelium of $Pkd1^{-/-}$ kidneys, were both ion channels were strongly colocalized (Fig. 6.3a-c, Supplementary Figs. 6.1, 6.2a). In contrast to cystic kidneys, Tmem16a is much less abundant in normal kidneys where it is found to be expressed in apical membranes and in the primary cilium [38] (Supplementary Fig. 6.2b,c).

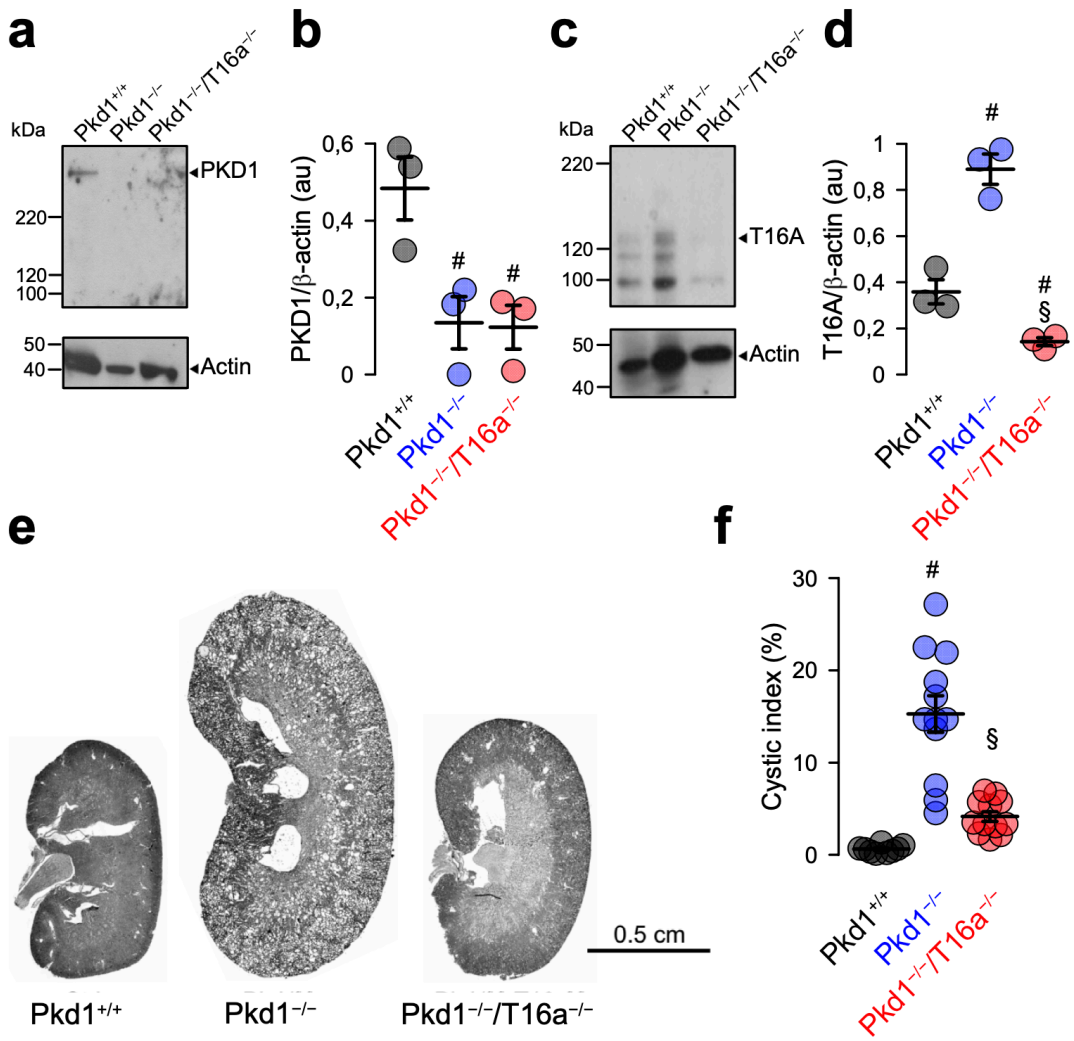

Figure 6.2 | *Tubule-specific deletion of TMEM16a reduces cyst progression in an ADPKD mouse model.*

a-d Western blotting from whole kidney lysates (n = 3) detecting tubule-specific deletion of Pkd1 (450 kDa) and increase in Tmem16a expression (glycosylated 130 kDa and non-glycosylated forms [59]) induced at postnatal day 20 – 22 using tamoxifen. Results obtained in $Pkd1^{-/-}$ mice were compared with those obtained in wt ($Pkd1^{fl;fl}$) mice ($PKD^{+/+}$) and mice co-deleted for Tmem16a ($Pkd1^{-/-}T16a^{-/-}$; $Pkd1^{fl/fl}$; tam-KspCad-Cre). **e** Tubule-specific knockout of Pkd1 ($Pkd1^{-/-}$; n = 12 animals) induced polycystic kidney disease, which was almost completely abolished in mice with an additional knockout of Tmem16a ($Pkd1^{-/-}T16a^{-/-}$; n = 12 animals). **f** Corresponding cystic indices. Mean ± SEM. $^{\#}$significant difference when compared to $Pkd1^{+/+}$ ($p<0.05$, unpaired t-test), §significant difference when compared to $Pkd1^{-/-}$ ($p<0.05$, unpaired t-test).

Remarkably, enhanced expression of CFTR in cystic kidneys was entirely reversible upon additional knockout of TMEM16A in $Pkd1^{fl/fl}$;$Tmem16a^{fl/fl}$; tam-KspCad-Cre animals (Fig. 6.3a-d). These results indicate an intimate relationship between CFTR and TMEM16A and correspond to earlier results demonstrating the requirement of Tmem16a for proper

expression and function of Cftr in mouse and human airway and intestinal epithelial tissues [36]. Earlier studies showed a strong correlation between expression of Tmem16a and cell proliferation (reviewed in [142]). This was also observed in the present study using the proliferation marker ki67. Proliferation was enhanced in Pkd1$^{-/-}$ kidneys, but was lowered to almost normal levels in Pkd1$^{-/-}$/Tmem16a$^{-/-}$ double knockout kidney (Fig. 6.3e,f).

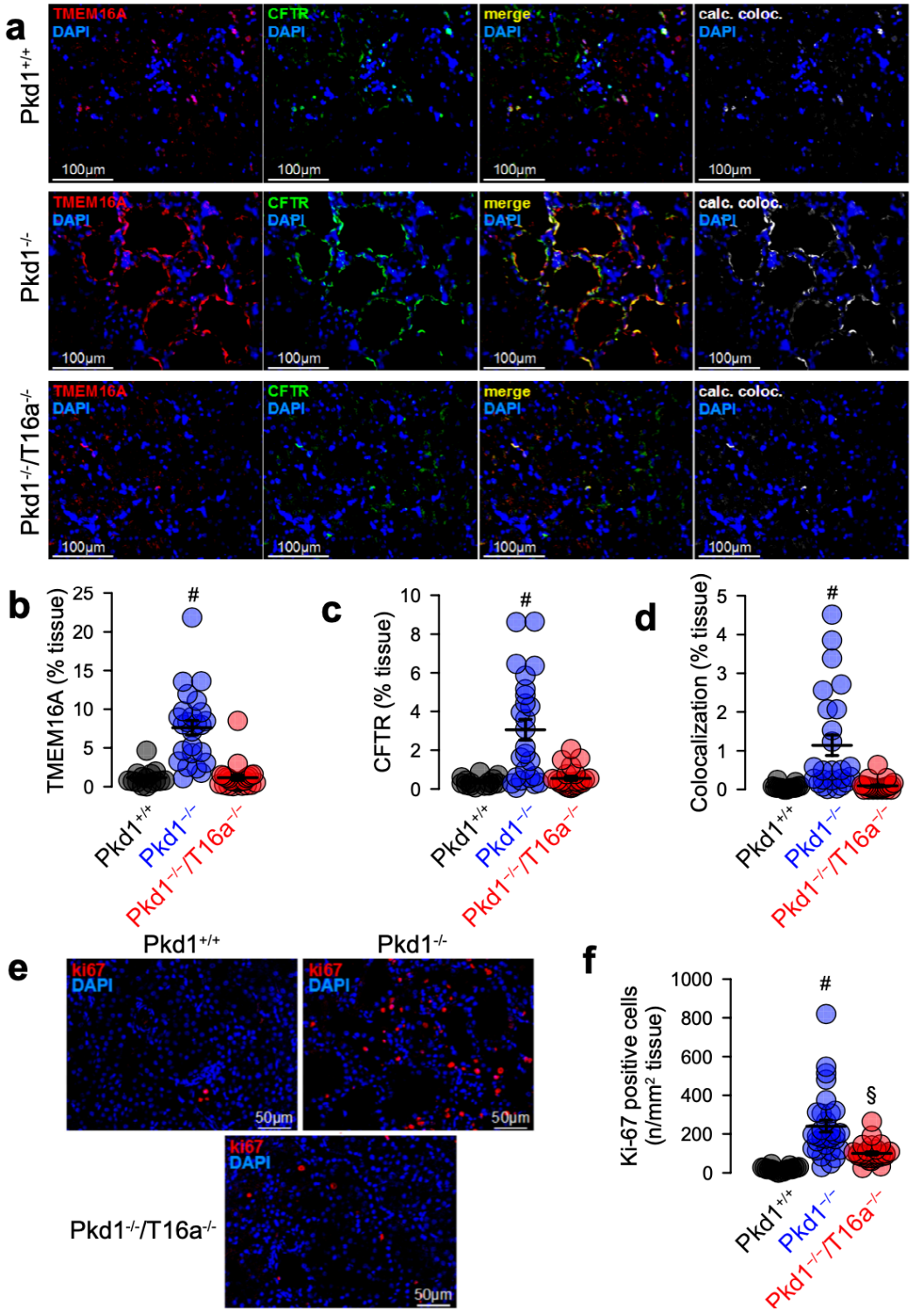

Figure 6.3 | *Enhanced expression of CFTR and increased cell proliferation in PKD1$^{-/-}$ kidneys depends on overexpressed TMEM16A.*

a Enhanced tubular epithelial expression of Cftr and Tmem16a in kidneys from Pkd1$^{-/-}$ mice that was

abolished in kidneys from $Pkd1^{-/-}$/$T16a^{-/-}$ double knockout mice. Both Cftr and Tmem16a were colocalized in the apical membrane of the cyst epithelium. (blue; DAPI). **b-d** Expression of Tmem16a and cftr was quantified in n = 15 – 25 images from n = 3 - 5 animals each. Significant colocalization was detected using colocalization finder algorithm (ImageJ, V.1.49 by Laummonerie and Mutterer). **e,f** ki67 - positive tubular epithelial cells in $Pkd1^{+/+}$, $Pkd1^{-/-}$ and $Pkd1^{-/-}$/$T16a^{-/-}$ kidneys. ki-67 positive cells were quantified in n = 18 – 30 images from n = 3 – 5 animals. Mean ± SEM. $^{\#\S}$significant difference when compared to $Pkd1^{+/+}$ ($p<0.05$, ANOVA).

Isolated medullary epithelial cells were grown on permeable supports to analyze Ca^{2+} dependent ion transport by Tmem16a. Transepithelial voltage deflection was induced by purinergic stimulation with UTP, and both basal and UTP-activated short circuit currents were enhanced in renal epithelium lacking Pkd1 (Fig. 6.4a-c). In contrast, renal epithelium from mice with double knockout of Pkd1 and Tmem16a demonstrated normal ion transport properties, indicating the role of Tmem16a for enhanced ion transport in ADPKD (Fig. 6.4a-c, Supplmentary Fig. 6.3a-c). Enhanced Ca^{2+}-dependent ion transport in $Pkd1^{-/-}$ cells was also well detected in whole cell patch clamp recordings as well as iodide quenching experiments (Supplementary Fig. 6.3d-g). Importantly, Cl^- secretion activated by increase in intracellular cAMP (IBMX and forskolin; IF) was also enhanced in $Pkd1^{-/-}$ cells, but not in epithelial cells from Pkd1/Tmem16a-double knockout animals (Supplementary Fig. 6.3h,i).

Enhanced ion secretion in Pkd1-/- animals is due to up-regulated Ca^{2+} signaling. We previously described enhanced intracellular Ca^{2+} signaling in cells expressing Tmem16a [348]. We therefore compared intracellular Ca^{2+} signals in primary medullary epithelial cells isolated from $Pkd1^{-/-}$ animals, $Pkd1^{-/-}$/$Tmem16a^{-/-}$ double knockout and wt ($Pkd1^{+/+}$) animals. Basal Ca^{2+} levels and ATP-induced Ca^{2+} rise were both enhanced in $Pkd1^{-/-}$ cells when compared to double knockout and wt cells (Fig. 6.4d-f). ATP-induced Ca^{2+} increase was strongly inhibited by the Tmem16a-inhibitor benzbromarone [127], supporting the role of Tmem16a for intracellular Ca^{2+} signaling (Fig. 6.4g,h). We employed a Ca^{2+} store release protocol by removing extracellular Ca^{2+} and emptying the endoplasmic reticulum (ER) Ca^{2+} store using the ER Ca^{2+} pump inhibitor cyclopiazonic acid (CPA). We found that deletion of Pkd1 enhanced Ca^{2+} release and largely enhanced store operated Ca^{2+} entry (SOCE) after re-adding extracellular Ca^{2+} (Fig. 6.4i,j). Thus, Ca^{2+} release and store operated Ca^{2+} entry (SOCE) are augmented by deletion of Pkd1 and are probably due to upregulation of Tmem16a [348]. SOCE was potently blocked by the inhibitors of transient receptor potential (Trp) and Orai channels, SK&F96365 and YM58483, respectively, suggesting a contribution of both channels to enhanced SOCE in $PKD1^{-/-}$ cells (Supplementary Fig. 6.4).

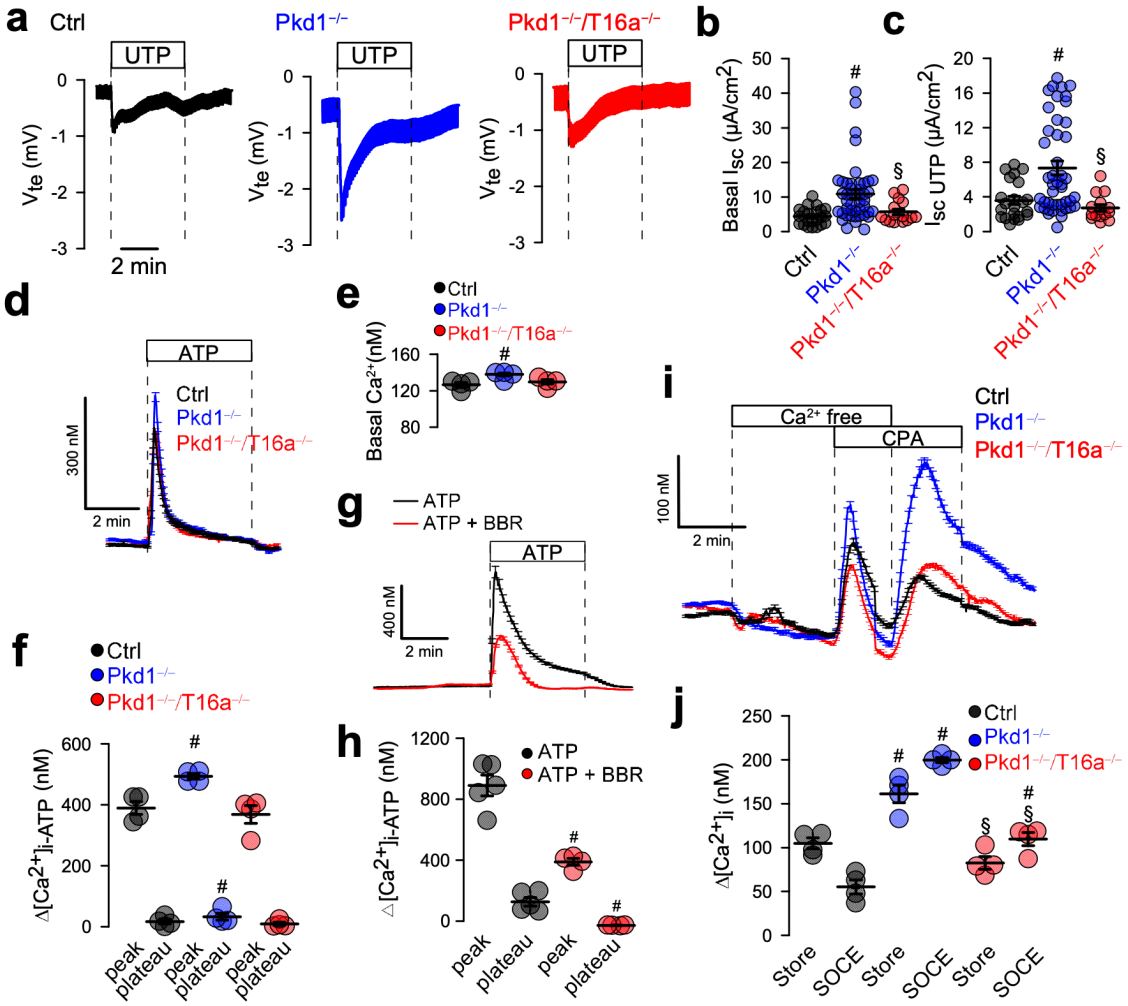

Figure 6.4 | *Induction of Cl^- secretion and enhanced Ca^{2+} signaling by knockdown of PKD1 in medullary primary epithelial cells.*

a Original Ussing chamber recordings from polarized grown primary medullary epithelial cells from Pkd1$^{+/+}$, Pkd1$^{-/-}$, and Pkd1$^{-/-}$/T16a$^{+/+}$ kidneys. **b,c.** Summaries for calculated basal and UTP (100 µM) activated short circuit currents (I_{sc}) demonstrating enhanced Cl^- secretion in epithelia lacking expression of Pkd1. **d-f** Original recordings of ATP-induced Ca^{2+} increase and summaries for basal and ATP (100 µM) induced Ca^{2+} peak and plateau in primary epithelial cells from Pkd1$^{+/+}$, Pkd1$^{-/-}$, and Pkd1$^{-/-}$/T16a$^{+/+}$ kidneys. **g,h** Original recording and summary demonstrating the inhibitory effect of benzbromarone (10 µM) on ATP (100 µM) induced Ca^{2+} peak and plateau. **i,j** Original recording and summary of cyclopiazonic acid (CPA,10 µM) induced ER Ca^{2+} store release and activation of store operated Ca^{2+} influx in medullary primary epithelial cells from Pkd1$^{+/+}$, Pkd1$^{-/-}$, and Pkd1$^{-/-}$/T16a$^{+/+}$ kidneys. Mean ± SEM (n = 15 - 45 filters and cells, respectively, from 4 - 5 mice for each series. #significant difference when compared Pkd1$^{+/+}$ ($p<0.05$; ANOVA). §significant difference when compared to Pkd1$^{-/-}$ ($p<0.05$; ANOVA).

FDA-approved inhibitors of TMEM16A inhibit renal cyst growth *in vivo*. The present data indicate an essential contribution of Tmem16a to the development of polycystic kidney disease. Recent studies identified two FDA-approved drugs, niclosamide and

benzbromarone, as potent inhibitors of TMEM16A [127,344]. We therefore examined if treatment with niclosamide and benzbromarone in vivo would inhibit development of renal cysts in $PKD1^{-/-}$ animals. To that end, $PKD1^{-/-}$ animals were maintained at normal diet or were fed a diet supplemented with 0.2 % niclosamide, which was well tolerated. Animals were sacrificed 30 days later and kidneys were analyzed. Cyst development was strongly attenuated in niclosamide-treated mice when compared to animals on standard diet (Fig. 6.5a,b).

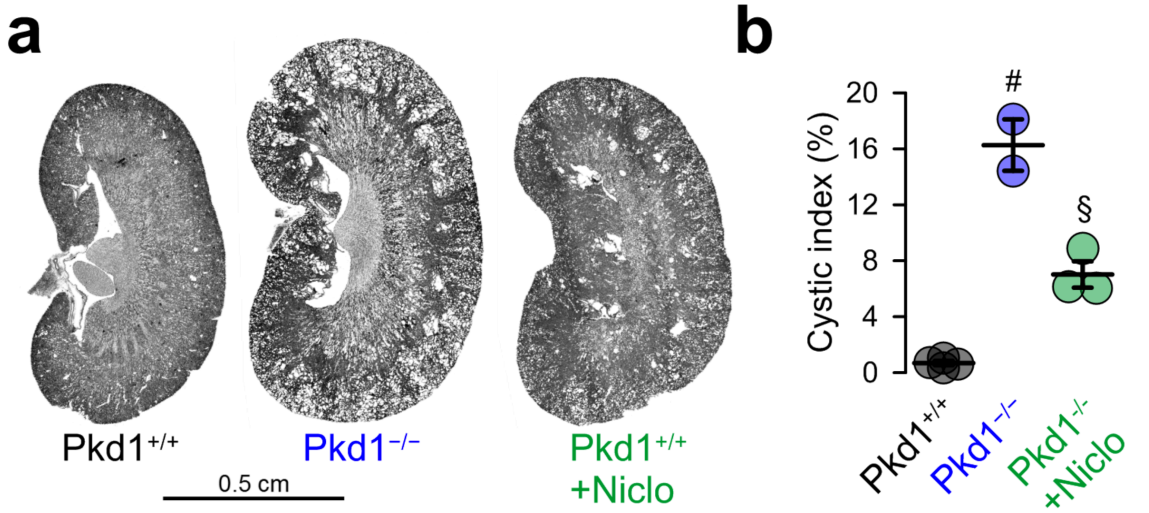

Figure 6.5 | *Niclosamide inhibits polycystic kidney disease in a mouse model for ADPKD.*

a Tubule-specific deletion of Pkd1 ($Pkd1^{-/-}$) was induced at postnatal day 20 - 22. Thereafter, mice were either treated with standard diet (n = 2) or diet supplemented with 0.2 % niclosamide (Niclo, n = 3). $Pkd1^{+/+}$ mice fed with standard diet served as control (n = 4). Niclosamide treatment strongly attenuated the cystic phenotype. **b** Analysis of cystic indices. #significant difference when compared to $Pkd1^{+/+}$. §significant inhibition by niclosamide ($p<0.05$; ANOVA).

A very similar inhibition of polycystic kidney disease was observed in animals treated with benzbromarone: Intraperitoneal injection of benzbromarone for 8 weeks dramatically reduced renal cysts when compared to sham treated animals (Fig. 6.6a,b). Notably, weight gain caused by polycystic kidneys was completely abolished by treatment with benzbromarone (Fig. 6.6c). Proliferative activity was analyzed by staining medullary epithelial cells with the proliferation marker Ki-67. Knockdown of Pkd1 largely enhanced proliferation, which was almost completely eliminated by treatment with benzbromarone (Fig. 6.6d,e). These data identify the crucial role of Tmem16a in polycystic kidney disease. We propose inhibitors of Tmem16a such as niclosamide or benzbromarone as novel therapeutics to potently suppress cyst development in patients with ADPKD.

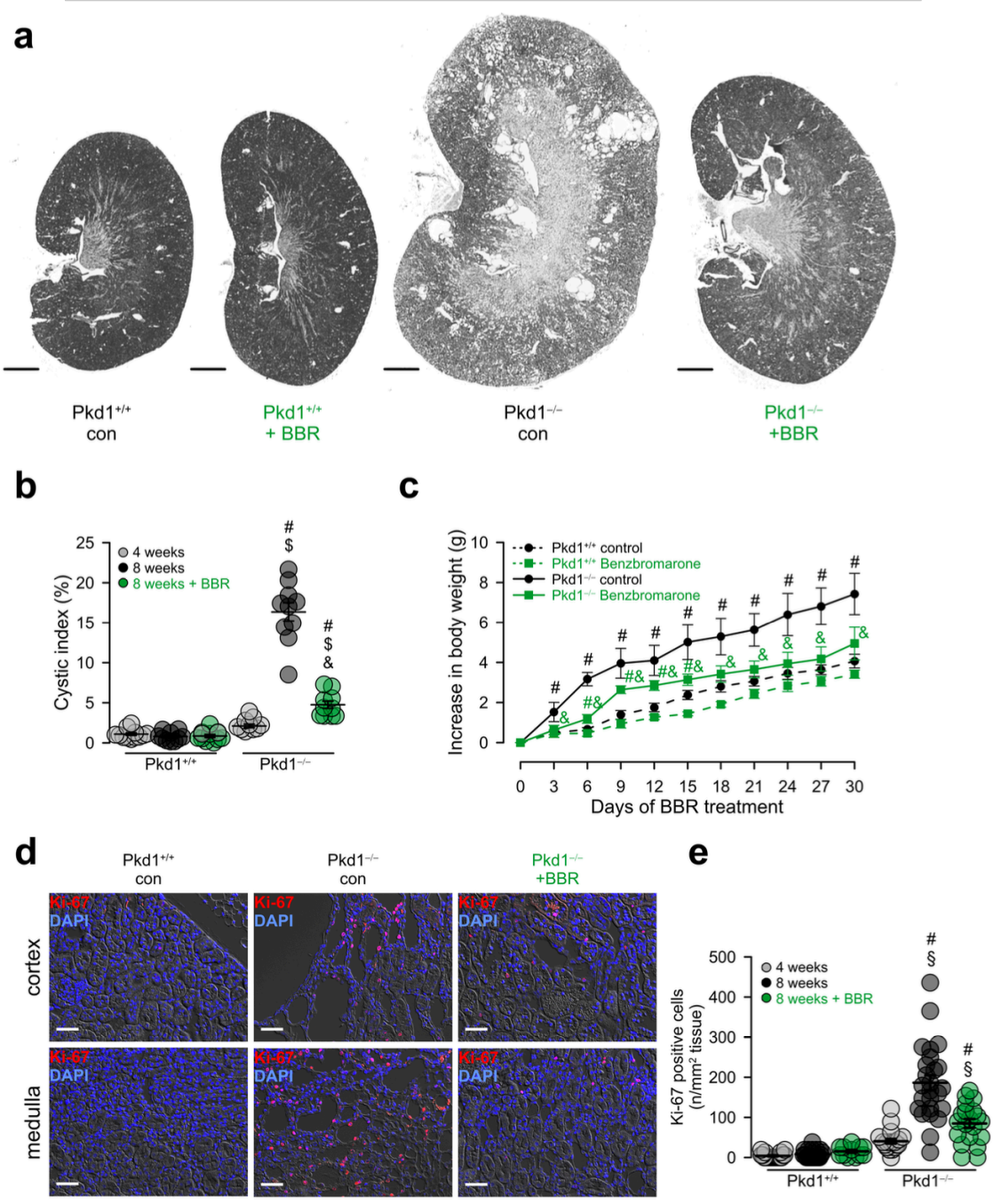

Figure 6.6 | *Benzbromarone inhibits polycystic kidney disease in a mouse model for ADPKD.*

a Representative images of kidneys from non-induced ($Pkd1^{+/+}$) and induced ($Pkd1^{-/-}$) mice, untreated (ip injection of corn oil) or treated with benzbromarone in corn oil (BBR, 1 mg/kg/day, i.p.) for 30 days. Scale bars: 1000 µm. **b** Cystic index (%) of 8 weeks old $Pkd1^{+/+}$ and $Pkd1^{-/-}$ mice, untreated or treated with benzbromarone. Benzbromarone impressively reduced cysts formation in $Pkd1^{-/-}$ mice (n = 2 kidneys from each 5 mice analyzed). **c** Time course of body weight for untreated and benzbromarone-treated $Pkd1^{+/+}$ and $Pkd1^{-/-}$ mice. **d,e** Proliferating tubular epithelial cells identified in $Pkd1^{+/+}$ and $Pkd1^{-/-}$ kidneys by the proliferation marker ki-67 (red). Benzbromarone largely inhibited cell proliferation. ki-67 positive cells were normalized to the tissue area. Mean ± SEM (Analysis of n = 12 - 25 images from n = 2 kidneys / 5 mice each). #significant increase when compared to $Pkd1^{+/+}$, §significant increase compared to 4 weeks ($p<0.05$; ANOVA).

Discussion

The present data demonstrate the crucial role of Tmem16a for the growth of renal cysts in a mouse model for ADPKD and in MDCK cells *in vitro*. Tmem16a was shown previously to be expressed at low levels in renal epithelial cells of normal human and mouse kidney, and was suggested to be upregulated in polycystic kidneys [38,44]. The present data now provide clear evidence that Tmem16a supports cyst development by at least two independent mechanisms, i) by supporting electrolyte secretion and ii) by enhancing cell proliferation.
The essential role of CFTR for cAMP-regulated chloride secretion in intestine, airways, exocrine glands and numerous other epithelial organs is undisputed [383]. Traditionally Ca^{2+} activated transport by TMEM16A was seen as a separate and independent mechanism for transepithelial chloride secretion. Recent studies however suggest that both pathways partially overlap and cannot be separated easily. Thus, CFTR dependent secretion is also activated through Ca^{2+} dependent stimulation [58,59], while knockout of TMEM16A in ciliated airway epithelial cells or intestinal epithelial cells abrogated cAMP/CFTR-dependent chloride secretion [36]. In differentiated epithelial cells plasma membrane expression and activation of CFTR appears to rely on the presence of TMEM16A [384]. Although the relationship of both channels is incompletely understood, plasma membrane tethering of the ER by TMEM16A and increase of compartmentalized Ca^{2+} signals close to the plasma membrane is likely to provide a clue as to the mechanism [79,348].

The present report demonstrates enhanced Ca^{2+} signals in renal epithelial cells from polycystic kidneys that are clearly correlated to enhanced expression of TMEM16A (Fig. 6.4, Supplementary Fig. 6.4). Increase in purinergic Ca^{2+} signaling and increase in Ca^{2+} dependent chloride secretion upon knockout of Pkd1 was observed in medullary (Fig. 6.4, Supplementary Figs. 6.3, 6.4) as well as cortical tubular epithelial cells (Supplementary Figs. 6.5, 6.6). Thus, enhanced Ca^{2+} signals caused by upregulation of TMEM16A appears as the predominant mechanism in ADPKD and also explains the increase in proliferation. In contrast to some previous studies we did not find evidence for attenuated Ca^{2+} levels in renal epithelial cells lacking expression of PKD1 [370]. Moreover, we were unable to detected a role of ryanodine receptors (RyR), as renal tubular expression of RyR could not be detected [166,370] (data not shown). A large number of studies demonstrate the crucial role of TMEM16A for cell proliferation and there is a long list of reports describing its contribution to cellular dedifferentiation and cancer development (reviewed in [142,388]). Along the same line, knockdown of TMEM16A also reduced the number of renal glomeruli and caused albuminuria in another study [46]. The pro-cancerous role of upregulated TMEM16A may also contribute to the higher risk of cancer suggested for patients with polycystic kidney disease [389].

The present data strongly suggest TMEM16A as a potential therapeutic target in ADPKD. Two well established FDA-approved drugs and potent inhibitors of TMEM16A, niclosamide and benzbromarone, strongly suppressed cyst development and ADPKD *in vivo* (Figs. 6.5, 6.6). Benzbromarone is an uricosuric compound that has been suggested to reduce the risk of progression to dialysis in chronic kidney disease (CKD) [390]. Inhibition of TMEM16A reduced pulmonary arterial hypertension and inflammatory airway disease in asthma *in vivo* [130,142]. Likewise, niclosamide inhibited airway inflammation and mucus hypersecretion *in vivo* [344,391] and is currently evaluated as a broad anticancer drug [142,392]. As both compounds and related drugs potently inhibit members of the TMEM16 protein family and interfere with intracellular Ca^{2+} signaling [348,391], we propose inhibition of TMEM16-mediated intracellular signaling as a new therapeutic principle in ADPKD.

Acknowledgements

Supported by Supported by Deutsche Forschungsgemeinschaft (DFG) – Projektnummer 387509280 – SFB 1350. We thank Dr. Björn Buchholz (Department of Nephrology and Hypertension, University of Erlangen-Nuremberg, Erlangen, Germany) for critical discussions and for providing the MDCK clones.

Supplementary material

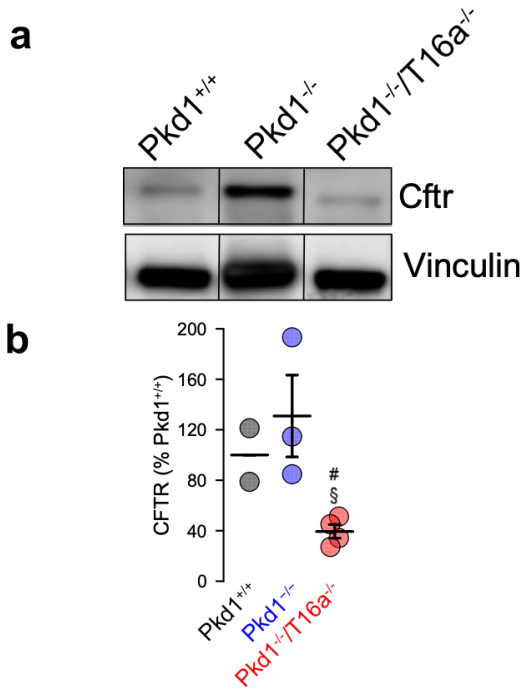

Supplementary Figure 6.1 | *Deletion of Tmem16a inhibits expression of Cftr.*

a Analysis of Cftr expression in protein lysates from whole kidneys of 10 weeks old $Pkd1^{+/+}$, $Pkd1^{-/-}$, and $Pkd1^{-/-}$/$Tmem16a^{-/-}$ double knockout mice. **b** Densitometric quantification of Cftr expression indicating slightly augmented and inhibited expression of CFTR on $Pkd1^{-/-}$ and $Pkd1^{-/-}$/$Tmem16a^{-/-}$ kidneys, respectively. Mean ± SEM; n = 3 animals each. $^{\#\S}$significant difference compared to $Pkd1^{+/+}$ and $Pkd1^{-/-}$ (p<0.5; ANOVA).

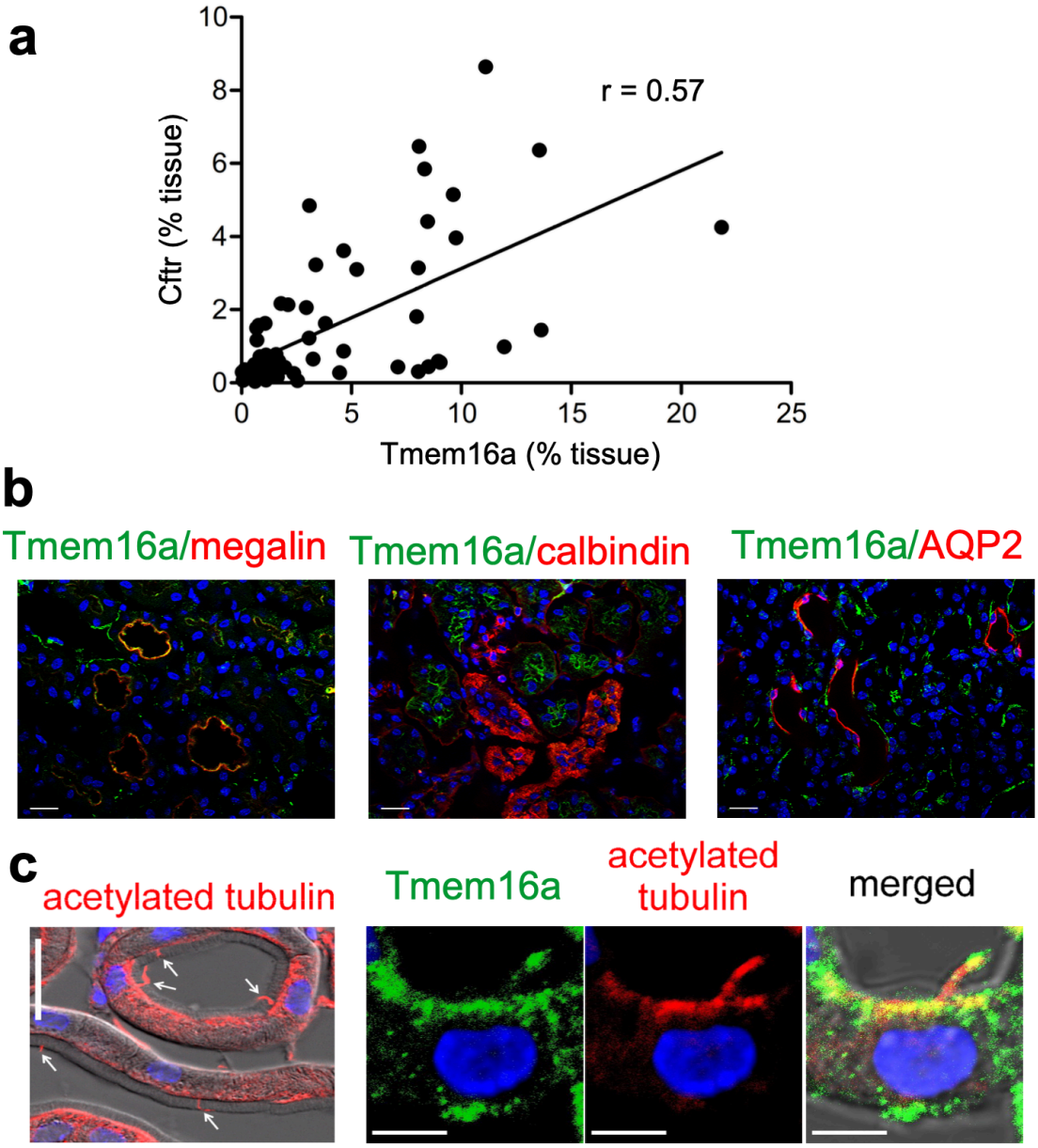

Supplementary Figure 6.2 | *Expression of Tmem16a and Cftr in murine kidney.*

a Correlation between expression of Tmem16a and cftr in the cyst epithelium of $Pkd1^{-/-}$ kidneys. Expression of Tmem16a and cftr was analyzed in n = 15 – 25 images from n = 3 – 5 mice, and was normalized to tissue area. A significant correlation was detected with a Pearson coefficient (r) of 0.57. **b** Expression of Tmem16a in wt $Pkd1^{+/+}$ kidneys. Colocalization was detected for Tmem16a and megalin (proximal tubular epithelial cells), but not for Tmem16a and calbindin (distal tubule) or Tmem16a and AQP2 (collecting duct). Bar 20 µm. **c** Primary cilia in $Pkd1^{+/+}$ renal tubules were identified using acetylated tubulin staining, which expressed Tmem16a. Bar 5 µm.

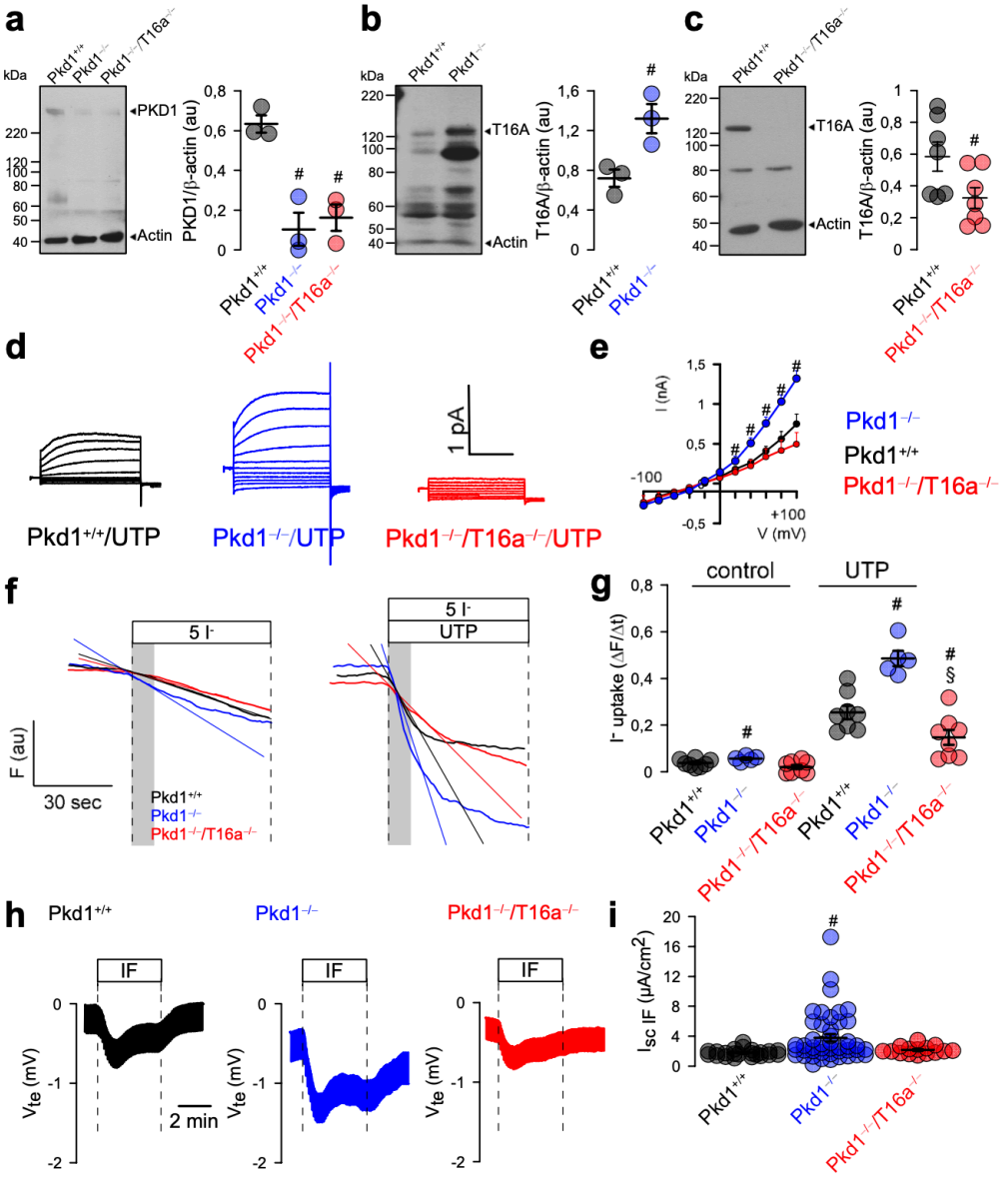

Supplementary Figure 6.3 | *Tmem16a is essential for upregulated chloride conductance in primary Pkd1$^{-/-}$ cells.*

a Western blots and densitometric analysis indicating knockdown of Pkd1 in renal epithelial cells from Pkd1$^{-/-}$ and Pkd1$^{-/-}$/T16a$^{-/-}$ mice (n = 3). **b,c** Western blots and densitometric analysis indicating increased and abolished expression of Tmem16a in renal epithelial cells from Pkd1$^{-/-}$ and Pkd1$^{-/-}$/T16a$^{-/-}$ mice, respectively (n = 3). Actin was used as loading control. **d,e** Original recordings of whole cell currents and corresponding current/voltage relationships obtained in UTP-stimulated medullary primary epithelial cells isolated from Pkd1$^{+/+}$, Pkd1$^{-/-}$ and Pkd1$^{-/-}$/T16a$^{-/-}$ mice. **f** Basal and Ca2+-activated (100 μM UTP) anion conductances detected by YFP quenching. Initial slopes correlate with size of anion conductance. **g** Summary of initial slopes, (ΔFluorescence/s). **h,i** Original recordings and summaries of Ussing chamber experiments with primary medullary epithelial cells from Pkd1$^{+/+}$, Pkd1$^{-/-}$ and Pkd1$^{-/-}$/T16a$^{-/-}$ double knockout mice, showing enhanced Cl^- secretion by activation of CFTR with IBMX/forskolin (100 μM/ 2 μM) in Pkd1$^{-/-}$ cells. Mean ± SEM; n = 15 – 25 cells and filters, respectively from 3 – 5 mice per series. #significant difference compared to Pkd1$^{+/+}$; §significant difference to Pkd1$^{-/-}$ (p<0.05; ANOVA).

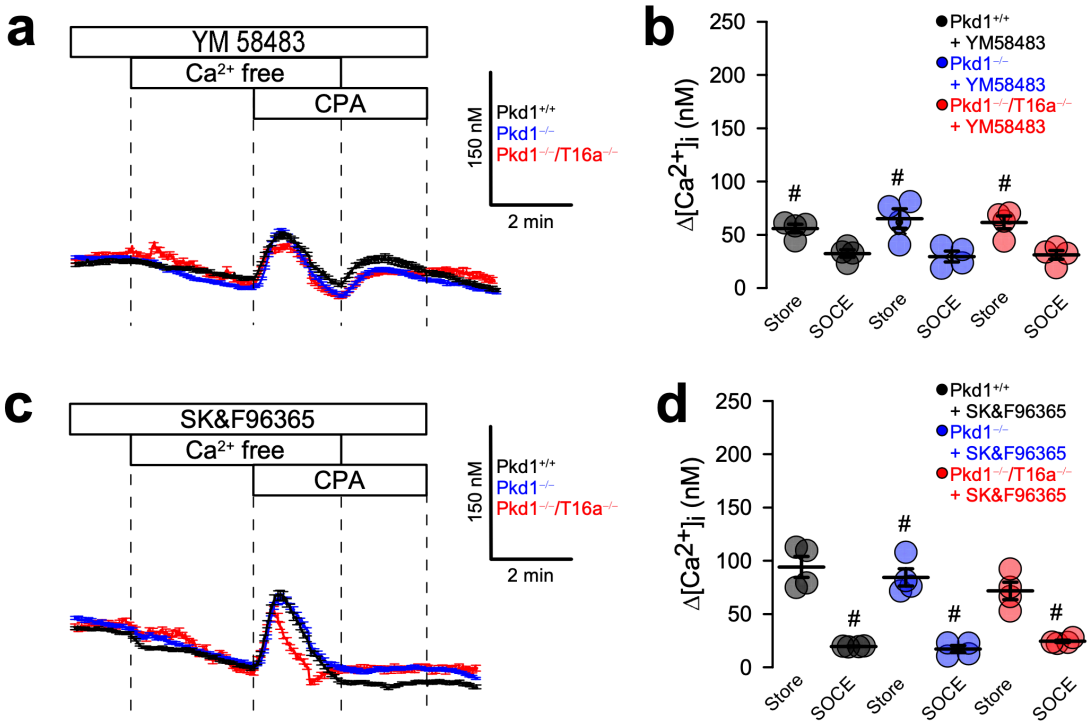

Supplementary Figure 6.4 | *Inhibition of enhanced store operated Ca^{2+} entry (SOCE) by TRP and Orai channel inhibitors.*

Original recordings and summaries showing inhibition of upregulated ER Ca^{2+} store release and store operated Ca^{2+} entry (SOCE) in primary renal epithelial cells from $Pkd1^{-/-}$ mice in the presence of TRP-channel inhibitor SK&F96365 and Orai channel inhibitor YM58483 (both 5 µM). Mean ± SEM (6 – 8 cells measured from n = 4 mice for each). #significant difference when compared to the absence of inhibitors (c.f. Fig. 6.4i) (p<0.05; ANOVA).

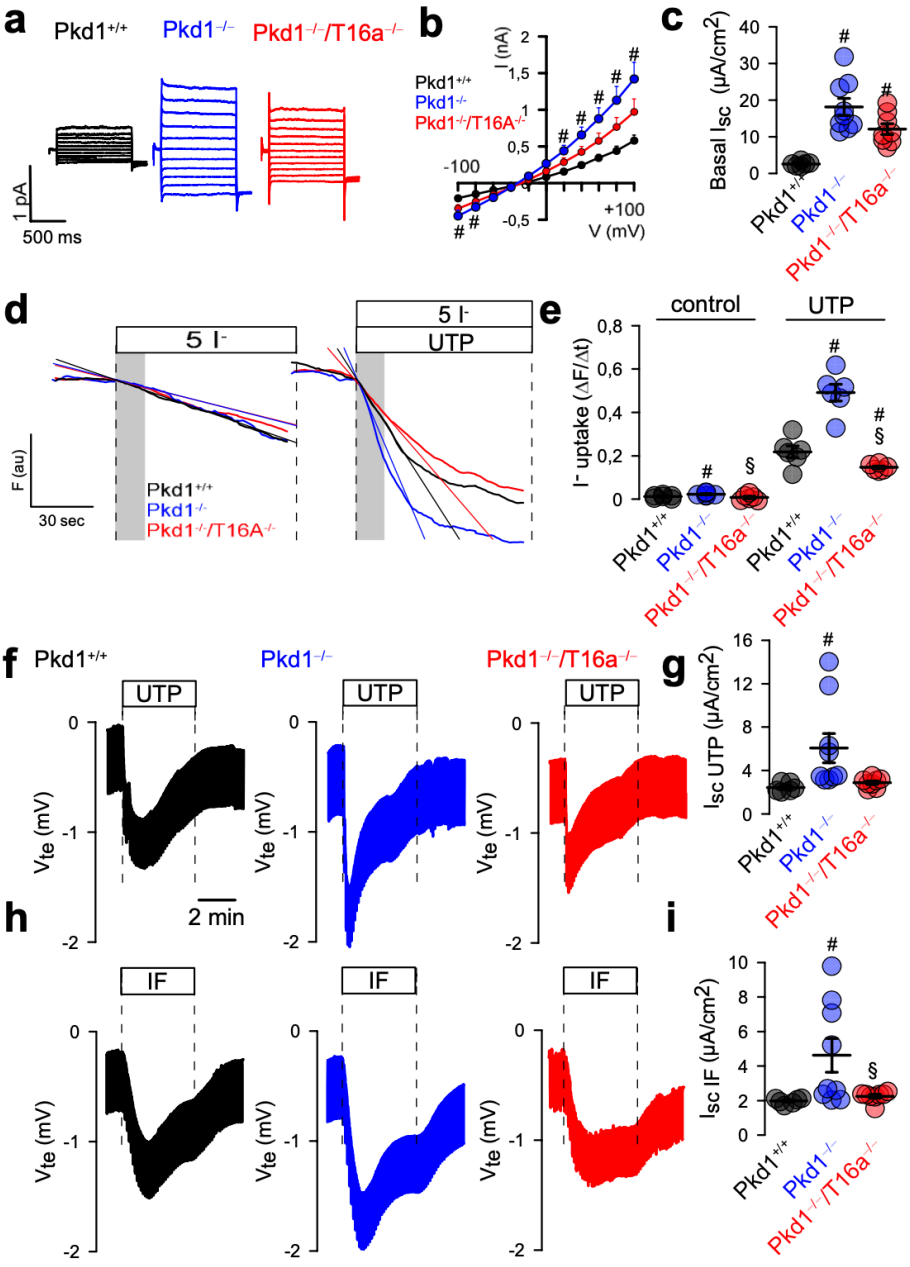

Supplementary Figure 6.5 | *Tmem16a is essential for upregulated chloride conductance in cortical primary epithelial cells from Pkd1$^{-/-}$ mice.*

a,b Whole cell currents and corresponding current/voltage relationships obtained in primary cortical epithelial cells isolated from Pkd1$^{+/+}$, Pkd1$^{-/-}$ and Pkd1$^{-/-}$/T16a$^{-/-}$ mice. **c** Summary of short circuit currents measured in Ussing chamber recordings showed upregulated transport in Pkd1$^{-/-}$ cells, which was lower in Pkd1$^{-/-}$/T16a$^{-/-}$ cells. **d,e** Basal and Ca^{2+}-activated (100 µM UTP) anion permeability assessed by YFP quenching. Summaries of YFP quenching (initial slope, ΔFluorescence/s) indicate upregulation of UTP-activated anion conductance in Pkd1$^{-/-}$ cells, which was inhibited in Pkd1$^{-/-}$/T16a$^{-/-}$ double knockout cells. **f-i** Original Ussing chamber recordings and calculated short circuit currents indicate upregulated Cl^- conductance activated by UTP (100 µM) or IBMX/forskolin (I/F; 100 µM, 2 µM) in Pkd1$^{-/-}$ cells, which was undetectable in Pkd1$^{-/-}$/T16a$^{-/-}$ cells. Mean ± SEM; n = 9 – 15 cells/filters from 4 mice each. #significant difference when compared to Pkd1$^{+/+}$, §significant difference compared to Pkd1 (p<0.05; ANOVA).

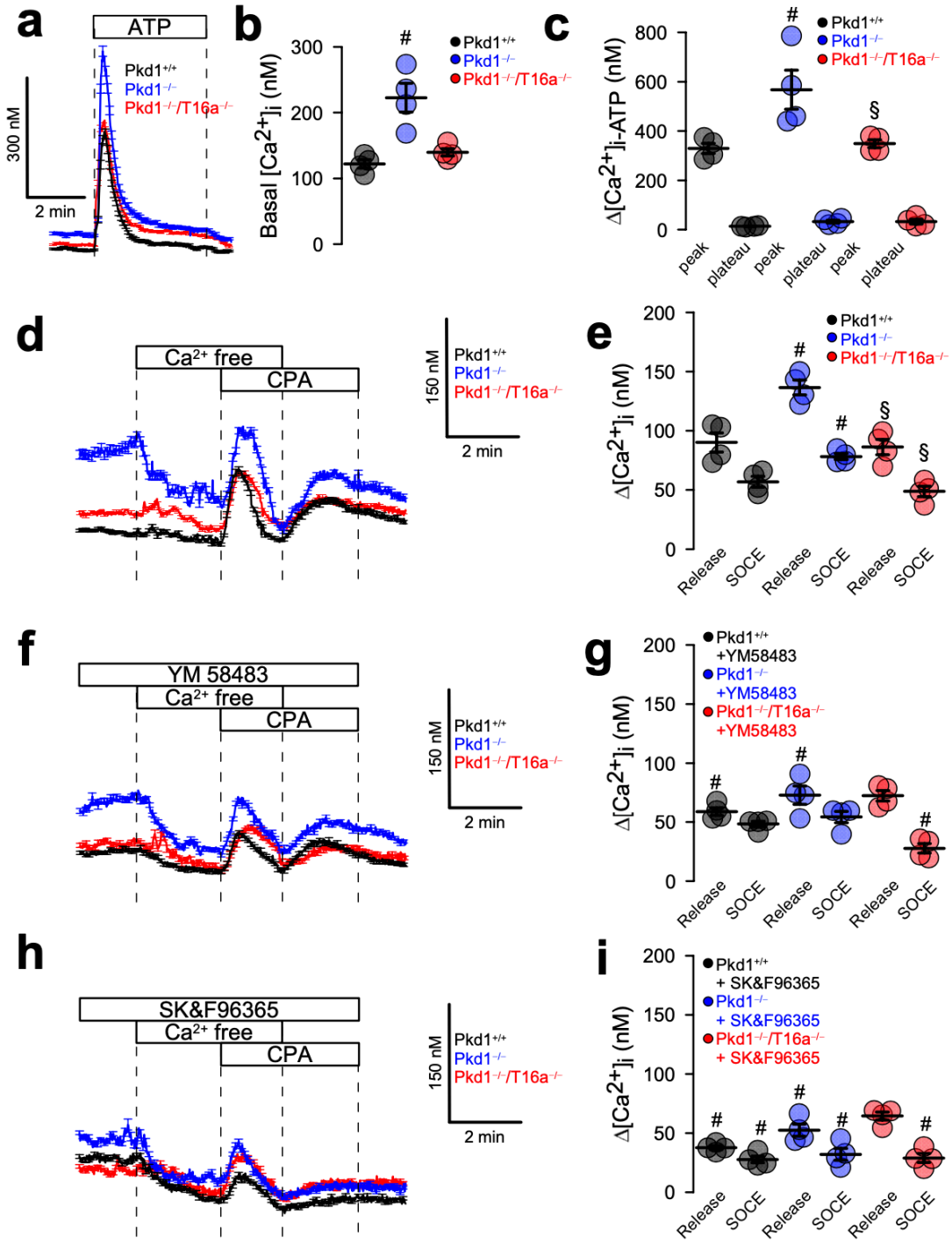

Supplementary Figure 6.6 | *Augmented Ca^{2+} signals in renal cortical primary epithelial cells.*

a-c Original recordings and summaries for basal and ATP-induced increase in intracellular Ca^{2+}. Ca^{2+} peak (store release from the ER) was enhanced in primary cells from Pkd1$^{-/-}$ but not Pkd1$^{-/-}$/T16a$^{-/-}$ kidneys. **d,e** Original recordings and summaries for cyclopiazonic acid (CPA, 10 µM) induced store release in Pkd1$^{+/+}$, Pkd1$^{-/-}$ and Pkd1$^{-/-}$/T16a$^{-/-}$ cells. Store release and store operated Ca^{2+} entry (SOCE) was augmented in cells from Pkd1$^{-/-}$ but not Pkd1$^{-/-}$/T16a$^{-/-}$ kidneys. **f-i** Original recordings and summaries from experiments performed in the presence of TRP-inhibitor SK&F96365 and Orai-inhibitor YM58483 (both 5 µM), which both inhibited upregulated SOCE. Mean ± SEM; n = 4 mice for each series. #significant difference when compared to Pkd1$^{+/+}$ and absence of inhibitors, respectively (p<0.05; ANOVA). §significant difference when compared to Pkd1$^{-/-}$ (p<0.05; ANOVA).

CHAPTER 7 | DISCUSSION

In the project presented here, I tried to unravel novel functions of TMEM16 proteins. I studied the impact of TMEM16A and other TMEM16 paralogs on intracellular Ca^{2+} signaling. This was done by overexpressing TMEM16 proteins *in vitro*, knockdown by siRNA, introducing mutations and pharmacologically inhibiting the channels in various cell types. I compared TMEM16-related Ca^{2+} signals in various tissues from wild type and TMEM16-knockout animals and in cell lines. The intracellular Ca^{2+} concentration was measured along with a number of Ca^{2+}-associated cellular parameters [27,72,371].

TMEM16 PROTEINS MODULATE CA^{2+} SIGNALING IN MICRODOMAINS

When measuring global intracellular Ca^{2+} signals, activation of purinergic receptors by ATP induced the typical peak and plateau increase of $[Ca^{2+}]_i$, caused by a fast release of Ca^{2+} from the ER (peak), followed by a Ca^{2+} influx through store-operated Ca^{2+} entry (SOCE) channels [393]. To measure local Ca^{2+} concentration close to the plasma membrane, I made use of membrane-bound Ca^{2+} sensor GCaMP2, modified by addition of a N-terminal signal peptide from neuromodulin (Pl-G-CaMP2). In contrast to Fura-2, the Ca^{2+} sensor Pl-G-CaMP2 is targeted to the plasma membrane and detects Ca^{2+} signals in the proximity of the plasma membrane. I found that Pl-G-CaMP2 only detects Ca^{2+} release from IP_3-sensitive ER stores (peak), but not Ca^{2+} influx (SOCE; plateau) (Chapter 2). Therefore, the transient peak is also detectable under extracellular Ca^{2+}-free conditions. From past and additional experiments [273,394] it became clear that TMEM16A and the Ca^{2+} sensor Pl-G-CaMP2 are targeted to lipid raft-like membrane microdomains, which are well isolated from other domains that contain Ca^{2+} influx (SOCE) channels. The Ca^{2+}-activated Cl^- channel TMEM16A is homologous to the yeast protein Ist2. Both proteins were shown to tether the cortical ER to the plasma membrane [76,78]. In Chapter 2, I examined whether TMEM16A and other members of the TMEM16 family affect intracellular Ca^{2+} signals. We found that expression of TMEM16A augments Ca^{2+} store release upon stimulation of G-protein coupled receptors, while knockdown of endogenous TMEM16A or lack of TMEM16A expression in TMEM16A$^{-/-}$ animals inhibits Ca^{2+} store release [36,37,125,395] (Chapter 5). Moreover, overexpression of TMEM16A, E, F, and K augmented Ca^{2+} store release, whereas TMEM16D, H and J largely reduced Ca^{2+} store release (Chapter 2).

TMEM16A and TMEM16D were found to affect compartmentalized calcium signals and ER Ca^{2+} stores in opposite fashion: TMEM16A is localized in lipid rafts in the plasma membrane[78], facilitating local Ca^{2+} release from the ER (Chapter 2). Surprisingly, it also increases Ca^{2+} store content, possibly by indirectly augmenting SOCE and Ca^{2+} uptake through SERCA (Chapter 2). In contrast, TMEM16D, which may also be permeable to

calcium [11], is localized in the ER membrane and lowers the Ca^{2+} store content by mediating Ca^{2+} leakage out of the ER. Thus, resulting in an overall decreased Ca^{2+} signaling. Moreover, TMEM16D interacts with SERCA pump and Orai1 and it is activated by SOCE (Chapter 2). Maniero *et al.* speculated that decreased intracellular Ca^{2+} signals in TMEM16D-overexpressing cells explains the decreased ATP and ionomycin-stimulated aldosterone secretion they observed in their studies [396]. More recently, Jha *et al.* showed that TMEM16J also tethers the ER to the PM, facilitating STIM1-Orai1 interactions [353]. The data also support the concept that TMEM16F is activated by Ca^{2+} influx (SOCE) through ORAI and maybe other Ca^{2+} influx channels. In addition, it may increase intracellular Ca^{2+} by operating as a Ca^{2+}-permeable ion channel [14] (Chapter 2).

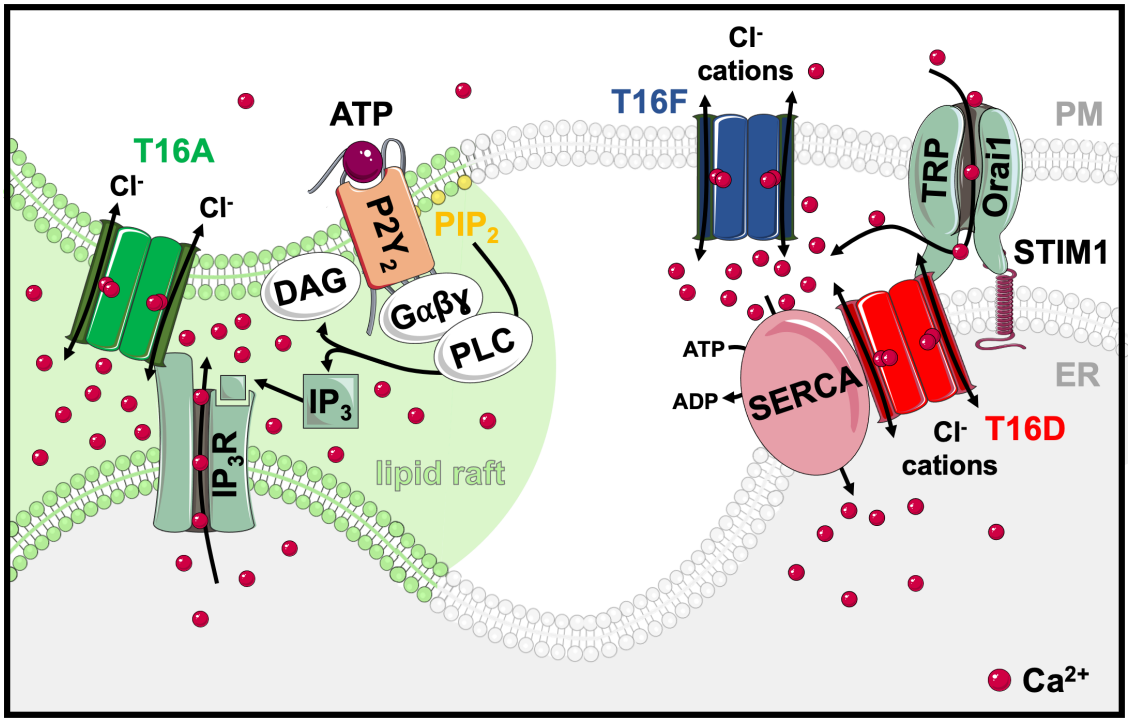

Figure 7.1 | *Compartmentalized Ca^{2+} signaling by TMEM16 proteins.*

Scheme illustrating the effects of TMEM16 proteins on Ca^{2+} signaling. TMEM16A (T16A) tethers ER Ca^{2+} stores close to the plasma membrane in lipid rafts, through IP_3R interaction, which leads to enriched ATP-induced apical Ca^{2+} signaling. Release of Ca^{2+} from the ER store results in Ca^{2+} influx through store-operated Orai1 and TRP Ca^{2+} influx channels. TMEM16D (T16D) decreases intracellular Ca^{2+} signaling as a Ca^{2+} leakage channel, or by inhibiting SERCA pumps in the ER. Activation of Ca^{2+} influx, activates TMEM16F (T16F) in the plasma membrane, which further increases Ca^{2+} signaling by operating as Ca^{2+}-permeable channel.

TMEM16K is expressed as an intracellular protein in renal proximal tubules, and along the intestinal epithelium, particularly in jejunum (Chapter 2 and 3, respectively) [3,27]. Overexpression of TMEM16K in HeLa cells resulted in enhanced compartmentalized ATP-induced Ca^{2+} store release (Chapter 2). Our results show that ATP-induced Ca^{2+} store

release and Ca^{2+} influx were largely impaired in TMEM16K-knockout animals when compared to *wild-type* animals (Chapter 2 and Chapter 3) [27]. Intracellular Ca^{2+} signals in intestinal epithelial cells are relevant to maintain cell size by volume regulation (Chapter 3). TMEM16K therefore supports Ca^{2+}-dependent activation of VRAC currents (Chapter 3)[93]. Moreover, intracellular Ca^{2+} concentration is crucial for cell proliferation and cellular apoptosis. TMEM16K knockout resulted in reduced proliferation as well as attenuated apoptotic activity in mouse jejunum and macrophages (Chapter 3). Finally, TMEM16K mutations, which were found to be associated with cerebellar ataxia [23,25,26], caused enhanced Ca^{2+} signals [23](Chapter 3). Increased Ca^{2+} signaling with enhanced local Ca^{2+} concentrations is known to harm Purkinje cells of the cerebellum which explains cell death in cerebellar ataxia [75,321-325].

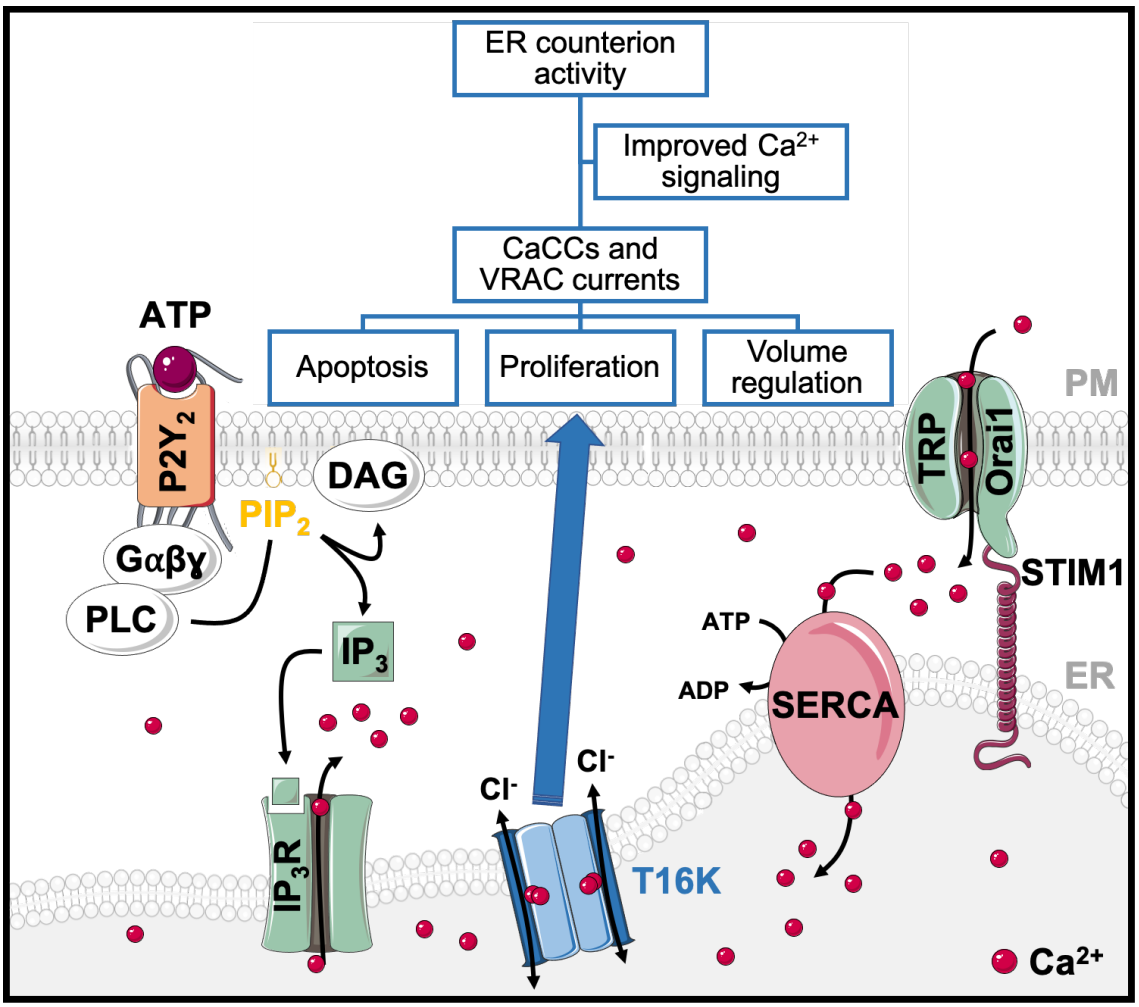

Figure 7.2 | *TMEM16K regulates calcium signaling in the ER modulating apoptosis, proliferation and volume regulation.*

Scheme illustrating the cellular effects of TMEM16K by possibly operating das ER counterion channel.

TMEM16K could also be acting as an ER-localized counterion channel for Cl^- to balance accumulation of negative charge within the ER, during IP3- or leakage channel-induced Ca^{2+}

release. Movement of Cl^- over the ER membrane is necessary for charge compensation to allow for efficient Ca^{2+} store release, and for re-uptake of Ca^{2+} into the ER by the SERCA pump (Fig. 7.2) [291,397]. Endogenous and overexpressed TMEM16K is typically intracellular and co-localizes with acetylated tubulin (Chapter 3). However, expression and localization of TMEM16K is tissue- and cell cycle-dependent. For example, endogenous TMEM16K in rapidly proliferating Fisher Rat Thyroid (FTR) cells is located mostly intracellularly and appears upregulated during mitosis (Chapter 3). Once FRT cells form a dense monolayer and stop proliferating in serum free media, TMEM16K moves to the cell membrane and co-localizes with the centrioles. Non-proliferating cells on permeable supports in the absence of serum seem to further lower expression of TMEM16K, which is then preferentially expressed close to the centriole (Chapter 3).

TMEM16A and TMEM16F regulate constitutive mucus secretion

TMEM16A is essential for secretion of mucus by goblet epithelial cells in airways and intestine [125]. In the intestine this appears to be due to a direct pro-secretory function: TMEM16A enhances sub-apical intracellular Ca^{2+} signals that are required to fuse mucus-filled granules with the apical membrane. In the airways, the situation is somewhat more complicated due to the larger number of different cell types. On the one hand TMEM16A, together with TMEM16F, seem to directly support mucus release by airway goblet cells, similar to intestinal goblet cells. On the other hand, TMEM16A/F seem to control the release of morphogenic factors such as Notch-receptor ligands or they support vesicular shedding and thus release exosomes carrying Notch-receptors. Notch receptors and ligands are known to regulate cellular differentiation in the airways. They control transdifferentiation from ciliated into club (Clara) cells and further differentiation into goblet cells. Thus, TMEM16A plays an essential role in the so-called goblet cell metaplasia in asthma and possibly in the hyperplasia of goblet cells, as observed in cystic fibrosis. Moreover, we also showed in the present studies that TMEM16A/F support cellular exocytosis and release of pro-secretory cytokines [125]. Indeed, release of IL-8 induced by lipopolysaccharide (LPS) was significantly reduced by knockdown of TMEM16A (Chapter 4). Along the same lines, IL-13-induced production and secretion of MUC5AC were inhibited by the TMEM16A blocker and antiproliferative/anticancer drug, niclosamide (Chapter 4).

A recent paper by Hilgemann and colleagues demonstrates massive membrane expansion by activation of TMEM16F, with induction of subsequent membrane shedding [97]. These results are reminiscent of our earlier observations of TMEM16F-dependent blebbing and membrane shedding in macrophages [16]. Taken together, there is now strong evidence that anoctamins, particularly TMEM16A and TMEM16F, control endolysosomal trafficking [16,38,40,93,125], while more recent findings show that TMEM16A contributes to membrane

exocytosis. TMEM16A/F are therefore able to increase membrane surface area and to insert proteins into the plasma membrane [36,59,125,304,378,384,394]. As outlined above, TMEM16A and TMEM16F control intracellular calcium concentration $[Ca^{2+}]_i$, which is the essential regulator of exocytosis (Fig. 7.3). Thus, compartmentalized $[Ca^{2+}]_i$ close to the plasma membrane is required for docking of exocytic vesicles and granules. This process requires the so-called Munc13 proteins and the soluble N-ethylmaleimide-sensitive factor-attachment protein receptor machinery [398,399]. TMEM16F, similarly to TMEM16A, was recently reported to support membrane exocytosis in HEK293 and B lymphocyte cells [97,125].

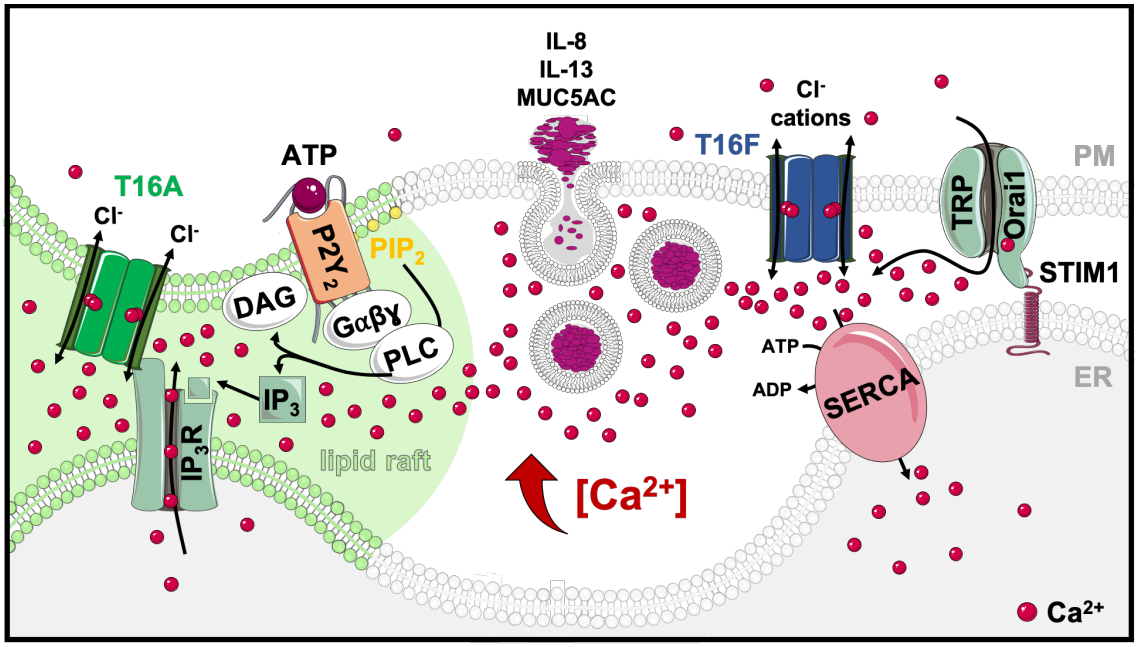

Figure 7.3 | *TMEM16A and TMEM16F regulate constitutive mucus and pro-secretory cytokine secretion.*

Scheme illustrating the effects of TMEM16A and TMEM16F on Ca^{2+} signaling resulting in ATP-induced constitutive exocytosis.

Niclosamide is a FDA-approved drug that was shown to inhibit Notch signaling [400], a pathway that is well known to participate in tumorigenesis [401]. In several reports, additional antineoplastic mechanisms of niclosamide have been described. This drug is used as an anthelmintic to treat tapeworm infestations. In addition, niclosamide was found to be a potent bronchodilator [344] and was shown to inhibit cellular signaling by nuclear factor kappa B (NF-κB), Wnt/ß-catenin, IL-6-JAK1-STAT3, GSK-3 and many more [352,368,402-408]. Notably, blockade of Notch signaling inhibits goblet cell metaplasia in asthmatic mice, which could be part of the mechanism how niclosamide inhibits mucus production [344,409,410]. Excessive mucus secretion represents one of the main clinical hallmarks in respiratory diseases, as well as in ulcerative colitis and irritable bowel syndrome [411,412]. Therefore, the need for novel drugs to control mucus hyperproduction is compelling. We investigated the effect of two

compounds which are known as potent TMEM16A-inhibitors: niclosamide and niflumic acid (NFA). Niclosamide and NFA inhibited purinergic Cl^- currents in HEK293 cells expressing TMEM16A or TMEM16F (Chapter 4). In addition, both drugs showed a marked effect on Ca^{2+} signals in freshly isolated intestinal cells (Chapter 4). Similarly, freshly isolated crypts from jejunum and colonic crypts from TMEM16F$^{fl/fl}$ Vil1Cre mice showed a reduced ATP-induced Ca^{2+} store release, while the CCH-induced Ca^{2+} signaling was unaffected (Chapter 4). In asthmatic mice, niclosamide and NFA reduced mucus production and attenuated bronchoconstriction after acute application of cholinergic stimuli. Moreover, both inhibitors reduced the inflammation in asthmatic mice (Chapter 4). Taken together, these results strongly suggest the use of TMEM16A-inhibitors for the treatment of inflammatory airway disease.

In contrast, potentiators of TMEM16A have been developed with the aim of treating cystic fibrosis lung disease. However, potentiation of TMEM16A activity [413] might be counterproductive, because TMEM16A is upregulated in inflamed airways of asthma and probably also in those of CF patients. Strong upregulation is found in airway smooth muscle and mucus-producing goblet cells. Thus, TMEM16A supports mucus secretion and bronchoconstriction [125,339,344,378], and therefore seems to abrogate airway function. Th2-induced goblet cell metaplasia occurs at the same rate in both control asthmatic mice and asthmatic mice lacking TMEM16A. Therefore, we speculated that not TMEM16A, but other members of TMEM16 family are in charge of mucus production. Deletion of TMEM16F in the airways (TMEM16F$^{fl/fl}$ FoxJ1-Cre) displayed mucus accumulation similar to TMEM16A knockout mice [125] but showed attenuated mucus production after inducing asthma (Chapter 4). In contrast to mouse lungs, mucus production was clearly TMEM16A-dependent in cultured human airway epithelial cells. Taken together, TMEM16A/F are relevant for mucus production and secretion and therefore represent pharmacological targets in inflammatory airway disease.

In the intestine, ATP-induced mucus secretion was attenuated in tissue-specific TMEM16F knockout mice (TMEM16F$^{fl/fl}$ Vil1Cre) similarly to the TMEM16A$^{fl/fl}$ Vil1Cre mice [125], while, cholinergic release was similar to control mice (Chapter 4). Interestingly, treatment with niclosamide either as acute application, via intraperitoneal injection or by gavage, inhibited apical ATP-induced mucus release, but not basolateral cholinergic-induced mucus secretion (Chapter 4). These results indicate a role for TMEM16F in mucus production and probably mucus secretion induced by purinergic stimulation. Given the fact that niclosamide inhibits both TMEM16A and TMEM16F, it appears to be a suitable drug to treat excessive mucus secretion *in vivo*.

As pointed out above, upregulation of TMEM16A in airway smooth muscle during airway inflammation strongly supports bronchoconstriction. The role of TMEM16A in provoking bronchoconstriction was further shown in asthmatic mice, by activating TMEM16A directly using the activator E_{ACT}. As expected, E_{ACT} induced a massive mucus release and airway contraction [125]. Therefore, inhibition of TMEM16A and TMEM16F activity will not only block the release of mucus and inflammatory mediators but also promote bronchorelaxation. As pointed out above, we propose inhibitors of TMEM16A/F as a new class of drugs that reduce mucus secretion in inflammatory airway diseases. Given the tight regulatory relationship between TMEM16A and CFTR, blocking TMEM16A would potentially inhibit CFTR, which could be counterproductive. However, it should be noted that CFTR is not functional in CF patients. Moreover, the benefit gained by inhibition of mucus secretion through inhibition of TMEM16A/F may well exceed potential negative effects caused by inhibition of TMEM16A. In addition, CF-typical airway plugging will be reduced by the bronchodilation induce by TMEM16A-inhibitors. In this regards it is important to note that around 50% of all CF patients show an asthmatic phenotype. Little information is currently available on the true importance of TMEM16A-dependent Cl^- secretion in human airways, which would be compromised by the use of TMEM16A-inhibitors. Thus, it is indispensable to perform additional *in vivo* studies, pre-clinical trials in animals and clinical pilot trials.

TMEM16A modulates cyst development in the kidney

The glomerular filtrate is reabsorbed by 99% during the renal tubular passage. Evidence suggests that most of the cysts are disconnected from the original tubule of origin, forming a secretory spherical structure [248]. Additionally, cysts continue to grow after separation from the renal tubule, which indicates that this fluid is not derived from the glomerular filtrate, but instead is caused by upregulated epithelial Cl^- secretion. We showed earlier that in the kidney, TMEM16A is predominantly expressed in human and mouse renal proximal tubules and collecting ducts [38]. Our studies and those by other teams, demonstrated that CFTR is mainly expressed in the proximal tubule. Expression of TMEM16A and CFTR was shown to coincide with the appearance of renal cysts during ADPKD. As outlined above, TMEM16A plays a central role in fluid secretion and proliferation of cysts in an embryonic kidney cyst models, as well as in cysts formed by Madin-Darby Canine Kidney (MDCK) cells in a collagen matrix. Moreover, TMEM16A is also expressed in the cyst epithelium from human ADPKD tissues of different patients [44]. Notably, secretion and cyst growth are inhibited by inhibitors of TMEM16A.

TMEM16A is typically activated through purinergic stimulation via $P2Y_2$ receptors. Dr. Buchholz and our team found that expression of $P2Y_2$ and Cl^- secretion in ADPKD are strongly upregulated due to hypoxia and hypoxia-inducible factor-1α, and that this is further

boosted by high blood glucose levels [249,251,252]. We recently detected pronounced lipid peroxidation in polycystic kidneys and found that lipid peroxidation strongly activates TMEM16A/F, which further augments Cl^- secretion and cyst growth [22,48]. Expression and localization of TMEM16A is dynamic and has a clear effect on intracellular Ca^{2+} signaling, as well as cell proliferation. Luminal ATP activates TMEM16A via $P2Y_2R$ and leads to cyst growth. During the course of ADPKD, expression and membrane localization of TMEM16A is enhanced [386] along with cellular dedifferentiation and loss of the primary cilium. This also seem to result in activation of Cl^- secretion by CFTR, which strongly enhances fluid secretion and cyst growth. The present study demonstrates the importance of intracellular Ca^{2+} signaling as a central messenger in ADPKD. There is an ongoing controversy whether Ca^{2+} signals are increased or decreased in ADPKD [414]. This discrepancy might be due different model organisms and it is known that TMEM16-dependent intracellular Ca^{2+} signals parallel changes of cellular properties [2,36,125,415,416]. In my thesis I tried to examine this question in detail *in vitro* and *in vivo*. I found in both MDCK and primary tubular epithelial cells lacking expression of PKD1, upregulation of TMEM16A which was responsible for enhanced $[Ca^{2+}]_i$, purinergic receptors-induced Ca^{2+} store release, and parallel upregulation of transepithelial Cl^- transport (Chapter 5).

In order to understand the process of renal cysts development during ADPKD, we also investigated the role of TMEM16A on cell proliferation and apical Cl^- secretion. M1 cells were grown as renal spheroids in 3D cultures (Chapter 5). This was done to assess whether the induction of the cystic phenotype through knockdown of PDK1 or PDK2 would truly alter epithelial ion transport. Overall, the M1 cell line with stable downregulation of PKD1 or PKD2 mimicked the *in vivo* situation quite well, by showing an increased lumen when grown under 3D conditions and increased proliferation, compared with control cells. This increased lumen fluid content was due to increased Cl^- secretion (Chapter 5). Upregulation of TMEM16A, resulting from downregulation of PKD1 or PKD2 explains the increased proliferative activity of spheroids (Chapter 5). Furthermore, in this M1 model we found that TMEM16A is most important for Cl^- secretion, with little contribution of CFTR (Chapter 5). This is in agreement with Hooper *et al.* [417], who found that ATP stimulation of Cl^- secretion depends on PKD1. M1 cells presented enhanced Ca^{2+} signaling (Chapter 5), which may be responsible for the phenotypic switch from absorptive to secretory tissue. A shift in the gene expression profile after knockdown of PKD1 or PKD2 appears possible [418]. In fact, in cells lacking PKD1 or PKD2, TMEM16A was found to be upregulated (Chapter 5) [377].

Several studies have shown that TMEM16A colocalizes and interacts with the IP_3R in the ER [78] and facilitates IP_3-mediated Ca^{2+} release from the intracellular stores. It is also reported that PKD2 and IP_3R interact and promote Ca^{2+} release from the ER [197,198]. PKD1 is

thought to disrupt this interaction, thus limiting ER Ca^{2+} release [198]. In absence of PKD1, PKD2-IP_3R interaction is apparently enhanced and, together with increased TMEM16A activity, a higher Ca^{2+} release after IP_3R activation, can occur. On the other hand, downregulation of Pkd2 led to an increase of intracellular Ca^{2+} concentration in the cytosol and ER. This is explained by the expression of PKD2 in the absence of PKD1 in the membrane of the ER [419]. In this condition, PKD2 could contribute to ER Ca^{2+} leakage and to an increase in the cytosolic Ca^{2+} concentration (Chapter 5). I propose a new model for Cl^- secretion in ADPKD. Under basal conditions, knockdown of PKD1 deregulates PKD2 function. This leads to a higher $[Ca^{2+}]_i$ and a slight increase of basal chloride conductance by TMEM16A and CFTR. After purinergic stimulation, Ca^{2+} release from the ER and Ca^{2+} uptake into the cell is enhanced and facilitates TMEM16A and CFTR dependent chloride secretion and cyst development in ADPKD.

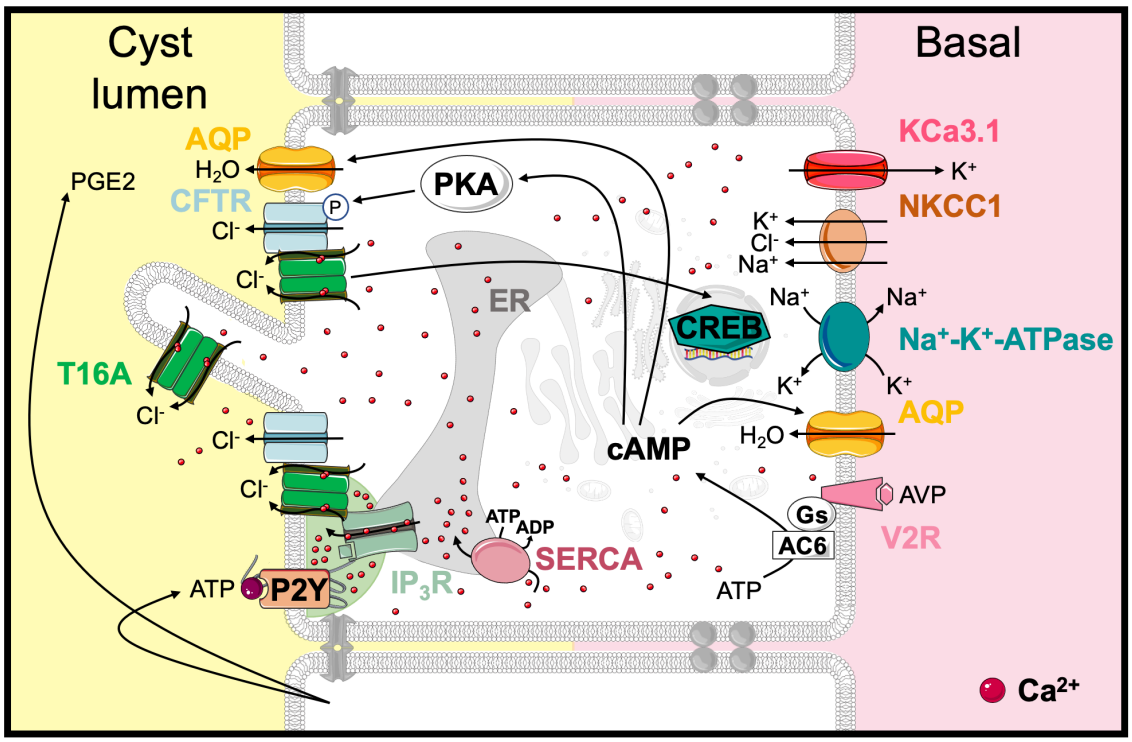

Figure 7.4 | *TMEM16A upregulation increases Ca^{2+} signaling, secretes chloride and increases proliferation activity in ADPKD.*

Scheme illustrating the effects of TMEM16A on Ca^{2+} signaling, resulting in cysts growth. Apical TMEM16A and CFTR crosstalk thereby increasing Cl^- secretion. TMEM16A tethers the ER to the PM increasing apical Ca^{2+} signaling. Moreover, upregulated TMEM16A increases the cellular proliferative activity.

Several studies claim that cystic cells contain higher cAMP levels [258] that lead to a higher Cl^- secretion, which is blocked by inhibiting CFTR with $CFTR_{inh}172$. According to this, CFTR has a role as Cl^- secreting channel in the cyst epithelium. Indeed, in this work, we found that CFTR is upregulated together with TMEM16A in PKD1 KO cells (Chapter 6). Notably, and as reported by Benedetto *et al.* [36], CFTR and TMEM16A seem to interact, and this interaction

is necessary for CFTR activation. Moreover, we found in primary cortical cells that Tmem16a knockout also reduced CFTR-dependent Cl^- secretion that was found to be augmented by Pkd1 knockout (Chapter 6).

THERAPIES FOR AUTOSOMAL DOMINANT POLYCYSTIC KIDNEY DISEASE

Tolvaptan, a vasopressin 2 receptor antagonist (V2RA), blocks the renal effects of AVP and inhibits Cl^- secretion and growth *in vitro* [240]. In preclinical studies, tolvaptan delayed the progression of cystic disease in several animal models of PKD [420-423]. Clinical trials finally demonstrated that V2 receptor antagonism effectively slowed kidney volume increase and the decline in estimated glomerular filtration rate in ADPKD patients [424-426]. Thus, tolvaptan has been approved as a therapy for ADPKD in individuals at high risk of progression to end stage renal disease (ESRD). However, Tolvaptan has its disadvantages due to its cost and adverse effects, which include polyuria and potentially severe liver injury[424,426]. Moreover, disease progression is slowed down but not blocked. Additional treatments that target dysregulated signaling pathways are needed to improve patient outcomes [427]. Inhibitors of mTORC1 include rapamycin and its analogues (rapalogs) [428], and metformin (an activator of AMP-activated protein kinase (AMPK) that inhibits 4E-BP and S6K phosphorylation) [429]. Both inhibitors have been suggested as potential therapies for PKD. In addition to suppressing mTORC1 signaling, metformin may reduce fluid secretion in cysts by inhibiting CFTR, and have additional beneficial metabolic effects [430,431]. Moreover, rapamycin reduced the cystic volume in a mouse model [432] but its analogues failed in clinical trials in ADPKD patients [433,434].

The present data indicate an essential contribution of TMEM16A in the development of polycystic kidney disease. The treatment with TMEM16A inhibitor niclosamide resulted in inhibition of development of renal cysts in $PKD1^{-/-}$ animals (Chapter 6). Cyst development was also strongly attenuated in benzbromarone-treated mice when compared to sham-treated animals (Chapter 6). Furthermore, proliferative activity was analyzed again by staining the proliferation marker Ki-67. The largely enhanced proliferation was almost completely eliminated by treatment with benzbromarone (Chapter 6) [435]. Our data suggest TMEM16A as a novel and very potent pharmacological target to inhibit cyst growth in ADPKD. In addition, inhibition of TMEM16A is clearly anti-inflammatory, which would also be beneficial to patients with PKD as they present pro-inflammatory cytokines in the cyst fluid and chemoattractants in the urine [436,437].

CONCLUSIONS AND FURTHER PERSPECTIVES

This work presents strong evidence that TMEM16A is of fundamental importance for intracellular calcium signaling, cell proliferation and fluid secretion in renal cystic epithelium. We present data indicating the beneficial effects of two FDA-approved drugs, niclosamide and benzbromarone, which both demonstrate to be most potent in suppressing polycystic kidney disease and probably inflammatory airway disease.

However, a larger number of studies demonstrate CFTR as the crucial Cl^- channel in ADPKD [216,218,219,238-243,258]. To rule out the true contribution of CFTR in ADPKD, generation of an additional animal model with double knockout for both *Pkd1* and *Cftr* would be determinant.

Another interesting aspect is the observation that males exhibit a more severe phenotype in ADPKD. In the kidney, evidence exists for sex differences in water transport [438], organic anion handling [439], transporters [440] and gene expression patterns [441]. These differences may have important functional consequences. For example, in ischemia-reperfusion experiments in rodent models of kidney injury, males demonstrate significantly worse outcomes than females. This is often attributed to hormonal differences [442-444]. Disease progression in patients with chronic kidney disease is also thought to be affected by sex, with an increased prevalence of end-stage renal disease (ESRD) being present in males [445,446]. Sex was evaluated as a biological variable in human PKD. It was shown that males indeed presented a more severe kidney disease than females [445]. Males also showed an earlier onset of ESRD in human ADPKD [447,448]. We also observed in our mouse model a more pronounced ADPKD in male Pkd1-/- mice. We speculate that androgen receptors play a key role in developing ADPKD. Further analysis of the effects of testosterone on expression and function of TMEM16A therefore will be very interesting. These experiments appear particularly promising as these androgens have been shown to upregulate expression of TMEM16A and to induce TMEM16A-dependent Ca^{2+}-activated Cl^- currents as well as proliferation in prostate epithelial cells [449].

ACKNOWLEDGEMENTS

For the success of my work presented in this thesis, I would like to thank all the people that in one or the other way contributed to the work presented here. I would like to show my sincere gratitude to my supervisor, Prof. Karl Kunzelmann, for the unique opportunity to work in his lab. His immense knowledge and ability to see a silver lining in every set of data kept me motivated for more than 4 years and made me always strive for my best capacities. I want to express my huge gratitude to Prof. Rainer Schreiber for all the support, orientation, motivation, patience and for sharing his insightful ideas always with a contagious positive attitude. Many thanks to Jiraporn Ousingsawat, for all her suggestions, advice and concerns, not only on the scientific but also on the personal side. I thank my mentors, Prof. Wolf Hayo Castrop and Prof. Jens Georg Leipziger for their input during my yearly reports. A special thanks also goes to the great support of Patricia, Brigitte, Ernestine and Silvia. Their help and continuous support transformed our laboratory life into a much easier and cheerful one. I would like to extend my gratitude to all the grants that supported my thesis work: Deutsche Forschungsgemeinschaft (DFG) SFB699-A7, DFG SFB699-A12, DFG SFB1350-A3, DFG KU756/12-1, DFG KU756/14-1, Cystic Fibrosis Trust SRC003, Cystic Fibrosis Trust SRC013, and Gilead Stiftung.

To Podchanart Wanitchakool (aka Kip) and Lalida Sirianant (“Gam”), whom I deadly miss, a warm thank you for your great PhD examples and work-wise best friendships! To the younger pals that I had the pleasure to meet and work with side-by-side, I leave here my heartfelt thank you to all: Filipa Simões, Ana Fonseca, Filipe Saúde and Raquel Centeio. Thank you, for your eagerness to learn the ways of science, for your questions and for your teachings. Thank you all for your great friendships. You can always count on me in the future. Raquel Centeio, I leave to you my Nature paper! My deepest gratitude goes to Roberta for her brightness and lovely friendship, which accompanied me through all these years. For all the good laughs and memorable stories. I also thank all the groups in the Vorklinikum and in Anatomie that were always helpful. Bunino, I thank you for sharing in this adventure, for your prompt availability to help me with my brain tornados and for your music that served as motivation to carry on. It will always be a source of inspiration throughout my life.

Aos meus amigos e à minha querida família (que neste último ano duplicou), obrigada por me apoiarem, por estarem lá para mim quando preciso de desabafar. É sempre bom reencontrar-vos quando vou a Portugal e, apesar da distância, obrigada por continuarem por perto. Obrigada ao meu primo Miguel e família por continuarem a incentivar-me neste mundo científico. Ao Nuno, aos meus pais e irmão que eu tanto amo, dedico este trabalho! Obrigada por toda a força que me transmitem, por todo o vosso incansável apoio, dedicação e confiança!

ERKLÄRUNGEN

Hiermit erkläre ich, gem. § 6 Abs. 2, Nr. 6 der Promotionsordnung der Math.-Nat.-Fachbereiche zur Erlangung des Dr. rer. nat., dass ich die vorliegende Dissertation selbständig verfasst und mich keiner anderen als der angegebenen Hilfsmittel bedient habe.

Regensburg, den

CURRICULUM VITAE

INÊS MARIA SANTOS CABRITA BUSTORFF SILVA

October 13th, 1992
Hochweg 56A, 93049 Regensburg, Germany
+49 (0)176 4349 6951
inesmscabrita @gmail.com

Academic Background	2016–2020	**PhD in Biomedicine** Faculty of Biology and Pre-clinical Medicine of University of Regensburg, Regensburg, Germany
	2013–2014	**ERASMUS Program: MSc in Biochemistry (6 months)** Faculty of Chemical Sciences of Complutense University of Madrid Madrid, Spain
	2013–2015	**MSc in Biochemistry** Faculty of Sciences of Lisbon University, Lisbon, Portugal
	2010–2013	**BSc in Biochemistry** Faculty of Sciences of Lisbon University, Lisbon, Portugal
Research Experience and Training	2016	**FELASA B course** University of Regensburg, Regensburg, Germany
	2014–2015	**Master thesis** "Anoctamins, a novel family of ion channels and their role in intracellular calcium signaling" University of Regensburg, Regensburg, Germany
Awards	2019	**98th Meeting of the German Physiological Society** Ulm, Germany – Best poster presentation
	2015	**12th ECFS Basic Science Conference** Albufeira, Portugal – Travel grant from Mukoviszidose e.V.; Travel grant from European Cystic Fibrosis Society
Conferences and Meetings	2019	**SFB 1350 Retreat 2019 (Oral presentation)** Beilngries, Germany
	2019	**98th Annual Meeting of the German Physiological Society (Symposium and poster)** Ulm, Germany
	2018	**Europhysiology (Poster)** London, England
	2018	**12th European CF Young Investigators' Meeting (Oral presentation and Poster)** Paris, France
	2017	**96th Annual Meeting of the German Physiological Society (Oral presentation)** Greifswald, Germany
	2016	**95th Annual Meeting of the German Physiological Society (Oral presentation)** Lübeck, Germany

	2015	**12th ECFS Basic Science Conference (Oral presentation)** Albufeira, Portugal

Publications

1. Centeio R., **Cabrita I.,** Benedetto R., Talbi K., Ousingsawat J., Schreiber R., Sullivan JK., Kunzelmann K. Pharmacological Inhibition and Activation of the Ca^{2+} Activated Cl^- Channel TMEM16A. *Int J Mol Sci.* 2020 Apr 7;21(7). pii: E2557.

2. Cabrita I., Buchholz B., Schreiber R., Kunzelmann K. TMEM16A drives renal cyst growth by augmenting Ca^{2+} signaling in M1 cells. *J Mol Med (Berl)*. 2020 Mar 18; 98, 659–671.

3. Kunzelmann K., Centeio R., Wanitchakool P., **Cabrita I**., Benedetto R., Saha T., Hoque KM., Schreiber R. Control of Ion Transport by Tmem16a Expressed in Murine Intestine. *Front Physiol.* 2019 Oct 4;10:1262.

4**. Cabrita I.**, Benedetto R., Schreiber R., Kunzelmann K. Niclosamide repurposed for the treatment of inflammatory airway disease. *JCI Insight*. 2019 Aug 8;4(15).

5. Benedetto R., Ousingsawat J., **Cabrita I.**, Pinto M., Lérias J.R., Wanitchakool P., Schreiber R., Kunzelmann K. Plasma membrane-localized TMEM16 proteins are indispensable for expression of CFTR. J *Mol Med (Berl).* 2019 May; 97(5):711-722.

6. Kunzelmann K., Ousingsawat J., Benedetto R., **Cabrita I.**, Schreiber R. Contribution of Anoctamins to Cell Survival and Cell Death. *Cancers (Basel).* 2019 Mar; 19;11(3). pii: E382.

7. Kunzelmann K., Ousingsawat J., **Cabrita I.**, Doušová T., Bähr A., Janda M., Schreiber R., Benedetto R. TMEM16A in Cystic Fibrosis: Activating or Inhibiting? *Front Pharmacol.* 2019 Jan; 29;10:3.

8. Benedetto R., **Cabrita I.**, Schreiber R., Kunzelmann K. TMEM16A is indispensable for basal ATP-induced mucus secretion in airways and intestine. *FASEB J.* 2018 Dec:fj201801333RRR.

9. Simões F., Ousingsawat J., Wanitchakool P., Fonseca A., **Cabrita I.**, Benedetto R., Schreiber R., Kunzelmann K. CFTR supports cell death through ROS-dependent activation of TMEM16F (anoctamin 6). *Pflugers Arch.* 2018 Feb; 470(2):305-314.

10. Cabrita I., Benedetto R., Fonseca A., Wanitchakool P., Sirianant L., Skryabin B.V., Schenk L.K., Pavenstadt H., Schreiber R., Kunzelmann K. Differential effects of anoctamins on intracellular calcium signals*. FASEB J.* 2017 May; 31(5): 2123-2134.

11. Wanitchakool P., Ousingsawat J., Sirianant L., **Cabrita I.**, Faria D., Schreiber R., Kunzelmann K. Cellular Defects by Deletion of ANO10 are due deregulated local Calcium Signaling. *Cell Signal*. 2017 Jan; 30:41-49.

12. Ousingsawat J., **Cabrita I.**, Wanitchakool P., Sirianant L., Krautwald S., Linkermann A., Schreiber R., Kunzelmann K. Ca^{2+} signals, cell membrane disintegration, and activation of TMEM16F during necroptosis. *Cell Mol Life Sci.* 2017 Jan; 74(1):173-181.

13. Benedetto R., Sirianant L., Pankonien I., Wanitchakool P., Ousingsawat J., **Cabrita I.,** Schreiber R., Amaral M., Kunzelmann K. Relationship between TMEM16A/anoctamin 1 and LRRC8A. *Pflugers Arch.* 2016 Oct; 468(10):1751-63.

14. Sirianant L., Wanitchakool P., Ousingsawat J., Benedetto R., Zormpa A., **Cabrita I.,** Schreiber R., Kunzelmann K. Non-essential contribution of LRRC8A to volume regulation. *Pflugers Arch.* 2016 May; 468(5):805-16.

15. Kunzelmann K., **Cabrita I.**, Wanitchakool P., Ousingsawat J., Sirianant L., Benedetto R., Schreiber R. Modulating Ca^{2+} signals: a common theme for TMEM16, Ist2, and TMC. *Pflugers Arch* 2016 Mar; 468(3):475-90.

Language	Portuguese — native	English — fluent	Spanish — fluent

REFERENCE LIST

1. Pedemonte, N. & Galietta, L.J. Structure and Function of TMEM16 Proteins (Anoctamins). *Physiol Rev* **94**, 419-459 (2014).
2. Kunzelmann, K. & Schreiber, R. Chloride secretion, anoctamin 1 and Ca2+ signaling. *Channels (Austin)* **8**, 387-388 (2014).
3. Schreiber, R.*, et al.* Expression and Function of Epithelial Anoctamins. *J. Biol. Chem* **285**, 7838-7845 (2010).
4. Caputo, A.*, et al.* TMEM16A, A Membrane Protein Associated With Calcium-Dependent Chloride Channel Activity. *Science* **322**, 590-594 (2008).
5. Brunner, J.D., Schenck, S. & Dutzler, R. Structural basis for phospholipid scrambling in the TMEM16 family. *Current opinion in structural biology* **39**, 61-70 (2016).
6. Paulino, C., Kalienkova, V., Lam, A.K.M., Neldner, Y. & Dutzler, R. Activation mechanism of the calcium-activated chloride channel TMEM16A revealed by cryo-EM. *Nature* (2017).
7. Falzone, M.E., Malvezzi, M., Lee, B.-C. & Accardi, A. Known structures and unknown mechanisms of TMEM16 scramblases and channels. *The Journal of general physiology* **150**, 933-947 (2018).
8. Yang, Y.D.*, et al.* TMEM16A confers receptor-activated calcium-dependent chloride conductance. *Nature* **455**, 1210-1215 (2008).
9. Ousingsawat, J.*, et al.* Loss of TMEM16A causes a defect in epithelial Ca2+ dependent chloride transport. *J Biol Chem* **284**, 28698-28703 (2009).
10. Romanenko, V.G.*, et al.* Tmem16A encodes the Ca2+-activated Cl- channel in mouse submandibular salivary gland acinar cells. *J Biol. Chem* **285**, 12990-13001 (2010).
11. Tian, Y., Schreiber, R. & Kunzelmann, K. Anoctamins are a family of Ca2+ activated Cl- channels. *J Cell Sci* **125**, 4991-4998 (2012).
12. Suzuki, J., Umeda, M., Sims, P.J. & Nagata, S. Calcium-dependent phospholipid scrambling by TMEM16F. *Nature* **468**, 834-838 (2010).
13. Martins, J.R.*, et al.* Anoctamin 6 is an essential component of the outwardly rectifying chloride channel. *Proc. Natl. Acad. Sci. U. S. A* **108**, 18168-18172 (2011).
14. Yang, H.*, et al.* TMEM16F Forms a Ca(2+)-Activated Cation Channel Required for Lipid Scrambling in Platelets during Blood Coagulation. *Cell* **151**, 111-122 (2012).
15. Kmit, A.*, et al.* Calcium-activated and apoptotic phospholipid scrambling induced by Ano6 can occur independently of Ano6 ion currents. *Cell death and disease* **25**, 4:e611 (2013).
16. Ousingsawat, J.*, et al.* Anoctamin 6 mediates effects essential for innate immunity downstream of P2X7-receptors in macrophages. *Nat. Commun* **6**, 6245- (2015).
17. Bevers, E.M. & Williamson, P.L. Phospholipid scramblase: an update. *FEBS Lett* **584**, 2724-2730 (2010).
18. Yu, K.*, et al.* Identification of a lipid scrambling domain in ANO6/TMEM16F. *Elife* **4. doi**, 10 (2015).
19. Brunner, J.D., Lim, N.K., Schenck, S., Duerst, A. & Dutzler, R. X-ray structure of a calcium-activated TMEM16 lipid scramblase. *Nature* **516**, 207-212 (2014).
20. Lee, B.C.*, et al.* Gating mechanism of the extracellular entry to the lipid pathway in a TMEM16 scramblase. *Nature communications* **9**, 3251 (2018).
21. Alvadia, C.*, et al.* Cryo-EM structures and functional characterization of the murine lipid scramblase TMEM16F. *Elife* **8**(2019).
22. Schreiber, R.*, et al.* Regulation of TMEM16A/ANO1 and TMEM16F/ANO6 ion currents and phospholipid scrambling by Ca2+ and plasma membrane lipid. *J Physiology (London)* **596**, 217-229 (2018).
23. Vermeer, S.*, et al.* Targeted next-generation sequencing of a 12.5 Mb homozygous region reveals ANO10 mutations in patients with autosomal-recessive cerebellar ataxia. *Am J Hum. Genet* **87**, 813-819 (2010).
24. Kunzelmann, K.*, et al.* Anoctamins. *Pflugers Arch* **462**, 195-208 (2011).

25. Chamova, T.*, et al.* ANO10 c.1150_1151del is a founder mutation causing autosomal recessive cerebellar ataxia in Roma/Gypsies. *J Neurol* **259**, 906-911 (2012).
26. Renaud, M.*, et al.* Autosomal recessive cerebellar ataxia type 3 due to ANO10 mutations: delineation and genotype-phenotype correlation study. *JAMA neurology* **71**, 1305-1310 (2014).
27. Hammer, C.*, et al.* A coding variant of ANO10, affecting volume regulation of macrophages, is associated with Borrelia seropositivity. *Mol. Med* **21**, 26-37 (2015).
28. Chamard, L., Sylvestre, G., Koenig, M. & Magnin, E. Executive and Attentional Disorders, Epilepsy and Porencephalic Cyst in Autosomal Recessive Cerebellar Ataxia Type 3 Due to ANO10 Mutation. *European neurology* **75**, 186-190 (2016).
29. Duran, C., Thompson, C.H., Xiao, Q. & Hartzell, H.C. Chloride Channels: Often Enigmatic, Rarely Predictable. *Annu. Rev. Physiol* **17**, 95-121 (2010).
30. Duran, C. & Hartzell, H.C. Physiological roles and diseases of Tmem16/Anoctamin proteins: are they all chloride channels? *Acta Pharmacol. Sin* **32**, 685-692 (2011).
31. Rottgen, T.S., Nickerson, A.J. & Rajendran, V.M. Calcium-Activated Cl(-) Channel: Insights on the Molecular Identity in Epithelial Tissues. *International journal of molecular sciences* **19**(2018).
32. Hartzell, H.C., Putzier, I. & Arreola, J. Calcium-Activated Chloride Channels. *Annu. Rev. Physiol* **67**, 719-758 (2005).
33. Wasserman, S.I.*, et al.* Immune-related intestinal Cl- secretion. I. Effect of histamine on the T84 cell line. *Am J Physiol* **254**, C53-C62 (1988).
34. Dho, S., Stewart, K. & Foskett, J.K. Purinergic receptor activation of Cl- secretion in T84 cells. *Am J Physiol* **262**, C67-74 (1992).
35. Barrett, K.E. & Keely, S.J. Chloride secretion by the intestinal epithelium: molecular basis and regulatory aspects. *Annu. Rev Physiol* **62**, 535-572 (2000).
36. Benedetto, R.*, et al.* Epithelial Chloride Transport by CFTR Requires TMEM16A. *Scientific Reports* **7**, 12397 (2017).
37. Schreiber, R.*, et al.* Anoctamins support calcium-dependent chloride secretion by facilitating calcium signaling in adult mouse intestine. *Pflugers Arch* **467**, 1203-1213 (2015).
38. Faria, D.*, et al.* The calcium activated chloride channel Anoctamin 1 contributes to the regulation of renal function. *Kindey Int* **85**, 1369-1381 (2014).
39. Ruppersburg, C.C. & Hartzell, H.C. The Ca2+-activated Cl- channel ANO1/TMEM16A regulates primary ciliogenesis. *Mol. Biol. Cell* **25**, 1793-1807 (2014).
40. He, M.*, et al.* Cytoplasmic Cl(-) couples membrane remodeling to epithelial morphogenesis. *Proceedings of the National Academy of Sciences of the United States of America* **114**, E11161-e11169 (2017).
41. Schwiebert, E.M.*, et al.* Autocrine extracellular purinergic signaling in epithelial cells derived from polycystic kidneys. *Am. J Physiol Renal Physiol* **282**, F763-F775 (2002).
42. Hovater, M.B., Olteanu, D., Welty, E.A. & Schwiebert, E.M. Purinergic signaling in the lumen of a normal nephron and in remodeled PKD encapsulated cysts. *Purinergic. Signal* **4**, 109-124 (2008).
43. Liu, Y.*, et al.* Prostaglandin E2 mediates proliferation and chloride secretion in ADPKD cystic renal epithelia. *Am. J Physiol Renal Physiol* **303**, F1425-F1434 (2012).
44. Buchholz, B.*, et al.* Anoctamin 1 induces calcium-activated chloride secretion and tissue proliferation in polycystic kidney disease. *Kidney Int* **85**, 1058-1067 (2014).
45. Tanaka, T. & Nangaku, M. ANO1: an additional key player in cyst growth. *Kidney Int* **85**, 1007-1009 (2014).
46. Schenk, L.K.*, et al.* Nephron-specific knockout of TMEM16A leads to reduced number of glomeruli and albuminuria. *Am J Physiol Renal Physiol* (2018).
47. Juul, C.A.*, et al.* Anoctamin 6 differs from VRAC and VSOAC but is involved in apoptosis and supports volume regulation in the presence of Ca. *Pflugers Arch* **466**, 1899-1910 (2014).
48. Simoes, F.*, et al.* CFTR supports cell death through ROS-dependent activation of TMEM16F (anoctamin 6). *Pflugers Arch* **470**, 305-314 (2018).

49. Fujii, T., Sakata, A., Nishimura, S., Eto, K. & Nagata, S. TMEM16F is required for phosphatidylserine exposure and microparticle release in activated mouse platelets. *Proc. Natl. Acad. Sci U. S A*, 201516594 (2015).
50. Cheng, S.H.*, et al.* Phosphorylation of the R domain by cAMP-dependent protein kinase regulates the CFTR chloride channel. *Cell* **66**, 1027-1036 (1991).
51. Kunzelmann, K., Kathöfer, S. & Greger, R. Na+ and Cl- conductances in airway epithelial cells: Increased Na+ conductance in cystic fibrosis. *Pflügers Arch* **431**, 1-9 (1995).
52. Shei, R.J., Peabody, J.E., Kaza, N. & Rowe, S.M. The epithelial sodium channel (ENaC) as a therapeutic target for cystic fibrosis. *Current opinion in pharmacology* **43**, 152-165 (2018).
53. Schwiebert, E.M.*, et al.* CFTR regulates outwardly rectifying chloride channels through an autocrine mechanism involving ATP. *Cell* **81**, 1063-1073 (1995).
54. Kunzelmann, K. & Schreiber, R. CFTR, a regulator of channels. *J. Membr. Biol* **168**, 1-8 (1999).
55. Cutting, G.R. Cystic fibrosis genetics: from molecular understanding to clinical application. *Nature reviews. Genetics* **16**, 45-56 (2015).
56. Collins, F.S. Cystic fibrosis: molecular biology and therapeutic implications. *Science* **256**, 774-778 (1992).
57. Liu, F., Zhang, Z., Csanady, L., Gadsby, D.C. & Chen, J. Molecular Structure of the Human CFTR Ion Channel. *Cell* **169**, 85-95 (2017).
58. Billet, A. & Hanrahan, J.W. The secret life of CFTR as a calcium-activated chloride channel. *The Journal of physiology* **591**, 5273-5278 (2013).
59. Lerias, J.*, et al.* Compartmentalized crosstalk of CFTR and TMEM16A (ANO1) through EPAC1 and ADCY1. *Cellular signalling* **44**, 10-19 (2018).
60. Faria, D., Schreiber, R. & Kunzelmann, K. CFTR is activated through stimulation of purinergic P2Y2 receptors. *Pflügers Arch* **457**, 1373-1380 (2009).
61. Namkung, W., Finkbeiner, W.E. & Verkman, A.S. CFTR-Adenylyl Cyclase I Association Is Responsible for UTP Activation of CFTR in Well-Differentiated Primary Human Bronchial Cell Cultures. *Mol. Biol. Cell* **21**, 2639-2648 (2010).
62. Kunzelmann, K. & Mehta, A. CFTR: a hub for kinases and cross-talk of cAMP and Ca. *FEBS J* **280**, 4417-4429 (2013).
63. Jia, Y., Mathews, C.J. & Hanrahan, J.W. Phosphorylation by protein kinase C is required for acute activation of cystic fibrosis transmembrane conductance regulator by protein kinase A. *J. Biol. Chem* **272**, 4978-4984 (1997).
64. Ousingsawat, J., Kongsuphol, P., Schreiber, R. & Kunzelmann, K. CFTR and TMEM16A are Separate but Functionally Related Cl Channels. *Cell Physiol Biochem* **28**, 715-724 (2011).
65. Berridge, M.J., Lipp, P. & Bootman, M.D. The versatility and universality of calcium signalling. *Nature reviews. Molecular cell biology* **1**, 11-21 (2000).
66. Schreiber, R. Ca2+ signaling, intracellular pH and cell volume in cell proliferation. *J Membr. Biol* **205**, 129-137 (2005).
67. Caulfield, M.P. Muscarinic receptors--characterization, coupling and function. *Pharmacol. Ther* **58**, 319-379 (1993).
68. Mikoshiba, K. IP3 receptor/Ca2+ channel: from discovery to new signaling concepts. *J Neurochem* **102**, 1426-1446 (2007).
69. Wang, Y., Deng, X., Hewavitharana, T., Soboloff, J. & Gill, D.L. Stim, ORAI and TRPC channels in the control of calcium entry signals in smooth muscle. *Clin Exp Pharmacol Physiol* **35**, 1127-1133 (2008).
70. Pozzan, T., Rizzuto, R., Volpe, P. & Meldolesi, J. Molecular and cellular physiology of intracellular calcium stores. *Physiol Rev* **74**, 595-636 (1994).
71. Blaustein, M.P. & Lederer, W.J. Sodium/calcium exchange: its physiological implications. *Physiol Rev* **79**, 763-854 (1999).
72. Kunzelmann, K.*, et al.* Modulating Ca2+signals: a common theme for TMEM16, Ist2, and TMC. *Pflügers Arch* **468**, 475-490 (2016).
73. Wise, D. & Wolniak, S.M. A calcium-rich intraspindle membrane system in

spermatocytes of wolf spiders. *Chromosoma* **90**, 156-161 (1984).
74. Kramer, J. & Hawley, R.S. The spindle-associated transmembrane protein Axs identifies a membranous structure ensheathing the meiotic spindle. *Nature cell biology* **5**, 261-263 (2003).
75. Kasumu, A. & Bezprozvanny, I. Deranged calcium signaling in Purkinje cells and pathogenesis in spinocerebellar ataxia 2 (SCA2) and other ataxias. *Cerebellum (London, England)* **11**, 630-639 (2012).
76. Wolf, W.*, et al.* Yeast Ist2 recruits the endoplasmic reticulum to the plasma membrane and creates a ribosome-free membrane microcompartment. *PLoS. ONE* **7**, e39703 (2012).
77. Stefan, C.J., Manford, A.G. & Emr, S.D. ER-PM connections: sites of information transfer and inter-organelle communication. *Curr. Opin. Cell Biol* **25**, 434-442 (2013).
78. Jin, X.*, et al.* Activation of the Cl- Channel ANO1 by Localized Calcium Signals in Nociceptive Sensory Neurons Requires Coupling with the IP3 Receptor. *Sci. Signal* **6**, ra73 (2013).
79. Jin, X., Shah, S., Du, X., Zhang, H. & Gamper, N. Activation of Ca2+-activated Cl- channel ANO1 by localized Ca2+ signals. *The Journal of physiology* **594**, 19-30 (2016).
80. Perez-Cornejo, P.*, et al.* Anoctamin 1 (Tmem16A) Ca2+-activated chloride channel stoichiometrically interacts with an ezrin-radixin-moesin network. *Proc. Natl. Acad. Sci. U. S. A* **109**, 10376-10381 (2012).
81. Sudhof, T.C. The synaptic vesicle cycle. *Annu Rev Neurosci* **27**, 509-547 (2004).
82. Kasai, H., Takahashi, N. & Tokumaru, H. Distinct initial SNARE configurations underlying the diversity of exocytosis. *Physiol Rev* **92**, 1915-1964 (2012).
83. Rorsman, P. & Braun, M. Regulation of insulin secretion in human pancreatic islets. *Annu Rev Physiol* **75**, 155-179 (2013).
84. Alabi, A.A. & Tsien, R.W. Perspectives on kiss-and-run: role in exocytosis, endocytosis, and neurotransmission. *Annu Rev Physiol* **75**, 393-422 (2013).
85. Wu, L.G., Hamid, E., Shin, W. & Chiang, H.C. Exocytosis and endocytosis: modes, functions, and coupling mechanisms. *Annu Rev Physiol* **76**, 301-331 (2014).
86. Leikin, S.L., Kozlov, M.M., Chernomordik, L.V., Markin, V.S. & Chizmadzhev, Y.A. Membrane fusion: overcoming of the hydration barrier and local restructuring. *J Theor Biol* **129**, 411-425 (1987).
87. Headland, S.E.*, et al.* Neutrophil-derived microvesicles enter cartilage and protect the joint in inflammatory arthritis. *Sci. Transl. Med* **7**, 315ra190 (2015).
88. Zwaal, R.F., Comfurius, P. & Bevers, E.M. Scott syndrome, a bleeding disorder caused by defective scrambling of membrane phospholipids. *Biochim Biophys Acta* **1636**, 119-128 (2004).
89. Sims, P.J., Wiedmer, T., Esmon, C.T., Weiss, H.J. & Shattil, S.J. Assembly of the platelet prothrombinase complex is linked to vesiculation of the platelet plasma membrane. Studies in Scott syndrome: an isolated defect in platelet procoagulant activity. *J Biol Chem* **264**, 17049-17057 (1989).
90. Ehlen, H.W.*, et al.* Inactivation of anoctamin-6/Tmem16f, a regulator of phosphatidylserine scrambling in osteoblasts, leads to decreased mineral deposition in skeletal tissues. *Journal of bone and mineral research : the official journal of the American Society for Bone and Mineral Research* **28**, 246-259 (2013).
91. Gyorgy, B.*, et al.* Membrane vesicles, current state-of-the-art: emerging role of extracellular vesicles. *Cell Mol Life Sci* **68**, 2667-2688 (2011).
92. Raposo, G. & Stoorvogel, W. Extracellular vesicles: exosomes, microvesicles, and friends. *J Cell Biol* **200**, 373-383 (2013).
93. Ousingsawat, J.*, et al.* Anoctamin 6 controls bone mineralization by activating the calcium transporter NCX1. *J Biol Chem* **290**, 6270-6280 (2015).
94. Anderson, H.C. Matrix vesicles and calcification. *Curr Rheumatol Rep* **5**, 222-226 (2003).
95. Batti, L.*, et al.* TMEM16F Regulates Spinal Microglial Function in Neuropathic Pain States. *Cell reports* **15**, 2608-2615 (2016).

96. Han, T.W.*, et al.* Chemically induced vesiculation as a platform for studying TMEM16F activity. *Proceedings of the National Academy of Sciences of the United States of America* **116**, 1309-1318 (2019).
97. Bricogne, C.*, et al.* TMEM16F activation by Ca(2+) triggers plasma membrane expansion and directs PD-1 trafficking. *Sci Rep* **9**, 619 (2019).
98. Bevers, E.M.*, et al.* Defective Ca(2+)-induced microvesiculation and deficient expression of procoagulant activity in erythrocytes from a patient with a bleeding disorder: a study of the red blood cells of Scott syndrome. *Blood* **79**, 380-388 (1992).
99. Cooper, S.T. & McNeil, P.L. Membrane Repair: Mechanisms and Pathophysiology. *Physiol Rev* **95**, 1205-1240 (2015).
100. Griffin, D.A.*, et al.* Defective membrane fusion and repair in Anoctamin5 -deficient muscular dystrophy. *Hum. Mol. Genet*, ddw063 (2016).
101. Sellers, L.A., Allen, A., Morris, E.R. & Ross-Murphy, S.B. Mucus glycoprotein gels. Role of glycoprotein polymeric structure and carbohydrate side-chains in gel-formation. *Carbohydr Res* **178**, 93-110 (1988).
102. Johansson, M.E., Larsson, J.M. & Hansson, G.C. The two mucus layers of colon are organized by the MUC2 mucin, whereas the outer layer is a legislator of host-microbial interactions. *Proceedings of the National Academy of Sciences of the United States of America* **108 Suppl 1**, 4659-4665 (2011).
103. Rose, M.C. & Voynow, J.A. Respiratory tract mucin genes and mucin glycoproteins in health and disease. *Physiol Rev* **86**, 245-278 (2006).
104. Kreda, S.M., Davis, C.W. & Rose, M.C. CFTR, mucins, and mucus obstruction in cystic fibrosis. *Cold Spring Harbor perspectives in medicine* **1**, 9 (2012).
105. Rodriguez-Pineiro, A.M.*, et al.* Studies of mucus in mouse stomach, small intestine, and colon. II. Gastrointestinal mucus proteome reveals Muc2 and Muc5ac accompanied by a set of core proteins. *American journal of physiology. Gastrointestinal and liver physiology* **305**, G348-356 (2013).
106. Thornton, D.J., Rousseau, K. & McGuckin, M.A. Structure and function of the polymeric mucins in airways mucus. *Annu Rev Physiol* **70**, 459-486 (2008).
107. Quinton, P.M. Role of epithelial HCO3(-) transport in mucin secretion: lessons from cystic fibrosis. *Am J Physiol Cell Physiol* **299**, C1222-C1233 (2010).
108. Gustafsson, J.K.*, et al.* Bicarbonate and functional CFTR channel are required for proper mucin secretion and link cystic fibrosis with its mucus phenotype. *J Exp Med* **209**, 1263-1272 (2012).
109. Ridley, C.*, et al.* Assembly of the respiratory mucin MUC5B: a new model for a gel-forming mucin. *J Biol Chem* **289**, 16409-16420 (2014).
110. Fukuda, M. & Kuroda, T.S. Slac2-c (synaptotagmin-like protein homologue lacking C2 domains-c), a novel linker protein that interacts with Rab27, myosin Va/VIIa, and actin. *J Biol Chem* **277**, 43096-43103 (2002).
111. Rudolf, M.T., Dinkel, C., Traynor-Kaplan, A.E. & Schultz, C. Antagonists of myo-inositol 3,4,5,6-tetrakisphosphate allow repeated epithelial chloride secretion. *Bioorg. Med. Chem* **11**, 3315-3329 (2003).
112. Barral, D.C. & Seabra, M.C. The melanosome as a model to study organelle motility in mammals. *Pigment Cell Res* **17**, 111-118 (2004).
113. Li, Y., Martin, L.D., Spizz, G. & Adler, K.B. MARCKS protein is a key molecule regulating mucin secretion by human airway epithelial cells in vitro. *J Biol Chem* **276**, 40982-40990 (2001).
114. Singer, M.*, et al.* A MARCKS-related peptide blocks mucus hypersecretion in a mouse model of asthma. *Nature medicine* **10**, 193-196 (2004).
115. Hammer, J.A., 3rd & Wu, X.S. Rabs grab motors: defining the connections between Rab GTPases and motor proteins. *Current opinion in cell biology* **14**, 69-75 (2002).
116. Oliver, M.G. & Specian, R.D. Cytoskeleton of intestinal goblet cells: role of actin filaments in baseline secretion. *Am J Physiol* **259**, 991-997 (1990).
117. Hong, W. SNAREs and traffic. *Biochim Biophys Acta* **1744**, 120-144 (2005).
118. Okada, S.F.*, et al.* Coupled nucleotide and mucin hypersecretion from goblet-cell metaplastic human airway epithelium. *American journal of respiratory cell and*

molecular biology **45**, 253-260 (2011).
119. Adler, K.B., Tuvim, M.J. & Dickey, B.F. Regulated mucin secretion from airway epithelial cells. *Front Endocrinol. (Lausanne)* **4**, 129 (2013).
120. Specian, R.D. & Neutra, M.R. Mechanism of rapid mucus secretion in goblet cells stimulated by acetylcholine. *J Cell Biol* **85**, 626-640 (1980).
121. Voets, T.*, et al.* Intracellular calcium dependence of large dense-core vesicle exocytosis in the absence of synaptotagmin I. *Proceedings of the National Academy of Sciences of the United States of America* **98**, 11680-11685 (2001).
122. Demetrios Papahadjopoulos, S.N.D. Molecular mechanisms of calcium-induced membrane fusion. *Journal of Bioenergetics and Biomembranes* **22**, 157-179 (1990).
123. Schutte, A.*, et al.* Microbial-induced meprin beta cleavage in MUC2 mucin and a functional CFTR channel are required to release anchored small intestinal mucus. *Proceedings of the National Academy of Sciences of the United States of America* **111**, 12396-12401 (2014).
124. Halm, D.R. & Halm, S.T. Secretagogue response of goblet cells and columnar cells in human colonic crypts(1). *Am J Physiol Cell Physiol* **278**, C212-C233 (2000).
125. Benedetto, R., Cabrita, I., Schreiber, R. & Kunzelmann, K. TMEM16A is indispensable for basal mucus secretion in airways and intestine. *Faseb j* **33**, 4502-4512 (2019).
126. Huang, F.*, et al.* Studies on expression and function of the TMEM16A calcium-activated chloride channel. *Proc. Natl. Acad. Sci. U. S. A* **106**, 21413-21418 (2009).
127. Huang, F.*, et al.* Calcium-activated chloride channel TMEM16A modulates mucin secretion and airway smooth muscle contraction. *Proc. Natl. Acad. Sci U. S. A* **109**, 16354-16359 (2012).
128. Gallos, G.*, et al.* Functional Expression of the TMEM16 Family of Calcium Activated Chloride Channels in Airway Smooth Muscle. *Am J Physiol Lung Cell Mol. Physiol* **305**, L625-L634 (2013).
129. Danielsson, J., Goldklang, M.P., Xu, D., Armiento, M.D. & Emala, C.W. Antagonists Of The Tmeml6a Calcium-Activated Chloride Channel Attenuate Mucus Production induced By Cigarette Smoke Extract. *American journal of respiratory and critical care medicine* **191**, A3872 (2015).
130. Kondo, M.*, et al.* Chloride ion transport and overexpression of TMEM16A in a guinea pig asthma model. *Clin Exp Allergy* (2017).
131. Boynton, A.L. Calcium and epithelial cell proliferation. *Miner Electrolyte Metab* **14**, 86-94 (1988).
132. Whitfield, J.F. Calcium signals and cancer. *Crit Rev Oncog* **3**, 55-90 (1992).
133. Short, A.D.*, et al.* Intracellular Ca2+ pool content is linked to control of cell growth. *Proceedings of the National Academy of Sciences of the United States of America* **90**, 4986-4990 (1993).
134. Santella, L. The role of calcium in the cell cycle: facts and hypotheses. *Biochem Biophys Res Commun* **244**, 317-324 (1998).
135. Kahl, C.R. & Means, A.R. Regulation of cell cycle progression by calcium/calmodulin-dependent pathways. *Endocr. Rev* **24**, 719-736 (2003).
136. Lipskaia, L. & Lompre, A.M. Alteration in temporal kinetics of Ca2+ signaling and control of growth and proliferation. *Biol Cell* **96**, 55-68 (2004).
137. Britschgi, A.*, et al.* Calcium-activated chloride channel ANO1 promotes breast cancer progression by activating EGFR and CAMK signaling. *Proc. Natl. Acad. Sci U. S. A* **110**, E1026-E1034 (2013).
138. Deng, L.*, et al.* Knockdown of TMEM16A suppressed MAPK and inhibited cell proliferation and migration in hepatocellular carcinoma. *Onco. Targets. Ther* **9**, 325-333 (2016).
139. Duvvuri, U.*, et al.* TMEM16A, induces MAPK and contributes directly to tumorigenesis and cancer progression. *Cancer Res* **72**, 3270-3281 (2012).
140. Greenwood, I.A., Ledoux, J. & Leblanc, N. Differential regulation of Ca(2+)-activated Cl(-) currents in rabbit arterial and portal vein smooth muscle cells by Ca(2+)-calmodulin-dependent kinase. *The Journal of physiology* **534**, 395-408 (2001).

141. Wang, M.*, et al.* Downregulation of TMEM16A Calcium-Activated Chloride Channel Contributes to Cerebrovascular Remodeling during Hypertension through Promoting Basilar Smooth Muscle Cell Proliferation. *Circulation* **125**, 697-707 (2012).
142. Kunzelmann, K., Ousingsawat, J., Benedetto, R., Cabrita, I. & Schreiber, R. Contribution of Anoctamins to Cell Survival and Cell Death. *Cancers (Basel)* **11**(2019).
143. Chang, Z.*, et al.* Anoctamin5 regulates cell migration and invasion in thyroid cancer. *International journal of oncology* **51**, 1311-1319 (2017).
144. Whitlock, J.M., Yu, K., Cui, Y.Y. & Hartzell, H.C. Anoctamin 5/TMEM16E facilitates muscle precursor cell fusion. *The Journal of general physiology* (2018).
145. Zhao, P.*, et al.* Anoctamin 6 Regulates C2C12 Myoblast Proliferation. *PLoS. ONE* **9**, e92749 (2014).
146. Das, S.*, et al.* NGEP, a prostate-specific plasma membrane protein that promotes the association of LNCaP cells. *Cancer Res* **67**, 1594-1601 (2007).
147. Bera, T.K.*, et al.* NGEP, a gene encoding a membrane protein detected only in prostate cancer and normal prostate. *Proc. Natl. Acad. Sci. U. S. A* **101**, 3059-3064 (2004).
148. Li, C., Cai, S., Wang, X. & Jiang, Z. Identification and characterization of ANO9 in stage II and III colorectal carcinoma. *Oncotarget* **6**, 29324-29334 (2015).
149. Jun, I.*, et al.* ANO9/TMEM16J promotes tumourigenesis via EGFR and is a novel therapeutic target for pancreatic cancer. *British journal of cancer* **117**, 1798-1809 (2017).
150. Torres, V.E., Harris, P.C. & Pirson, Y. Autosomal dominant polycystic kidney disease. *Lancet (London, England)* **369**, 1287-1301 (2007).
151. Ibraghimov-Beskrovnaya, O. & Bukanov, N. Polycystic kidney diseases: from molecular discoveries to targeted therapeutic strategies. *Cell Mol Life Sci* **65**, 605-619 (2008).
152. Harris, P.C. & Torres, V.E. Polycystic kidney disease. *Annual review of medicine* **60**, 321-337 (2009).
153. Torra, R. Autosomal dominant policystic kidney disease, more than a renal disease. *Minerva Endocrinol* **39**, 79-87 (2014).
154. Hughes, J.*, et al.* The polycystic kidney disease 1 (PKD1) gene encodes a novel protein with multiple cell recognition domains. *Nat Genet* **10**, 151-160 (1995).
155. Mochizuki, T.*, et al.* PKD2, a gene for polycystic kidney disease that encodes an integral membrane protein. *Science* **272**, 1339-1342 (1996).
156. Igarashi, P. & Somlo, S. Genetics and pathogenesis of polycystic kidney disease. *J Am Soc Nephrol* **13**, 2384-2398 (2002).
157. Cornec-Le Gall, E.*, et al.* PKD2-Related Autosomal Dominant Polycystic Kidney Disease: Prevalence, Clinical Presentation, Mutation Spectrum, and Prognosis. *Am J Kidney Dis* **70**, 476-485 (2017).
158. Qian, F., Watnick, T.J., Onuchic, L.F. & Germino, G.G. The molecular basis of focal cyst formation in human autosomal dominant polycystic kidney disease type I. *Cell* **87**, 979-987 (1996).
159. Piontek, K., Menezes, L.F., Garcia-Gonzalez, M.A., Huso, D.L. & Germino, G.G. A critical developmental switch defines the kinetics of kidney cyst formation after loss of Pkd1. *Nature medicine* **13**, 1490-1495 (2007).
160. Tan, A.Y.*, et al.* Somatic Mutations in Renal Cyst Epithelium in Autosomal Dominant Polycystic Kidney Disease. *J Am Soc Nephrol* **29**, 2139-2156 (2018).
161. Lantinga-van Leeuwen, I.S.*, et al.* Kidney-specific inactivation of the Pkd1 gene induces rapid cyst formation in developing kidneys and a slow onset of disease in adult mice. *Hum Mol Genet* **16**, 3188-3196 (2007).
162. Takakura, A., Contrino, L., Beck, A.W. & Zhou, J. Pkd1 inactivation induced in adulthood produces focal cystic disease. *J Am Soc Nephrol* **19**, 2351-2363 (2008).
163. Weimbs, T. Polycystic kidney disease and renal injury repair: common pathways, fluid flow, and the function of polycystin-1. *Am J Physiol Renal Physiol* **293**, F1423-1432 (2007).

164. Weimbs, T. Third-hit signaling in renal cyst formation. *J Am Soc Nephrol* **22**, 793-795 (2011).
165. Takakura, A.*, et al.* Renal injury is a third hit promoting rapid development of adult polycystic kidney disease. *Hum Mol Genet* **18**, 2523-2531 (2009).
166. Nauli, S.M.*, et al.* Polycystins 1 and 2 mediate mechanosensation in the primary cilium of kidney cells. *Nat Genet* **33**, 129-137 (2003).
167. Duning, K.*, et al.* Polycystin-2 activity is controlled by transcriptional coactivator with PDZ binding motif and pals1-associated tight junction protein. *J Biol. Chem* **285**, 33584-33588 (2010).
168. Delmas, P. Polycystins: from mechanosensation to gene regulation. *Cell* **118**, 145-148 (2004).
169. Wilson, P.D. Polycystic kidney disease. *N Engl J Med* **350**, 151-164 (2004).
170. Delmas, P. Polycystins: polymodal receptor/ion-channel cellular sensors. *Pflugers Arch* **451**, 264-276 (2005).
171. Ong, A.C. & Harris, P.C. Molecular pathogenesis of ADPKD: the polycystin complex gets complex. *Kidney Int* **67**, 1234-1247 (2005).
172. Zhou, J. Polycystins and primary cilia: primers for cell cycle progression. *Annu Rev Physiol* **71**, 83-113 (2009).
173. Chauvet, V.*, et al.* Expression of PKD1 and PKD2 transcripts and proteins in human embryo and during normal kidney development. *Am J Pathol* **160**, 973-983 (2002).
174. Huan, Y. & van Adelsberg, J. Polycystin-1, the PKD1 gene product, is in a complex containing E-cadherin and the catenins. *The Journal of clinical investigation* **104**, 1459-1468 (1999).
175. Dell, K.M. The role of cilia in the pathogenesis of cystic kidney disease. *Curr Opin Pediatr* **27**, 212-218 (2015).
176. Tsiokas, L.*, et al.* Specific association of the gene product of PKD2 with the TRPC1 channel. *Proceedings of the National Academy of Sciences of the United States of America* **96**, 3934-3939 (1999).
177. Gifford, J.L., Walsh, M.P. & Vogel, H.J. Structures and metal-ion-binding properties of the Ca2+-binding helix-loop-helix EF-hand motifs. *Biochem J* **405**, 199-221 (2007).
178. Shen, P.S.*, et al.* The Structure of the Polycystic Kidney Disease Channel PKD2 in Lipid Nanodiscs. *Cell* **167**, 763-773.e711 (2016).
179. Wilkes, M.*, et al.* Molecular insights into lipid-assisted Ca(2+) regulation of the TRP channel Polycystin-2. *Nat Struct Mol Biol* **24**, 123-130 (2017).
180. Grieben, M.*, et al.* Structure of the polycystic kidney disease TRP channel Polycystin-2 (PC2). *Nat Struct Mol Biol* **24**, 114-122 (2017).
181. Gonzalez-Perrett, S.*, et al.* Polycystin-2, the protein mutated in autosomal dominant polycystic kidney disease (ADPKD), is a Ca2+-permeable nonselective cation channel. *Proc. Natl. Acad. Sci. U. S. A* **98**, 1182-1187 (2001).
182. Vassilev, P.M.*, et al.* Polycystin-2 is a novel cation channel implicated in defective intracellular Ca(2+) homeostasis in polycystic kidney disease. *Biochem Biophys Res Commun* **282**, 341-350 (2001).
183. Koulen, P.*, et al.* Polycystin-2 is an intracellular calcium release channel. *Nat. Cell Biol* **4**, 191-197 (2002).
184. Arif Pavel, M.*, et al.* Function and regulation of TRPP2 ion channel revealed by a gain-of-function mutant. *Proceedings of the National Academy of Sciences of the United States of America* **113**, E2363-2372 (2016).
185. Lemos, F.O. & Ehrlich, B.E. Polycystin and calcium signaling in cell death and survival. *Cell Calcium* **69**, 37-45 (2018).
186. Köttgen, M.*, et al.* TRPP2 and TRPV4 form a polymodal sensory channel complex. *J Cell Biol* **182**, 437-447 (2008).
187. Zhang, P.*, et al.* The multimeric structure of polycystin-2 (TRPP2): structural-functional correlates of homo- and hetero-multimers with TRPC1. *Hum Mol Genet* **18**, 1238-1251 (2009).
188. Semmo, M., Kottgen, M. & Hofherr, A. The TRPP subfamily and polycystin-1 proteins. *Handb Exp Pharmacol* **222**, 675-711 (2014).

189. Casuscelli, J.*, et al.* Analysis of the cytoplasmic interaction between polycystin-1 and polycystin-2. *Am J Physiol Renal Physiol* **297**, F1310-1315 (2009).
190. Yu, Y.*, et al.* Structural and molecular basis of the assembly of the TRPP2/PKD1 complex. *Proceedings of the National Academy of Sciences of the United States of America* **106**, 11558-11563 (2009).
191. Zhu, J.*, et al.* Structural model of the TRPP2/PKD1 C-terminal coiled-coil complex produced by a combined computational and experimental approach. *Proceedings of the National Academy of Sciences of the United States of America* **108**, 10133-10138 (2011).
192. Su, Q.*, et al.* Structure of the human PKD1-PKD2 complex. *Science* **361**(2018).
193. Grimm, D.H.*, et al.* Polycystin-1 distribution is modulated by polycystin-2 expression in mammalian cells. *J Biol Chem* **278**, 36786-36793 (2003).
194. Hanaoka, K. & Guggino, W.B. cAMP Regulates Cell Proliferation and Cyst Formation in Autosomal Polycystic Kidney Disease Cells. *J Am Soc. Nephrol* **11**, 1179-1187 (2000).
195. Li, Y.*, et al.* Polycystin-1 interacts with inositol 1,4,5-trisphosphate receptor to modulate intracellular Ca2+ signaling with implications for polycystic kidney disease. *J Biol Chem* **284**, 36431-36441 (2009).
196. Sammels, E.*, et al.* Polycystin-2 activation by inositol 1,4,5-trisphosphate-induced Ca2+ release requires its direct association with the inositol 1,4,5-trisphosphate receptor in a signaling microdomain. *J Biol. Chem* **285**, 18794-18805 (2010).
197. Li, Y., Wright, J.M., Qian, F., Germino, G.G. & Guggino, W.B. Polycystin 2 interacts with type I inositol 1,4,5-trisphosphate receptor to modulate intracellular Ca2+ signaling. *J Biol Chem* **280**, 41298-41306 (2005).
198. Santoso, N.G., Cebotaru, L. & Guggino, W.B. Polycystin-1, 2, and STIM1 interact with IP(3)R to modulate ER Ca release through the PI3K/Akt pathway. *Cell Physiol Biochem* **27**, 715-726 (2011).
199. Anyatonwu, G.I., Estrada, M., Tian, X., Somlo, S. & Ehrlich, B.E. Regulation of ryanodine receptor-dependent calcium signaling by polycystin-2. *Proceedings of the National Academy of Sciences of the United States of America* **104**, 6454-6459 (2007).
200. Kuo, I.Y.*, et al.* Polycystin 2 regulates mitochondrial Ca(2+) signaling, bioenergetics, and dynamics through mitofusin 2. *Sci Signal* **12**(2019).
201. Fliegauf, M., Benzing, T. & Omran, H. When cilia go bad: cilia defects and ciliopathies. *Nat. Rev. Mol. Cell Biol* **8**, 880-893 (2007).
202. Chavez, M.*, et al.* Modulation of Ciliary Phosphoinositide Content Regulates Trafficking and Sonic Hedgehog Signaling Output. *Developmental cell* **34**, 338-350 (2015).
203. Praetorius, H.A. & Leipziger, J. Primary cilium-dependent sensing of urinary flow and paracrine purinergic signaling. *Semin. Cell Dev. Biol* **24**, 3-10 (2013).
204. Delling, M.*, et al.* Primary cilia are not calcium-responsive mechanosensors. *Nature* **531**, 656-660 (2016).
205. Delling, M., DeCaen, P.G., Doerner, J.F., Febvay, S. & Clapham, D.E. Primary cilia are specialized calcium signalling organelles. *Nature* **504**, 311-314 (2013).
206. Praetorius, H.A. & Spring, K.R. A physiological view of the primary cilium. *Annu Rev Physiol* **67**, 515-529 (2005).
207. Pan, J. & Snell, W. The primary cilium: keeper of the key to cell division. *Cell* **129**, 1255-1257 (2007).
208. Wanitchakool, P.*, et al.* Role of Anoctamins in Cancer and Apoptosis. *Philosophical transactions of the Royal Society of London. Series B, Biological sciences* **369**, 20130096 (2014).
209. Forschbach, V.*, et al.* Anoctamin 6 is localized in the primary cilium of renal tubular cells and is involved in apoptosis-dependent cyst lumen formation. *Cell death & disease* **6**, e1899 (2015).
210. Theunissen, J.W. & de Sauvage, F.J. Paracrine Hedgehog signaling in cancer. *Cancer Res* **69**, 6007-6010 (2009).

211. Mochizuki, T., Tsuchiya, K. & Nitta, K. Autosomal dominant polycystic kidney disease: recent advances in pathogenesis and potential therapies. *Clin Exp Nephrol* **17**, 317-326 (2013).
212. Paul, B.M. & Vanden Heuvel, G.B. Kidney: polycystic kidney disease. *Wiley Interdiscip Rev Dev Biol* **3**, 465-487 (2014).
213. Grantham, J.J., Mulamalla, S. & Swenson-Fields, K.I. Why kidneys fail in autosomal dominant polycystic kidney disease. *Nature reviews. Nephrology* **7**, 556-566 (2011).
214. Roos, K.P., Strait, K.A., Raphael, K.L., Blount, M.A. & Kohan, D.E. Collecting duct-specific knockout of adenylyl cyclase type VI causes a urinary concentration defect in mice. *Am J Physiol Renal Physiol* **302**, F78-84 (2012).
215. Rieg, T*., et al.* Adenylyl cyclase 6 enhances NKCC2 expression and mediates vasopressin-induced phosphorylation of NKCC2 and NCC. *Am J Pathol* **182**, 96-106 (2013).
216. Wallace, D.P., Grantham, J.J. & Sullivan, L.P. Chloride and fluid secretion by cultured human polycystic kidney cells. *Kidney Int* **50**, 1327-1336 (1996).
217. Yamaguchi, T*., et al.* Cyclic AMP activates B-Raf and ERK in cyst epithelial cells from autosomal-dominant polycystic kidneys. *Kidney Int* **63**, 1983-1994 (2003).
218. Sullivan, L.P., Wallace, D.P. & Grantham, J.J. Chloride and fluid secretion in polycystic kidney disease. *J Am Soc Nephrol* **9**, 903-916 (1998).
219. Wallace, D.P., Rome, L.A., Sullivan, L.P. & Grantham, J.J. cAMP-dependent fluid secretion in rat inner medullary collecting ducts. *Am. J Physiol Renal Physiol* **280**, F1019-F1029 (2001).
220. Wallace, D.P*., et al.* Electrolyte and fluid secretion by cultured human inner medullary collecting duct cells. *Am J Physiol Renal Physiol* **283**, F1337-1350 (2002).
221. Grantham, J.J. & Wallace, D.P. Return of the secretory kidney. *Am J Physiol Renal Physiol* **282**, F1-9 (2002).
222. Montesano, R., Ghzili, H., Carrozzino, F., Rossier, B.C. & Feraille, E. cAMP-dependent chloride secretion mediates tubule enlargement and cyst formation by cultured mammalian collecting duct cells. *Am J Physiol Renal Physiol* **296**, F446-457 (2009).
223. Odgaard, E., Praetorius, H.A. & Leipziger, J. AVP-stimulated nucleotide secretion in perfused mouse medullary thick ascending limb and cortical collecting duct. *Am J Physiol Renal Physiol* **297**, F341-349 (2009).
224. Cuffe, J.E., Bielfeld-Ackermann, A., Thomas, J., Leipziger, J. & Korbmacher, C. ATP stimulates Cl- secretion and reduces amiloride-sensitive Na+ absorption in M-1 mouse cortical collecting duct cells. *J Physiol (Lond.)* **524 Pt 1**, 77-90 (2000).
225. Rajagopal, M., Kathpalia, P.P., Thomas, S.V. & Pao, A.C. Activation of P2Y1 and P2Y2 receptors induces chloride secretion via calcium-activated chloride channels in kidney inner medullary collecting duct cells. *Am. J Physiol Renal Physiol* **301**, F544-F553 (2011).
226. Rajagopal, M., Kathpalia, P.P., Widdicombe, J.H. & Pao, A.C. Differential effects of extracellular ATP on chloride transport in cortical collecting duct cells. *Am J Physiol Renal Physiol* **303**, F483-491 (2012).
227. Piwkowska, A., Rogacka, D., Jankowski, M. & Angielski, S. Extracellular ATP through P2 receptors activates AMP-activated protein kinase and suppresses superoxide generation in cultured mouse podocytes. *Exp Cell Res* **317**, 1904-1913 (2011).
228. Svenningsen, P., Nielsen, M.R., Marcussen, N., Walter, S. & Jensen, B.L. TMEM16A is a Ca -activated Cl channel expressed in the renal collecting duct. *Acta Physiol (Oxf)* **212**, 166-174 (2014).
229. Buchholz, B., Teschemacher, B., Schley, G., Schillers, H. & Eckardt, K.U. Formation of cysts by principal-like MDCK cells depends on the synergy of cAMP- and ATP-mediated fluid secretion. *J Mol. Med* **89**, 251-261 (2011).
230. Wallace, D.P., Reif, G., Hedge, A.M., Thrasher, J.B. & Pietrow, P. Adrenergic regulation of salt and fluid secretion in human medullary collecting duct cells. *Am J Physiol Renal Physiol* **287**, F639-648 (2004).
231. Belibi, F.A*., et al.* Cyclic AMP promotes growth and secretion in human polycystic

kidney epithelial cells. *Kidney Int* **66**, 964-973 (2004).
232. Welch, B.D., Carlson, N.G., Shi, H., Myatt, L. & Kishore, B.K. P2Y2 receptor-stimulated release of prostaglandin E2 by rat inner medullary collecting duct preparations. *Am J Physiol Renal Physiol* **285**, F711-721 (2003).
233. Xia, M. & Zhu, Y. Signaling pathways of ATP-induced PGE2 release in spinal cord astrocytes are EGFR transactivation-dependent. *Glia* **59**, 664-674 (2011).
234. Gonzalez, A.A., Cespedes, C., Villanueva, S., Michea, L. & Vio, C.P. E Prostanoid-1 receptor regulates renal medullary alphaENaC in rats infused with angiotensin II. *Biochem Biophys Res Commun* **389**, 372-377 (2009).
235. Sandrasagra, S., Cuffe, J.E., Regardsoe, E.L. & Korbmacher, C. PGE2 stimulates Cl- secretion in murine M-1 cortical collecting duct cells in an autocrine manner. *Pflugers Arch* **448**, 411-421 (2004).
236. Ye, W.*, et al.* Expression and function of COX isoforms in renal medulla: evidence for regulation of salt sensitivity and blood pressure. *Am J Physiol Renal Physiol* **290**, F542-549 (2006).
237. Rajagopal, M., Thomas, S.V., Kathpalia, P.P., Chen, Y. & Pao, A.C. Prostaglandin E2 induces chloride secretion through crosstalk between cAMP and calcium signaling in mouse inner medullary collecting duct cells. *Am J Physiol Cell Physiol* **306**, C263-C278 (2014).
238. Lu, M.*, et al.* Mouse cystic fibrosis transmembrane conductance regulator forms cAMP-PKA-regulated apical chloride channels in cortical collecting duct. *Proc. Natl. Acad. Sci. U. S. A* (2010).
239. Wallace, D.P. Cyclic AMP-mediated cyst expansion. *Biochim Biophys Acta* **1812**, 1291-1300 (2011).
240. Reif, G.A.*, et al.* Tolvaptan inhibits ERK-dependent cell proliferation, Cl(-) secretion, and in vitro cyst growth of human ADPKD cells stimulated by vasopressin. *Am J Physiol Renal Physiol* **301**, F1005-1013 (2011).
241. Magenheimer, B.S.*, et al.* Early embryonic renal tubules of wild-type and polycystic kidney disease kidneys respond to cAMP stimulation with cystic fibrosis transmembrane conductance regulator/Na(+),K(+),2Cl(-) Co-transporter-dependent cystic dilation. *J Am Soc Nephrol* **17**, 3424-3437 (2006).
242. Yang, B., Sonawane, N.D., Zhao, D., Somlo, S. & Verkman, A.S. Small-Molecule CFTR Inhibitors Slow Cyst Growth in Polycystic Kidney Disease. *J Am Soc. Nephrol* **19**, 1300-1310 (2008).
243. Yanda, M.K., Liu, Q. & Cebotaru, L. A potential strategy for reducing cysts in autosomal dominant polycystic kidney disease with a CFTR corrector. *J Biol Chem* **293**, 11513-11526 (2018).
244. Morales, M.M.*, et al.* Both the wild type and a functional isoform of CFTR are expressed in kidney. *Am. J. Physiol* **270**, F1038-F1048 (1996).
245. Jouret, F.*, et al.* Cystic fibrosis is associated with a defect in apical receptor-mediated endocytosis in mouse and human kidney. *J Am Soc. Nephrol* **18**, 707-718 (2007).
246. Davidow, C.J., Maser, R.L., Rome, L.A., Calvet, J.P. & Grantham, J.J. The cystic fibrosis transmembrane conductance regulator mediates transepithelial fluid secretion by human autosomal dominant polycystic kidney disease epithelium in vitro. *Kidney Int* **50**, 208-218 (1996).
247. O'Sullivan, D.A.*, et al.* Cystic fibrosis and the phenotypic expression of autosomal dominant polycystic kidney disease [see comments]. *Am J Kidney Dis* **32**, 976-983 (1998).
248. Persu, A.*, et al.* CF gene and cystic fibrosis transmembrane conductance regulator expression in autosomal dominant polycystic kidney disease. *J Am Soc Nephrol* **11**, 2285-2296 (2000).
249. Buchholz, B.*, et al.* Hypoxia-Inducible Factor-1a Causes Renal Cyst Expansion through Calcium-Activated Chloride Secretion. *J Am Soc Nephrol* **25**, 465-474 (2014).
250. Rieg, T. & Vallon, V. ATP and adenosine in the local regulation of water transport and homeostasis by the kidney. *Am J Physiol Regul Integr Comp Physiol* **296**, R419-427 (2009).

251. Kraus, A.*, et al.* P2Y2R is a direct target of HIF-1alpha and mediates secretion-dependent cyst growth of renal cyst-forming epithelial cells. *Purinergic signalling* **12**, 687-695 (2016).
252. Kraus, A.*, et al.* Glucose promotes secretion-dependent renal cyst growth. *J Mol. Med. (Berl)* **94**, 107-117 (2015).
253. Bachinsky, D.R.*, et al.* Water channel expression in human ADPKD kidneys. *Am J Physiol* **268**, F398 (1995).
254. Agre, P. The aquaporin water channels. *Proc Am Thorac Soc* **3**, 5-13 (2006).
255. Devuyst, O.*, et al.* Expression of aquaporins-1 and -2 during nephrogenesis and in autosomal dominant polycystic kidney disease. *Am J Physiol* **271**, F169-183 (1996).
256. Matsuzaki, T.*, et al.* The distribution and function of aquaporins in the kidney: resolved and unresolved questions. *Anat Sci Int* **92**, 187-199 (2017).
257. Hayashi, M.*, et al.* Expression and localization of the water channels in human autosomal dominant polycystic kidney disease. *Nephron* **75**, 321-326 (1997).
258. Mangoo-Karim, R., Ye, M., Wallace, D.P., Grantham, J.J. & Sullivan, L.P. Anion secretion drives fluid secretion by monolayers of cultured human polycystic cells. *Am J Physiol* **269**, F381-388 (1995).
259. Gamba, G. Molecular physiology and pathophysiology of electroneutral cation-chloride cotransporters. *Physiol Rev* **85**, 423-493 (2005).
260. Lebeau, C.*, et al.* Basolateral chloride transporters in autosomal dominant polycystic kidney disease. *Pflugers Arch* **444**, 722-731 (2002).
261. Thomson, R.B.*, et al.* Histopathological analysis of renal cystic epithelia in the Pkd2WS25/- mouse model of ADPKD. *Am J Physiol Renal Physiol* **285**, F870-880 (2003).
262. Alper, S.L. Let's look at cysts from both sides now. *Kidney Int* **74**, 699-702 (2008).
263. Brill, S.R.*, et al.* Immunolocalization of ion transport proteins in human autosomal dominant polycystic kidney epithelial cells. *Proc. Natl. Acad. Sci. U. S. A* **93**, 10206-10211 (1996).
264. Albaqumi, M.*, et al.* KCa3.1 potassium channels are critical for cAMP-dependent chloride secretion and cyst growth in autosomal-dominant polycystic kidney disease. *Kidney Int* **74**, 740-749 (2008).
265. Suzuki, J.*, et al.* Calcium-dependent Phospholipid Scramblase Activity of TMEM16 Family Members. *J Biol Chem* **288**, 13305-13316 (2013).
266. Huang, W.C.*, et al.* Calcium-activated chloride channels (CaCCs) regulate action potential and synaptic response in hippocampal neurons. *Neuron* **74**, 179-192 (2012).
267. Huang, F.*, et al.* TMEM16C facilitates Na(+)-activated K(+) currents in rat sensory neurons and regulates pain processing. *Nat. Neurosci* **16**, 1284-1290 (2013).
268. Heinze, C.*, et al.* Disruption of vascular Ca2+-activated chloride currents lowers blood pressure. *J Clin. Invest* **124**, 675-686 (2014).
269. Takayama, Y., Uta, D., Furue, H. & Tominaga, M. Pain-enhancing mechanism through interaction between TRPV1 and anoctamin 1 in sensory neurons. *Proc. Natl. Acad. Sci U. S A* **112**, 5213-5218 (2015).
270. Ehlen, H.W.*, et al.* Inactivation of Anoctamin-6/Tmem16f, a regulator of phosphatidylserine scrambling in osteoblasts, leads to decreased mineral deposition in skeletal tissues. *J Bone Miner. Res* **28**, 246-259 (2012).
271. Balreira, A.*, et al.* ANO10 mutations cause ataxia and coenzyme Q deficiency. *J Neurol* **261**, 2192-2198 (2014).
272. Fischer, M.A., Temmerman, K., Ercan, E., Nickel, W. & Seedorf, M. Binding of plasma membrane lipids recruits the yeast integral membrane protein Ist2 to the cortical ER. *Traffic* **10**, 1084-1097 (2009).
273. Courjaret, R. & Machaca, K. Mid-range Ca2+ signalling mediated by functional coupling between store-operated Ca2+ entry and IP3-dependent Ca2+ release. *Nat. Commun* **5**, 3916 (2014).
274. Sirianant, L., Ousingsawat, J., Tian, Y., Schreiber, R. & Kunzelmann, K. TMC8 (EVER2) attenuates intracellular signaling by Zn2+ and Ca2+ and suppresses activation of Cl- currents. *Cellular signalling* **26**, 2826-2833 (2014).

275. Almaca, J.*, et al.* TMEM16 proteins produce volume regulated chloride currents that are reduced in mice lacking TMEM16A. *J Biol Chem* **284**, 28571-28578 (2009).
276. Watts, S.D., Suchland, K.L., Amara, S.G. & Ingram, S.L. A sensitive membrane-targeted biosensor for monitoring changes in intracellular chloride in neuronal processes. *PLoS. ONE* **7**, e35373 (2012).
277. Lee, M.Y.*, et al.* Local subplasma membrane Ca2+ signals detected by a tethered Ca2+ sensor. *Proc. Natl. Acad. Sci. U. S A* **103**, 13232-13237 (2006).
278. Sones, W.R., Davis, A.J., Leblanc, N. & Greenwood, I.A. Cholesterol depletion alters amplitude and pharmacology of vascular calcium-activated chloride channels. *Cardiovasc. Res* **87**, 476-484 (2010).
279. Fischer, K.G., Leipziger, J., Rubini-Illes, P., Nitschke, R. & Greger, R. Attenuation of stimulated Ca2+ influx in colonic epithelial (HT29) cells by cAMP. *Pflugers Arch* **432**, 735-740 (1996).
280. Szentpetery, Z., Balla, A., Kim, Y.J., Lemmon, M.A. & Balla, T. Live cell imaging with protein domains capable of recognizing phosphatidylinositol 4,5-bisphosphate; a comparative study. *BMC cell biology* **10**(2009).
281. Kabouridis, P.S., Janzen, J., Magee, A.L. & Ley, S.C. Cholesterol depletion disrupts lipid rafts and modulates the activity of multiple signaling pathways in T lymphocytes. *European journal of immunology* **30**, 954-963 (2000).
282. Diaz, O.*, et al.* Disruption of lipid rafts stimulates phospholipase d activity in human lymphocytes: implication in the regulation of immune function. *J Immunol* **175**, 8077-8086 (2005).
283. Grubb, S.*, et al.* TMEM16F (Anoctamin 6), an anion channel of delayed Ca2+ activation. *J Gen. Physiol* **141**, 585-600 (2013).
284. Sirianant, L., Ousingsawat, J., Wanitchakool, P., Schreiber, R. & Kunzelmann, K. Cellular Volume regulation by Anoctamin 6:Ca2+, phospholipase A2,osmosensing. *Pflügers Arch* **468**, 335-349 (2015).
285. Zhang, W.M.*, et al.* ET-1 activates Ca2+ sparks in PASMC: local Ca2+ signaling between inositol trisphosphate and ryanodine receptors. *American journal of physiology. Lung cellular and molecular physiology* **285**, 680-690 (2003).
286. Tones, M.A.*, et al.* The effect of heparin on the inositol 1,4,5-trisphosphate receptor in rat liver microsomes. Dependence on sulphate content and chain length. *FEBS Lett* **252**, 105-108 (1989).
287. Ohga, K., Takezawa, R., Arakida, Y., Shimizu, Y. & Ishikawa, J. Characterization of YM-58483/BTP2, a novel store-operated Ca2+ entry blocker, on T cell-mediated immune responses in vivo. *International immunopharmacology* **8**, 1787-1792 (2008).
288. Derler, I.*, et al.* The action of selective CRAC channel blockers is affected by the Orai pore geometry. *Cell Calcium* **53**, 139-151 (2013).
289. Maniero, C.*, et al.* Role of ANO4 in regulation of aldosterone secretion in the zona glomerulosa of the human adrenal gland. *Lancet (London, England)* **385 Suppl 1**, 4 (2015).
290. Pritchard, H.A., Leblanc, N., Albert, A.P. & Greenwood, I.A. Inhibitory role of phosphatidylinositol 4,5 bisphosphate on TMEM16A encoded calcium-activated chloride channels in rat pulmonary artery. *Br. J Pharmacol*, 10 (2014).
291. Barro Soria, R.*, et al.* ER localized bestrophin1 acts as a counter-ion channel to activate Ca2+ dependent ion channels TMEM16A and SK4. *Pflügers Arch* **459**, 485-497 (2009).
292. Kunzelmann, K.*, et al.* Expression and function of epithelial anoctamins. *Exp. Physiol* **97**, 184-192 (2012).
293. Maass, K.*, et al.* A signal comprising a basic cluster and an amphipathic alpha-helix interacts with lipids and is required for the transport of Ist2 to the yeast cortical ER. *J Cell Sci* **122**, 625-635 (2009).
294. Liu, B.*, et al.* The acute nociceptive signals induced by bradykinin in rat sensory neurons are mediated by inhibition of M-type K+ channels and activation of Ca2+-activated Cl- channels. *J. Clin. Invest* **120**, 1240-1252 (2010).
295. Vocke, K.*, et al.* Calmodulin-dependent activation and inactivation of anoctamin

calcium-gated chloride channels. *J Gen. Physiol* **142**, 381-404 (2013).
296. Singh, R.D.*, et al.* Ano1, a Ca2+-activated Cl- channel coordinates contractility in mouse intestine by ca2+ transient coordination between interstitial cells of cajal. *The Journal of physiology* **592**, 4051-4068 (2014).
297. Zhu, M.H., Sung, T.S., O'Driscoll, K., Koh, S.D. & Sanders, K.M. Intracellular Ca(2+) release from endoplasmic reticulum regulates slow wave currents and pacemaker activity of interstitial cells of Cajal. *Am J Physiol Cell Physiol* **308**, C608-C620 (2015).
298. Zhang, C.H.*, et al.* The transmembrane protein 16A Ca(2+)-activated Cl- channel in airway smooth muscle contributes to airway hyperresponsiveness. *Am J Respir. Crit Care Med* **187**, 374-381 (2013).
299. Namkung, W., Yao, Z., Finkbeiner, W.E. & Verkman, A.S. Small-molecule activators of TMEM16A, a calcium-activated chloride channel, stimulate epithelial chloride secretion and intestinal contraction. *FASEB J* **25**, 4048-4062 (2011).
300. Takayama, Y., Shibasaki, K., Suzuki, Y., Yamanaka, A. & Tominaga, M. Modulation of water efflux through functional interaction between TRPV4 and TMEM16A/anoctamin 1. *FASEB J* **28**, 2238-2248 (2014).
301. Concepcion, A.R.*, et al.* Store-operated Ca2+ entry regulates Ca2+-activated chloride channels and eccrine sweat gland function. *The Journal of clinical investigation* (2016).
302. Wanitchakool, P.*, et al.* Cellular defects by deletion of ANO10 are due to deregulated local calcium signaling. *Cellular signalling* **30**, 41-49 (2017).
303. Schroeder, B.C., Cheng, T., Jan, Y.N. & Jan, L.Y. Expression cloning of TMEM16A as a calcium-activated chloride channel subunit. *Cell* **134**, 1019-1029 (2008).
304. Sirianant, L.*, et al.* Non-essential contribution of LRRC8A to volume regulation. *Pflügers Arch* **468**, 1789-1796 (2016).
305. Wanitchakool, P.*, et al.* Cellular defects by deletion of ANO10 are due to deregulated local calcium signaling. *Cellular signalling* **30**, 41-49 (2016).
306. Warth, R.*, et al.* Molecular and functional characterization of the small Ca2+-regulated K+ channel (rSK4) of colonic crypts. *Pflügers Arch* **438**, 437-444 (1999).
307. Zhivotovsky, B. & Orrenius, S. Calcium and cell death mechanisms: a perspective from the cell death community. *Cell Calcium* **50**, 211-221 (2011).
308. Reuter, S. & Lang, D. Life span of monocytes and platelets: importance of interactions. *Frontiers in bioscience (Landmark edition)* **14**, 2432-2447 (2009).
309. Eastman, A. Activation of programmed cell death by anticancer agents: cisplatin as a model system. *Cancer cells (Cold Spring Harbor, N.Y. : 1989)* **2**, 275-280 (1990).
310. Maeno, E., Ishizaki, Y., Kanaseki, T., Hazama, A. & Okada, Y. Normotonic cell shrinkage because of disordered volume regulation is an early prerequisite to apoptosis. *Proc. Natl. Acad. Sci. U. S. A* **97**, 9487-9492 (2000).
311. Lee, E.L.*, et al.* Impaired activity of volume-sensitive Cl- channel is involved in cisplatin resistance of cancer cells. *J Cell Physiol* **211**, 513-521 (2007).
312. Poulsen, K.A.*, et al.* Deregulation of apoptotic volume decrease and ionic movements in multidrug-resistant tumor cells: role of chloride channels. *Am J Physiol Cell Physiol* **298**, C14-C25 (2010).
313. Lang, F. & Hoffmann, E.K. CrossTalk proposal: Cell volume changes are an essential step in the cell death machinery. *The Journal of physiology* **591**, 6119-6121 (2013).
314. Voss, F.K.*, et al.* Identification of LRRC8 Heteromers as an Essential Component of the Volume-Regulated Anion Channel VRAC. *Science* **344**, 634-638 (2014).
315. Qiu, Z.*, et al.* SWELL1, a Plasma Membrane Protein, Is an Essential Component of Volume-Regulated Anion Channel. *Cell* **157**, 447-458 (2014).
316. Planells-Cases, R.*, et al.* Subunit composition of VRAC channels determines substrate specificity and cellular resistance to Pt-based anti-cancer drugs. *EMBO J* **34**, 2993-3008 (2015).
317. Min, X.J.*, et al.* Dysfunction of volume-sensitive chloride channels contributes to cisplatin resistance in human lung adenocarcinoma cells. *Experimental biology and medicine (Maywood, N.J.)* **236**, 483-491 (2011).
318. Gunther, C., Buchen, B., Neurath, M.F. & Becker, C. Regulation and

pathophysiological role of epithelial turnover in the gut. *Seminars in cell & developmental biology* **35**, 40-50 (2014).
319. Kramer, J. & Hawley, R.S. The spindle-associated transmembrane protein Axs identifies a new family of transmembrane proteins in eukaryotes. *Cell cycle (Georgetown, Tex.)* **2**, 174-176 (2003).
320. Whitaker, M. Calcium microdomains and cell cycle control. *Cell Calcium* **40**, 585-592 (2006).
321. Zhuchenko, O.*, et al.* Autosomal dominant cerebellar ataxia (SCA6) associated with small polyglutamine expansions in the alpha 1A-voltage-dependent calcium channel. *Nat Genet* **15**, 62-69 (1997).
322. van de Leemput, J.*, et al.* Deletion at ITPR1 underlies ataxia in mice and spinocerebellar ataxia 15 in humans. *PLoS genetics* **3**, e108 (2007).
323. Saegusa, H.*, et al.* Properties of human Cav2.1 channel with a spinocerebellar ataxia type 6 mutation expressed in Purkinje cells. *Molecular and cellular neurosciences* **34**, 261-270 (2007).
324. Liu, J.*, et al.* Deranged calcium signaling and neurodegeneration in spinocerebellar ataxia type 2. *J Neurosci* **29**, 9148-9162 (2009).
325. Egorova, P., Popugaeva, E. & Bezprozvanny, I. Disturbed calcium signaling in spinocerebellar ataxias and Alzheimer's disease. *Seminars in cell & developmental biology* **40**, 127-133 (2015).
326. Parkinson, M.H., Schulz, J.B. & Giunti, P. Co-enzyme Q10 and idebenone use in Friedreich's ataxia. *J Neurochem* **126 Suppl 1**, 125-141 (2013).
327. Seo, Y.*, et al.* Inhibition of ANO1/TMEM16A Chloride Channel by Idebenone and Its Cytotoxicity to Cancer Cell Lines. *PLoS. ONE* **10**, e0133656 (2015).
328. Boucher, R.C. Airway surface dehydration in cystic fibrosis: pathogenesis and therapy. *Annu. Rev. Med* **58**, 157-170 (2007).
329. Stoltz, D.A., Meyerholz, D.K. & Welsh, M.J. Origins of cystic fibrosis lung disease. *N. Engl. J Med* **372**, 351-362 (2015).
330. Fahy, J.V. & Dickey, B.F. Airway mucus function and dysfunction. *N Engl J Med* **363**, 2233-2247 (2010).
331. Kunzelmann, K., Schreiber, R. & Hadorn, H.B. Bicarbonate in cystic fibrosis. *Journal of Cystic Fibrosis* **16**, 653-662 (2017).
332. Pezzulo, A.A.*, et al.* Reduced airway surface pH impairs bacterial killing in the porcine cystic fibrosis lung. *Nature* **487**, 109-113 (2012).
333. Schultz, A.*, et al.* Airway surface liquid pH is not acidic in children with cystic fibrosis. *Nature communications* **8**, 1409 (2017).
334. Scudieri, P.*, et al.* Increased expression of ATP12A proton pump in cystic fibrosis airways. *JCI insight* **3**(2018).
335. Colombo, J.L. Long-acting bronchodilators in cystic fibrosis. *Curr Opin Pulm Med* **9**, 504-508 (2003).
336. Matusovsky, O.S.*, et al.* Contractile Properties of Intrapulmonary Airway Smooth Muscle in Cystic Fibrosis. *American journal of respiratory cell and molecular biology* **60**, 434-444 (2019).
337. Pascoe, C.D. & Halayko, A.J. Shot Down Inflamed: Airway Smooth Muscle Bronchodilator Insensitivity in Cystic Fibrosis. *American journal of respiratory cell and molecular biology* **60**, 379-381 (2019).
338. Caci, E.*, et al.* Upregulation of TMEM16A Protein in Bronchial Epithelial Cells by Bacterial Pyocyanin. *PLoS. ONE* **10**, e0131775 (2015).
339. Wang, P.*, et al.* Inflammatory mediators mediate airway smooth muscle contraction through a G protein-coupled receptor-transmembrane protein 16A-voltage-dependent Ca(2+) channel axis and contribute to bronchial hyperresponsiveness in asthma. *J Allergy Clin Immunol* **141**, 1259-1268.e1211 (2018).
340. Papp, R.*, et al.* Targeting TMEM16A to reverse vasoconstriction and remodelling in idiopathic pulmonary arterial hypertension. *The European respiratory journal* **53**(2019).
341. Forrest, A.S.*, et al.* Increased TMEM16A-Encoded Calcium-Activated Chloride

Channel Activity Is Associated With Pulmonary Hypertension. *Am. J Physiol Cell Physiol* **303**, C1229-C1243 (2012).
342. Harkness, L.M., Kanabar, V., Sharma, H.S., Westergren-Thorsson, G. & Larsson-Callerfelt, A.K. Pulmonary vascular changes in asthma and COPD. *Pulm Pharmacol Ther* **29**, 144-155 (2014).
343. Wells, J.M*., et al.* Pulmonary artery enlargement and cystic fibrosis pulmonary exacerbations: a cohort study. *The Lancet. Respiratory medicine* **4**, 636-645 (2016).
344. Miner, K*., et al.* Drug Repurposing: The Anthelmintics Niclosamide and Nitazoxanide Are Potent TMEM16A Antagonists That Fully Bronchodilate Airways. *Frontiers in pharmacology* **10**, 51 (2019).
345. Schenk, L.K*., et al.* Regulation and Function of TMEM16F in Renal Podocytes. *International journal of molecular sciences* **19**(2018).
346. Schreiber, R., Castrop, H. & Kunzelmann, K. Allergen induced airway hyperresponsiveness is absent in ecto-5´-nucleotidase (CD73) deficient mice. *Pflugers Arch* **457**, 431-440 (2008).
347. Garcia, M.A., Yang, N. & Quinton, P.M. Normal mouse intestinal mucus release requires cystic fibrosis transmembrane regulator-dependent bicarbonate secretion. *J Clin. Invest* **119**, 2613-2622 (2009).
348. Cabrita, I*., et al.* Differential effects of anoctamins on intracellular calcium signals. *Faseb j* **31**, 2123-2134 (2017).
349. Kunzelmann, K. & Schreiber, R. Airway epithelial cells-Hyperabsorption in CF? *Int. J Biochem Cell Biol* **44**, 1232-1235 (2012).
350. Liang, L*., et al.* Inhibitory effects of niclosamide on inflammation and migration of fibroblast-like synoviocytes from patients with rheumatoid arthritis. *Inflammation research : official journal of the European Histamine Research Society ... [et al.]* **64**, 225-233 (2015).
351. Cheng, J., Wang, H. & Guggino, W.B. Modulation of mature cystic fibrosis transmembrane regulator protein by the PDZ domain protein CAL. *J Biol Chem***.**(2003).
352. Chen, W., Mook, R.A., Jr., Premont, R.T. & Wang, J. Niclosamide: Beyond an antihelminthic drug. *Cellular signalling* **41**, 89-96 (2018).
353. Jha, A*., et al.* Anoctamin 8 tethers endoplasmic reticulum and plasma membrane for assembly of Ca(2+) signaling complexes at the ER/PM compartment. *Embo j* **38**(2019).
354. Walker, N.M., Simpson, J.E., Levitt, R.C., Boyle, K.T. & Clarke, L.L. Talniflumate increases survival in a cystic fibrosis mouse model of distal intestinal obstructive syndrome. *J Pharmacol Exp Ther* **317**, 275-283 (2006).
355. Scudieri, P*., et al.* ASSOCIATION OF TMEM16A CHLORIDE CHANNEL OVEREXPRESSION WITH AIRWAY GOBLET CELL METAPLASIA. *The Journal of physiology* **590**, 6141-6155 (2012).
356. Mazzone, A*., et al.* Identification and characterization of a novel promoter for the human ANO1 gene regulated by the transcription factor signal transducer and activator of transcription 6 (STAT6). *FASEB J*, fj-258541 (2015).
357. Qin, Y*., et al.* Interleukin-13 stimulates MUC5AC expression via a STAT6-TMEM16A-ERK1/2 pathway in human airway epithelial cells. *International immunopharmacology* **40**, 106-114 (2016).
358. Schreiber, R*., et al.* Lipid Peroxidation Drives Renal Cyst Growth In Vitro through Activation of TMEM16A. *J Am Soc Nephrol* **30**, 228-242 (2019).
359. Mall, M.A. & Galietta, L.J. Targeting ion channels in cystic fibrosis. *Journal of cystic fibrosis : official journal of the European Cystic Fibrosis Society* **14**, 561-570 (2015).
360. Ruffin, M*., et al.* Anoctamin 1 Dysregulation Alters Bronchial Epithelial Repair in Cystic Fibrosis. *Biochim. Biophys. Acta* **1832**, 2340-2351 (2013).
361. Mall, M*., et al.* Modulation of Ca2+ activated Cl- secretion by basolateral K+ channels in human normal and cystic fibrosis airway epithelia. *Pediatric Research* **53**, 608-618 (2003).
362. Ratjen, F*., et al.* Long term effects of denufosol tetrasodium in patients with cystic

fibrosis. *Journal of cystic fibrosis : official journal of the European Cystic Fibrosis Society* **11**, 539-549 (2012).
363. Moss, R.B. Pitfalls of drug development: lessons learned from trials of denufosol in cystic fibrosis. *J Pediatr* **162**, 676-680 (2013).
364. Imperi, F.*, et al.* New life for an old drug: the anthelmintic drug niclosamide inhibits Pseudomonas aeruginosa quorum sensing. *Antimicrobial agents and chemotherapy* **57**, 996-1005 (2013).
365. Costabile, G.*, et al.* Toward Repositioning Niclosamide for Antivirulence Therapy of Pseudomonas aeruginosa Lung Infections: Development of Inhalable Formulations through Nanosuspension Technology. *Molecular pharmaceutics* **12**, 2604-2617 (2015).
366. Gwisai, T.*, et al.* Repurposing niclosamide as a versatile antimicrobial surface coating against device-associated, hospital-acquired bacterial infections. *Biomedical materials (Bristol, England)* **12**, 045010 (2017).
367. Morin, F.*, et al.* Improvement of Sclerodermatous Graft-Versus-Host Disease in Mice by Niclosamide. *J Invest Dermatol* **136**, 2158-2167 (2016).
368. Li, Y.*, et al.* Multi-targeted therapy of cancer by niclosamide: A new application for an old drug. *Cancer Lett* **349**, 8-14 (2014).
369. Ma, M., Gallagher, A.R. & Somlo, S. Ciliary Mechanisms of Cyst Formation in Polycystic Kidney Disease. *Cold Spring Harbor perspectives in biology* **9**(2017).
370. Mekahli, D., Parys, J.B., Bultynck, G., Missiaen, L. & De Smedt, H. Polycystins and cellular Ca2+ signaling. *Cell Mol Life Sci* **70**, 2697-2712 (2013).
371. Schreiber, R. & Kunzelmann, K. Expression of anoctamins in retinal pigment epithelium (RPE). *Pflugers Arch* **468**, 1921-1929 (2016).
372. Gao da, Y.*, et al.* Coupling of TRPV6 and TMEM16A in epithelial principal cells of the rat epididymis. *The Journal of general physiology* **148**, 161-182 (2016).
373. Kappes, J.C., Wu, X. & Wakefield, J.K. Production of trans-lentiviral vector with predictable safety. *Methods Mol Med* **76**, 449-465 (2003).
374. Mendes, F.*, et al.* Establishment and Characterization of a novel polarized MDCK epithelial cellular model for CFTR studies. *Cell Physiol Biochemc* **16**, 281-290 (2005).
375. Su, S.*, et al.* Genetically encoded calcium indicator illuminates calcium dynamics in primary cilia. *Nat. Methods* **10**, 1105-1107 (2013).
376. Wu, J.*, et al.* Red fluorescent genetically encoded Ca2+ indicators for use in mitochondria and endoplasmic reticulum. *Biochem. J* **464**, 13-22 (2014).
377. Wegierski, T.*, et al.* TRPP2 channels regulate apoptosis through the Ca2+ concentration in the endoplasmic reticulum. *EMBO J* **28**, 490-499 (2009).
378. Kunzelmann, K.*, et al.* TMEM16A in Cystic Fibrosis: Activating or Inhibiting? *Frontiers in pharmacology* **10**, 3 (2019).
379. Gainullin, V.G., Hopp, K., Ward, C.J., Hommerding, C.J. & Harris, P.C. Polycystin-1 maturation requires polycystin-2 in a dose-dependent manner. *J Clin Invest* **125**, 607-620 (2015).
380. Woodward, O.M.*, et al.* Identification of a polycystin-1 cleavage product, P100, that regulates store operated Ca entry through interactions with STIM1. *PLoS One* **5**, e12305 (2010).
381. Low, S.H.*, et al.* Polycystin-1, STAT6, and P100 function in a pathway that transduces ciliary mechanosensation and is activated in polycystic kidney disease. *Dev Cell* **10**, 57-69 (2006).
382. Guo, S.*, et al.* Ginsenoside Rb1, a novel activator of the TMEM16A chloride channel, augments the contraction of guinea pig ileum. *Pflugers Arch* (2017).
383. Kunzelmann, K. The Cystic Fibrosis Transmembrane Conductance Regulator and its function in epithelial transport. *Rev. Physiol. Biochem. Pharmacol* **137**, 1-70 (1999).
384. Benedetto, R.*, et al.* Plasma membrane-localized TMEM16 proteins are indispensable for expression of CFTR. *Journal of molecular medicine (Berlin, Germany)* **97**, 711-722 (2019).
385. Danielsson, J.*, et al.* Antagonists of the TMEM16A Calcium-activated Chloride

Channel Modulate Airway Smooth Muscle Tone and Intracellular Calcium. *Anesthesiology (in press)* **123**, 569-581 (2015).
386. Kraus, A.*, et al.* HIF-1alpha promotes cyst progression in a mouse model of autosomal dominant polycystic kidney disease. *Kidney Int* (2018).
387. Lantinga-van Leeuwen, I.S.*, et al.* Transgenic mice expressing tamoxifen-inducible Cre for somatic gene modification in renal epithelial cells. *Genesis* **44**, 225-232 (2006).
388. Wang, H.*, et al.* Cell-specific mechanisms of TMEM16A Ca2+-activated chloride channel in cancer. *Molecular cancer* **16**, 152 (2017).
389. Yu, H.*, et al.* Extended synaptotagmins are Ca2+-dependent lipid transfer proteins at membrane contact sites. *Proceedings of the National Academy of Sciences of the United States of America* **113**, 4362-4367 (2016).
390. Chou, H.W.*, et al.* Comparative effectiveness of allopurinol, febuxostat and benzbromarone on renal function in chronic kidney disease patients with hyperuricemia: a 13-year inception cohort study. *Nephrol Dial Transplant* **33**, 1620-1627 (2018).
391. Cabrita, I., Benedetto, R., Schreiber, R. & Kunzelmann, K. Niclosamide repurposed for the treatment of inflammatory airway disease. *JCI insight* **4**(2019).
392. Burock, S.*, et al.* Phase II trial to investigate the safety and efficacy of orally applied niclosamide in patients with metachronous or sychronous metastases of a colorectal cancer progressing after therapy: the NIKOLO trial. *BMC Cancer* **18**, 297 (2018).
393. Grynkiewicz, G., Poenie, M. & Tsien, R.Y. A new generation of Ca2+ indicators with greatly improved fluorescence properties. *J Biol Chem* **260**, 3440-3450 (1985).
394. Benedetto, R.*, et al.* Relationship between TMEM16A/anoctamin 1 and LRRC8A. *Pflugers Arch* **468**, 1751-1763 (2016).
395. Schreiber, R., Faria, D., Skryabin, B.V., Rock, J.R. & Kunzelmann, K. Anoctamins support calcium-dependent chloride secretion by facilitating calcium signaling in adult mouse intestine. *Pflügers Arch* **467**, 1203-1213 (2015).
396. Maniero, C.*, et al.* ANO4 (Anoctamin 4) Is a Novel Marker of Zona Glomerulosa That Regulates Stimulated Aldosterone Secretion. *Hypertension (Dallas, Tex. : 1979)* **74**, 1152-1159 (2019).
397. Martins, J.R.*, et al.* F508del-CFTR increases intracellular Ca2+ signaling that causes enhanced calcium-dependent Cl- conductance in cystic fibrosis. *Biochim Biophys Acta* **1812**, 1385-1392 (2011).
398. Oheim, M., Kirchhoff, F. & Stuhmer, W. Calcium microdomains in regulated exocytosis. *Cell Calcium* **40**, 423-439 (2006).
399. Chieregatti, E. & Meldolesi, J. Regulated exocytosis: new organelles for non-secretory purposes. *Nature reviews. Molecular cell biology* **6**, 181-187 (2005).
400. Suliman, M.A.*, et al.* Niclosamide inhibits colon cancer progression through downregulation of the Notch pathway and upregulation of the tumor suppressor miR-200 family. *Int J Mol Med* **38**, 776-784 (2016).
401. Meurette, O. & Mehlen, P. Notch Signaling in the Tumor Microenvironment. *Cancer cell* **34**, 536-548 (2018).
402. Jin, Y.*, et al.* Antineoplastic mechanisms of niclosamide in acute myelogenous leukemia stem cells: inactivation of the NF-kappaB pathway and generation of reactive oxygen species. *Cancer Res* **70**, 2516-2527 (2010).
403. Ren, X.*, et al.* Identification of Niclosamide as a New Small-Molecule Inhibitor of the STAT3 Signaling Pathway. *ACS medicinal chemistry letters* **1**, 454-459 (2010).
404. Osada, T.*, et al.* Antihelminth compound niclosamide downregulates Wnt signaling and elicits antitumor responses in tumors with activating APC mutations. *Cancer Res* **71**, 4172-4182 (2011).
405. Kim, S.Y.*, et al.* Role of the IL-6-JAK1-STAT3-Oct-4 pathway in the conversion of non-stem cancer cells into cancer stem-like cells. *Cellular signalling* **25**, 961-969 (2013).
406. Arend, R.C.*, et al.* Niclosamide and its analogs are potent inhibitors of Wnt/beta-catenin, mTOR and STAT3 signaling in ovarian cancer. *Oncotarget* **7**, 86803-86815

(2016).
407. Ahn, S.Y.*, et al.* Anti-helminthic niclosamide inhibits Ras-driven oncogenic transformation via activation of GSK-3. *Oncotarget* **8**, 31856-31863 (2017).
408. Wang, L.H., Xu, M., Fu, L.Q., Chen, X.Y. & Yang, F. The Antihelminthic Niclosamide Inhibits Cancer Stemness, Extracellular Matrix Remodeling, and Metastasis through Dysregulation of the Nuclear beta-catenin/c-Myc axis in OSCC. *Sci Rep* **8**, 12776 (2018).
409. Lafkas, D.*, et al.* Therapeutic antibodies reveal Notch control of transdifferentiation in the adult lung. *Nature* **528**, 127-131 (2015).
410. Danahay, H.*, et al.* Notch2 is required for inflammatory cytokine-driven goblet cell metaplasia in the lung. *Cell reports* **10**, 239-252 (2015).
411. Cohn, L. Mucus in chronic airway diseases: sorting out the sticky details. *The Journal of clinical investigation* **116**, 306-308 (2006).
412. Hansson, G.C. Role of mucus layers in gut infection and inflammation. *Curr Opin Microbiol* **15**, 57-62 (2012).
413. Danahay, H.L.*, et al.* TMEM16A Potentiation: A Novel Therapeutic Approach for the Treatment of Cystic Fibrosis. *American journal of respiratory and critical care medicine* (2020).
414. Chebib, F.T., Sussman, C.R., Wang, X., Harris, P.C. & Torres, V.E. Vasopressin and disruption of calcium signalling in polycystic kidney disease. *Nat. Rev. Nephrol*, 10 (2015).
415. Malysz, J.*, et al.* Conditional genetic deletion of Ano1 in interstitial cells of Cajal impairs Ca2+ transients and slow-waves in adult mouse small intestine. *American journal of physiology. Gastrointestinal and liver physiology*, ajpgi.00363.02016 (2016).
416. Zak, J.D., Grimaud, J., Li, R.C., Lin, C.C. & Murthy, V.N. Calcium-activated chloride channels clamp odor-evoked spike activity in olfactory receptor neurons. *Sci Rep* **8**, 10600 (2018).
417. Hooper, K.M., Unwin, R.J. & Sutters, M. The isolated C-terminus of polycystin-1 promotes increased ATP-stimulated chloride secretion in a collecting duct cell line. *Clin Sci (Lond)* **104**, 217-221 (2003).
418. Chen, W.C., Tzeng, Y.S. & Li, H. Gene expression in early and progression phases of autosomal dominant polycystic kidney disease. *BMC Res Notes* **1**, 131 (2008).
419. Xu, C.*, et al.* Human ADPKD primary cyst epithelial cells with a novel, single codon deletion in the PKD1 gene exhibit defective ciliary polycystin localization and loss of flow-induced Ca2+ signaling. *Am J Physiol Renal Physiol* **292**, F930-F945 (2007).
420. Gattone, V.H., 2nd, Maser, R.L., Tian, C., Rosenberg, J.M. & Branden, M.G. Developmental expression of urine concentration-associated genes and their altered expression in murine infantile-type polycystic kidney disease. *Dev Genet* **24**, 309-318 (1999).
421. Gattone, V.H., 2nd, Wang, X., Harris, P.C. & Torres, V.E. Inhibition of renal cystic disease development and progression by a vasopressin V2 receptor antagonist. *Nature medicine* **9**, 1323-1326 (2003).
422. Wang, X., Gattone, V., 2nd, Harris, P.C. & Torres, V.E. Effectiveness of vasopressin V2 receptor antagonists OPC-31260 and OPC-41061 on polycystic kidney disease development in the PCK rat. *J Am Soc Nephrol* **16**, 846-851 (2005).
423. Torres, V.E.*, et al.* Effective treatment of an orthologous model of autosomal dominant polycystic kidney disease. *Nature medicine* **10**, 363-364 (2004).
424. Torres, V.E.*, et al.* Tolvaptan in patients with autosomal dominant polycystic kidney disease. *N Engl J Med* **367**, 2407-2418 (2012).
425. Muto, S.*, et al.* The effect of tolvaptan on autosomal dominant polycystic kidney disease patients: a subgroup analysis of the Japanese patient subset from TEMPO 3:4 trial. *Clin Exp Nephrol* **19**, 867-877 (2015).
426. Torres, V.E.*, et al.* Tolvaptan in Later-Stage Autosomal Dominant Polycystic Kidney Disease. *N Engl J Med* **377**, 1930-1942 (2017).
427. Lanktree, M.B. & Chapman, A.B. New treatment paradigms for ADPKD: moving

towards precision medicine. *Nature reviews. Nephrology* **13**, 750-768 (2017).
428. Thoreen, C.C*., et al.* An ATP-competitive mammalian target of rapamycin inhibitor reveals rapamycin-resistant functions of mTORC1. *J Biol Chem* **284**, 8023-8032 (2009).
429. Larsson, O*., et al.* Distinct perturbation of the translatome by the antidiabetic drug metformin. *Proceedings of the National Academy of Sciences of the United States of America* **109**, 8977-8982 (2012).
430. Hallows, K.R., McCane, J.E., Kemp, B.E., Witters, L.A. & Foskett, J.K. Regulation of channel gating by AMP-activated protein kinase modulates cystic fibrosis transmembrane conductance regulator activity in lung submucosal cells. *J Biol Chem* **278**, 998-1004 (2003).
431. Takiar, V*., et al.* Activating AMP-activated protein kinase (AMPK) slows renal cystogenesis. *Proc. Natl. Acad. Sci. U. S. A* (2011).
432. Shillingford, J.M*., et al.* The mTOR pathway is regulated by polycystin-1, and its inhibition reverses renal cystogenesis in polycystic kidney disease. *Proc. Natl. Acad. Sci. U. S. A* **103**, 5466-5471 (2006).
433. Serra, A.L*., et al.* Sirolimus and kidney growth in autosomal dominant polycystic kidney disease. *N Engl J Med* **363**, 820-829 (2010).
434. Walz, G*., et al.* Everolimus in patients with autosomal dominant polycystic kidney disease. *N Engl J Med* **363**, 830-840 (2010).
435. Pandey, R.N*., et al.* Structure-activity relationships of benzbromarone metabolites and derivatives as EYA inhibitory anti-angiogenic agents. *PloS one* **8**, e84582 (2013).
436. Gardner, K.D., Jr., Burnside, J.S., Elzinga, L.W. & Locksley, R.M. Cytokines in fluids from polycystic kidneys. *Kidney Int* **39**, 718-724 (1991).
437. Zheng, D*., et al.* Urinary excretion of monocyte chemoattractant protein-1 in autosomal dominant polycystic kidney disease. *J Am Soc Nephrol* **14**, 2588-2595 (2003).
438. Liu, J*., et al.* Sex differences in vasopressin V(2) receptor expression and vasopressin-induced antidiuresis. *Am J Physiol Renal Physiol* **300**, F433-440 (2011).
439. Ljubojevic, M*., et al.* Rat renal cortical OAT1 and OAT3 exhibit gender differences determined by both androgen stimulation and estrogen inhibition. *Am J Physiol Renal Physiol* **287**, F124-138 (2004).
440. Veiras, L.C*., et al.* Sexual Dimorphic Pattern of Renal Transporters and Electrolyte Homeostasis. *J Am Soc Nephrol* **28**, 3504-3517 (2017).
441. Menezes, L.F., Lin, C.C., Zhou, F. & Germino, G.G. Fatty Acid Oxidation is Impaired in An Orthologous Mouse Model of Autosomal Dominant Polycystic Kidney Disease. *EBioMedicine* **5**, 183-192 (2016).
442. Muller, V*., et al.* Sexual dimorphism in renal ischemia-reperfusion injury in rats: possible role of endothelin. *Kidney Int* **62**, 1364-1371 (2002).
443. Park, K.M., Kim, J.I., Ahn, Y., Bonventre, A.J. & Bonventre, J.V. Testosterone is responsible for enhanced susceptibility of males to ischemic renal injury. *J Biol Chem* **279**, 52282-52292 (2004).
444. Tanaka, R*., et al.* Sex differences in ischemia/reperfusion-induced acute kidney injury are dependent on the renal sympathetic nervous system. *European journal of pharmacology* **714**, 397-404 (2013).
445. Neugarten, J., Acharya, A. & Silbiger, S.R. Effect of gender on the progression of nondiabetic renal disease: a meta-analysis. *J Am Soc Nephrol* **11**, 319-329 (2000).
446. Neugarten, J. & Golestaneh, L. Gender and the prevalence and progression of renal disease. *Adv Chronic Kidney Dis* **20**, 390-395 (2013).
447. Magistroni, R*., et al.* Genotype-renal function correlation in type 2 autosomal dominant polycystic kidney disease. *J Am Soc Nephrol* **14**, 1164-1174 (2003).
448. Reed, B.Y*., et al.* Variation in age at ESRD in autosomal dominant polycystic kidney disease. *Am J Kidney Dis* **51**, 173-183 (2008).
449. Cha, J.Y*., et al.* Anoctamin 1 (TMEM16A) is essential for testosterone-induced prostate hyperplasia. *Proc. Natl. Acad. Sci U. S A*, 201423827 (2015).